An Introduction to Bioreactor Hydrodynamics and Gas-Liquid Mass Transfer

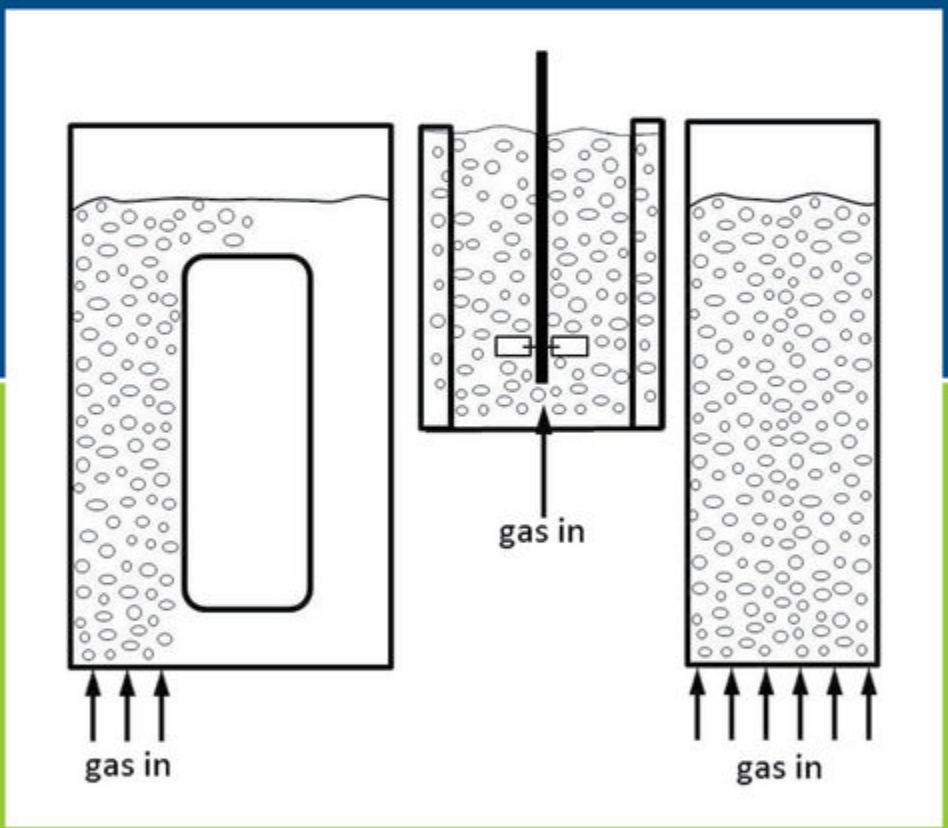

Enes Kadic and Theodore J. Heindel

WILEY

AN INTRODUCTION TO BIOREACTOR HYDRODYNAMICS AND GAS-LIQUID MASS TRANSFER

AN INTRODUCTION TO BIOREACTOR HYDRODYNAMICS AND GAS-LIQUID MASS TRANSFER

Enes Kadic and Theodore J. Heindel
Department of Mechanical Engineering
Iowa State University
Ames, Iowa

WILEY

Published by John Wiley & Sons, Inc., Hoboken, New Jersey
Published simultaneously in Canada

Library of Congress Cataloging-in-Publication Data:

Kadic, Enes, 1973-
An introduction to bioreactor hydrodynamics and gas-liquid mass transfer / Enes Kadic, Theodore J. Heindel.
pages cm
Includes bibliographical references and index.
ISBN 978-1-118-10401-9 (hardback)
1. Bioreactors. 2. Bioreactors–Fluid dynamics. I. Heindel, Theodore J., 1964- II. Title.
TP248.25.B55K33 2014
620.1′064–dc23

2013042733

Printed in the United States of America

10 9 8 7 6 5 4 3 2 1

EK would like to thank his parents, MK and EK, for their continued support and love.
TJH would like to thank MLH, HMH, and OLH for their love and support.

CONTENTS

1 Introduction

The biological production of renewable fuels, chemicals, medicines, and proteins is not possible without a properly functioning bioreactor. Bioreactors are expected to meet several basic requirements and create conditions favorable to the biological matter such that the desired production is maximized. The basic requirements may include minimal damage to the biological matter, maximum bioreactor volume utilization, maximum gas–liquid mass transfer, and/or maximum mass transfer from the liquid to the biological species (Bliem and Katinger, 1988a). Even though gas–liquid mass transfer is often the limiting reaction process, the biological species may incur additional limitations. For example, biological species can be very sensitive to shear while others may not grow well in laminar flow conditions but thrive in very turbulent conditions (Bliem and Katinger, 1988a; Hoffmann et al., 2008). In other words, the bioreactor has to accommodate very specific environmental conditions, and the operator has to be mindful of those when choosing bioreactor design and operating conditions.

Once the broadness of the problem is absorbed, it becomes clear that one bioreactor design or design ideology is insufficient to meet the operational requirements for all bioreactor operations (Bliem and Katinger, 1988a). Therefore, each bioreactor design tries to produce a very specific set of conditions applicable to a certain cell or bacteria line. In order to help with this decision process, this book provides a survey of relevant gas–liquid and gas–liquid–solid bioreactors; defines the respective bioreactor pros, cons, hydrodynamic considerations, and gas–liquid mass transfer correlations; and identifies research needs and figures of merit that have yet to be addressed. Since a large portion of the bioreactor designs have been ported over from the chemical and petrochemical industries, a significant portion of the basic bioreactor knowledge has originated from those areas. Hence, bioreactors will often be referred to as simple reactors in order to signal that some of the research used for the discussion and conclusion have been adapted from nonbiological research areas.

The remainder of this book is organized as follows. All bioreactors have common modes of operation, which are described in Chapter 2. General gas–liquid mass transfer considerations are then summarized in Chapter 3. Various hydrodynamic and gas–liquid mass transfer measure techniques are then outlined in Chapter 4, followed by a summary of multiphase flow modeling

An Introduction to Bioreactor Hydrodynamics and Gas-Liquid Mass Transfer, First Edition.
Enes Kadic and Theodore J. Heindel.

methods in Chapter 5. Chapters 6–8 then cover the three common bioreactor types, including stirred-tank bioreactors, bubble column bioreactors, and airlift bioreactors, respectively. Chapters 9 and 10 then cover less common bioreactor types, including fixed bed bioreactors and novel bioreactor designs. Some general figures of merit are then described in Chapter 11, followed by general conclusions.

2 Modes of Operation

Batch, semibatch, and continuous modes of operation are classified by the flow rates in and out of the system. Virtually all bioreactor types are capable of operating in one of these modes, depending on hardware configuration. This section will review the different modes by presenting some general information, operating procedures, and advantages and disadvantages. Discussion of operational modes for specific bioreactors can be found in the respective chapters.

2.1 BATCH BIOREACTORS

The batch bioreactor is the oldest and most used bioreactor in industry (Bellgardt, 2000b; Branyik et al., 2005). Its historical and most familiar use is in the production of alcoholic beverages (beer, wine, whiskey, etc.) and bread. Batch bioreactors combine all the necessary ingredients and then operate until the desired product concentration is reached at which point the product is extracted. In well-known processes where the final product is relatively cheap, product concentration can be correlated with time, leading to some process automation, lower capital needs, and lower operational costs (Bellgardt, 2000b). Batch bioreactor systems are also useful in modeling environmental issues (Fogler, 2005).

Biological application and experience have led to a differentiation based on substrate input or sterilization frequency. The simplest and least applicable variant is the batch cultivation system (Bellgardt, 2000b). Bioreactor sterilization is undertaken prior to the start of the process, followed by the medium being fed into the bioreactor creating a high substrate concentration (Bellgardt, 2000b; Williams, 2002). Inoculated microorganisms are introduced into the batch bioreactor at a low concentration to allow proper growth, which is practically uncontrollable until the process is finished. Ideally, the product is extracted once a satisfactory concentration is achieved, but the product in the batch cultivation system is also extracted if a necessary ingredient has been exhausted (Bellgardt, 2000b). Finally, the bioreactor is cleaned, and the process starts over again with bioreactor sterilization.

The need for more control over the biological process created the fed-batch (also known as the semibatch) cultivation system, which is the most widely used batch

An Introduction to Bioreactor Hydrodynamics and Gas-Liquid Mass Transfer, First Edition.
Enes Kadic and Theodore J. Heindel.

bioreactor. This deviation is a variable volume process that introduces additives at specific time intervals, gradually creating a more responsive and friendly growth environment (Bellgardt, 2000b). In other words, the bacteria receives the right amount and type of nutrients at the appropriate growth stage, creating a more efficient and controllable process. The final result is a product that can be adjusted or extracted when it achieves the desired properties.

The fed-batch and batch cultivation systems share the same cleaning and sterilization process in which the bioreactor operation is stopped and the bioreactor is emptied. This stoppage creates considerable costs and operational downtime. The repeated or cyclic system, which can be applied to both batch and fed-batch cultivation systems, may be installed in order to maximize the productivity. The cyclic cultivation system does not enter the cleaning and sterilization process, but rather empties a portion of the bioreactor while preserving part of the batch for the next cycle. Another method to increase productivity is cell retention techniques such as fluidized beds, membranes, or external separators. These options allow multiple cycles without cleaning and sterilization, which is initiated only if it is deemed that mutation risks exceed tolerable levels (Bellgardt, 2000b).

Variations of the batch bioreactor try to limit problems or expand batch bioreactor applications, but some systematic advantages and disadvantages exist. For the most part, batch bioreactors have lower fixed costs due to the simple concept, design, and process control (Bellgardt, 2000b; Donati and Paludetto, 1999; Williams, 2002); however, variable costs are generally higher for several reasons. First, cleaning and sterilization often add significant downtime and labor costs (Donati and Paludetto, 1999; Williams, 2002). These costs, however, can be limited in the cyclic cultivation system. Second, batch bioreactors have heat recovery difficulties leading to high environmental impact and energy consumption (Donati and Paludetto, 1999; Schumacher, 2000; Williams, 2002). Third, the additive nature of fed-batch and cyclic cultivation systems force the operator to prepare several subcultures for inoculation, which adds further variable cost pressures (Williams, 2002). Finally, batch bioreactors are not steady-state processes. The biological matter grows uncontrollably, leading to a changing environment that can bring about safety issues, runaway growth, or unexpected products when mutations occur (Westerterp and Molga, 2006).

Runaway reactions are unlikely in biological systems, but the variable environment can create conditions that change the competitive situation favoring a different bacterial species than the initially dominant one (Hoffmann et al., 2008). Batch bioreactors have limited, albeit relatively simple, process control that can lead to inconsistent or unwanted products, especially in a batch cultivation system. This problem can get even more pronounced in operations with a high potential contact amid pathogenic microorganisms or toxins, adding to variable costs if more stringent cleaning and sterilization procedures are needed (Williams, 2002).

The fed-batch cultivation system makes process control more challenging by creating a variable volume process. Any control mechanisms, therefore, require much more labor or capital (Bellgardt, 2000b; Donati and Paludetto, 1999; Simon et al., 2006; Williams, 2002). According to Simon et al. (2006), a fed-batch

system can have thousands of control variables requiring a modern and powerful supervisory control and data acquisition system, programmable logic controllers, trained personnel, and an 8-year upgrade cycle, all of which eliminate or limit upgradability of older systems or construction of larger batch bioreactor systems (Heijnen and Lukszo, 2006; Simon et al., 2006). The complexity limits practical batch bioreactor application beyond a certain size, while other bioreactor modes enjoy economies of scale for much larger operations (Donati and Paludetto, 1999; Heijnen and Lukszo, 2006; Simon et al., 2006; Williams, 2002).

Some of the batch system costs can be offset by its flexibility. Batch bioreactors are able to produce the desired product consistently. They are also capable of producing several types of products with the same equipment or making the same type of product with different equipment. Significant product modifications can also be implemented online (Donati and Paludetto, 1999; Heijnen and Lukszo, 2006). These traits offer flexibility and competitive advantages to batch bioreactor operations; however, many problems and complications are encountered when these bioreactor schemes are used for multiple separation processes, which is often the case in industry (Barakat and Sorensen, 2008).

Most batch bioreactors operate in a changing external environment especially with respect to product and ecological demands (Heijnen and Lukszo, 2006). Researchers are able to take batch bioreactors and investigate reactions, both chemical and biological, for which data are unavailable or have never been documented, while limiting contamination and experimental or dangerous risks (Donati and Paludetto, 1999). These research bioreactors should be used for scaling purposes with care since most reactions and biological growth are affected by hydrodynamics, which are a function of bioreactor scale and type.

Ultimately, batch bioreactors contain biological matter that tends to mutate. Growth periods, therefore, need to be kept short and controlled to prevent these microbial mutations, which could produce inconsistent or undesirable products (Williams, 2002). Some fermentation processes, however, are characterized by biological matter that mutates very little allowing for long reaction times (Donati and Paludetto, 1999). Either way, a positive side effect of the controlled growth period is a higher conversion level (Williams, 2002).

A specific batch bioreactor application depends on multiple internal and external factors; however, general rules of thumb and process-specific improvements can be employed to make a smarter and more profitable selection. Batch bioreactor selectivity is based on the following factors: economic balance, production scale, reaction times, production flexibility, and the nature of the process and product (Donati and Paludetto, 1999). Typically, batch bioreactors are used for smaller operations, specialty products, long growth periods (bioreactor of choice by elimination), operations in which flexibility is vital, unsteady processes, and experimental development (Donati and Paludetto, 1999; Simon et al., 2006; Williams, 2002).

Batch bioreactor operation can be made more efficient by implementing several simple managerial procedures. First, a disturbance strategy should be developed by which personnel are trained to respond and actively scan for problems in the

process leading to "lines of defense" that limit contamination and loss of product (Westerterp and Molga, 2006). These "lines of defense" should include an operating condition within which personnel and management are comfortable, an early warning system, and a reaction procedure to accidents and malfunctions including proper training and equipment (Westerterp and Molga, 2006). Second, a decision support framework (DSF) should be developed so that all personnel and management are familiar with operating costs, benefits, objectives, etc. The DSF will make production more efficient and profitable; it provides a clear outline of benefits and costs associated with general and specific options. General models, such as ANSI/ISA88 or ANSI/ISA95, are available and can be applied to all batch bioreactors (Heijnen and Lukszo, 2006). Finally, two improvement strategies can be implemented to make batch reactions more efficient. The "cook book" or "recipe" approach has been shown to improve yields in batch process operations. The user is able to adjust the biological reaction online as needed and is able to draw on extensive experience and/or knowledge to have better process control and product quality and consistency. The second strategy, production schedule optimization, has been proven effective in situations where products are made with different equipment, or equipment is used to make different products by optimizing capacity utilization (Schumacher, 2000).

2.2 CONTINUOUS BIOREACTORS

Continuous bioreactors have several intrinsic properties that differentiate them from batch bioreactors. The largest distinction is that substrate and product continuously flow in and out of the bioreactor, which does not allow for cleaning or sterilization processes and extracts product regardless of identity or quality (Bellgardt, 2000b). If output does not meet specifications, the resulting product has to be either discarded or separated and recycled back into the bioreactor. Either option creates a negative economic impact by increasing (i) initial investment due to the necessary installation of a recycling system and (ii) variable costs due to the discarded product and the associated inputs (Williams, 2002). Product properties are controlled by substrate residence time which, by design, can only be controlled by material flow rate and bioreactor geometry. In order to ensure a homogeneous product, the process is assumed to be in steady state and conditions within the bioreactor are typically assumed to be independent of time (Williams, 2002). Therefore, continuous bioreactors are agitated mechanically and/or by gas injection. Substrate input is not used for agitation so as to decouple it from bioreactor hydrodynamics. In order to make the steady-state conditions easier to achieve and maintain, most continuous bioreactors are run in a constant volume setting, which induces uniform volumetric substrate and product flow rates. Efficiency is enhanced using cell retention techniques such as fluidized beds, membrane bioreactors, or cell recycle (Bellgardt, 2000b). The semicontinuous bioreactor, a hybrid between the batch and continuous bioreactor, is run in batch mode during start-up. Once necessary conditions are achieved, this bioreactor

is operated continuously unless the product has not achieved the necessary properties, in which case the bioreactor is operated in batch mode until the desired specifications are met (Williams, 2002).

Any continuous bioreactor discussion is ultimately related to batch systems which are seen as a proven technology with processes designed around their capabilities and properties. In addition, operators have more experience and are more comfortable dealing with batch disturbances (Branyik et al., 2005). Continuous bioreactors, however, offer many advantages such as control, production, and the potential for optimization (Williams, 2002). Control can be achieved with several schemes. Substrate and cell concentrations or bioreactor conditions can be modified online to influence bacterial growth rates which, in turn, modify bioreactor and reaction dynamics (Bellgardt, 2000b; Gonzalez et al., 1998; Ramaswamy et al., 2005; Reddy and Chidambaram, 1995; Sokol and Migiro, 1996). These changes provide an indirect influence over product type and properties (Ramaswamy et al., 2005).

The continuous bioreactor offers more operational control and flexibility over batch bioreactors. Practical production is made simpler and more profitable due to the possibility for automation and the lack of cleaning and sterilization processes (Bellgardt, 2000b). The added equipment cost is offset with operational savings while control schemes, which are limited to a few hundred variables, are often much simpler than the corresponding batch bioreactor systems (Simon et al., 2006; Williams, 2002).

In addition to the control advantages, the steady-state operation of continuous bioreactors allows for the production of a consistent and economically attainable product quality (Williams, 2002). It also rectifies a major downside in the batch system—the bacterial concentration is very low in the initial stages while growth rates are sluggish at maturity, both leading to decreased productivity. The continuous system allows high bacterial concentrations throughout the process, boosting production capacity and consistency (Bellgardt, 2000b). Combined with the lack of cleaning and sterilization processes, continuous bioreactors maximize production time while providing lower labor and variable costs and maximum capital utilization (Bellgardt, 2000b; Williams, 2002).

Finally, continuous bioreactors allow for optimization. Operators are able to vary inputs and bioreactor conditions online, creating an optimized environment for the growth stage and age of the cell culture, resulting in a more consistent output (Bellgardt, 2000b; Williams, 2002). In some series bioreactor applications, process augmentation is necessary to prevent washout or inconsistent product (in case of an upstream disturbance and varying substrate concentration). These disturbances and variances are often experienced when a batch bioreactor or other limiting cycles are used to prepare a substrate for the continuous process (Ramaswamy et al., 2005).

Disturbance management depends greatly on the ability to investigate the cause of the disturbance. Batch reaction systems have complicated procedures to identify the cause of disturbances with the operator often left guessing (Schumacher, 2000). The continuous process provides a clear plan of attack. The effect of changing one variable while keeping all others constant allows for a clear relationship and better

understanding (Williams, 2002). Researchers are able to form global correlations or models aiding development, adoption, or ongoing operations.

Much higher production capacity, efficiency, capital utilization, and lower variable costs for continuous bioreactors may make operations appear efficient, but continuous systems have a number of disadvantages. Biological growth typically requires a batch start-up period to achieve conditions within the bioreactor to promote optimal production (Bisang, 1997; Gonzalez et al., 1998; Williams, 2002). In addition, bacterial matter, especially in recycle and retention processes, age and mutate, which negatively impacts their productivity and efficiency, and may even lead to the production of unwanted products (Branyik et al., 2005; Domingues and Teixeira, 2000). Because of this, a continuous system may be unable to produce the prescribed product quality or it may require more equipment and control systems (Williams, 2002). Long-lasting processes also have contamination problems and biological growth on the walls, requiring the bioreactor to be controlled more closely; otherwise, faster growing cultures overtake the desired ones (Bellgardt, 2000b; Williams, 2002).

Controlling continuous production is also made more difficult because it is usually nonlinear (Ramaswamy et al., 2005; Reddy and Chidambaram, 1995). Several control mechanisms exist, but most make the mistake of varying substrate or bacterial concentrations based on indirect data, such as temperature or pH, and assuming a first-order response (Bellgardt, 2000b; Ramaswamy et al., 2005). This type of control mechanism usually results in a system that is too slow and has stability problems (Reddy and Chidambaram, 1995). Nonlinear controllers are available, but have been shown to be unreliable and complicated and usually report excessive variations (Gonzalez et al., 1998; Reddy and Chidambaram, 1995). Operators may also be limited to a certain gas or liquid input range. Bacteria require a certain amount of gas for proper growth, and a low gas flow rate could suffocate the bacteria or create a hostile environment decreasing bioreactor productivity. On the other hand, too much gas may create suboptimal conditions and have a negative impact on bacterial growth or bioreactor hydrodynamics (Bellgardt, 2000b).

The flexibility, reliability, efficiency, and cost reductions which the continuous systems are supposed to deliver can be offset by control issues, making the pure continuous bioreactor ineffective and even more expensive to operate than batch systems (Williams, 2002). In addition, some fermentation processes, such as beer production, are not able to easily use continuous systems since they change basic product properties, such as taste, color, and/or odor (Branyik et al., 2005).

Several scenarios exist for which continuous bioreactors are feasible and preferred, such as high volume production, use of mutation-resistant bacteria culture, wastewater treatment, and processes that do not require a sterile environment. Currently, continuous bioreactors are used for the production of vinegar, baker's yeast, alcohols, and solvents, and for wastewater treatment (Bellgardt, 2000b; Simon et al., 2006; Williams, 2002). Proper control systems also allow continuous principles to be used in other production systems. These requirements include that the process does not necessitate a sterile environment or that it can be easily controlled through alternative means such as flocculation, substrate and

cell concentrations, or the use of secondary or genetically altered cell cultures (Bellgardt, 2000b; Bisang, 1997; Domingues and Teixeira, 2000; Gonzalez et al., 1998; Ramaswamy et al., 2005; Reddy and Chidambaram, 1995; Simon et al., 2006; Sokol and Migiro, 1996; Williams, 2002). The most practical option for the use of the continuous system would be with the semicontinuous bioreactor. This variant would require a smaller initial investment, offer productivity and optimization possibilities, and have less control problems than a continuous bioreactor (Williams, 2002). It would allow for start-up, residence time variations, more flexibility, and some positive batch bioreactor traits.

2.3 SUMMARY

The batch bioreactor is the oldest and most widely used bioreactor. The advantages of using a batch bioreactor are lower fixed cost, flexibility, and operational simplicity. Operational costs can be lowered if the process is well known. These bioreactors are preferred for use in smaller operations, specialty products, long growth periods, operations in which flexibility is vital, unsteady-state processes, and experimental development. Continuous bioreactors, on the other hand, provide for more production optimization, automation, and capital utilization. If the continuous process is used properly, the larger initial investment can be easily offset by lower variable costs and faster production times. Therefore, this process is preferred for high volume production, processes using mutation-resistant bacteria, and processes that do not require a sterile media. The production of alcohols, solvents, vinegar, or baker's yeast, and wastewater treatment are a few examples that take advantages of the continuous process.

Although the choice may seem simple, the experience has been otherwise. The continuous process has had a hard time breaking into industries that have traditionally used batch bioreactors. Some operators have found the switch to a continuous process to be laborious. Unknown challenges provide a situation which could be critical to the project's survival. For example, even though the continuous process offers huge time savings in the production of beer, the batch bioreactor remains the most popular. More risk loving and high volume operators, such as producers of industrial alcohols and solvents and wastewater treatment plants, find the continuous system to be a huge economic advantage. The choice should be made with an understanding of risk capacity for the particular application. The analysis should also include an economic sensitivity analysis and a foresight into the equipment availability. The process selection may ultimately limit the type of bioreactor used or its operational conditions.

3 Gas–Liquid Mass Transfer Models

Mass transfer operations in biological systems depend on a myriad of intermediate and parallel processes. Reactors for gas–liquid applications, which account for about 25% of all chemical reactions (Tatterson, 1994), fulfill two needs: dispersion and absorption (Oldshue, 1983). Dispersion requires that the entire reactor volume be used to mix the gas into the liquid. This step, however, is usually easily achieved or is not the critical system constraint (Oldshue, 1983). The low solubility of most gases limits the gas absorption to the point that gas–liquid mass transfer becomes the rate-limiting step for the overall reaction (Bouaifi et al., 2001; Fogler, 2005; Garcia-Ochoa and Gomez, 1998; Linek et al., 1996a; Moo-Young and Blanch, 1981; Ogut and Hatch, 1988; Oldshue, 1983; Vazquez et al., 1997). This limitation is even more severe in systems using very low solubility gases, such as carbon monoxide found in synthesis gas, some of which are very important in industrial applications (Moo-Young and Blanch, 1981). Thus, the easiest way to increase the productivity of gas–liquid bioreactors is to increase the gas–liquid mass transfer rate (Kapic, 2005).

3.1 GAS-LIQUID TRANSPORT PATHWAYS

The transfer of gas from the gas phase to a microorganism suspended in a bioreactor must take place along a certain pathway. Figure 3.1 schematically describes the general transport route and includes eight resistances to gas mass transfer that may exist between the gas bubble and the microorganism (Chisti, 1989); these resistances include (i) in the gas film inside the bubble, (ii) at the gas–liquid interface, (iii) in the liquid film at the gas–liquid interface, (iv) in the bulk liquid, (v) in the liquid film surrounding the cell, (vi) at the liquid–cell interface, (vii) the internal cellular resistance, and (viii) at the site of the biochemical reaction.

It should be noted that all resistances are purely physical except for the last resistance, and that not all mass transfer resistances may be significant for a given system. Many of the resistances may be neglected in most bioreactors except for those around the gas–liquid interface (Chisti, 1989; Moo-Young and Blanch, 1981). Thus, the transport problem is greatly simplified to a gas–liquid interfacial

An Introduction to Bioreactor Hydrodynamics and Gas-Liquid Mass Transfer, First Edition.
Enes Kadic and Theodore J. Heindel.

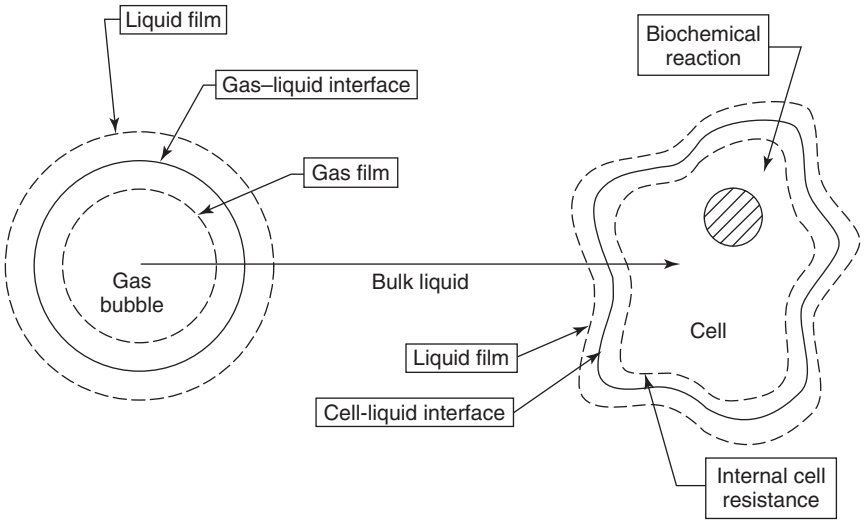

Figure 3.1 Mass transfer resistances encountered in gas–liquid dispersions containing active cells. Adapted from Chisti (1989).

mass transfer problem around the bubble. At this location, two transfer coefficients may be considered at the gas–liquid interface. The liquid-phase mass transfer coefficient is represented by k_L, whereas the gas-phase mass transfer coefficient is identified by k_G. Since the gas-phase mass transfer resistance is typically much smaller than the liquid phase, $k_G >> k_L$ and gas–liquid mass transfer is controlled by k_L (Chisti, 1989); this value is modulated by the specific (gas–liquid) interfacial area a. The driving force for mass transfer is the gas concentration gradient between the gas phase C^* and the dissolved gas C. The mass transfer rate is then determined by

$$\frac{dC}{dt} = k_L a(C^* - C) \tag{3.1}$$

The volumetric gas–liquid mass transfer coefficient $k_L a$ is typically used when determining the mass transfer coefficient because it is difficult to measure k_L or a independently. Variations in the volumetric gas–liquid mass transfer coefficient during operation are often thought to be a direct result of changes in the interfacial area (Hoffmann et al., 2007; Stenberg and Andersson, 1988b), which would imply that homogeneous (bubbly) operation is more desirable than heterogeneous flow (Bouaifi et al., 2001). However, according to Linek et al. (2005b), concise conclusions are often troublesome because liquid-phase mass transfer is calculated using the gas–liquid mass transfer coefficient (k_L) and the specific interfacial area (a). Any measurement errors in either variable cause false conclusions or improper use of mass transfer models.

3.2 BASIC MASS TRANSFER MODELS

Many mass transfer models exist, but most of them depend on three assumptions and are simplified versions of actual mass transfer mechanisms, many of which occur simultaneously. The first assumption is that the different phases and the phase interface offer resistance to mass transfer in series, in a similar manner to heat transfer resistances. The second assumption maintains that mass transfer is controlled by the phase equilibrium near the interface, which changes more quickly than the bulk phase equilibrium (Azbel, 1981). In other words, mass transfer occurs at the microscale level (van Elk et al., 2007). Finally, gases are assumed to be single component. Multiple component problems are more complicated because each individual gas component making up the mixture has to be considered for the limiting gas–liquid mass transfer step. The complexity grows further once the relationships between each gas component and, for example, the bacteria in a bioreactor are considered.

Single-component gases are preferred for research purposes because direct and mechanistic relationships can be drawn. However, air has been used in many oxygen mass transfer studies because it is easily accessible; in this case, air is typically assumed to be composed of two components: oxygen and an inert gas comprised primarily of nitrogen. Nevertheless, its utilization in gas–liquid processes is often seen as inferior relative to other gases such as pure oxygen, carbon monoxide, carbon dioxide, or hydrogen (Bliem and Katinger, 1988b; Worden and Bredwell, 1998). For experimental purposes, air is often treated as a single-component gas with the realization that the driving force could change due to nontransferred gases (Worden and Bredwell, 1998). Multiple component gases, however, are often encountered in industrial settings mainly due to biological or chemical reactions. Therefore, mass transfer models and correlations are typically used to provide mass transfer estimates and possibly production bounds.

The oldest and most simplistic mass transfer model, which is often presented in undergraduate chemical reaction engineering textbooks (e.g., Fogler (2005)), is the film model originally presented by Nernst in 1904. The interface is assumed to be infinitesimally thin and its resistance is usually ignored. The liquid phase has a constant and definite boundary layer, or film, of thickness δ_{eff} which limits mass transfer (Azbel, 1981). Since these assumptions are made about the boundary layer characteristics, mass transfer is concluded to occur in a steady-state environment. Other limiting factors are the molecular diffusivity D and the driving force represented by the concentration gradient. The film model equation, therefore, predicts mass flux J as

$$J = \frac{-D}{\delta_{\text{eff}}}(C^* - C) \tag{3.2}$$

Molecular diffusivity and film thickness are combined into the liquid-phase mass transfer coefficient k_{L} such that

$$J = k_{\text{L}}(C^* - C) \tag{3.3}$$

This model has several limitations. The film model assumes that mass transfer is controlled by the liquid-phase film, which is often not the case because the interface characteristics can be the limiting factor (Linek et al., 2005a). The liquid film thickness and diffusivity may not be constant over the bubble surface or swarm of bubbles. Experiments also indicate that mass transfer does not have a linear dependence on diffusivity. Azbel (1981) indicates that others have shown that turbulence can have such a significant effect on mass transfer such that eddy turbulence becomes the controlling mechanism in which diffusivity does not play a role. In most instances, however, eddy turbulence and diffusivity combine to play a significant role in mass transfer (Azbel, 1981).

The border diffusion layer model was introduced as an amendment to the film model to present a more realistic description. It accounts for an undefined film thickness, turbulence effects, and the role of molecular diffusion. When the flow is turbulent, the flow around the bubble is split into four sections: the main turbulent stream, the turbulent boundary layer, the viscous sublayer, and the diffusion sublayer. Eddy turbulence accounts for mass transfer in the main turbulent stream and the turbulent boundary layer. The viscous sublayer limits eddy turbulence effects so that the flow is laminar and mass transfer is controlled by both molecular diffusion and eddy turbulence. Microscale eddy turbulence is assumed to be dominant in the viscous sublayer. Mass transfer in the diffusion sublayer is controlled almost completely by molecular diffusion (Azbel, 1981).

This model can be used as a rough estimate. It is still plagued by the steady-state assumption which is oftentimes an inadequate description of mass transfer. The diffusion sublayer δ is a function of viscosity (ν), diffusivity (D), and viscous sublayer thickness (δ_0), but realistic measurements are difficult, if not impossible, to obtain. An empirical correlation has been suggested for δ (Azbel, 1981):

$$\delta = \left(\frac{D}{\nu}\right)^{1/n} \delta_0 \tag{3.4}$$

The power n is an experimental variable with a value of about 2 for gas–liquid mass transfer. The liquid-phase mass transfer coefficient can therefore be related to diffusivity as (Azbel, 1981; Moo-Young and Blanch, 1981)

$$k_{\mathrm{L}} \approx D^{1/n} \tag{3.5}$$

The Higbie penetration model for mass transfer compensates for transient behavior. It assumes that mass transfer occurs during brief phase contacts that do not allow enough time for steady-state conditions. In other words, the phases collide but do not have a definitive and continuous interface with respect to time. The mass transfer is prompted by turbulence that refreshes the interface, and the refresh rate is the limiting step in mass transfer. Eddies approach the surface at which point mass transfer by molecular diffusion is initiated and is described by Azbel (1981):

$$\frac{\partial C}{\partial t} = -D\frac{\partial^2 C}{\partial y^2} \tag{3.6}$$

Equation (3.6) assumes that the gas phase is not reacted during the mass transfer process at the interface. Fast reactions, however, predominantly occur very close to the interface and have to be accounted for by van Elk et al. (2007)

$$\frac{\partial C}{\partial t} = -D\frac{\partial^2 C}{\partial y^2} - r_C \tag{3.7}$$

where r_C represents the reaction rate of the gas phase at the liquid interface. In this case, fast reactions are assumed to occur when $Ha > 2$, where Ha is the Hatta number defined as the ratio of species absorption with and without reactions. The reactive absorption provides the advantage of separating the investigation of the interfacial area from the mass transfer coefficient (Hoffmann et al., 2007).

All turbulent eddies spend approximately the same amount of time at the interface defined by τ. This interface contact time is assumed to be proportional to the amount of time it takes the bubble to rise one bubble diameter d_B or

$$\tau = \frac{d_B}{U_B} \tag{3.8}$$

where U_B is the bubble rise velocity. The Higbie penetration model predicts (Azbel, 1981; Moo-Young and Blanch, 1981)

$$k_L = 2\left(\frac{D}{\pi\tau}\right)^{1/2} \tag{3.9}$$

The assumption that each turbulent eddy spends the same amount of time at the interface is unrealistic. Modified penetration models, such as Danckwerts' surface renewal theory model, allow each eddy to have an independent, variable interface contact time based on a statistical probability function. It uses a fractional renewal s to account for the rate of surface renewal, in which case:

$$k_L = (Ds)^{1/2} \tag{3.10}$$

The surface renewal theory model still shares the same power as the two previous models (Azbel, 1981). The difficulty with the surface renewal model is that the unknown variable s depends on operational conditions and reactor geometry. Hence, it would be difficult to use this model as a scale-up guide.

Later research concluded that reality lies somewhere between the film and penetration models. These film–penetration models, such as those of Hanratty and Toor (Azbel, 1981; van Elk et al., 2007), concluded that the original film model is accurate for highly diffusive gases, large interface contact times, or a small boundary layer thickness (relative to a penetration depth). If a penetration model is used during these situations, predicted mass transfer will be too high (van Elk et al., 2007). Other penetration-type or hybrid models allow for further modifications making their predictions more accurate or applicable for certain conditions. A common ground has been found in the exponential dependence of the diffusivity. Gas–liquid

applications show the power n ranging from 0.5 to 1. If water is used as the liquid, the power ranges from 0.65 to 0.985 (Azbel, 1981).

Current research falls into one of two schools of thought: Calderbank's slip velocity model and Lamont and Scott's eddy turbulence model (Linek et al., 2004; Linek et al., 2005b). Even though both models are penetration-type models, they make very different assumptions. The slip velocity model assumes different behavior for small and large bubbles. It also assumes a significant difference between average velocities for the two phases. The slip velocity and the surface mobility control mass transfer and, in terms of penetration theory, surface renewal.

Small bubbles with a diameter $d_B < 1$ mm act as rigid spheres with an immobile surface and slipless interface (Linek et al., 2005a; Scargiali et al., 2007). The surface and its phase interface limit mass transfer. In this case, turbulence indirectly affects mass transfer by influencing the terminal bubble rise velocity and, therefore, the residence time (Poorte and Biesheuvel, 2002). Larger bubbles, those with $d_B > 2.5$ mm, have a mobile, ellipsoidal surface experiencing much larger drag forces than rigid spherical bubbles with the same total volume (Scargiali et al., 2007). Therefore, mass transfer in large bubbles is limited by eddy turbulence. In this case, other penetration models can properly describe mass transfer behavior. The transition area is highly variable. Bubble surface mobility in this region is dependent on liquid properties and surfactants (Linek et al., 2005a).

The eddy turbulence model, or simply eddy model, assumes that the small-scale eddies control surface renewal and, subsequently, mass transfer. This model acknowledges a scale dependence. Macroscale movements, those represented by the Reynolds number, Re, are assumed to have a small impact on surface renewal, where the Reynolds number is defined as

$$Re = \frac{U d_B}{\nu} \tag{3.11}$$

where U is the velocity, d_B is the (hydraulic) bubble diameter, and ν is the fluid kinematic viscosity. The eddy model postulates that small bubbles would not recognize macroscale motions. Small-scale effects are needed to incur a relative impact. Eddies are assumed to pound the bubble surface and cause surface renewal regardless of bubble size and interface properties (Linek et al., 2004; Linek et al., 2005a; Linek et al., 2005b).

Some of these models predict opposing results. For example, the slip velocity model predicts mass transfer to decrease with increasing turbulence once the bubble surface becomes rigid. The eddy turbulence model predicts the opposite. These theories represent effects that occur concurrently. The strength of each mode depends on the bioreactor type and process. For example, complex reactions, such as polymerization or cellular cultures, are highly sensitive to micromixing (Nauman and Buffman, 1983). Mass transfer during these highly complex processes is affected more by micromixing than by macromixing (Hoffmann et al., 2008). These models and their predictions will be revisited in the appropriate bioreactor sections. Furthermore, the models do not account for surfactant effects on the interface, nor its influence on mass transfer behavior (Vazquez et al., 1997).

3.3 SUMMARY

The fundamental gas–liquid mass transfer models lack the ability to obtain and process all necessary information and factors integral to bioreactor operation. Gas–liquid systems are simply too complex. Therefore, a theoretical equation, which is widely applicable, does not exist (Garcia-Ochoa and Gomez, 2004). Empirical correlations have been developed to simplify analysis and design and have become exclusive in the literature and practice (Kawase and Moo-Young, 1988). Model parameters are chosen that are thought to influence the operation, and their powers and constants are fitted to the experimental data. The correlations are used for design and scale-up while theoretical mass transfer models are used to explain the influence of various operational inputs.

4 Experimental Measurement Techniques

A significant difficulty in characterizing and quantifying gas–liquid, liquid–solid, and gas–liquid–solid mixtures commonly found in bioreactor flows is that the systems are typically opaque (e.g., even an air–water system becomes opaque at fairly low volumetric gas fractions); this necessitates the use of specially designed invasive measurement probes or noninvasive techniques when determining internal flow and transport characteristics. Many of these probes or techniques were developed for a particular type of gas–liquid flow or bioreactor. This chapter first introduces experimental techniques to gauge bioreactor hydrodynamics and then summarizes gas–liquid mass transfer measurement techniques used in bioreactors.

4.1 MEASURING BIOREACTOR HYDRODYNAMIC CHARACTERISTICS

Hydrodynamics in gas–liquid systems have been studied extensively in the past due to their wide range of applications. Characteristics of interest include flow regimes, local pressure drop, gas residence time, axial diffusion coefficients, bubble size, bubble rise velocity, gas holdup, and power consumption. This section will summarize various experimental techniques to quantify some of these characteristics.

In general, the experimental techniques used in gas–liquid flows can be classified as intrusive where invasive probes are used to record local measurements, or noninvasive where data are recorded without altering the flow conditions. Measurement techniques can further be classified as time-average or transient techniques as well as local, regional, or global techniques. Depending on the bioreactor of interest, one technique may be more applicable than another. For example, global time-average gas holdup may be all that is desired in an internal-loop airlift bioreactor investigation, whereas local transient conditions may be required to validate turbulence modeling simulations in bubble columns. Several reviews of one or more experimental methods used in multiphase systems have appeared in the literature, and these can be applied in bioreactor characterization; additional details can be found in several of these publications (Azzopardi et al., 2011; Beck and

An Introduction to Bioreactor Hydrodynamics and Gas-Liquid Mass Transfer, First Edition.
Enes Kadic and Theodore J. Heindel.

Williams, 1996; Boyer et al., 2002; Ceccio and George, 1996; Chaouki et al., 1996, 1997; Cheremisinoff, 1986; Heindel, 2011; Hewitt, 1978, 1982; Kumar et al., 1997; Mudde, 2010a; Powell, 2008; Prasser, 2008; Vatanakul et al., 2004; Vial et al., 2003; Williams and Beck, 1995).

4.1.1 Flow Regime Measurements

Flow regime identification is dependent on the geometry of the bioreactor. For example, flow regimes in bubble columns will be different from those identified in stirred-tank bioreactors. In some cases, the experimental techniques used to identify flow regimes are system independent, while in other cases, the technique was developed for a particular geometry. The specific flow regime definitions in common bioreactor types are described in detail in their respective chapters.

Many of the early flow regime studies were based on visual observations in optically accessible flow systems. In cases were optical access is problematic, techniques have been developed to analyze local process measurements such as local pressure fluctuations to correlate various measures with the observed flow regimes. For example, Boyer et al. (2002) indicate many different process measurements can be analyzed to identify bioreactor flow regimes, including measures from wall pressure transducers, microelectrodes imbedded in the wall, conductivity probes, acoustic receivers, optical probes, optical transmittance probes, temperature probes, hot film anemometry, and electrochemical probes. Many of these techniques are invasive to the bioreactor. The fluctuating signals from these probes have been analyzed with various signal processing techniques including classical statistical or spectral techniques, as well as newer fractal, chaotic, or time–frequency analysis techniques. Boyer et al. (2002) and Vial et al. (2000) provide an excellent overview of the flow regime identification methods based on pressure signal fluctuation analysis. Tomographic techniques have also been used to identify flow regimes in multiphase systems (Chaouki et al., 1996, 1997).

4.1.2 Local Pressure Drop

The pressure drop between two locations in a bioreactor is an important hydrodynamic characteristic because the actual measure is needed to size pumps and compressors. Average and transient pressure drop measures can also be analyzed to quantify phase holdup or identify flow regime.

Local pressure drop can be recorded through a variety of methods. Manometers were initially installed along multiphase flow columns to measure pressure signals (Hills, 1976; Kara et al., 1982; Merchuk and Stein, 1981; Zahradnik et al., 1997). More recently, pressure transducers have been used (Letzel et al., 1999; Lin et al., 1998; Luo et al., 1997; Su and Heindel, 2003, 2004, 2005a; Tang and Heindel, 2004; Tang and Heindel, 2005a; Tang and Heindel, 2005b; Tang and Heindel, 2006a; Ueyama et al., 1989), and they are usually flush mounted to the bioreactor wall so that the disturbance to the flow caused by the pressure transducers is minimized.

Local pressure drop measurements with flush-mounted sensors are an easy way to determine gas holdup in the region in which the pressure drop was measured

(Tang and Heindel, 2006a), is noninvasive, and does not interrupt bioreactor operation. With the price drop of piezoelectric pressure transducers and the development of computer data acquisition technology, this method is a convenient low cost measurement technique and is applicable to systems at high temperature and pressure (Letzel et al., 1999; Lin et al., 1998). This technique does not require a transparent fluid or containment vessel, nor does it have requirements on liquid electrical properties. Bioreactor pressure drop can be analyzed to measure the overall average gas holdup in a multiphase region between the two pressure measurement locations, as well as the global average gas holdup. Thus, it can be used to probe the axial gas holdup variation in a column (Hol and Heindel, 2005). Compared to radiation attenuation methods (e.g., γ-ray or X-ray tomography), the pressure difference method is much safer. Furthermore, in addition to estimating gas holdup, pressure signals can also be used to determine flow regime transition (Ruthiya et al., 2005; Vial et al., 2000) and average bubble size (Chilekar et al., 2005) in bubble columns. When a solid phase is present, the pressure difference method can be used to measure gas holdup if the liquid–solid slurry behaves as a pseudo-homogeneous mixture or if the solid concentration as a function of height is known (Kumar et al., 1997; Tang and Heindel, 2005b; Tang and Heindel, 2006a, 2007).

4.1.3 Mixing or Residence Time

Mixing time is defined as the time required to achieve a specified quality of mixing or homogeneity after the addition of some materials (Merchuk, 1985; Weiland and Onken, 1981). Mixing time is very important to several processes, including fermentation. If, for example, an additive does not disperse adequately or takes too long to mix, a local high concentration may be observed, which could lead to cell damage in that region. In batch processes, mixing time is typically associated with the time it takes to fully disperse an additive in the entire tank after a localized input. In continuous processes, mixing time and residence time are coupled, where residence time is the time a particular fluid element (or slug) remains in a given region of the bioreactor. For example, in an airlift bioreactor, residence time is typically associated with the length of time a fluid element remains in the riser and is used extensively as a key parameter in airlift bioreactor modeling.

As indicated by Rodgers et al. (2011), there are several experimental methods that have been used to determine mixing or residence time, including dye injection, pH shift, tracer monitoring, flow followers, and tomography imaging. For example, neutrally buoyant tracer particles were tracked by Kawase and Moo-Young (1986b) to determine the circulation time in an airlift bioreactor. The time it took the tracer particles to complete one loop was determined through multiple measures to calculate the average circulation time.

4.1.4 Axial Diffusion Coefficient

The axial diffusion (or dispersion) coefficient is a measure of mixing in a vertical bioreactor like a bubble column or airlift bioreactor. It has also been used to quantify

backmixing in bubble columns. A simple method to measure the axial diffusion coefficient is to add a small amount of salt tracer to the liquid surface, and then measure the local fluid conductivity at a particular distance from the column surface as a function of time (Ohki and Inoue, 1970). Lorenz et al. (2005) extended this idea using a thermal pulse. In this method, a pulse of the same liquid, but at a higher or lower temperature than the bulk fluid, is injected into the system. Thermocouples placed along the column record the local fluid temperature as a function of time to track the thermal pulse. The axial dispersion coefficient D_L is then determined using a 1D dispersion model of the form (Ohki and Inoue, 1970):

$$T = \left(1 + 2\sum_{n=1}^{\infty}\left[\left(\cos\frac{n\pi}{H}z\right)\exp\left\{-\left(\frac{n\pi}{H}\right)^2 D_L t\right\}\right]\right)(T_0 - T_\infty)e^{\alpha t} + T_\infty \quad (4.1)$$

where H is the bioreactor height, z is the axial location within the reactor where the temperature is recorded, T_0 is the initial temperature, T_∞ is the final temperature, α and n are the constants, and t is the time.

4.1.5 Gas–Liquid Interfacial Area

The gas–liquid interfacial area (a) is a fundamental parameter in designing bioreactors because the knowledge of this parameter is required to calculate individual gas–liquid mass transfer rates (Vasquez et al., 2000). The interfacial area is a challenge to quantify because it is influenced by the bioreactor geometry and operating conditions, as well as the physical and chemical properties of the gas–liquid system. In some cases, the interfacial area is estimated by assuming a uniform bubble diameter d_B and measuring the overall gas holdup ϵ. In this case, the gas–liquid interfacial area is estimated from Chisti (1989):

$$a = \frac{6\epsilon}{d_B} \quad (4.2)$$

If the bubble size is not uniform, the bubble size distribution can be measured using a variety of measurement tools such as optical probes, multipoint needle probes, or hot-film anemometers, and the Sauter mean diameter (d_{SM}) can be substituted for the bubble diameter (Azzopardi et al., 2011) (see also Eq. (4.3)).

The interfacial area can be measured in specific systems using chemical reactions in which the absorption rate kinetics are a known function of the gas–liquid interfacial area. For example, Vasquez et al. (2000) compared three different chemical methods: (i) Danckwerts' method using the absorption of CO_2 in sodium or potassium carbonate buffer solutions, (ii) the sodium sulfite method involving the oxidation of sulfite ions, and (iii) the sodium dithionite method involving the oxidation of dithionite ions. All three methods were shown to produce similar interfacial area measurements.

4.1.6 Bubble Size and Velocity

Bubble size and bubble velocity measurement techniques have been reviewed by Saxena et al. (1988) and Boyer et al. (2002); the interested reader is directed to these sources for detailed descriptions of the available hardware and data analysis procedures.

It is common to report the average bubble diameter as the Sauter mean diameter d_{SM}, which is defined as the diameter of a bubble equivalent to the volume-to-surface area ratio of the entire dispersion (Saxena et al., 1988). Assuming all bubbles are spheres,

$$d_{SM} = \frac{6\epsilon}{a} = \frac{\sum d_B^3}{\sum d_B^2} \tag{4.3}$$

where ϵ is the total gas holdup, a is the total interfacial area, and d_B is the individual bubble diameter. Bubble size can be determined through visual observations and image analysis techniques.

If the time difference between successive frames of the same bubble is known and the bubble displacement can be measured, then bubble rise velocity can also be measured. However, visual methods are limited to systems with optical access, so observations are limited to regions near the wall even under moderate gassing rates in gas–liquid systems. The wall and liquid must also be transparent.

In addition to optical methods, bubble size can be determined using optical probes and electrical conductivity (resistivity) probes (Saxena et al., 1988). For example, Magaud et al. (2001) used dual optical probes to determine the local instantaneous presence of the liquid or gas in a bubble column. With this information, local bubble chord length and bubble rise velocity can be determined. One advantage of optical probes is that its operation is independent of the electrical properties of the medium surrounding the probe (Saxena et al., 1988). Electrical conductivity or resistivity probes can be configured as needle probes, which have been used to determine mean bubble chord length, bubble size, and bubble rise velocity.

Bubble size in opaque systems has been determined by Heindel and coworkers using flash X-ray radiography (Garner and Heindel, 2000; Heindel, 1999, 2000, 2002; Heindel and Garner, 1999). In this process, an intense burst of radiation is produced for a fraction of a second to provide stop-motion X-ray projections of bubble motion. Image analysis is then completed to determine bubble size and bubble size distribution. A significant drawback of this technique was that the flow was limited to quasi-2D flows and the bubble number density had to be small enough to distinguish individual bubbles.

Ultrasound Doppler velocimetry (UDV) has also been used to measure bubble velocity by measuring the frequency shift between the emitted ultrasound beam and the echo reflected from the gas–liquid interface (Vial et al., 2003).

Many researchers have used two or more measurement methods to characterize multiple aspects of gas–liquid flows. For example, Broder and Sommerfeld (2003) used a specially designed particle image velocimetry (PIV) and particle tracking velocimetry (PTV) techniques to simultaneously measure the bubble size as well as bubble and liquid velocities. Their experimental equipment was mounted on a traversing system that allowed them to follow rising bubbles with a high speed camera system. Knowing the bubble size and bubble and liquid velocities, and using sophisticated data analysis procedures, they could further determine bubble–bubble collision rates, coalescence rates, and coalescence efficiencies. Another example is provided by Kiambi et al. (2011) who used a bioptical probe and hot-film anemometry to measure local gas holdup, bubble velocity, bubble size, and liquid velocity in an external airlift reactor. They were able to provide radial distributions of the various measures of interest.

4.1.7 Global and Local Liquid Velocity

In fermentation processes like those found in airlift reactors, the difference in riser and downcomer gas holdup creates a hydrostatic pressure difference between the bottom of the riser and the bottom of the downcomer, which in turn acts as the driving force for liquid circulation. A mean circulation velocity U_c is defined as (Blenke, 1979)

$$U_c = \frac{x_c}{t_c} \tag{4.4}$$

where x_c is the circulation path length and t_c is the average circulation time for one complete circulation. However, liquid circulation velocity is not commonly used as a characteristic parameter for gas–liquid fermentation processes. The superficial liquid velocity in the riser (U_{Lr}) or downcomer (U_{Ld}) is more commonly used as they are more meaningful and allow for direct comparison of liquid circulation rates in reactors of varying sizes. The superficial liquid velocity is different from the true linear velocity because the liquid flow occupies only a portion of the flow channel—the space occupied by rising gas bubbles reduces the local cross-sectional area available for liquid flow.

The superficial liquid velocity cannot be directly measured and is usually determined from the knowledge of the linear liquid velocity (V_L) and gas holdup. In airlift reactors, U_L and V_L have both riser and downcomer components, yet the riser superficial liquid velocity (U_{Lr}) is the parameter of greatest interest and the one commonly reported in the literature.

The determination of riser and downcomer U_L is often accomplished using a tracer technique or specially calibrated flow meters and mathematical relationships to convert the measurable V_L to U_L. The tracer techniques commonly used to determine V_L are based on determining the time it takes for a given tracer to travel a set distance. For example, a potassium chloride salt tracer and conductivity electrodes are commonly used to measure the time it takes an injection of the salt solution to travel past two fixed locations from which V_L is calculated (Bello et al.,

1984; Chisti, 1989; Jones, 2007; Van't Riet and Tramper, 1991). Knowing V_L, the superficial liquid velocity is determined from Chisti (1989)

$$U_L = (1 - \epsilon)V_L \tag{4.5}$$

While the superficial liquid velocity is a function of riser and downcomer gas holdup, it also influences these holdups. Hence, for a given airlift reactor geometry, the superficial liquid velocity is a function of gas holdup. The superficial liquid velocity can only be changed in this reactor through geometry modifications (which will also affect gas holdup values) or through the use of a throttling device (Popovic and Robinson, 1988).

Local instantaneous liquid velocity measurements in bioreactors that can quantify turbulence statistics are challenging using conventional laser-based techniques because optical access is critical for effective signal acquisition. Laser Doppler anemometry (LDA) and PIV have been used to determine local liquid velocities within multiphase flows. Reviews of LDA and PIV with applications to multiphase flows have appeared in the literature (Boyer et al., 2002; Chaouki et al., 1997; Cheremisinoff, 1986).

Liquid velocity may also be determined using hot film anemometry (Boyer et al., 2002; Magaud et al., 2001). One advantage of this technique is that it is fairly inexpensive, accurate, and relatively easy to implement. However, proper implementation requires a uniform temperature in the bioreactor as well as a limited solid content, and the measurement technique is invasive.

Radioactive particle tracking using neutrally buoyant γ-ray-emitting particles has been used to determine liquid velocity within various bioreactors (Devanathan et al., 1990; Dudukovic, 2000; Khopkar et al., 2005; Luo and Al-Dahhan, 2008). In this technique, a single neutrally buoyant particle that has been tagged to emit γ-rays is inserted into a bioreactor, and γ-ray detectors are located at several locations around the periphery of the bioreactor. With proper signal calibration, the location of the tracer particle is then determined at any instant in time. By following the particle over long time intervals (several hours), mean and fluctuating liquid velocity components can be determined within the multiphase flow.

X-ray particle tracking velocimetry (XPTV) is an X-ray imaging technique where several X-ray absorbing objects (particles) are simultaneously tracked as a function of time (Seeger et al., 2001a). By tracking neutrally buoyant X-ray absorbing particles, Seeger and coworkers (Kertzscher et al., 2004; Seeger et al., 2001b; Seeger et al., 2003) were able to record the 3D liquid velocity field in a slurry bubble column.

4.1.8 Gas Holdup

Gas holdup (or gas fraction or void fraction) is defined as the volumetric fraction occupied by the gas phase in the total volume of a two- or three-phase mixture. It is one of the most important parameters characterizing gas–liquid and gas–liquid–solid hydrodynamics, because it not only gives the volume fraction of

the gas phase but also is needed to estimate the interfacial area and thus the mass transfer rate between the gas and liquid phases (Shah et al., 1982).

Gas holdup can be measured by numerous invasive or noninvasive techniques, which have been reviewed by Kumar et al. (1997) and Boyer et al. (2002), and include changes in total bed expansion upon gassing, pressure drop measurements, dynamic gas disengagement (DGD), and tomographic techniques.

4.1.8.1 Bed Expansion. One of the simplest methods to measure global gas holdup, ϵ, is to measure the bed expansion upon gassing. Assuming that the containment vessel has a constant cross-sectional area:

$$\epsilon = \frac{H - H_0}{H} \tag{4.6}$$

where H is the liquid height at a given gas flow rate and H_0 corresponds to the initial liquid height. This assumes that the bulk liquid velocity is zero. The liquid expansion height is very easy to identify at low gas flow rates, but this identification is more challenging at high gas flow rates due to fluctuations at the free surface caused by bubble disengagement. In industry, this level may be identified with an electronic float to continuously monitor the gas holdup.

4.1.8.2 Pressure Drop Measurements. Pressure drop measurements are one of the most widely used techniques for measuring gas holdup. This method has been used in semibatch bubble columns (Letzel et al., 1999; Lin et al., 1998; Luo et al., 1997; Su and Heindel, 2003, 2004, 2005a; Su et al., 2006; Tang and Heindel, 2005a; Tang and Heindel, 2005b; Tang and Heindel, 2006a; Ueyama et al., 1989; Zahradnik et al., 1997), as well as airlift reactors (Al-Masry, 2001; Hills, 1976; Merchuk and Stein, 1981), and concurrent bubble columns (Kara et al., 1982; Tang and Heindel, 2004, 2005b; Tang and Heindel, 2006a), where there is a net upward liquid flow. With this method, gas holdup is measured using the time-average static pressure drop along the column. The resulting gas holdup is an average value (both temporal and spatial) over the volume of the dispersion between the corresponding pressure taps. In semibatch bubble column operations, Kara et al. (1982) and Tang and Heindel (2005b) showed that the gas holdup values obtained via the pressure difference method matched well (within $\pm 3\%$) with those obtained via direct gas holdup measurement (i.e., estimating gas holdup by measuring the mixture or liquid level before and after DGD).

Assuming 1D isothermal flow, steady-state, constant cross-sectional area, negligible mass transfer between the gas and liquid phases, and constant properties in a cross section, Merchuk and Stein (1981) used a separated flow model of Wallis (1969) for vertical gas–liquid cocurrent flows to determine gas holdup in gas–liquid bubble columns and airlift reactors:

$$\epsilon = \left(1 + \frac{1}{\rho_L g}\frac{dp}{dz}\right) + \frac{4\tau_w}{\rho_L D_c g} + \frac{U_L^2}{g}\frac{1}{(1-\epsilon)^2}\frac{d\epsilon}{dz} \tag{4.7}$$

where ϵ and p are the local gas holdup and pressure at position z, respectively, ρ_L is the liquid density, g is the acceleration due to gravity, D_c is the column inner diameter, U_L is the superficial liquid velocity, and τ_w is the wall shear stress. Hills (1976) obtained a similar expression assuming a pseudo-homogeneous two-phase mixture.

The first term on the right-hand side of Eq. (4.7) accounts for the hydrostatic head, the second term describes wall shear effects, and the third term represents fluid acceleration due to void changes. The contribution of the acceleration term is typically $\sim 1\%$ of the total gas holdup (Merchuk and Stein, 1981). Hills (1976) has shown that in the worst case in a study with superficial liquid and gas velocities as high as 2.7 and 3.5 m/s, respectively, the acceleration term amounted to less than 10% of the total gas holdup. As a result, the acceleration term is usually neglected in practice (Al-Masry, 2001; Hills, 1976; Merchuk and Stein, 1981; Tang and Heindel, 2004; Zahradnik et al., 1997). Without the acceleration term, Eq. (4.7) becomes

$$\epsilon = \left(1 + \frac{1}{\rho_L g}\frac{dp}{dz}\right) + \frac{4\tau_w}{\rho_L D_c g} \tag{4.8}$$

To obtain the average gas holdup $\overline{\epsilon}$ in a column section between two locations separated by a distance $\Delta z = z_2 - z_1 (> 0)$, average both sides of Eq. (4.8) from z_1 to z_2:

$$\frac{1}{\Delta z}\int_{z_1}^{z_2} \epsilon\, dz = \frac{1}{\Delta z}\int_{z_1}^{z_2} \left(1 + \frac{1}{\rho_L g}\frac{dp}{dz}\right) dz + \frac{1}{\Delta z}\int_{z_1}^{z_2} \frac{4\tau_w}{\rho_L D_c g}\, dz \tag{4.9}$$

Thus,

$$\overline{\epsilon}_I = \overline{\epsilon} = \left(1 - \frac{1}{\rho_L g}\frac{\Delta p}{\Delta z}\right) + \frac{4\overline{\tau}_w}{\rho_L D_c g} \tag{4.10}$$

where $\Delta p = p_1 - p_2 (> 0)$ with p_1 and p_2 the pressures at locations z_1 and z_2, respectively, and $\overline{\tau}_w$ represents the average wall shear stress in the same column section. Tang and Heindel (2006a) denoted the gas holdup measurement based on Eq. (4.10) as Method I ($\overline{\epsilon}_I$) where it totally accounts for the wall shear stress effects and provides accurate gas holdup values based on the assumptions above.

The wall shear term in Eq. (4.10) is usually neglected for semibatch bubble columns (Su and Heindel, 2003, 2004, 2005a; Su et al., 2006; Ueyama et al., 1989; Zahradnik et al., 1997). For cocurrent bubble columns and airlift reactors, this term is small at low superficial liquid velocities (e.g., $U_L \sim 1\,\text{cm/s}$ in air–water systems). When the wall shear term is negligible, Eq. (4.10) can be simplified to

$$\overline{\epsilon}_{II} = 1 - \frac{1}{\rho_L g}\frac{\Delta p}{\Delta z} \tag{4.11}$$

The gas holdup measurement based on Eq. (4.11) completely neglects the effects of wall shear stress and has been identified by Tang and Heindel (2006a) as Method II ($\overline{\epsilon}_{II}$).

The wall shear term in Eq. (4.10) increases significantly with increasing superficial liquid (U_L) and gas (U_g) velocities and can amount to $\sim 20\%$ of the total gas holdup (Hills, 1976; Merchuk and Stein, 1981). This is because the wall shear stress $\overline{\tau}_w$ increases significantly with U_L and U_g (Liu, 1997; Magaud et al., 2001; Wallis, 1969). When the liquid phase is highly viscous, the wall shear term can be significant even at superficial liquid velocities on the order of $\sim 2-10\,\text{cm/s}$ (Al-Masry, 2001). Hence, it is necessary to include the wall shear effect in the total gas holdup value for most cocurrent or viscous flow bioreactors.

Calculation of the wall shear term in Eq. (4.10) requires estimation of the two-phase wall shear stress $\overline{\tau}_w$, which is a complex function of gas holdup, superficial gas and liquid velocity, liquid-phase rheological properties, and wall roughness. The models for $\overline{\tau}_w$ in gas–liquid two-phase flows are limited, and most are not general and cannot be extended beyond their restricted conditions (Gharat and Joshi, 1992). The two-phase wall shear stress is even more difficult to estimate when the liquid phase is non-Newtonian (Al-Masry, 2001). Even when a model for $\overline{\tau}_w$ is known, the model is usually a highly nonlinear function of gas holdup (Beyerlein et al., 1985; Herringe and Davis, 1978; Merchuk and Stein, 1981), and one has to solve a nonlinear version of Eq. (4.10) to obtain the gas holdup. This is inconvenient, especially when a large number of data points are acquired.

Tang and Heindel (2006a) have shown that Eq. (4.11) can be modified for concurrent multiphase flow systems to estimate gas holdup based on differential pressure measurements, with

$$\overline{\epsilon}_{III} = 1 - \frac{\Delta p}{\Delta p_{0,U_L}} \tag{4.12}$$

where $\Delta p_{0,U_L}$ is the pressure difference between z_1 and z_2 (the same locations corresponding to Δp) when $U_g = 0$ ($\overline{\epsilon} = 0$) and U_L is the same superficial liquid velocity at which Δp is measured. Equation (4.12) becomes Eq. (4.11) when $U_L = 0$; Tang and Heindel (2006a) define this as Method III ($\overline{\epsilon}_{III}$). As described by Tang and Heindel (2006a), Eq. (4.12) considers an estimation of the wall shear stress effect without modeling the two-phase wall shear stress or solving a nonlinear form of Eq. (4.10). The procedure is as simple as Eq. (4.11) but provides more accurate gas holdup values in cocurrent systems. Hence, using Eq. (4.12), more accurate gas holdup measurements in cocurrent multiphase systems can be made with only pressure measurements, and the calculation is as simple as that required by Eq. (4.11). Furthermore, no knowledge of wall shear stress is required for Eq. (4.12), which is not the case for Eq. (4.10). Tang and Heindel (2006a) have shown that gas holdup in a cocurrent air–water–fiber bubble column was simple and accurate with Eq. (4.12), while error could be significant for selected operational conditions with Eq. (4.11).

4.1.8.3 Dynamic Gas Disengagement (DGD). DGD abruptly stops the aeration process in a gas–liquid or gas–liquid–solid bioreactor and then records the liquid level or pressure at different locations as a function of time (Daly et al., 1992; Deshpande et al., 1995; Fransolet et al., 2005; Patel et al., 1989; Schumpe and

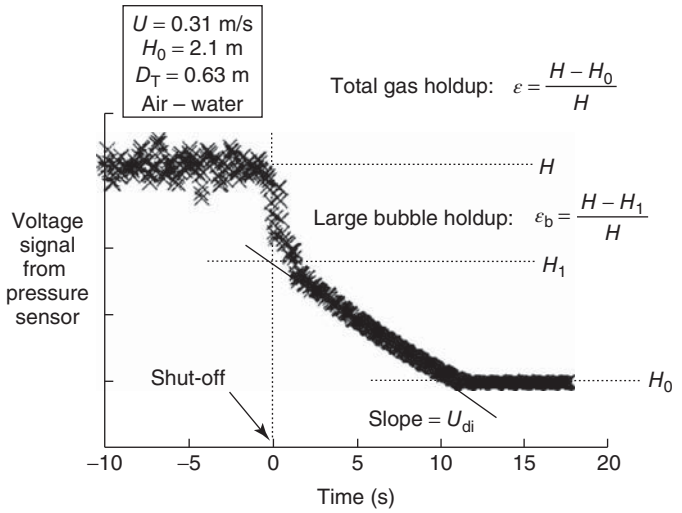

Figure 4.1 Sample data from a dynamic gas disengagement experiment (Krishna and Ellenberger, 1996).

Grund, 1986; Sriram and Mann, 1977). As summarized by Boyer et al. (2002), DGD can be used to record global gas and solid holdup, as well as estimate the holdup make-up according to different bubble size classes.

Krishna and coworkers (Ellenberger and Krishna, 1994; Krishna et al., 1997; Krishna and Ellenberger, 1996; Krishna et al., 2000; Krishna et al., 1999; Vermeer and Krishna, 1981) have employed the DGD technique extensively to determine dense and dilute phase gas holdup values. As shown in Figure 4.1, Krishna and Ellenberger (1996) followed the fluid-level decline as a function of time and identified the dilute phase with the large fast-rising bubbles that disengage first and the dense phase with the small bubbles that disengage after the large bubbles. The demarcation between the dilute and dense phase bubble region was the change in the rate of fluid-level decline. The gas holdup for each phase, as well as the total gas holdup, can be determined from these data. Lee et al. (1999) determined that the disengagement of large bubbles had a significant influence on small bubbles, but the overall gas holdup was similar when measured by differential pressure drop, dispersion height, and PIV.

In general, the DGD technique is fairly straightforward and easy and inexpensive to implement, but has limited applications beyond the laboratory.

4.1.8.4 Tomographic Techniques. Tomography refers to the cross-sectional imaging of a system from either transmission or reflection data collected by illuminating the systems from many different directions (Kak and Slaney, 1988). A variety of tomographic techniques have been developed to determine local time-average phase fractions within an imaging volume. Current tomographic

techniques for phase fraction determination include electrical impedance tomography (Ceccio and George, 1996; George et al., 2000; Tortora et al., 2006), electrical resistance tomography (Fransolet et al., 2005; Toye et al., 2005), electrical capacitance tomography (Du et al., 2006; Gamio et al., 2005; Ismail et al., 2005; Makkawi and Wright, 2002; Makkawi and Wright, 2004; Marashdeh et al., 2008; Pugsley et al., 2003; Warsito and Fan, 2003a, 2003b, 2005), ultrasonic computed tomography (Utomo et al., 2001; Vatanakul et al., 2004; Zheng and Zhang, 2004), gamma densitometry tomography (Dudukovic, 2000; George et al., 2001; Jin et al., 2005; Kumar and Dudukovic, 1996; Kumar et al., 1995; Mudde et al., 2005; Rados et al., 2005; Shaikh and Al-Dahhan, 2005; Tortora et al., 2006; Yin et al., 2002), X-ray computed tomography (Drake and Heindel, 2011, 2012; Ford et al., 2008; Franka and Heindel, 2009; Hubers et al., 2005; Kantzas, 1994; Marchot et al., 2001; Mudde, 2010a, 2010b; Prasser et al., 2005; Schmit and Eldridge, 2004; Schmit et al., 2004), positron emission tomography (Dechsiri et al., 2005), neutron transmission tomography (Harvel et al., 1999; Prasser, 2008), and magnetic resonance imaging (Muller et al., 2008; Powell, 2008; Rees et al., 2006).

As summarized by Marashdeh et al. (2008), tomographic systems are generally classified into soft field or hard field measurement systems. In soft field methods such as electrical capacitance tomography, a change in the measured property (e.g., capacitance) in one location changes the recorded field throughout the entire domain, resulting in a very complex reconstruction process that could produce multiple solutions. Typically for soft field methods, iterative and optimization techniques are utilized to find the most likely reconstruction. In hard field methods such as X-ray tomography, the field lines of the measured property (e.g., X-ray attenuation) remain straight and they are not influenced by property changes outside the line of sight. This makes the reconstruction easier, but, because of the detection systems and source strength, data acquisition is typically slow.

Of the ionizing radiation (hard field) techniques, X-ray imaging is safest because the sources only emit X-rays when they are powered and their energy can be controlled by varying the input voltage (Chaouki et al., 1997; Toye et al., 1996). Toye et al. (1996) also note that X-rays are preferred over γ-rays because the X-rays provide better spatial resolution due to improvements in the X-ray detector technology in recent years. X-ray tubes also provide a smaller spot size when compared to γ-ray sources of equivalent strength, which also provides improved spatial resolution.

Thatte et al. (2004) used a 67 μCi ^{137}Cs source (γ-ray) to measure gas holdup in a transparent, flat-bottomed, 0.57-m-diameter cylindrical tank equipped with a pitched blade downflow turbine or a disk turbine. For both impellers, the average gas holdup was obtained by integrating the local gas holdup and it matched well with the results obtained by visual observations. The reproducibility of the measurements was within $\pm 10\%$. Khopkar et al. (2005) used a ^{137}Cs source with seven NaI detectors to measure gas holdup in a flat-bottomed, 0.2-m-diameter cylindrical tank with a shaft that extended to the vessel bottom. The total scan time was a little over 3 h. Khopkar et al. (2005) noted that CT results were sensitive with respect to the convergence criterion used during data processing. High energy γ-rays, unlike

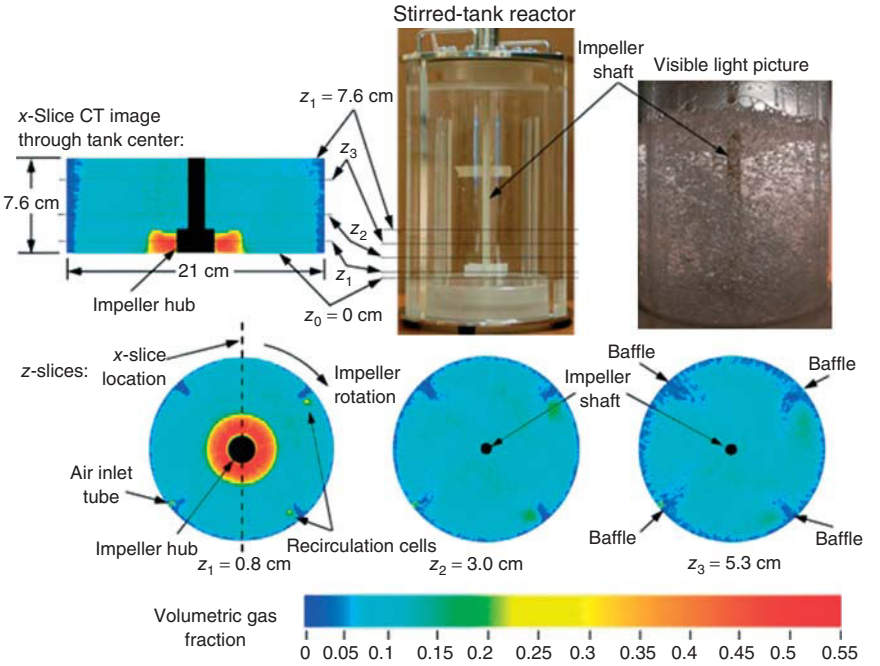

Figure 4.2 Gas holdup in a 21-cm-diameter stirred-tank reactor obtained using X-ray computed tomography imaging.

X-rays, also work on larger tanks because the γ-rays are strong enough to pass through substantial thicknesses of metals, overcoming the reactor wall thickness. For example, Veera et al. (2001) used a ^{137}Cs source to measure gas holdup in a three-phase, 4.9-m-diameter stirred-tank reactor equipped with two impellers.

Ford et al. (2008) used X-ray computed tomography to determine the local time-average gas holdup in a 21-cm-diameter stirred-tank reactor equipped with a Ruston-type turbine. The high resolution of the X-ray system allowed fine details such as recirculation cells behind the baffles to be visualized. An example of such imaging is shown in Figure 4.2, where X-ray CTs are used to determine the local time-average phase distribution anywhere within the imaging volume of the STR. The visible light picture shows a stop-motion image of the gas dispersion but there are so many bubbles that internal details are obscured. The details provided by the CT imaging show a high gas content in the impeller region and recirculation cells behind two of the baffles.

4.1.9 Liquid Holdup

Liquid holdup in a bioreactor can be measured by recording the residence time distribution (RTD) of a tracer that is injected into the bioreactor (Boyer et al., 2002). By following the tracer, the liquid mixing can also be characterized. The most common RTD method involves injecting a small amount of salt tracer and then measuring

the liquid conductivity at two fixed points. The time it takes for the conductivity to have a step change between the two locations is then related to the liquid velocity and holdup. Radioactive particle tracking has also been used as a tracer to determine liquid holdup (Devanathan et al., 1990).

4.1.10 Power Measurements

Stirred-tank bioreactors mechanically agitate the gas–liquid dispersion, and the resulting power draw is an important parameter in these bioreactors. The measured power draw is used to quantify two dimensionless numbers in air-sparged stirred-tank bioreactors, the ungassed and gassed power numbers.

The ungassed power number (N_{po}) represents the ratio of the pressure differences producing flow to the inertial forces of the liquid dispersion and it is analogous to a friction factor or drag coefficient. N_{po} is usually based on the power input by the impeller for agitated vessels and takes the form:

$$N_{po} = \frac{P_o}{\rho N^3 D_i^5} \tag{4.13}$$

where P_o is the impeller power input into the liquid without sparged gas, ρ is the fluid density, N is the impeller speed, and D_i is the impeller diameter. The gassed power number N_{pg} is a dimensionless parameter that provides a measure of the power requirements for the impeller operation in a gas–liquid dispersion. The gassed power number represents the ratio of the pressure differences producing flow to the inertial forces of a gas–liquid dispersion. When gas is introduced into ungassed agitated vessels, the mixing power will drop and is related to a gassed power number defined by

$$N_{pg} = \frac{P_g}{\rho N^3 D_i^5} \tag{4.14}$$

where P_g is the impeller power input into the liquid when gas is sparged into the vessel.

A thorough review of power consumption in stirred-tank reactors has been provided by Ascanio et al. (2004). There are four main techniques for measuring power consumption in stirred-tank bioreactors, including electric measurements, calorimetric measurements, torque measurements, and strain measurement. Although calorimetric and strain techniques can be very accurate, particularly in a laboratory setting, the setup and required controls can be complicated and they are generally not utilized in an industrial setting. Torque measurements through dynamometers or torquemeters can provide accurate measurements of the power imparted to the fluid, provided losses due to no-load conditions are accounted for accurately. In an industrial scale, however, the operating torques can be very large, making these measurement systems impractical.

In an industrial setting, electrical measurement of the power consumption is the simplest and most commonly utilized technique. A wattmeter can be used to determine the total power draw by the motor. This measurement includes the power lost

in the motor, gearbox (if any), and seal (if any), as well as the power imparted to the fluid to create the mixing process. Provided the losses can be accurately quantified, typically by running the system in air and then assuming the losses are constant, electrical measurements can provide the needed information and are commonly monitored in process control applications.

4.2 GAS–LIQUID MASS TRANSFER[1]

In the fermentation industry, usually two fermentation types are distinguished: (i) aerobic fermentation and (ii) anaerobic fermentation as discussed in detail by Bellgardt (2000c). Aerobic fermentations require an oxygen supply, which is normally acquired from the surrounding environmental air. Anaerobic fermentations are conducted in an oxygen-free environment and may utilize carbon monoxide (CO) as the sole carbon source from a gas mixture. In both fermentation types, a general premise is that microorganisms take one component and biologically convert it to another component. Therefore, dissolved O_2 and CO mass transfer rates are very important to determine bioreactor performance. The gas–liquid mass transfer rate is typically measured by recording the dissolved gas content as a function of time. Many methods are available to measure dissolved oxygen content (Gogate and Pandit, 1999b; Linek et al., 1987; Sobotka et al., 1982; Stenberg and Andersson, 1988a; Tobajas and Garcia-Calvo, 2000; Van't Riet, 1979; Wilkin et al., 2001) and they are discussed in Section 4.2.1. Details of a specific method to measure dissolved CO content as a function of time are described in Section 4.2.2 because it is important to synthesis gas fermentation processes (Brown, 2005; Henstra et al., 2007; Kapic et al., 2006; Riggs and Heindel, 2006; Ungerman and Heindel, 2007; Zhu et al., 2008, 2009) and no dissolved CO sensors are currently available.

4.2.1 Dissolved Oxygen Measurement Techniques

There are several techniques used to determine the dissolved oxygen content in a fluid. In practice, five general methods exist: chemical, volumetric, tubing, optodes, and the electrochemical electrode (Carroll, 1991; van Dam-Mieras et al., 1992). This section will discuss these methods and some of their limitations and uses; the emphasis, however, will be on electrochemical electrodes as they are the most common dissolved O_2 sensors.

4.2.1.1 Chemical Method. In the chemical method, a sample is taken from the reactor and the dissolved oxygen concentration is determined off-line using a titrimetric method. The use of chemical methods for systems that have rapidly changing dissolved oxygen content is limited because these methods are laborious, slow, and prone to error if not done correctly.

[1]Material in this section is based on the information summarized by Samuel T. Jones in "Gas-Liquid Mass Transfer in an External Airlift Loop Reactor for Syngas Fermentation," PhD Dissertation, Department of Mechanical Engineering, Iowa State University, 2007. Used with permission.

The most widely used chemical method is the Winkler method (iodometric method) developed by Lajos Winkler in 1888 (Anonymous, 2005), and is considered to be the most reliable and precise titrimetric procedure for dissolved oxygen analysis. This method involves several steps. First, adding a divalent manganese solution followed by a strong alkali to a sample in a gas tight container; this causes the dissolved oxygen to oxidize an equivalent amount of manganese ions to hydroxide. Second, an acid is added to convert the hydroxide to iodine. Third, the solution is titrated with a thiosulfate solution in the presence of a starch indicator to determine the number of iodine molecules in solution. The number of measured iodine molecules is proportional to the number of dissolved oxygen molecules in the original sample as shown by

$$1\,\text{mol}\ O_2 \rightarrow 4\,\text{mol}\ Mn(OH)_3 \rightarrow 2\,\text{mol}\ I_2 \tag{4.15}$$

As with any analytical method, the success of the Winkler method is highly dependent on how the sample is collected and prepared. Care must be taken during all steps of the analysis to ensure that oxygen is neither introduced nor lost from the sample. Furthermore, care must be taken to ensure that the sample is free of contaminants because they may oxidize the iodide or reduce the iodine, which are challenges commonly encountered with fermentation broths. Wilkin et al. (2001) stated that the Winkler method is the most accurate and precise of all methods for determining dissolved oxygen concentrations, and that it is also the most challenging technique to master and the most time consuming.

Other chemical methods such as the NADH oxidation and phenylhydrazine oxidation have been employed to determine dissolved oxygen content (van Dam-Mieras et al., 1992), but are not frequently used.

4.2.1.2 Volumetric Method. The volumetric method is simple and robust in principle, but rather inaccurate in practice. This method relies on the conversion of dissolved oxygen to carbon dioxide which is then driven out of solution. As the carbon dioxide is driven out of solution, it is collected and its volume is determined at a known pressure and temperature. Then, using the ideal gas law and an elemental balance for the oxygen to carbon dioxide reaction, the oxygen concentration is determined. While simple in theory and nearly unaffected by other compounds that might be in the sample, this method, similar to the chemical method, is slow and lacks the sensitivity needed for dynamic biological applications (van Dam-Mieras et al., 1992).

4.2.1.3 Tubing Method. The tubing method consists of using a very small-diameter thin-walled tube of semi-permeable material that is immersed in a fermentation broth (Turner and White, 1999; van Dam-Mieras et al., 1992). A slow stream of oxygen-free carrier gas is pumped through the immersed tube and allowed to absorb oxygen from the fermentation broth by diffusion. The oxygen concentration in the exit gas stream is then measured using a gas analyzer or electrode. This method is strongly influenced by the tubing type, length, diameter,

carrier gas flow rate, wall thickness, temperature, and the mixing characteristics within the reactor vessel. Owing to the many factors that may influence the operation of this method, extensive calibration is required. The tubing method is also very slow and has been shown to have response times of 2–10 min (Turner and White, 1999). However, despite the long response times and the need for extensive calibration, this method can be very accurate, robust, and can withstand repeated sterilization cycles.

4.2.1.4 Optode Method. A photometric transducer or optode can be used to measure gaseous and dissolved oxygen concentrations (Koeneke et al., 1999). Many types of optodes exist, of these the fluorescence quenching optode is most widely used for oxygen measurements (Turner and White, 1999).

Optodes for oxygen sensing are constructed using an immobilized fluorophore (a special dye) attached directly to the end of an optic fiber. When excited by a reference light wave, the fluorophore will emit another light wave having a different wavelength with an intensity that depends on the quencher concentration. Thus, when the quencher is oxygen, the intensity of the emitted light is proportional to the dissolved oxygen concentration.

These sensors can be used in very harsh environments, do not consume oxygen, are very small, are very sensitive to oxygen concentration changes, and are not prone to response time issues common to other methods (Glazer et al., 2004; Koeneke et al., 1999; Kohls and Scheper, 2000; Terasaka et al., 1998; Turner and White, 1999). However, a few drawbacks such as ambient light interactions and photobleaching are issues that must be addressed before their use is widespread.

4.2.1.5 Electrochemical Electrode Method. Membrane-coated dissolved oxygen electrodes were developed in the 1950s and have become one of the most important process instruments for aerobic fermentations (van Dam-Mieras et al., 1992). Normally, the membrane used with these electrodes is only gas permeable and impermeable to most ions such as those used in the electrolyte solution, thus these electrodes do not disturb the biological process. For this reason, and the fact that dissolved oxygen electrodes are relatively easy to use, they are very popular and widely used in industry. Today nearly all oxygen electrodes can be classified as either polarographic or galvanic.

Polarographic or galvanic electrodes are based on the reduction of oxygen at the cathode, which is negatively polarized with respect to the anode. While these electrodes are similar in construction and operation, the main difference between the two is the source of the needed polarization voltage. Polarographic electrodes are typically charged with a negative voltage of 0.75 V by an external source, while galvanic electrodes utilize a negative 0.75-V potential created by the use of dissimilar metals.

It is important to note that both the polarographic and galvanic electrodes measure the oxygen tension of the medium in which they are placed (Doran, 2013). So when an electrode is placed in a liquid, it does not measure dissolved oxygen, but rather the dissolved oxygen partial pressure, which is proportional to oxygen

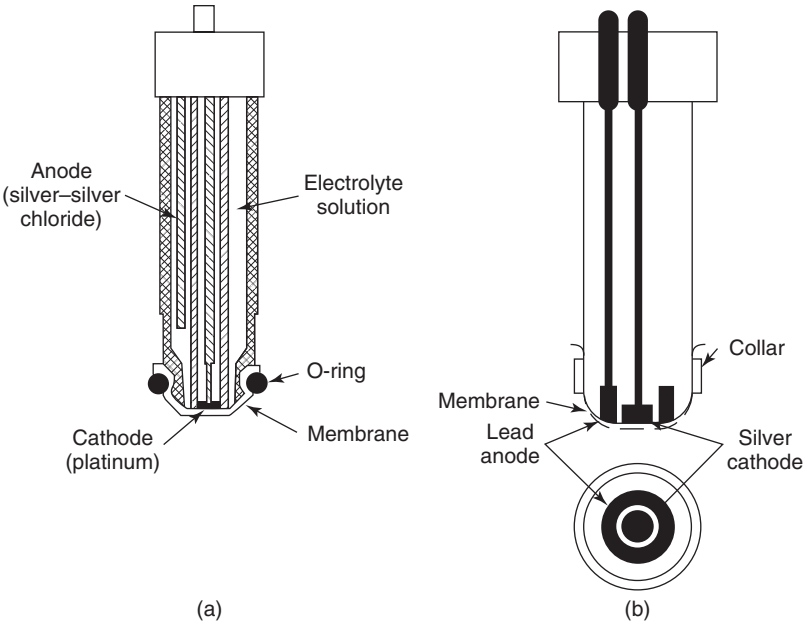

Figure 4.3 Schematics showing the typically construction of (a) polarographic and (b) galvanic electrodes. Adapted from Linek (1988).

tension in the fluid. It is necessary to know the oxygen solubility, pressure, and temperature of the fluid medium in order to determine the exact dissolved oxygen concentration.

Polarographic Electrodes. Polarographic electrodes usually contain a platinum or gold cathode, a silver/silver chloride anode, and a potassium chloride electrolyte. Figure 4.3a shows a schematic representation of a polarographic electrode. When the anode of the electrode is polarized by an external power supply, the following reactions take place at the surface of the electrode (Linek et al., 1985; Turner and White, 1999; van Dam-Mieras et al., 1992):

$$\begin{aligned} \text{cathode}: \quad & O_2 + 2H_2O + e^- \rightarrow H_2O_2 + 2OH^- \\ & H_2O_2 + 2e^- \rightarrow 2OH^- \\ \text{anode}: \quad & Ag + Cl^- \rightarrow AgCl + e^- \\ \text{overall}: \quad & 4Ag + O_2 + 2H_2O + 4Cl^- \rightarrow 4AgCl + 4OH^- \end{aligned} \tag{4.16}$$

The potassium chloride electrolyte solution between the membrane and probe tip provides the chloride ions needed for the above reactions. Since chloride ions are consumed over time with this type of probe, it is necessary to periodically replace

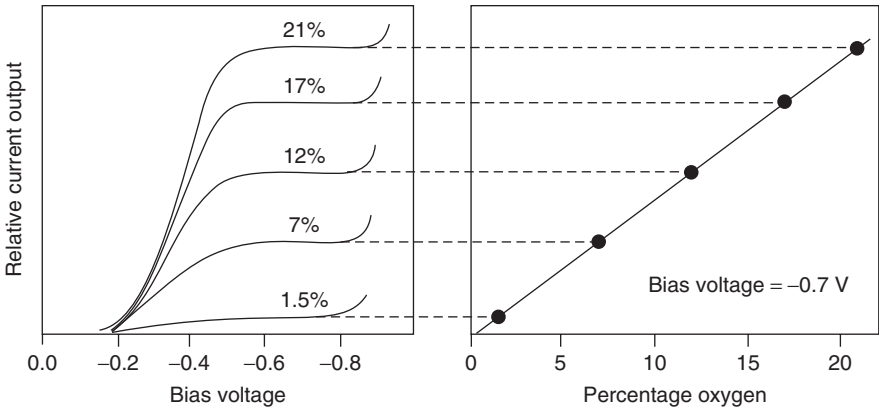

Figure 4.4 Typical polarographic electrode polarogram. Adapted from Lee and Tsao (1979).

the electrolyte solution. Owing to the reactions that take place at the electrode surface, a voltage-dependent current is created that can be related to the oxygen partial pressure as shown in the polarogram (current vs voltage diagram) in Figure 4.4. The rate at which the current-producing reaction takes place at the electrode surface in the plateau region shown in Figure 4.4 is limited by the diffusion rate of dissolved oxygen through the membrane and electrolyte as schematically represented in Figure 4.5 (Linek, 1988; Linek et al., 1985; van Dam-Mieras et al., 1992). Since these reactions are very quick, the diffusion rate is a function of the bulk fluid oxygen concentration. As shown in Figure 4.4, when the correct polarization voltage is selected for a particular electrode, the current output is linear with respect to dissolved oxygen concentration. Care must be taken to ensure that the voltage is not too high to prevent the formation of hydrogen peroxide due to water electrolysis as this will increase the current generation. On the other hand, if the voltage is too low, the current response will be nonlinear. Care must also be taken to ensure that the reaction at the electrode is sufficiently fast to prevent the built up of hydrogen peroxide that may promote hydrogen peroxide diffusion from the electrode tip. If hydrogen peroxide diffuses away, the electrode reaction stoichiometry will be altered. Likewise, it has been shown that the accumulation of OH^- ions also retards the probe reaction rates (Linek et al., 1985). Thus, it can be concluded that a careful balance must be achieved to ensure proper electrode operation; however, on a positive note, this balance is relatively easy to achieve and maintain in practice.

Galvanic Probes. In contrast to the polarographic electrode, a galvanic probe utilizes an anode of zinc, lead, or cadmium and a cathode of silver or gold, where a silver cathode and lead anode are the most common (Linek et al., 1985). Figure 4.3b shows a schematic representation of a typical galvanic probe. The electrochemical reactions that take place at the probe surface are as follows (Linek et al., 1985; Turner and White, 1999; van Dam-Mieras et al., 1992):

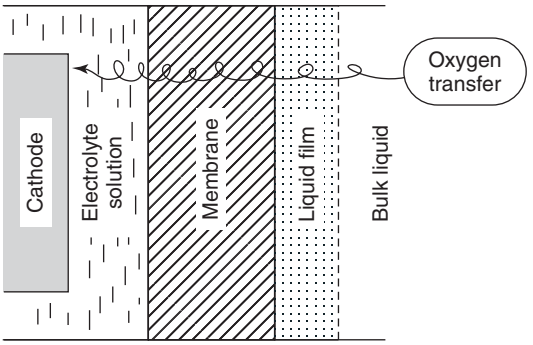

Figure 4.5 The typical oxygen transport path encountered at an electrode tip.

$$\begin{aligned} \text{cathode}: \quad & O_2 + 2H_2O + 4e^- \rightarrow 4OH^- \\ \text{anode}: \quad & Pb \rightarrow Pb^{2+} + 2e^- \\ \text{overall}: \quad & 2Pb + O_2 + 2H_2O \rightarrow 2Pb(OH)_2 \end{aligned} \tag{4.17}$$

Similar to the polarographic probe, the galvanic probe is constrained by the rate-limiting step of oxygen diffusion across the probe membrane. Thus, the current output of the probe is linearly related to the dissolved oxygen concentration in the bulk fluid.

Electrochemical Electrode Time Constant. Despite their fundamental differences, both electrochemical electrodes presented earlier operate on the same basic principles, where the electrode behavior can be predicted using a simplified electrode model with the following assumptions (Lee and Tsao, 1979):

1. The cathode is well polished and the membrane is placed over the cathode surface to minimize the thickness of the electrolyte layer, allowing the electrolyte layer to be neglected in the mathematical model.
2. The liquid around the probe is well mixed so that the oxygen partial pressure at the membrane surface is the same as in the bulk fluid.
3. The electrochemical reaction at the surface of the electrode is much faster than oxygen diffusion through the membrane.
4. Oxygen diffusion occurs only in one direction, perpendicular to the probe.

These assumptions led to the development of the so-called one-layer model (Aiba et al., 1968; Lee and Tsao, 1979). A schematic representation of the one-layer model is shown in Figure 4.6a where oxygen diffusion to the electrode surface is only a function of the membrane layer. Under steady-state conditions for the

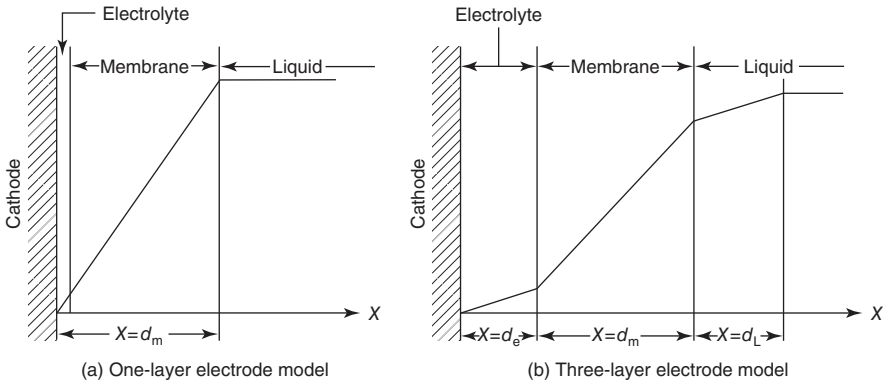

Figure 4.6 One- and three-layer electrode models used to estimate electrode time constants. Adapted from Linek (1988).

above-mentioned simplifications, Fick's first law describes oxygen diffusion from the bulk fluid to the membrane surface, showing that the electrode current output is linearly related to partial pressure of the bulk liquid oxygen. However, in application, the above-mentioned oversimplifications can rarely be used.

Although the one-layer model is an oversimplification of actual conditions, its application to the case where the oxygen partial pressure is allowed to change with time illustrates how electrode properties affect transient dissolved oxygen measurements. Fick's second law is needed to describe the unsteady-state diffusion in the membrane, and shows that the diffusion coefficient of the membrane directly determines how fast an electrode will respond to a step change in the oxygen partial pressure (Aiba et al., 1968; Lee and Tsao, 1979; Sobotka et al., 1982). Lee and Tsao (1979) showed mathematically that the electrode response time, for the one-layer model, depends on the electrode time constant defined as

$$\tau_e = \frac{\pi^2 D_m}{d_m^2} \tag{4.18}$$

where D_m is the membrane diffusion coefficient and d_m is the membrane thickness. A large τ_e results in a fast probe response, which means that either the membrane is very thin or it has a high D_m. However, a small τ_e indicates that the membrane is impermeable to oxygen or that the membrane is too thick. Since electrode stability relies on membrane-controlled diffusion, a compromise between electrode response and stability is required.

As stated earlier, the one-layer model is an oversimplification of actual conditions typically observed, and hence, a three-layer model is typically employed. This model accounts for the effects of the electrolyte and the stagnant boundary layer as shown in Figure 4.6b (Aiba et al., 1968; Lee and Tsao, 1979; Sobotka et al., 1982). While the three-layer model is more suited to quantifying the electrode response to transient conditions, it only provides the foundation for determining the electrode

response constant due to the many factors, as listed in the literature, that may affect it. Electrode design aspects such as membrane type, membrane thickness, cathode surface area, electrolyte, and electrode style all profoundly affect the behavior of the electrode response to oxygen partial pressure. Likewise, bulk fluid properties such as fluid type, viscosity, temperature, total pressure, oxygen partial pressure, fluid velocity, and solid loading can also affect electrode dynamics.

Electrochemical Electrode Response Time (τ_e). Owing to the complexity involved in estimating the probe time constant, most investigators opt to measure the electrode response time to a step change in the oxygen partial pressure. Typically, the electrode response time is defined as the time it takes the electrode to indicate 63% of the total change in dissolved oxygen concentration (Doran, 2013; Sobotka et al., 1982; Tribe et al., 1995; Vardar and Lilly, 1982). There are several experimental procedures described in the literature for obtaining τ_e when the probe is exposed to a stepwise concentration change (Linek et al., 1985) and these procedures are summarized below.

Procedure 1. The electrode is placed at the exit of a three-way valve and the interchange of fluids having different oxygen concentrations takes place when the valve is turned.

Procedure 2. The electrode is placed in a tube and the concentration change is produced by starting and stopping the flow of liquid saturated with air. While the flow of liquid is stopped, the concentration of oxygen in the liquid near the electrode decreases due to the chemical reaction at the electrode. The decrease in concentration will continue until nearly all the oxygen near the electrode is consumed. When this near-steady-state condition is reached, liquid flow is restarted causing a jump in the oxygen concentration near the electrode surface. This method is limited for use with electrodes that have a large cathode (i.e., ones that consume oxygen rapidly).

Procedure 3. The electrode is transferred between two vessels having liquids of different oxygen concentrations that are well mixed and thermostatically controlled (this may be the most popular).

Procedure 4. The electrode is transferred from air to a sulfite solution by inclining a vessel such that the probe, initially in air, is immersed in the sulfite solution.

Procedure 5. The electrode is rapidly transferred from a pure nitrogen environment to a vessel containing a liquid saturated with air. The liquid and hydrodynamic conditions in the test vessel should be the same as those in which the electrode will be used after calibration.

Procedure 6. The electrode is placed in a closed vessel containing a liquid saturated with oxygen and a stirrer. The stepwise concentration change is then facilitated by introducing a compound that immediately consumes all of the dissolved oxygen.

Regardless of the procedure used to find τ_e, care must be taken to ensure that the hydrodynamic conditions around the electrode during the response time test closely resemble those of the process in which the probe will be used, and that the step change is as rapid as possible.

To achieve reasonably accurate overall mass transfer values, a τ_e much smaller than $1/k_L a$ is recommended (Tribe et al., 1995; Van't Riet and Tramper, 1991) as problems occur when this is not the case. In practice, there are three gas–liquid mass transfer conditions of interest (Gaddis, 1999):

1. $\tau_e \ll 1/k_L a$. In this range, the response time of the electrode is much smaller than the dynamic oxygen concentration change in the reactor and the electrode is suitable for monitoring changes in oxygen concentration with a small error.
2. $\tau_e \approx 1/k_L a$. In this range, the response time is of the same order of magnitude as the reactor response time and considerable errors may be encountered when calculating the overall mass transfer coefficient. However, since this case is commonly encountered, models have been developed to account for this error.
3. $\tau_e \gg 1/k_L a$. In this range, the response time is much larger than that of the reactor and the use of electrodes to monitor changes in oxygen concentration is not recommended.

Electrochemical Electrode Response Models. Most oxygen-measuring electrodes used in biological processes have response times that range from 3 to 100 s (Gaddis, 1999; Van't Riet and Tramper, 1991), which may result in the need to correct oxygen concentration data depending on the reactor dynamics. Many models have been developed to correct for τ_e and are discussed in more detail in the literature (Chang et al., 1989; Chisti, 1989; Freitas and Teixeira, 2001; Gaddis, 1999; Kim and Chang, 1989; Lee and Luk, 1983; Lee and Tsao, 1979; Linek, 1988; Linek et al., 1981; Linek et al., 1991a; Linek et al., 1979, 1984, 1989; Linek et al., 1992; Linek et al., 1985; Lopez et al., 2006; Ruchti et al., 1981; Sobotka et al., 1982; Tobajas and Garcia-Calvo, 2000; Tribe et al., 1995; Van't Riet and Tramper, 1991; Vardar and Lilly, 1982). Lee and Luk (1983) and Sobotka et al. (1982) provide a good review of these model corrections. A selection of these models is presented below starting with the simplest and finishing with a few of the more popular complex models.

Models that Neglect the Electrode Dynamic Response. Van't Riet (1979) and Gaddis (1999) suggest that if $\tau_e < 3$ s, the overall mass transfer coefficient can be accurately measured without model correction. Hence, assuming ideal mixing and insignificant gas-phase concentration changes, the overall mass transfer coefficient may be calculated from

$$\frac{C^* - C_L}{C^* - C_0} = \exp(-k_L a \cdot t) \tag{4.19}$$

where C^* is the gas–liquid interface equilibrium molar concentration, C_L is the liquid-phase molar concentration, and C_0 is the steady-state molar concentration at

$t = 0$. Van't Riet (1979) cautioned that considerable corrections have to be made to coefficients calculated using this method if the gas residence time in the reactor is much greater than $1/k_L a$. These corrections were reported to greatly reduce the accuracy of Eq. (4.19). Linek et al. (1991b, 1987) also reported that the use of this model to relate experimental data to overall mass transfer coefficients would lead to an underestimation of $k_L a$ for air systems in which nitrogen transport is neglected, and that this model is really only sufficient for steady-state signals and marginally acceptable in the extreme case when oxygen concentration changes are much slower than τ_e.

Models Considering Membrane Diffusion. The following model has been used when assuming that the electrode response is a first-order lag function, the liquid and gas phases are perfectly mixed, there is negligible nitrogen diffusion, and the interfacial area and oxygen concentration in the gas phase are constant (Blazej et al., 2004a; Chisti, 1989; Freitas and Teixeira, 2001; Fuchs et al., 1971):

$$\frac{C^* - C_L}{C^* - C_0} = \frac{(e^{-k_L a \cdot t} - k_L a \cdot \tau_e \cdot e^{-t/\tau_e})}{(1 - k_L a \cdot \tau_e)} \tag{4.20}$$

In general, τ_e represents all the diffusional properties of the measurement system in the model (Sobotka et al., 1982). As with the previous model, the adequacy of this model depends on the ratio of τ_e and $1/k_L a$. When τ_e is much less than $1/k_L a$, Eq. (4.20) reduces to Eq. (4.19), and the resulting error associated with neglecting τ_e has been reported to be small (Gaddis, 1999; Merchuk et al., 1990; Nakanoh and Yoshida, 1983). This model is again subject to the same errors and limitations as the previous model, especially if nitrogen transport is neglected.

Jones and Heindel (2007) compared the $k_L a$ values calculated from dissolved oxygen measurements using the models described in Eqs (4.19) and (4.20). As shown in Figure 4.7a, when $\tau_e \ll 1/k_L a$, there is no real difference in how Eq. (4.19) and Eq. (4.20) represent the experimental data. When $\tau_e < 1/k_L a$ (Figure 4.7b), Eqs (4.19) and (4.20) begin to show a difference in how they model the experimental data. When $\tau_e \approx 1/k_L a$ (Figure 4.7c), Eq. (4.20) provides a better model of the experimental data. Table 4.1 summarizes the calculated $k_L a$ values using these two models for these three test conditions.

Linek et al. (1985) have suggested a different approach using a very sophisticated model in which the electrode time constant plays a major role. Rather than solving the model explicitly to determine $k_L a$, they suggested that since the electrode signal is most distorted during the initial response, one could find $k_L a$ by removing the distorted portion of the signal and using the remaining response and Eq. (4.19) to find $k_L a$. The proper application of this technique is discussed in detail in the literature (Linek, 1972; Linek et al., 1985).

If the system being studied can be assumed to have a perfectly mixed liquid phase and a constant oxygen concentration in the gas phase, Tobajas and

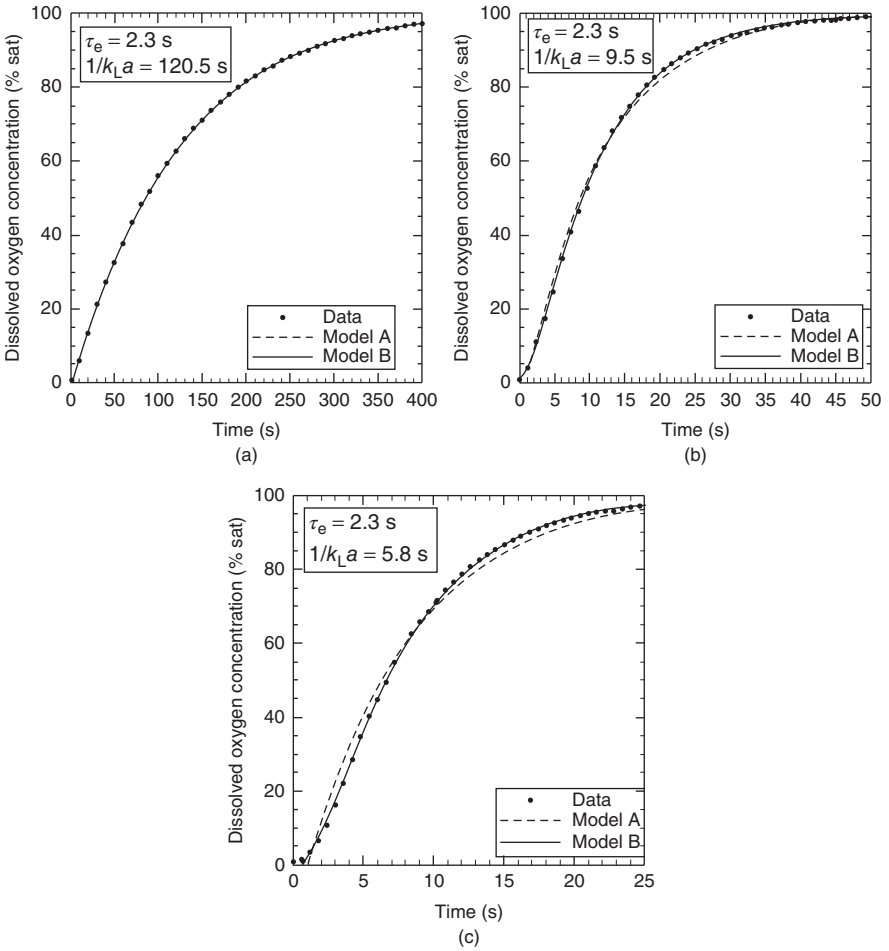

Figure 4.7 Comparison of the experimental data to Eq. (4.19) (Model A) and Eq. (4.20) (Model B) for (a) $\tau_e \ll 1/k_La$, (b) $\tau_e < 1/k_La$, and (c) $\tau_e \approx 1/k_La$. Adapted from Jones and Heindel (2007).

Garcia-Calvo (2000) suggested that the following model be used to determine k_La:

$$\frac{C^* - C_L}{C^* - C_0} = \frac{1}{1-m}\left[1 - \exp\left(\frac{-m \cdot t}{\tau_e}\right) - m\left(1 - \exp\left(\frac{-t}{\tau_e}\right)\right)\right] \tag{4.21}$$

where m is defined as

$$m = \frac{k_La \cdot \tau_e}{1-\epsilon} \tag{4.22}$$

and ϵ is the total gas holdup.

TABLE 4.1 Equations (4.19) and (4.20) k_La Estimates for the Three Experimental Conditions where τ_e Ranges from $\tau_e \ll 1/k_La$ to $\tau_e \approx 1/k_La$

	Time Constant (τ_e) (s)	$1/k_La$(s)	k_La from Eq. (4.19) (s^{-1})	k_La from Eq. (4.20) (s^{-1})	Difference (%)
$\tau_e \ll 1/k_La$ (Figure 4.7a)	2.3	120.5	0.0083	0.0083	0.1
$\tau_e < 1/k_La$ (Figure 4.7b)	2.3	9.5	0.0919	0.1052	12.6
$\tau_e \approx 1/k_La$ (Figure 4.7c)	2.3	5.8	0.1311	0.1711	23.4

Adapted from Jones and Heindel (2007).

Models Considering Membrane Diffusion and Time Delay. Lopez et al. (2006) and Vardar and Lilly (1982) suggested that when the electrode dynamic response was first order with a time delay, the following model can be used to correct the dissolved oxygen concentration data:

$$C_L(t - \tau_d) = C_E(t) + \tau_e \frac{dC_E(t)}{dt} \tag{4.23}$$

where $C_E(t)$ is the recorded electrode concentration at time t and τ_d is the dead time. The dead time represents the time from the beginning of the concentration step change to the beginning of the change in the electrode signal. Once the concentration data (C_L) is corrected for the electrode dynamic response, Eq. (4.19) can be used to determine k_La.

Sobotka et al. (1982), however, suggested that the following complex relationship be used to find k_La using the electrode data:

$$\frac{C^* - C_L}{C^* - C_0} = \frac{1}{(1 - k_La \cdot \tau_e)} \left[\frac{1}{(1 - k_La \cdot \tau_d)} e^{-k_La \cdot t} - \frac{k_La \cdot \tau_e^2}{(\tau_e - \tau_d)} e^{-t/\tau_e} + \left((1 - k_La \cdot \tau_e) - \frac{1}{(1 - k_La \cdot \tau_d)} + \frac{k_La \cdot \tau_e^2}{(\tau_e - \tau_d)} \right) e^{-t/\tau_d} \right] \tag{4.24}$$

When $\tau_d \ll \tau_e$, Eq. (4.24) reduces to Eq. (4.20), and when $\tau_d \ll \tau_e \ll 1/k_La$, Eq. (4.24) reduces to Eq. (4.19).

Models Considering Membrane and Liquid Film Diffusion. Models considering membrane and liquid film diffusion are quite complex as they are of second order in nature, and the solution to these models require numerical analysis or a method of moments due to their complexity (Sobotka et al., 1982). Linek et al. (1985), Ruchti et al. (1981), and Dang et al. (1977) suggested that while these models are more complex and involved, their solutions are much superior to any first-order model. However, due to their complexity, they are typically not used and the reader is referred to the literature for more information concerning these models.

Models Considering a Membrane Diffusion Model. Sobotka et al. (1982) claimed that the empirical time delay models previously described do not properly consider the physical nature of the electrode response. Instead, they insisted that models based on Fick's second law are superior and encouraged their use to more accurately model system dynamics. Sobotka et al. (1982), in their review, presented many of the different diffusional models that have been developed and discussed their usefulness.

Summary of Electrochemical Electrode Response Models. As has been shown by a review of just a few of the models presented in the literature, the use of electrochemical electrodes to accurately determine $k_L a$ can be complicated due to internal instrument dynamics as well as system dynamics. Hence, as implied by Tribe et al. (1995) and others (Keitel and Onken, 1981; Lee and Luk, 1983; Lee and Tsao, 1979; Linek et al., 1985; Sobotka et al., 1982), the proper selection of an electrode and method for evaluating its signal will greatly impact the accuracy of the experimental results.

4.2.2 Dissolved Carbon Monoxide Measurements

The determination of dissolved carbon monoxide concentrations and CO–liquid mass transfer rates is important to synthesis gas fermentation, where carbonaceous fuels, such as biomass, are gasified into flammable gas mixtures, sometimes known as synthesis gas or syngas, consisting of carbon monoxide (CO), carbon dioxide (CO_2), hydrogen (H_2), methane (CH_4), nitrogen (N_2), and smaller quantities of higher hydrocarbons and contaminants (Bridgwater, 1995). Syngas fermentation utilizes CO and H_2 as growth substrates to anaerobically produce a variety of fuels and chemicals, including methane, acetic acid, butyric acid, ethanol, and butanol (Bredwell et al., 1999). One potential bottleneck to the commercialization of syngas fermentation is the mass transfer limitations within gas–liquid bioreactors (Bredwell et al., 1999; Worden et al., 1997); this is a result of the low solubility of the major syngas components (CO and H_2) in the aqueous fermentation broth when it contains a high cell concentration. If the cell concentration is too low, the system yield will be low and mass transfer will be kinetically limited (Vega et al., 1989). To improve the CO–liquid mass transfer rates, actual dissolved CO concentrations and mass transfer rates must be determined, but there are no dissolved CO measurement probes like those used for dissolved O_2.

Dissolved CO concentrations can be determined using a myoglobin-protein assay as described by Kundu et al. (2003). This method was used by Riggs and Heindel (2006), Kapic et al. (2006), and Ungerman and Heindel (2007) to determine pure CO concentrations in water to assess CO–water mass transfer rates for various operating conditions. A summary of the bioassay measurement technique is provided next and further details can be found in Jones (2007).

4.2.2.1 Bioassay Overview. In the bioassay, a liquid sample is taken from the bioreactor and the dissolved carbon monoxide concentration is determined off-line using a protein-binding method. The use of the bioassay is limited, much like the

chemical methods for determining dissolved oxygen concentrations, because the method is laborious, slow, and prone to error if done incorrectly.

The method involves several steps that include, first, preparing a myoglobin protein solution that is free of dissolved oxygen and carbon monoxide. Second, the myoglobin protein solution is added to the withdrawn liquid sample in a gas tight container; this causes the dissolved carbon monoxide to bind to the myoglobin. Third, the change in the absorbance spectrum (400–700 nm) of the sample is measured after the addition of the protein solution. The change in the absorbance spectrum is proportional to the number of dissolved carbon monoxide molecules in the original sample.

As with any analytical method, the success of the bioassay is highly dependent on how the samples are collected and prepared. Care must be taken during all of the steps of the analysis to ensure that oxygen is not allowed to bind with myoglobin and that all measurements are carried out very carefully. Furthermore, attention to sample acquisition must be taken to ensure that small gas bubbles are not entrained in the samples when they are collected as this leads to errors (Kapic, 2005). Although difficult to use, the bioassay technique, once mastered, may be successfully used to accurately measure dissolved carbon monoxide concentrations.

4.2.2.2 Needed Materials. Jones (2007) used various materials to complete the dissolved CO measurements using the bioassay technique. An Ocean Optics ChemUSB2-VIS-NIR spectrophotometer was used to measure the absorbance spectrum in the liquid sample. Figure 4.8 displays several syringes and a sample cuvette that were used in the measurements. Samples were prepared and scanned in 1.5-ml polystyrene disposable cuvettes that have a 10-mm path length. These cuvettes are usable for wavelengths ranging from 340 to 800 nm and have polystyrene caps to reduce contamination. Syringes used for liquid sample collection were gastight high performance 10-μ*l* syringes from Hamilton (model 1701); the needles were cemented into this type of syringe by the manufacturer to minimize oxygen contamination. Several other syringes shown in Figure 4.8 are also used in the bioassay.

Myoglobin used in the dissolved carbon monoxide concentration measurements by Jones (2007) was purchased from Sigma-Aldrich (product number M1882) and derived from horse heart. The myoglobin comes as an essentially salt-free lyophilized powder of at least 90% pure that must be stored at minus 20 °C. One gram of the myoglobin powder is dissolved in approximately 25 ml of 0.1 M potassium phosphate at pH 7.0 buffer solution prepared by adding 3.3 g of dibasic potassium phosphate powder and 11.0 g of monobasic potassium phosphate powder to 1 l of deionized water. The final pH of the buffer solution is adjusted to 7.0 with either potassium hydroxide or *o*-phosphoric acid. To increase the shelf life of the myoglobin solution, the solution is run through a dialysis separation process for 24 h and then spun down in a centrifuge to remove impurities. The solution is then separated into 1-ml containers and frozen until needed.

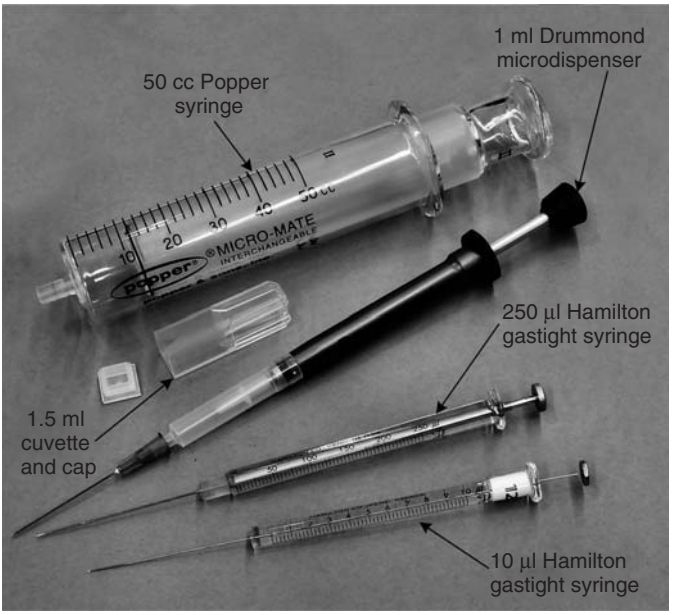

Figure 4.8 Syringes and cuvette used by Jones (2007) in the dissolved CO bioassay.

4.2.2.3 Liquid Sample Collection. Liquid samples were collected by Jones (2007) using 10-µ*l* syringes; he determined that it is best if several syringes are first numbered sequentially and then inserted into the bioreactor through a septum (see, e.g., Figure 4.9). Care must be taken to ensure the syringe tips are all located in close proximity. Prior to introducing carbon monoxide into the bioreactor, a single sample is taken with syringe number 0 to measure the carbon monoxide concentration at time $t = 0$ (assumed to be zero and the sample confirms this). Once the carbon monoxide is introduced into the bioreactor, transient samples are withdrawn at specified time intervals depending on the operating conditions. Once the bioreactor is saturated with CO, three additional samples are taken to determine the steady-state concentration.

4.2.2.4 Identifying the Concentrated Myoglobin Solution Concentration. Prior to testing, the myoglobin solution must be thawed and the myoglobin concentration determined to calibrate the test solution. The goal in preparing the test solution is to obtain a peak absorption value near Abs = 1.5 for a saturated oxygen sample (Figure 4.10). The saturated oxygen peak occurs at 409 nm for myoglobin.

The concentration is determined by putting 1 ml of buffer solution into a cuvette and adding 1 µ*l* of myoglobin protein. The absorbance is measured and more protein is added in 1 µ*l* increments until the peak absorbance is near 1.5.

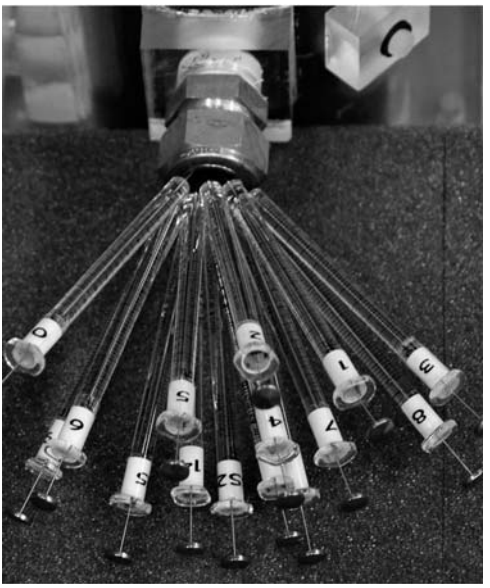

Figure 4.9 Sample syringes inserted into a bioreactor for liquid sample collection.

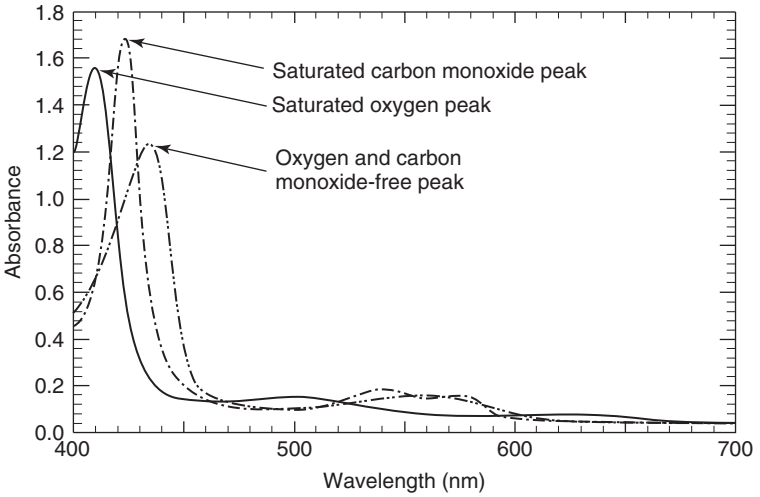

Figure 4.10 Reference absorbance spectrums.

Once the peak absorbance reaches Abs ≈ 1.5, the myoglobin concentration (C_p) and the dilution ratio (DR) are determined from

$$C_p = \frac{\text{Abs}}{\lambda \cdot \epsilon_m} \tag{4.25}$$

$$\text{DR} = \frac{\text{microliters of myoglobin solution}}{\text{milliliters of buffer solution}} \tag{4.26}$$

where Abs is the absorption value, λ is the path length of the cuvette, and ϵ_m is the extinction coefficient. For horse heart myoglobin, ϵ_m is reported to be 188 $\mu M/\text{cm}$ (Antonini and Brunori, 1971).

4.2.2.5 Sample Preparation for Analysis. The test solution used to analyze the liquid samples is prepared just prior to use because the myoglobin solution is temperature sensitive and its exposure to room temperature should be minimized. The test solution is prepared by pipetting 1 ml of buffer solution for every sample being analyzed into the 50-ml syringe. Then, using the previously calculated dilution ratio (Eq. (4.26)), an appropriate amount of myoglobin solution is added to the test solution, and the mixture is gently agitated. A 1 ml sample is set aside in a 1.5-ml cuvette and then placed in the spectrophotometer and scanned to record the "oxy" spectrum, corresponding to the test solution with dissolved oxygen. Finally, a small amount of sodium dithionite (Na_2SO_4) is added to the test solution to neutralize all the dissolved oxygen and the oxygen bonded to the myoglobin.

All measurements are initiated with 1 ml of the test solution being added to empty 1.5-ml cuvettes. A "deoxy" spectrum is determined by scanning a cuvette containing only the test solution; this spectrum corresponds to a sample containing no carbon monoxide. In a similar manner, a "saturated CO" spectrum is found by saturating the solution in one cuvette with an excess amount of carbon monoxide to ensure that all the myoglobin is bound to a carbon monoxide molecule. The resulting spectrum corresponds to the maximum amount of dissolved carbon monoxide that can be detected without increasing the myoglobin concentration in the test solution.

The liquid samples are analyzed after the three reference spectrums have been determined. After 1 ml of test solution has been placed in the cuvette, a 10 μl liquid sample is injected into the cuvette and the cuvette is capped, gently agitated, and then scanned. This process is repeated for each of the acquired liquid samples. The resulting spectra will follow the trend shown in Figure 4.11, where an increase in the amount of dissolved carbon monoxide results in the peaks of the spectra initially shifting down and to the left and then up and to the left. Errors may occur in these measurements because of gas bubbles becoming entrained in the liquid sample when it is drawn; thus, care must be taken to ensure that the syringes are clean and properly located in the sample port.

4.2.2.6 Determining the Dissolved CO Concentration. Dissolved CO concentration in the liquid sample is determined by loading the spectra data files into a data analysis program (i.e., JMP 6.0) to fit the liquid sample spectra between the "deoxy" and "saturated" spectra; effectively interpolating between CO-free and CO-saturated samples. The software package uses a least squares fitting routine that outputs a percent similarity to each of the reference spectra. These output data

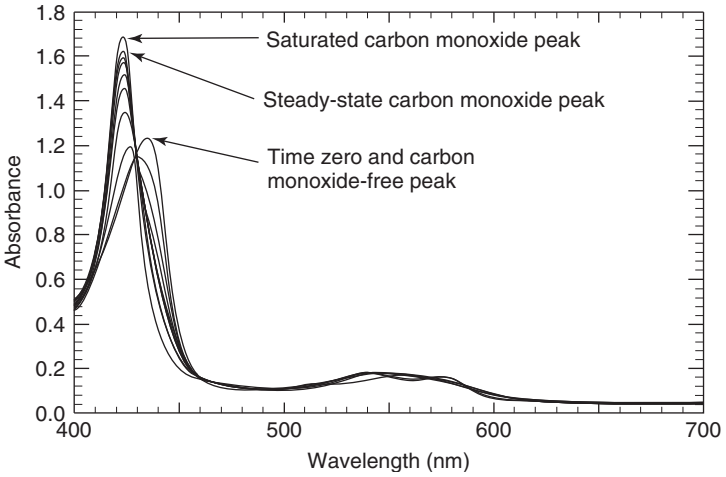

Figure 4.11 Absorbance spectra progression from carbon monoxide free state to a carbon monoxide saturated state.

are then used to determine the carbon monoxide concentration (C_{CO}) in the given liquid sample as a percent of the steady-state concentration using

$$C_{CO} = (C_p)(SS)\left(\frac{Vol_T}{Vol_S}\right) \tag{4.27}$$

where C_p is the myoglobin concentration in the test solution, SS is the percentage of the steady-state concentration exported from the data analysis program, Vol_T is the total liquid volume in the cuvette, and Vol_S is the sample volume of the dissolved carbon monoxide liquid. The CO concentration as a function of time is then used to determine the CO–liquid mass transfer rate using the models in Eq (4.19) or (4.20).

4.2.3 Determining Volumetric Gas–Liquid Mass Transfer Coefficient, $k_L a$

For two-phase gas–liquid systems, it has been shown that the gas transfer rate (GTR) can be described by

$$GTR = \frac{dC_L}{dt} = k_L a(C^* - C_L) = a \cdot J \tag{4.28}$$

where C^* and C_L are the equilibrium gas concentration at the gas–liquid interface and the dissolved gas concentration in the liquid phase, respectively. In bioreactors, dC_L/dt, C^*, and C_L can all be measured directly. However, as stated earlier, k_L and a are not so easily measured, so it is common to report the product of $k_L a$. This product is commonly called the *overall volumetric mass transfer coefficient* and has units of s^{-1}.

The most widely used methods for determining $k_L a$ in bioreactors have been summarized in the literature (Chisti, 1989; Gogate and Pandit, 1999b; Sobotka et al., 1982; Van't Riet and Tramper, 1991); they will be presented later. It is important to note that in using Eq. (4.28), it is assumed that the gas and liquid phases are well mixed so that $k_L a$ can be assumed constant over the entire gas–liquid system. These assumptions, however, are not always applicable to the system being evaluated, and further modeling of the gas–liquid system may be needed.

4.2.3.1 Gas Balance Method. The gas balance method can only be used in a gas-consuming system. Typically, this method is applied to a fermentation run where all the variables except $k_L a$ are measured. The gas concentration and the entering and exiting gas stream flow rates are monitored using a gas analyzer and mass flow meters. Using this information, the gas transfer rate (GTR) can be calculated from (Van't Riet and Tramper, 1991)

$$\text{GTR} = \frac{F_i \cdot C_i - F_o \cdot C_o}{\text{Vol}_L} \tag{4.29}$$

where F is the respective gas flow rate, C is the respective gas concentration, and Vol_L is the liquid volume. Once the GTR is known, $k_L a$ can be calculated using Eq. (4.28).

The gas balance method is claimed to be the most reliable method for determining $k_L a$ (Doran, 2013; Poughon et al., 2003). However, this method requires the precise measurement of the gas inlet and outlet concentrations and flow rates. Since the difference between inlet and outlet conditions is typically very small, the accuracy of this method is determined in large part by the accuracy of the instrumentation (Poughon et al., 2003; van Dam-Mieras et al., 1992). Because of this, very precise instruments are required and the instrumentation cost for this method is often high. Hence, this method is usually justified only when expensive gas-monitoring equipment is also needed for process control.

This method is also limited by the underlying assumption that the gas phase is constant throughout the bioreactor. For large systems where the gas concentration may vary widely from inlet to outlet, gas-phase modeling is required to accurately estimate GTR and $k_L a$ (Van't Riet and Tramper, 1991).

4.2.3.2 Dynamic Method. The dynamic method involves measuring the dissolved gas concentration as a function of time for a step change in the inlet gas concentration. Similar to the gas balance method, this method can be applied to an actual fermentation or it can be applied to systems containing no microorganisms. Owing to its versatility and ease of use, this method is widely used and discussed in the literature (Blanch and Clark, 1997; Chisti, 1989; Doran, 2013; Sobotka et al., 1982; Van't Riet and Tramper, 1991; van Dam-Mieras et al., 1992). As a result, many variations of this method exist of which a selected few are discussed in more detail.

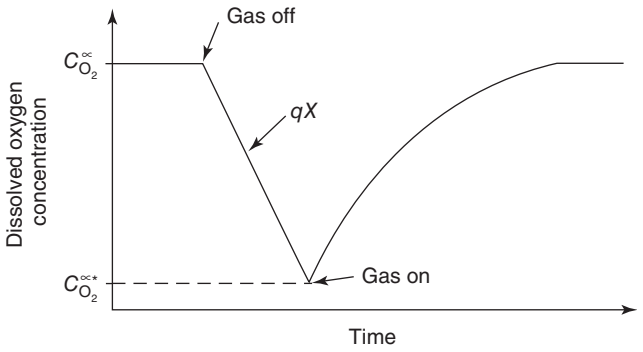

Figure 4.12 Typical dissolved oxygen concentration variation with time for the biological dynamic method. Adapted from Blanch and Clark (1997).

Biological Dynamic Method. The biological dynamic method is applied to actual fermentations using a step change in inlet gas concentration, where the change in dissolved gas concentration in the bulk fluid is recorded. The step change is initiated in one of several ways that will be discussed in more detail later. This method consists of three primary steps. First, the system is brought to an initial steady-state condition. Second, the inlet gas step change is initiated and the change in dissolved gas concentration is recorded. Typically, the dissolved gas concentration is reduced to a point just above the critical gas concentration needed to prevent cell death and/or an irreversible change in cell behavior (Blanch and Clark, 1997). Third, after a period of time, the inlet gas concentration is returned to its original state and the change in gas concentration is recorded as the system moves back to the original steady-state condition. Figure 4.12 illustrates the typical dissolved gas concentration profile obtained using the dynamic method.

The system mass balance for the dynamic method is as follows:

$$\frac{dC_L}{dt} = k_L a(C^* - C_L) - qX \tag{4.30}$$

where qX is the microbial gas consumption rate. If the gas phase disengages quickly from the liquid, then the transport term disappears in the above-mentioned relationship and it reduces to

$$\frac{dC_L}{dt} = -qX \tag{4.31}$$

Equation (4.31) can be used to find qX assuming that the microbial uptake of the gas is unaffected by stopping aeration. The volumetric mass transfer rate $k_L a$ is calculated using the overall system mass balance and does not require previous knowledge of qX, as qX can be replaced in Eq. (4.30) with the following expression (Doran, 2013):

$$qX = k_L a(C^* - C_\infty) \tag{4.32}$$

where C_∞ is the dissolved gas concentration in the liquid at steady state. Equation (4.30) then reduces to the following and can be solved directly for $k_L a$:

$$\frac{dC_L}{dt} = k_L a(C_\infty - C_L) \tag{4.33}$$

The instruments used in obtaining the liquid–gas concentration data for this method depend on the required fermentation gas. For processes that utilize oxygen, typically an oxygen electrode is used, although in rare situations another dissolved oxygen-measuring technique may be used. If an oxygen electrode is used, care must be taken to properly account for the probe dynamics as previously discussed (Chisti, 1989; Van't Riet and Tramper, 1991). For processes that utilize other gases such as hydrogen or carbon monoxide, specialized measuring instruments or techniques must be employed. For example, dissolved carbon monoxide concentration data can be obtained using the bioassay technique discussed in Section 4.2.2.

Blanch and Clark (1997) reported that the biological dynamic method is commonly used in both large- and small-scale equipment, primarily due to the fact that sterilizable oxygen probes permit the finding of $k_L a$ during fermentation without significantly upsetting the system.

Nonbiological Dynamic Method. This method is similar to the biological dynamic method in that it employs the use of an inlet gas concentration step change, though it differs from the previous method as the system either has microorganisms that have been terminated, had cell respiration blocked, or does not have any microorganisms present (van Dam-Mieras et al., 1992). This method is commonly used for systems that are void of microorganisms (Abashar et al., 1998; Sobotka et al., 1982; Van't Riet, 1979).

The nonbiological dynamic method begins by first removing the dissolved gas being studied from the vessel by (i) aerating the system with an inert gas such as nitrogen, (ii) using a vacuum to cause the dissolved gas to come out of solution, or (iii) adding a chemical compound to consume the dissolved gas. Once the dissolved gas has been removed, the system is then aerated and the change in gas concentration is recorded until steady state is reached.

Without cell respiration, the overall mass balance for the biological dynamic method simplifies from Eq. (4.30) to Eq. (4.28). The volumetric mass transfer coefficient $k_L a$ is then evaluated by integrating Eq. (4.28) and plotting $\ln[(C^* - C_L)/(C^* - C_o)]$ as a function of time, where $k_L a$ is the slope of the resulting line, or by curve fitting the data with a nonlinear regression software package.

This method is reported to offer accurate results if the system being studied does not vary significantly from the actual system containing respiring microorganisms (van Dam-Mieras et al., 1992). However, the accuracy of the results obtained using

this method was reported to depend on the procedure used to initiate the concentration step change and electrode dynamics (if a dissolved oxygen electrode is used) (Linek et al., 1993; Linek et al., 1989; Linek and Sinkule, 1990; Linek et al., 1987; Van't Riet and Tramper, 1991).

Variations of the Inlet Step Change. While variations for each of the dynamic methods have been reported in the literature, the variation of greatest importance seems to be in how to initiate the change in the dissolved gas concentration. The remainder of this section will review the most popular techniques used to initiate a step change in the inlet gas concentration.

Gas Off/On or Start-up. The gas off/on technique is used primarily for fermentations that have actively respiring cells. In such fermentation systems, the dynamic method is applied by turning the gas flow off and allowing the cells to deplete the dissolved gas until the critical gas concentration is reached and then the gas is turned back on (e.g., Figure 4.12).

One of the main advantages of using this technique is that the gas–liquid mass transfer is not affected by alternating the gas species, which has been reported to affect the calculation of $k_L a$ values (Linek et al., 1981). Another advantage is the low cost associated with this technique as it requires no additional equipment. However, this method has a couple of limitations that must also be realized. First, this method must be done quite rapidly and with extreme care to ensure that cell respiration is not affected by the change in dissolved gas concentration. Second, when the gas is turned off and then on again, the system hydrodynamics may be altered. Consideration must also be given to the time needed to once again reach steady-state hydrodynamic behavior because if the start-up time approaches or exceeds the length of the experiment, then the method cannot be used for calculating $k_L a$ (Gogate and Pandit, 1999b). For example, in the extreme case when vessels are very large or have a height greater than 1 m, the time to reestablish steady-state gas holdup conditions may be larger than the characteristic $k_L a$, resulting in inaccurate $k_L a$ estimates that are not representative of normal operation (Van't Riet and Tramper, 1991).

Gassing Out or Gassing In. Since dynamic methods are usually quite sensitive to the starting conditions of the experiment, a gas switching technique is used to eliminate hydrodynamic changes. The gassing-out technique is one of the most widely used techniques for the dynamic method when a simulated fermentation broth is used. This technique, as the name implies, begins by aerating with one gas and then switching at $t = 0$ to a second gas. For example, in an air–water system, the system may first be aerated with air until the water is completely saturated, and then aerated with nitrogen to replace the oxygen in solution (Figure 4.13). A wide variety of gas pairs have been used in the application of this technique in the literature, though air–nitrogen is the most common.

Van't Riet and Tramper (1991) reported that when deoxygenation with nitrogen was followed by an aeration switch, the average gas-phase residence time (τ_g) must

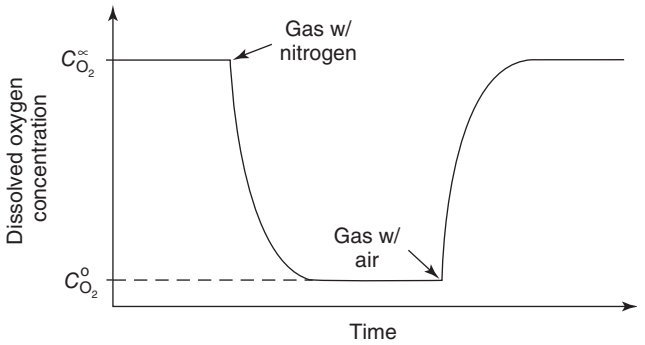

Figure 4.13 Typical dissolved oxygen concentration variation with time for the nonbiological dynamic method. Adapted from Blanch and Clark (1997).

be considered as the gas-phase concentration was no longer constant over the entire test. Van't Riet and Tramper defined τ_g as

$$\tau_g = \frac{H}{U_g}\left(\frac{\epsilon}{1-\epsilon}\right) \tag{4.34}$$

where H is the unaerated liquid height in the vessel, U_g is the superficial gas velocity, and ϵ is the gas holdup. If τ_g is the same order of magnitude as $1/k_La$, then the assumption of a constant gas-phase concentration used to derive Eq. (4.30) is no longer valid (Sobotka et al., 1982). Models to correct for this behavior have been proposed by Dunn and Einsele (1975) and Dang et al. (1977). These models have been reported to be useful only over a narrow range of conditions (Van't Riet and Tramper, 1991). Linek et al. (1981) reported that interphase nitrogen transport may significantly influence k_La estimations. Linek et al. (1993) indicated that errors in k_La estimation due to nitrogen transport can be as high as 25% for large k_La values. However, they also indicated that for low k_La values commonly encountered, the error due to nitrogen transport may be negligible. Stenberg and Andersson (1988a) found that the change from nitrogen to air had a small but significant effect on k_La measurements, but this error was smaller than other observed experimental errors.

Lopez et al. (2006) and Chang et al. (1989) suggested that a gas pair of air and oxygen-enriched air be used to improve this technique by eliminating the need for pure nitrogen. Lopez et al. (2006) showed that k_La values measured with this technique closely matched those obtained for the gas off/on technique. Kim and Chang (1989) indicated that the difference in inlet oxygen concentrations for this technique must be at least 20% in order to minimize errors.

Pressure Step. Another widely used form of the dynamic method is the pressure step technique where the gas concentration is changed by suddenly increasing or decreasing the system pressure. The system pressure is typically changed by a small amount, for example, from 15 to 20 kPa, by the addition of gas into the reactor

head space. The sudden pressure change is believed to instantaneously change the gas concentration in the gas phase throughout the vessel and be independent of system hydrodynamics.

The use of the pressure step technique was found by Blazej et al. (2004a) and Linek et al. (1991b) to be more accurate (by up to 60% for systems with non-coalescing liquids) in determining $k_L a$ values than the gassing-out technique. This increase in accuracy was attributed to model shortcomings related to the washing out of one gas by another for systems with non-coalescing liquids. The $k_L a$ values for the gassing-out method and pressure step method were found to be similar under some operating conditions. Linek et al. (1989, 1994) also reported that there was no difference in $k_L a$ values when gassing with air or pure oxygen, indicating that nitrogen transport was not a factor. They also reported that experimental results for this technique only match those from the gas off/on method for small values of $k_L a$.

NONIDEAL PRESSURE STEP. The nonideal pressure step technique is slightly different from the pressure step technique. The difference in the two is that in the pressure step technique, the pressure change is considered instantaneous or ideal. In the nonideal pressure step technique, however, the pressure step is actually achieved by throttling the exit gas stream to cause a pressure buildup, where the time lag for the pressure step depends on the gas flow rate and the vessel size. Linek et al. (1993) compared this technique with the pressure step technique and reported that the results from the two techniques agreed very well.

CONCENTRATION STEP. The concentration step technique is a rarely used technique that deoxygenates the liquid phase by the addition of a small amount of a chemical compound like sulfite without interrupting aeration. This technique should not be confused with the chemical sorption methods as only a small amount of the compound is added with the intent of causing a dissolved gas concentration step change. For this method to work properly, the system must be very well mixed to ensure uniform dissolved gas concentrations. Also, care must be taken to ensure that the chemical compound being added does not alter the hydrodynamics or enhance mass transfer rates.

Dynamic Method Drawbacks. The dynamic methods are affected by several factors:

1. These methods assume that both the gas and liquid phases are well mixed. However, if either one of these phases is anything other than well mixed, which is often the case, especially for large or tall vessels, the $k_L a$ measurement accuracy decreases (Blanch and Clark, 1997).
2. Since air is commonly used for experimental purposes, the effect of simultaneous oxygen and nitrogen transport may affect the accuracy of experimentally determined $k_L a$ values (Gogate and Pandit, 1999b; Letzel et al., 1999; Linek et al., 1981; Stenberg and Andersson, 1988a).

3. Changing from one steady state to another, where the gas-phase residence times are significant, will cause the $k_L a$ estimate to be inaccurate. This is especially true when the time to move from one steady-state condition to another is of the same order of magnitude as $1/k_L a$ (Gogate and Pandit, 1999b; Van't Riet, 1979).
4. The rapid change in dissolved oxygen concentrations with time may lead to oxygen electrode outputs that are not directly related to the instantaneous oxygen concentration unless the output is conditioned to adjust for electrode dynamics (Van't Riet, 1979). Tribe et al. (1995) showed that neglecting electrode probe response time, while using any of the dynamic measurement methods, would cause errors in $k_L a$ estimates, regardless of how much smaller τ_e is compared to $1/k_L a$. They emphasized that proper accounting for the electrode dynamics is needed for reliable measurements.

A comparison of methods done by Poughon et al. (2003) concluded, without explanation, that the use of the dynamic method always results in an underprediction of $k_L a$ when compared to other methods, such as the gas balance and chemical sorption methods, which are now described.

Chemical Sorption Methods. Chemical sorption methods to determine $k_L a$ are based on a chemical reaction between the absorbed gas and a chemical that is added to the liquid phase. Four of these methods will be presented here, although many others exist. The sulfite oxidation, hydrazine, and peroxide methods are applicable to systems studying oxygen transport, while the carbon dioxide absorption method, as its name implies, is for measuring dissolved carbon dioxide.

Sulfite Oxidation Method. The sulfite oxidation method is based on the oxidation of sulfite to sulfate in the presence of a catalyst, where dissolved oxygen is consumed by the reaction

$$Na_2SO_3 + \frac{1}{2}O_2 \xrightarrow{\text{catalyst}} Na_2SO_4 \tag{4.35}$$

Thus, to make this method work, the bulk fluid has to have a high concentration of sulfite and catalyst prior to aeration. Once aeration begins, any oxygen that dissolves into the fluid phase is immediately consumed by the sulfite reaction and the rate of sulfite oxidation is proportional to $k_L a$. Since the bulk fluid oxygen concentration remains at zero, $k_L a$ is estimated by

$$-\frac{dC_{\text{sulfite}}}{dt} \approx k_L a \cdot C^* \tag{4.36}$$

The sulfite concentration in the bulk fluid is followed by taking liquid samples over a given time interval. The samples are then quenched with excess iodine and back titrated with thiosulfate to determine the residual iodine concentration and, subsequently, the sample sulfite concentration (Sobotka et al., 1982). Knowing the sulfite concentration change with time, Eq. (4.36) can be used to determine $k_L a$.

Chisti (1989) and Blanch and Clark (1997) reported that this technique had severe limitations. First, there is a need for expensive high purity chemicals. Second, the chemical reaction produces a highly ionic fluid that is non-coalescing, which may alter the system hydrodynamics. Third, sample analysis is often slow and tedious (Sobotka et al., 1982). Fourth, the sulfite oxidation rate is very sensitive to fluid properties and impurities; thus, the reaction rate depends on the type of catalyst used, its concentration, trace metals, temperature, and fluid pH. Hence, $k_L a$ determination requires that the reaction conditions be carefully controlled, the sulfite concentration kept sufficiently high, and excess catalyst must be present in the bulk fluid to ensure that oxidation occurs in the bulk fluid and not at the gas–liquid interface (Chisti, 1989). Gogate and Pandit (1999b) indicated that this method is not suitable for use in systems using pure oxygen because bubble size in the system changes dramatically by the high chemical reaction rate. Van't Riet (1979) also reported that the reaction rate constant can vary in unknown ways and that this method should be avoided.

The Hydrazine Method. The steady-state hydrazine (N_2H_4) method makes use of the following reaction (Chisti, 1989):

$$N_2H_4 + O_2 \rightarrow N_2 + 2H_2O \tag{4.37}$$

This method uses a steady flow of hydrazine into an aerated reactor. The dissolved oxygen concentration is then followed by an oxygen electrode. The intent of this method is to introduce hydrazine into the system at a rate equal to $k_L a$ which, when accomplished, keeps the electrode signal at a constant level (i.e., the rate at which hydrazine is consumed is equal to $k_L a$).

The reaction in Eq. (4.37) does not form ionic species; therefore, the system hydrodynamics are not affected during the course of the test, unlike the sulfite oxidation method (Chisti, 1989).

Peroxide Method. The peroxide method is based on the following chemical reaction where oxygen is produced in the reactor liquid:

$$2H_2O_2 \xrightarrow{\text{catalase}} 2H_2O + O_2 \tag{4.38}$$

The oxygen is transferred to a carrier gas that is used to transport the oxygen out of the system. Under steady-state conditions, the oxygen production is equal to the oxygen transfer rate. To calculate the oxygen transfer rate, only the peroxide inlet flow rate and concentration, liquid volume, carrier gas flow rate, and dissolved oxygen concentrations are needed at steady-state conditions. This method uses catalase enzymes that are known to enhance foam formation and alter the gas bubble diameter, which is a severe limitation when considering the use of the method (Gogate and Pandit, 1999b).

Carbon Dioxide Absorption Method. Another commonly employed chemical technique is the absorption of carbon dioxide into a mild alkaline or an appropriately buffered solution (Andre et al., 1981). The carbon dioxide method is similar in principle and procedure to the sulfite oxidation method. Chisti (Chisti, 1989) indicated that the limitations for this method were similar to those of the sulfite oxidation method.

4.3 SUMMARY

Many different experimental techniques are available to characterize and quantify bioreactor hydrodynamics and gas–liquid mass transfer rates. Some of these techniques, including advantages and disadvantages, were outlined in this chapter. Current experimental methods are continually being modified and refined, and new techniques will always be developed. Hence, the development of experimental methods relevant to bioreactor operation is an evolutionary process and an area rich in application.

5 Modeling Bioreactors

Lab-scale and pilot-scale experimental bioreactor studies can be expensive and challenging to complete, but are needed before industrial-scale processes are implemented. To reduce the experimental costs, models of the various systems can be developed and simulations can be completed and validated with selected experimental results. In bioreactors, the hydrodynamics play a critical role, and multiphase computational fluid dynamics (CFD) models are needed to simulate the commonly encountered gas–liquid, liquid–solid, and gas–liquid–solid bioreactor mixtures. The overall bioreactor production can also be modeled through appropriate mass and energy balances combined with biological kinetic processes. This chapter will provide a general outline of multiphase flow CFD modeling, and then provide a brief overview of basic biological process modeling.

5.1 MULTIPHASE FLOW CFD MODELING

CFD can be used to simulate the hydrodynamics found in multiphase bioreactors. Although bioreactors typically involve heat and mass transfer operations, they are generally neglected in the hydrodynamic models (Joshi, 2001; Kulkarni et al., 2007). Monahan et al. (2005) have provided a summary of the various computational approaches and physical models used in gas–liquid hydrodynamic modeling. They point out that various aspects of gas–liquid hydrodynamic modeling have been considered in the literature, but the importance of various terms and their exact model form is still under debate; these include terms that address (i) bubble–bubble interactions; (ii) two-phase turbulence modeling; (iii) gas–liquid interfacial mass, momentum, and energy transfer mechanisms; and (iv) coupling between the phases. The required grid resolution and its effect on convergence have also been addressed. Comprehensive CFD overviews are available in the literature (Azzopardi et al., 2011; Delnoij et al., 1997a; Jakobsen et al., 2005a; Joshi, 2001; Kulkarni et al., 2007), and the interested reader is referred to these and other studies for additional details.

Multiphase flow CFD simulations typically employ Eulerian–Eulerian models (Monahan et al., 2005; Pan et al., 2000; Rampure et al., 2003; Sokolichin and

An Introduction to Bioreactor Hydrodynamics and Gas-Liquid Mass Transfer, First Edition.
Enes Kadic and Theodore J. Heindel.

Eigenberger, 1994), Eulerian–Lagrangian models (Delnoij et al., 1997a, 1997b; Delnoij et al., 1997c) or various direct numerical simulation (DNS) methods (Dijkhuizen et al., 2010; van Sint Annaland et al., 2006). The Eulerian–Eulerian model treats dispersed and continuous phases as interpenetrating continua and describes the motion for both phases in an Eulerian frame of reference. In gas–liquid bioreactors, for example, the bubbles act as the dispersed phase and the liquid is the continuous phase. In the Eulerian–Lagrangian model (Delnoij et al., 1997a, 1997b; Delnoij et al., 1997c), the continuous phase is described in an Eulerian representation while the dispersed phase (e.g., bubbles) is treated as discrete particles, and each discrete particle is tracked by solving the equations of motion for individual particles. The DNS methods, including level set, volume of fluid, lattice Boltzmann, and front-tracking methods (Dijkhuizen et al., 2010; van Sint Annaland et al., 2006), solve the instantaneous Navier–Stokes equations to obtain the dispersed and continuous phase flow field with an extremely high spatial resolution, and the interface between phases is tracked.

The main advantage of the Eulerian–Lagrangian formulation comes from the fact that each individual bubble is modeled, allowing consideration of additional effects related to bubble–bubble and bubble–liquid interactions. Mass transfer with and without chemical reaction, bubble coalescence, and redispersion, in principle, can be added directly to an Eulerian–Lagrangian hydrodynamic model. The main disadvantage of the Eulerian–Lagrangian approach is that only a limited number of particles (bubbles) can be tracked, such as when the superficial gas velocity is low (Chen et al., 2005), due to computer limitations.

The Eulerian–Eulerian method is more popular because memory storage requirements and computer power demand depend on the number of computational cells considered instead of the number of particles. Hence, the Eulerian–Eulerian approach can be applied to cases for low and high superficial gas velocities. The disadvantage of using the Eulerian–Eulerian method is that the bubble–bubble and bubble–liquid interactions cannot be considered as straightforward as the Eulerian–Lagrangian method, and models for these interactions are typically applied.

The DNS methods are the most detailed; they typically advance the gas–liquid interface through the flow field in an Eulerian mesh and do not require empirical constitutive equations. However, the DNS methods are limited to a very small number of particles/bubbles (e.g., typically 10s of bubbles in the flow field) due to computational limitations. Most industrial applications require high superficial gas velocities, and therefore the Eulerian–Eulerian method is preferred (Dudukovic, 2002; Pan et al., 2000) and will be summarized later.

Note that many bioreactor CFD simulations assume that the biological content has a negligible effect on the bioreactor hydrodynamics or, if there is an effect, only the fluid rheology is modified. Hence, many of the available bioreactor CFD studies focus on gas–liquid modeling (Roy et al., 2006). A few gas–liquid–solid CFD studies have been completed (Hamidipour et al., 2012; Jia et al., 2007; Rampure et al., 2003), and the interested reader is referred to these studies for further information.

5.1.1 Governing Equations for Gas–Liquid Flows

The two-fluid Eulerian–Eulerian model represents each phase as interpenetrating continua, and the conservation equations for mass and momentum for each phase are ensemble-averaged. Bubble coalescence and/or breakup are typically neglected in the models used in the literature. The subscript c refers to the continuous (liquid) phase and the subscript d refers to the dispersed (gas bubble) phase. The continuity equations for each phase are

$$\frac{\partial}{\partial t}(\alpha_c \rho_c) + \nabla \cdot (\alpha_c \rho_c \vec{u}_c) = R_c \tag{5.1}$$

$$\frac{\partial}{\partial t}(\alpha_d \rho_d) + \nabla \cdot (\alpha_d \rho_d \vec{u}_d) = R_d \tag{5.2}$$

where the volumetric phase fractions are denoted by α_c and α_d, respectively, and sum to 1, and ρ and $\vec{u}$ are the respective phase density and velocity. Note that α is used to specify the volumetric phase fractions in this chapter to avoid confusion with the dissipation of turbulent kinetic energy ϵ. The right-hand side of Eqs (5.1) and (5.2), R_c and R_d, are zero when mass transfer is neglected, which is common in many simulations. The momentum equations for each phase are

$$\begin{aligned}\frac{\partial}{\partial t}(\alpha_c \rho_c \vec{u}_c) + \nabla \cdot (\alpha_c \rho_c \vec{u}_c \vec{u}_c) \\ = -\alpha_c \nabla p + \nabla \cdot \bar{\bar{\tau}}_c + \vec{K}_{dc}(\vec{u}_d - \vec{u}_c) + \vec{F}_{vm} + \rho_c \alpha_c \vec{g}\end{aligned} \tag{5.3}$$

$$\begin{aligned}\frac{\partial}{\partial t}(\alpha_d \rho_d \vec{u}_d) + \nabla \cdot (\alpha_d \rho_d \vec{u}_d \vec{u}_d) \\ = -\alpha_d \nabla p + \nabla \cdot \bar{\bar{\tau}}_d + \vec{K}_{cd}(\vec{u}_c - \vec{u}_d) - \vec{F}_{vm} + \rho_d \alpha_d \vec{g}\end{aligned} \tag{5.4}$$

The terms on the right-hand side of Eqs (5.3) and (5.4) represent, from left to right, the pressure gradient, effective stress, interfacial momentum exchange terms (drag and virtual mass forces), and the gravitational force. Additional momentum exchange forces may be included, but there has been no consensus as to which forces are the most appropriate, which may also depend on the given system of interest (Joshi, 2001; Monahan et al., 2005). The closures for turbulence modeling and interfacial momentum exchange are discussed next.

5.1.2 Turbulence Modeling

Turbulence contributions for the continuous and dispersed phases have been based on a modified form of the standard multiphase k–ϵ equations, first presented by Kashiwa et al. (1993) and described in detail by Padial et al. (2000), to calculate turbulence at the gas–liquid interface in the form of a slip-production energy term.

The modified $k-\epsilon$ equations can be used for high superficial gas velocity flows (Law et al., 2008), and the equations for a general phase i are

$$\frac{\partial}{\partial t}(\alpha_i \rho_i k_i) + \nabla \cdot (\alpha_i \rho_i k_i \vec{u}_i) = \nabla \cdot \left(\alpha_i \frac{\mu_{t,i}}{\sigma_i} \nabla k_i \right) + \alpha_i G_i - \alpha_i \rho_i \epsilon_i + \sum_{j \neq i} \beta_{ij} K_{ij} |\vec{u}_i - \vec{u}_j|^2 + 2 \sum_{j \neq i} E_{ij}(k_j - k_i) \quad (5.5)$$

$$\frac{\partial}{\partial t}(\alpha_i \rho_i \epsilon_i) + \nabla \cdot (\alpha_i \rho_i \epsilon_i \vec{u}_i) = \nabla \cdot \left(\alpha_i \frac{\mu_{t,i}}{\sigma_\epsilon} \nabla \epsilon_i \right) + \alpha_i \frac{\epsilon_i}{k_i} (C_{1\epsilon} G_i - C_{2\epsilon} \rho_i \epsilon_i) + \frac{1}{\tau_{ij}} \left\{ \sum_{j \neq i} \beta_{ij} K_{ij} \left| \vec{u}_i - \vec{u}_j \right|^2 \right\} \quad (5.6)$$

where

$$\mu_{t,i} = \rho_i C_{\mu,i} \frac{k_i^2}{\epsilon_i} \quad (5.7)$$

$$G_i = \mu_{t,i} (\nabla \vec{u}_i + (\nabla \vec{u}_i)^T) : \nabla \vec{u}_i \quad (5.8)$$

$$C_{\mu,i} = \frac{C_\mu}{1 + (2 \sum_{j \neq i} E_{ij} k_i)/(\rho_i \epsilon_i)} \quad (5.9)$$

Note that if i is the continuous phase, then j is the dispersed phase, and vice versa.

The form of Eq. (5.9) models a return-to-isotropy effect due to fluctuating interfacial momentum coupling and reduces the turbulent viscosity from that predicted by the single-phase model. The turbulence energy exchange rate coefficient E_{ij} is given by

$$E_{ij} = \alpha_i \alpha_j \left(\frac{\rho_i \rho_j}{\rho_i + \rho_j} \right) \frac{\sqrt{k_i + k_j}}{d_B} (1 + Re_B^{0.6}) \quad (5.10)$$

where $Re_B = \rho_c |\vec{u}_d - \vec{u}_c| d_B / \mu_c$ is the bubble Reynolds number based on a characteristic (effective) bubble diameter, relative velocity between the two phases, and the liquid density and dynamic viscosity.

The first three terms on the right-hand side of Eq. (5.5) account for turbulent diffusion, mean flow shear production, and decay of turbulence kinetic energy of phase i. The fourth term on the right-hand side of Eq. (5.5) accounts for production of turbulence energy from slip between phases. The coefficient β_{ij} is given by

$$\beta_{ij} = \frac{\alpha_i}{\alpha_i + \alpha_j} \quad (5.11)$$

where

$$\alpha_i = \frac{{\alpha_i}^{1/3}}{\rho_i + \rho_c} \tag{5.12}$$

and ρ_c is the continuous phase density. The last term in Eq. (5.5) accounts for the exchange of turbulence energy among phases.

The first three terms on the right-hand side of Eq. (5.6) account for the diffusion of turbulence dissipation, the mean flow velocity gradient production term, and the homogeneous dissipation term. The last group of terms in Eq. (5.6) describes the effect of interfacial momentum transfer on the production of turbulence dissipation. The time constant τ_{ij} is given by the following empirical correlation:

$$\tau_{ij} = \left\{ 0.01 C_{2\epsilon} \left(\alpha_i \alpha_j\right)^{0.086} \left[\frac{\rho_i \left| \vec{u}_i - \vec{u}_j \right| d_B}{\mu_i} \right]^{0.562} \frac{|\vec{u}_i - \vec{u}_j|}{d_B} \right\}^{-1} \tag{5.13}$$

This correlation was obtained by fitting predictions of turbulence kinetic energy to data from experiments on homogeneous settling and bubbly systems (Lance and Bataille, 1991; Mizukami et al., 1992; Parthasarathy and Faeth, 1990a, 1990b). The term K_{ij} is the interfacial momentum exchange coefficient discussed next. Equations (5.7) and (5.8) are closure models for the turbulent viscosity $\mu_{t,i}$ and for the production of turbulent kinetic energy G_i of phase i. The turbulent parameters are set using standard empirical values for k–ϵ turbulence modeling where $C_{1\epsilon} = 1.44$, $C_{2\epsilon} = 1.92$, $C_\mu = 0.09$, $\sigma_k = 1.0$, and $\sigma_\epsilon = 1.3$.

5.1.3 Interfacial Momentum Exchange

The interfacial momentum exchange terms in the momentum conservation equations for each phase consist of drag and virtual mass force terms. The drag force for gas and liquid is modeled, respectively, as

$$\begin{aligned} \vec{K}_{cd}(\vec{u}_c - \vec{u}_d) &= \frac{3}{4}\rho_c \alpha_d \alpha_c \frac{C_D}{d_B} |\vec{u}_c - \vec{u}_d| (\vec{u}_c - \vec{u}_d) \\ \vec{K}_{dc}(\vec{u}_d - \vec{u}_c) &= \frac{3}{4}\rho_c \alpha_d \alpha_c \frac{C_D}{d_B} |\vec{u}_d - \vec{u}_c| (\vec{u}_d - \vec{u}_c) \end{aligned} \tag{5.14}$$

where C_D is the drag coefficient. There are many different drag coefficient models available in the literature and these have been summarized by Joshi (2001) and Monahan et al. (2005). Two particular models commonly found in commercial CFD packages were compared by Law et al. (2008). One was the model proposed by Schiller and Naumann (1933):

$$C_D = \begin{cases} 24\left(1 + 0.15 Re_B^{0.687}\right)/Re_B & Re_B \le 1000 \\ 0.44 & Re_B > 1000 \end{cases} \tag{5.15}$$

The second drag coefficient model was proposed by White (1974):

$$C_{\mathrm{D}} = C_{\mathrm{D},\infty} + \frac{24}{Re_{\mathrm{B}}} + \frac{6}{1+\sqrt{Re_{\mathrm{B}}}} \quad 0 \le Re_{\mathrm{B}} \le 2\times 10^5 \tag{5.16}$$

where $C_{\mathrm{D},\infty}$ is the drag coefficient when the bubble Reynolds number goes to infinity, which is set at 0.5 (Law et al., 2008).

The virtual mass force $\vec{F}_{\mathrm{vm}}$ is modeled as

$$\vec{F}_{\mathrm{vm}} = 0.5\alpha_{\mathrm{d}}\rho_{\mathrm{c}}\left(\frac{d\vec{u}_{\mathrm{c}}}{dt} - \frac{d\vec{u}_{\mathrm{d}}}{dt}\right) \tag{5.17}$$

and the coefficient of 0.5 is used for a spherical bubble.

5.1.4 Bubble Pressure Model

The bubble pressure (BP) model is reported in the literature to play an important role in bubble-phase stability and represents the transport of momentum arising from bubble–velocity fluctuations, collisions, and hydrodynamic interactions. According to Spelt and Sangani (1998), the kinetic contribution comes from fluctuations in the bubble motion; the collisional contribution is attributed to bubble–bubble collisions; and the hydrodynamic contribution arises from the relative motion of the bubbles and the spatial and velocity distribution of the bubbles. As the dispersed phase void fraction (α_{d}) increases from zero, the bubble-phase pressure will increase from zero, reach a maximum value, and then decrease. For low dispersed phase void fractions, the gradient in the BP with respect to the void fraction ($dP_{\mathrm{d}}/da_{\mathrm{d}}$) is positive and proportional to the slip velocity and gas holdup, and the collisional and hydrodynamic contributions can be neglected. In this case, Spelt and Sangani (1998) suggest the BP to be of the form

$$P_{\mathrm{B}} = \rho_{\mathrm{c}} C_{\mathrm{BP}} \alpha_{\mathrm{d}} (\vec{u}_{\mathrm{d}} - \vec{u}_{\mathrm{c}}) \cdot (\vec{u}_{\mathrm{d}} - \vec{u}_{\mathrm{c}}) \tag{5.18}$$

The virtual mass coefficient C_{BP} of an isolated spherical bubble is 0.5. The BP gradient is then added to the right-hand side of the gas momentum (Eq. (5.4)) and acts as a driving force for bubbles to move from areas of higher α_{d} to areas of lower α_{d} and facilitates stabilization of the bubbly flow regime. However, Sankaranarayanan and Sundaresan (2002) indicate that as α_{d} increases, the collisional and hydrodynamic contributions become important.

Biesheuvel and Gorissen (1990) proposed a modified BP model of the form

$$P_{\mathrm{B}} = \rho_{\mathrm{c}} C_{\mathrm{BP}} \alpha_{\mathrm{d}} (\vec{u}_{\mathrm{d}} - \vec{u}_{\mathrm{c}}) \cdot (\vec{u}_{\mathrm{d}} - \vec{u}_{\mathrm{c}}) \left(\frac{\alpha_{\mathrm{d}}}{\alpha_{\mathrm{dcp}}}\right)\left(1 - \frac{\alpha_{\mathrm{d}}}{\alpha_{\mathrm{dcp}}}\right) \tag{5.19}$$

The gas holdup at close packing α_{dcp} is typically set equal to 1.0 (Law et al., 2008; Monahan et al., 2005).

5.1.5 Bubble-Induced Turbulence

Bubbles contain potential energy when they are injected into a bioreactor. As they rise, some of the potential energy of the gas is converted into kinetic energy. The remaining energy is passed to the liquid through the gas–liquid interface, where some energy is dissipated. The energy that reaches the liquid phase is eventually dissipated in the small scales found in the wakes of the bubbles (Monahan et al., 2005). Several models have been proposed to account for this bubble-induced turbulence (BIT) (Sokolichin et al., 2004). Sato and Sekoguchi (1975) proposed a BIT model proportional to the bubble diameter and slip velocity of the rising bubbles:

$$\mu_{t,c} = \rho_c C_{BT} \alpha_d d_b |\vec{u}_d - \vec{u}_c| \tag{5.20}$$

where the value of the proportionality constant C_{BT} is 0.6 (Sato et al., 1981). The BIT model yields an effective viscosity in the liquid (continuous) phase, that is, the sum of the molecular viscosity of the continuous phase and the turbulent viscosity calculated from the BIT model, whereas the effective viscosity for the dispersed phase is assumed to equal the molecular viscosity of the dispersed phase. Equation (5.20) replaces Eq. (5.7) when the BIT model is applied (Law et al., 2008). Law et al. (2008) concluded that a BP model coupled with a BIT model is needed to produce stable solutions in gas–liquid bubble column reactors when the superficial gas velocity is low.

5.1.6 Modeling Bubble Size Distribution

Bubble size is required to calculate, for example, the drag force imparted on a bubble. Most Eulerian–Eulerian CFD codes assume a single (average) bubble size, which is justified if one is modeling systems in which the bubble number density is small (e.g., bubbly flow in bubble columns). In this case, the bubble–bubble interactions are weak and bubble size tends to be narrowly distributed. However, most industrially relevant flows have a very large bubble number density where bubble–bubble interactions are significant and result in a wide bubble size distribution that may be substantially different from the average bubble size assumption. In these cases, a bubble population balance equation (BPBE) model may be implemented to describe the bubble size distribution (Chen et al., 2005).

A general population balance equation for bubbles located at position vector $\vec{x}$ with a bubble volume V_b, at time t, can be written as (Chen et al., 2005)

$$\frac{\partial}{\partial t} f(\vec{x}, V_b, t) + \nabla \cdot [\vec{u}_b(\vec{x}, V_b, t) f(\vec{x}, V_b, t)] = S(\vec{x}, V_b, t) \tag{5.21}$$

where $f(\vec{x}, V_b, t)$ is the bubble number density function that is assumed to be continuous and specifies the probable number density of bubbles at a given time in the spatial range $d\vec{x}$ about $\vec{x}$ with a bubble volume between V_b and $V_b + dV_b$. The bubbles in $f(\vec{x}, V_b, t)$ travel at a velocity $\vec{u}_b(\vec{x}, V_b, t)$. The term on the right-hand

side of Eq. (5.21) is the source term described by

$$S(\vec{x}, V_b, t) = \frac{1}{2}\int_0^{V_b} a(V_b - V_b', V_b') f(\vec{x}, V_b - V_b', t) f(\vec{x}, V_b', t) dV_b'$$
$$- f(\vec{x}, V_b, t) \int_0^{\infty} a(V_b, V_b') f(\vec{x}, V_b', t) dV_b'$$
$$+ \int_0^{\infty} m(V_b') b(V_b') P(V_b, V_b') f(\vec{x}, V_b', t) dV_b'$$
$$- b(V_b') f(\vec{x}, V_b, t) + S_{ph} + S_p + S_r + \cdots \tag{5.22}$$

where the first term on the right-hand side is the birth rate of bubbles of volume V_b due to coalescence of bubbles of volume $V_b - V_b'$ and V_b', the second term is the death rate of bubbles of volume V_b due to coalescence with other bubbles, the third term is the birth rate of bubbles of volume V_b due to breakup of bubbles with a volume larger than V_b, and the fourth term is the death rate of bubbles of volume V_b due to breakup. The additional source/sink terms are because of the bubbles being added or subtracted from the bubble class of volume V_b due to phase change (S_{ph}), pressure change (S_p), or reaction (S_r). In addition, $a(V_b, V_b')$ is the coalescence frequency between bubbles of volume V_b and V_b', $b(V_b')$ is the breakup frequency of bubbles of volume V_b', $m(V_b')$ is the mean number of daughter bubbles produced by breakup of a parent bubble of volume V_b', and $P(V_b, V_b')$ is the probability density function of daughter bubbles produced on breakup of a parent bubble of volume V_b' (Chen et al., 2005). The various source terms in Eq. (5.22) require closure models for bubble breakup and coalescence; these models are beyond the scope of this review, but can be found in the literature (e.g., Chen et al., 2005; Jakobsen et al., 2005a; Sanyal et al., 2005).

5.2 BIOLOGICAL PROCESS MODELING

Biological process (bioprocess) models mathematically focus on describing the biological system's growth and product formation. Even simple biological processes are extremely complex from cellular component operations to overall bioreactor interactions. These complex systems, however, are often described by only a few mathematical equations, and rather simple growth kinetics, because the large cell population in the bioreactor hides individual variations in their growth and product formation; this leads to a smoothed average bioreactor behavior (Bellgardt, 2000a).

As described by Nielsen et al. (2003), biological process modeling uses a set of mathematical relationships developed through physical laws and/or empirical observations that relate the input variables of the system to the output variables. The input parameters include things such as flow rate(s), pH, temperature, agitation speed, and substrate concentration, while the output may include cell/product concentration, temperature, and flow rate. Kinetic expressions, which describe the

rates of input/output concentrations, coupled to system mass balances are utilized in the overall bioprocess model. The model is specified for a given control volume, defined as a region of interest where all variables of interest are uniform. In biological process modeling, the control volume is typically taken as the entire bioreactor. For extremely large systems, the bioreactor may be divided into several control volumes, each one being homogeneous but different from the adjacent control volume(s). In contrast, when using CFD to model the bioreactor hydrodynamics, the control volume is an individual grid cell with millions of grid cells comprising the entire bioreactor.

Nielsen et al. (2003) describes four general groups of biological process models. The simplest are unstructured, nonsegregated models where the biomass is described by a single variable (e.g., cell concentration) and the cell population is assumed to be homogeneous. These models can be extended to unstructured, segregated models where individual cells within a population are modeled (e.g., cell age). Structured, nonsegregated and structured, and segregated models mathematically incorporate the cellular structure and its effect on the transport characteristics in the overall process model.

5.2.1 Simple Bioprocess Models

Simple bioprocess models are typically based on batch fermentation processes where the change in cell concentration with respect to time is proportional to the current cell concentration. This first-order rate equation is mathematically described by

$$\frac{dC_c}{dt} = kC_c \tag{5.23}$$

where C_c is the cell concentration at a given instant in time and k is a proportionality constant. This description assumes an infinite substrate concentration to support cell production.

A batch process, however, typically has a finite substrate concentration C_S set at time $t = 0$. As shown in Figure 5.1, plotting experimentally observed substrate and cell concentrations as a function of time, where concentration is on a natural logarithmic scale, the entire life cycle of the batch process can be described. Cell production can be divided into four regions (Dunn et al., 2003). First, cells are inoculated into the batch reactor at a known concentration C_{c0} and a period a cell adjustment is observed during the lag period ($0 < t < t_1$). Second, cells undergo a period of exponential growth until the substrate concentration can no longer support growth because a particular substance is limited ($t_1 < t < t_2$). Third, a stationary period of constant cell concentration may be observed while the remaining substrate material is consumed ($t_2 < t < t_3$). If sufficient time is allowed, cell death may be reached because of lack of nutrients, toxicity effects on the cells, and/or cell aging ($t_3 < t$).

Solving Eq. (5.23) during the exponential growth period reveals

$$\frac{C_c}{C_{c0}} = e^{kt} = e^{\mu t} \tag{5.24}$$

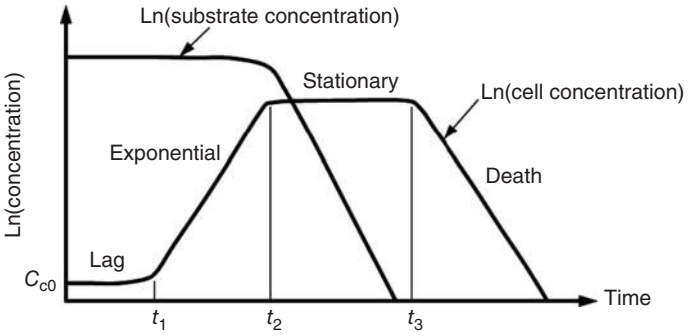

Figure 5.1 Cell life cycle in a batch fermentation process. Adapted from Dunn et al. (2003).

where the slope of linear part of Figure 5.1 ($t_1 < t < t_2$) is the growth rate per unit cell mass defined as the specific growth rate μ.

The exponential growth region can be described by a single relationship where the specific growth rate μ is a function of the substrate concentration C_S. Empirical evidence reveals that μ is a maximum when C_S is large, and μ is linear with C_S when C_S is small. The specific function that describes the entire relationship including the two limiting extremes is called the Monod equation

$$\mu = \frac{\mu_m C_S}{K_S + C_S} \tag{5.25}$$

where μ_m is the maximum specific growth rate and the saturation constant K_S is defined as the substrate concentration C_S when $\mu = 1/2\mu_m$. The Monod equation is shown in Figure 5.2 and is based on empirical observations. Although the Monod

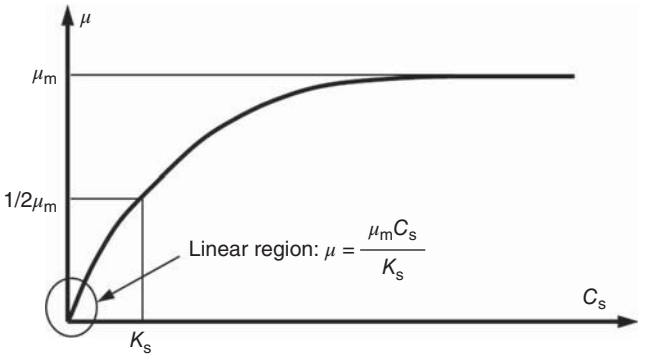

Figure 5.2 The Monod relationship describing specific growth rate as a function of substrate concentration C_S. Note that this is valid only in the exponential growth region ($t_1 < t < t_2$ in Fig. 5.1).

equation may appear to be rather simplistic, it generally describes the exponential growth rate for a wide variety of real systems (Dunn et al., 2003).

The Monod equation is not the only unstructured, nonsegregated empirical model of bioreactor cell growth. Others can be found in the summaries provided by Bellgardt (2000a), Dunn et al. (2003), or Nielsen et al. (2003).

5.3 SUMMARY

Modeling bioreactor performance is typically accomplished by focusing on either the bioreactor hydrodynamics using CFD modeling, which neglects the presence of microorganisms, or on biological process modeling assuming uniform flow condition within the bioreactor (or large sections of the bioreactor). Coupling the multiphase hydrodynamic models to the bioprocess models is needed for improved performance predictions.

6 Stirred-Tank Bioreactors

6.1 INTRODUCTION

Stirred-tank reactors (STRs) are one of the standard reactors in the chemical industry and have therefore been widely implemented for biological applications (Williams, 2002). We assume that the terms "stirred-tank reactor" and "stirred-tank bioreactor" can be used interchangeably and no distinction will be made between the two terms in this chapter; hence, the term *STR* will also be used to identify a stirred-tank bioreactor. They are used with viscous liquids, slurries, very low gas flow rates, and large liquid volumes (Charpentier, 1981; Fujasova et al., 2007; Garcia-Ochoa and Gomez, 1998). STRs are also popular because a well-mixed state is easily achieved, which aids in providing necessary substrate contact, pH and temperature control, removal of toxic by-products, uniform cell distribution, clog prevention, and particle size reduction (Branyik et al., 2005; Hoffmann et al., 2008). This chapter provides an overview of STR operation and summarizes issues related to STR gas–liquid mass transfer. Additional information can be found in the literature (Harnby et al., 1992; Linek et al., 2004; Linek et al., 1996a, 1996b; Linek et al., 1987; McFarlane and Nienow, 1995, 1996a, 1996b; McFarlane et al., 1995; Oldshue, 1983; Tatterson, 1991, 1994; Ulbrecht and Patterson, 1985).

STRs are widely applied in industry because of their low capital and operating costs (Williams, 2002). Popular applications are fermentation (Cabaret et al., 2008; Fujasova et al., 2007; Garcia-Ochoa and Gomez, 1998; Hoffmann et al., 2008; Scargiali et al., 2007; Vasconcelos et al., 2000), carbonation, oxidation (Oldshue, 1983; Scargiali et al., 2007), chlorination (Fujasova et al., 2007; Oldshue, 1983; Scargiali et al., 2007), hydrogenation (Fujasova et al., 2007; Murthy et al., 2007; Scargiali et al., 2007; Shewale and Pandit, 2006), dissolution, polymerization (Shewale and Pandit, 2006), chemical synthesis, and wastewater treatment (Cabaret et al., 2008; Ogut and Hatch, 1988; Shewale and Pandit, 2006). STRs are preferred when high gas–liquid mass transfer coefficients are needed (Bredwell et al., 1999). These reactors are usually made out of stainless steel for industrial units or out of clear materials, such as glass or certain plastics, for experimental applications (Williams, 2002).

An Introduction to Bioreactor Hydrodynamics and Gas-Liquid Mass Transfer, First Edition.
Enes Kadic and Theodore J. Heindel.

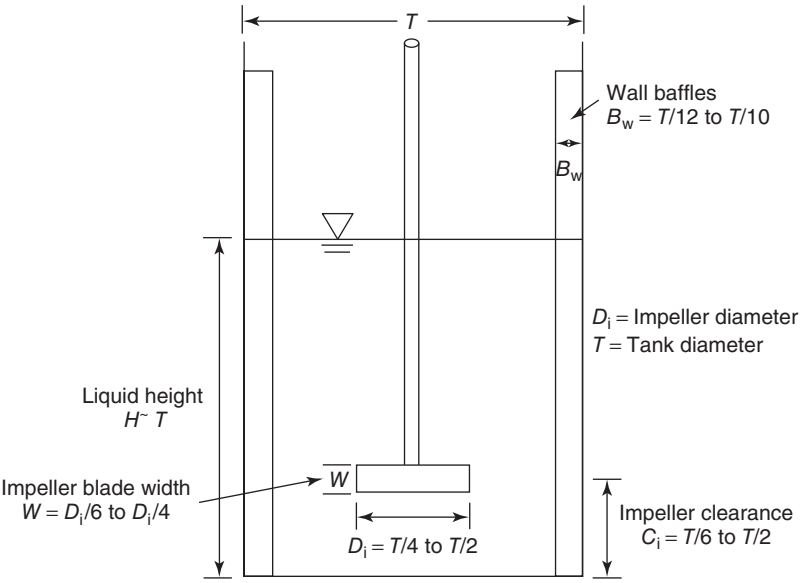

Figure 6.1 Standard single impeller stirred-tank reactor design. Adapted from Tatterson (1991).

Typical STR units (Figure 6.1) have a small height-to-diameter ratio relative to other reactor types (Charpentier, 1981). The diameter T can vary from about 0.1 m for experimental units to 10 m for industrial applications (Harnby et al., 1992). As shown in Figure 6.1, the impeller and baffle dimensions, as well as the impeller clearance, are typically a specified fraction of the tank diameter. The aspect ratio, defined as the liquid height-to-diameter ratio, is highly variable and depends on the number and arrangement of impellers and the reactor application. Single impeller systems typically have an aspect ratio of 1 (Charpentier, 1981; Tatterson, 1991), but certain exotic applications call for designs with aspect ratios up to 3 (Nielsen and Volladsen, 1993; Tatterson, 1991). Industrial multiple impeller designs are mostly limited to an aspect ratio of less than ~4 due to practical considerations (Charpentier, 1981).

Reactor shape, specifically the bottom, can vary greatly. The standard reactor design is cylindrical with a flat bottom (Ulbrecht and Patterson, 1985), but dished, conical, or curved bottoms have also been used (Harnby et al., 1992; Tatterson, 1991). The bottom shape does not seem to affect gas–liquid mass transfer or gas dispersion significantly, but the dished bottom is preferred for solid suspensions and mixing (Oldshue, 1983). Other reactor shapes, such as spherical or semispherical, are in use (Oldshue, 1983) but the standard design is preferred for gas–liquid dispersion due to operational experience and cost. Even though standard reactor designs exist in the chemical industry for liquid–liquid processes, customized STR's use for specific biological or gas–liquid applications precludes an optimized STR design for all applications (Tatterson, 1991).

6.2 STIRRED-TANK REACTOR FLOW REGIMES

Superficial gas velocity, defined as the volumetric gas flow rate divided by the STR cross-sectional area, influences gas–liquid mass transfer through two mechanisms: gas-filled cavities and gas holdup. The sweeping action of the impeller creates a low pressure void that quickly fills with sparged gas. These gas-filled cavities are the mechanism for gas dispersion and gassed power reduction (McFarlane et al., 1995). These cavities ultimately influence impeller loading, gas dispersion, and liquid circulation such that the impeller creates specific flow regimes which are of great importance for STR optimization.

6.2.1 Radial Flow Impellers

Radial flow impellers expel the fluid from the impeller region in the radial direction. The Rushton-type impeller is a standard example of radial flow impeller operation, and this impeller type is the basis for the typical flow regimes identified in radial flow impeller operation. As shown in Figure 6.2, three stable cavity groups are observed using this impeller: vortex cavities, clinging cavities, and large cavities. Vortex cavities form at constant impeller speeds and small gas flow rates. They are defined by two rolling vortices, one at the top and the other at the bottom of the impeller blade. Clinging cavities are formed with an increase in gas flow rate. They are larger than vortex cavities and cling to the blade backside, but still produce vortices at the gas tail. Large cavities, which form with another increase in the gas flow rate, are larger, smoother, and behave differently in terms of hydrodynamics (Nienow et al., 1985; Smith and Warmoeskerken, 1985).

Turbulent action forces the gas to break away from the cavity and exit the impeller zone. This breakage is the source of gas dispersion in STRs. The large cavity deserves special attention because it induces gas breaking away less violently than the other cavity types. Large cavities also have an advantage in that they hold more gas and have more surface area from which gas can break away.

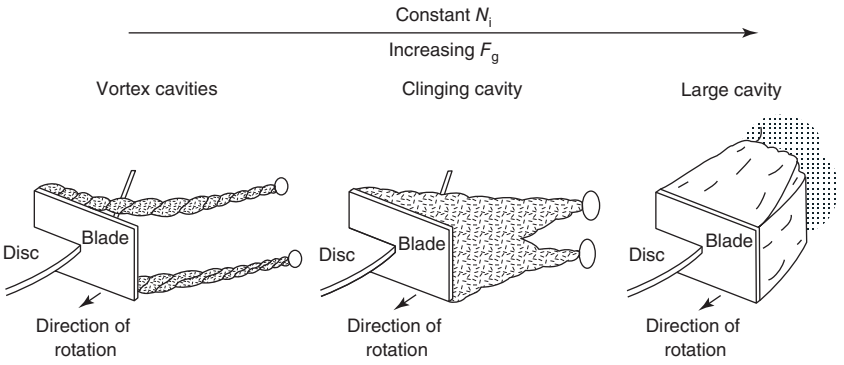

Figure 6.2 Cavity types for the Rushton-type impellers where N is the impeller speed and $Q_g(F_g)$ is the volumetric gas flow rate (Doran, 2013).

Since these cavities form at higher gas flow rates and thus superficial gas velocities, they are able to sustain a higher gas dispersion rate than the other two cavity types; however, there is a breakeven point. Cavities can become too large and hamper gas–liquid mass transfer. For example, if the cavity volume-to-surface area ratio is too large, gas dispersion will decrease (Nienow et al., 1985; Smith and Warmoeskerken, 1985).

Cavities also reduce the energy transfer between the impeller and liquid. A higher superficial gas velocity induces more gas dispersion at a lower power input. However, if too much gas is present and the cavities are too large, the energy transmission is reduced and the impeller's gas dispersion and mixing capabilities are hampered. In this case, the cavities produce an unwanted energy loss and a state described as flooding (Ogut and Hatch, 1988).

The exact nature of these events is accompanied by changes in the cavity structures for the Rushton-type turbine (Figure 6.3). Vortex and clinging cavities form symmetric structures (i.e., their size and shape are similar for every impeller blade). Although these transfer energy well, they do very little for gas dispersion making them undesirable for gas–liquid processes. If the gas flow rate is increased, a 3-3 structure is formed, which is defined by alternating large and clinging cavities. Its importance comes from its stability and gas-handling capacity. It offers the optimal gas dispersion for the lowest power input (i.e., most efficient). If the gas flow rate is increased further, the impeller is flooded. At this point, the stable 3-3 structure is replaced by a structure formed by large, unstable ragged cavities, which are inefficient for gas–liquid mass transfer and gas dispersion (Nienow et al., 1985; Smith and Warmoeskerken, 1985). The instability can also lead to varying impeller power draw that can damage the motor and gearbox system.

The observed cavity structures have inspired improvements to the Rushton-type turbine to increase the gas-handling capacity of the impeller to allow more gas and, hence, higher gas concentrations in the reactor. To accomplish this, impellers should create smaller cavities in similar structures while minimizing flooding. The concave blade disk turbine, discussed in Section 6.3, has been shown to accomplish these goals.

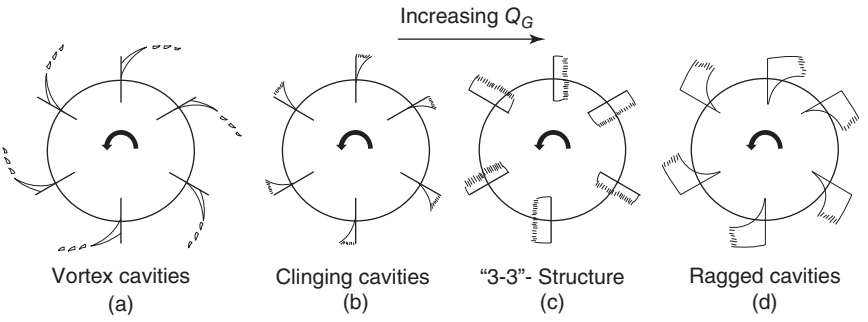

Figure 6.3 Cavity structures for the Rushton-type impeller. Adapted from Nienow et al. (1985).

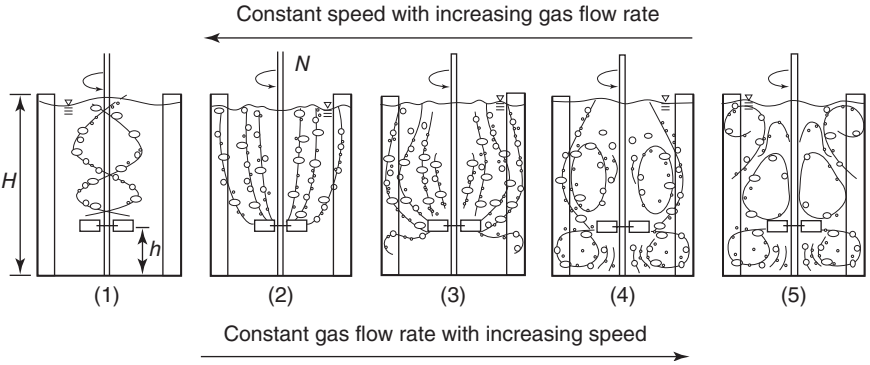

Figure 6.4 Bulk flow patterns for radial flow impellers at constant U_g. Adapted from Nienow et al. (1977).

The gas cavities on the impeller influence the gas dispersion and bulk flow regimes in an STR. For single impeller radial flow systems, five bulk flow regimes (Figure 6.4) have been defined (Nienow et al., 1977). The different regimes occur at increased impeller speeds while holding the gas flow rate constant. At low impeller speeds, the power input is very small and negligible dispersion occurs (regime (1) in Figure 6.4). Increasing the impeller speed begins to disperse the gas phase (regime (2)). The bulk flow above the impeller acts like a bubble column while the lower section is not contacted by the gas phase. Further increasing the impeller speed allows the gas to be recirculated in the upper reactor section, and some gas dispersion occurs in the lower region (regime (3)). Regime (4) is identified by gas recirculation throughout the reactor. This condition is optimal for gas–liquid mass transfer and mixing processes. At the highest impeller speeds (regime (5)), significant circulation loops and gross recirculation are observed and high turbulence at the surface promotes gas entrainment (surface aeration) (Nienow et al., 1977). The progression of these bulk flow regimes are also shown in Figure 6.5 (Nienow et al., 1985).

Nishikawa et al. (1984) determined that when negligible gas dispersion occurs, impeller type, location, or separation are irrelevant. In other words, if the total power input to the system is dominated by the sparged gas, the mixing in the STR approximates a bubble column. This effect was, however, recognized to occur at small power inputs, and the impeller power would start to dominate hydrodynamics and mass transfer at 30 W/m^3 for Rushton-type impellers (Gagnon et al., 1998). This power level is almost never observed in application since most gas–liquid dispersion with STRs occurs in the range of 500–4000 W/m^3 (Bliem and Katinger, 1988b; Bredwell and Worden, 1998; Oldshue, 1983).

The flow regime transitions can be determined from a gassed power number (or gassed-to-ungassed power ratio) versus flow number graph where the flow number is defined as

$$Fl_G = \frac{Q_G}{ND_i^3} \tag{6.1}$$

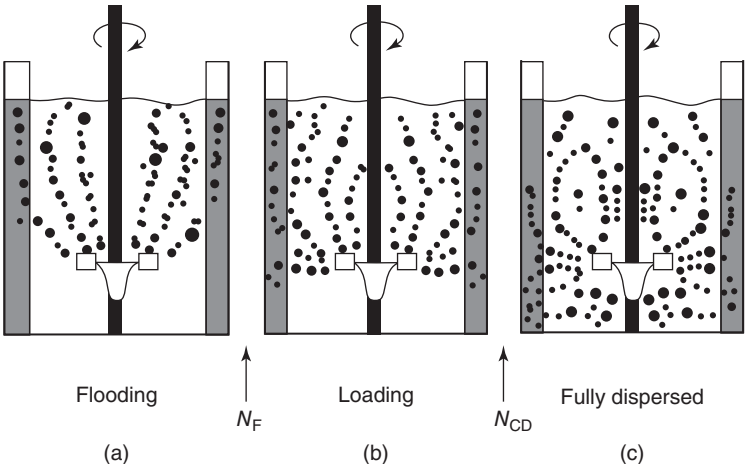

Figure 6.5 Loading regimes and transitions for radial flow impellers, where N_{FL} indicates a transition from flooded to loaded regimes and N_{CD} defines the transition to completely dispersed flow regime (Jade et al., 2006).

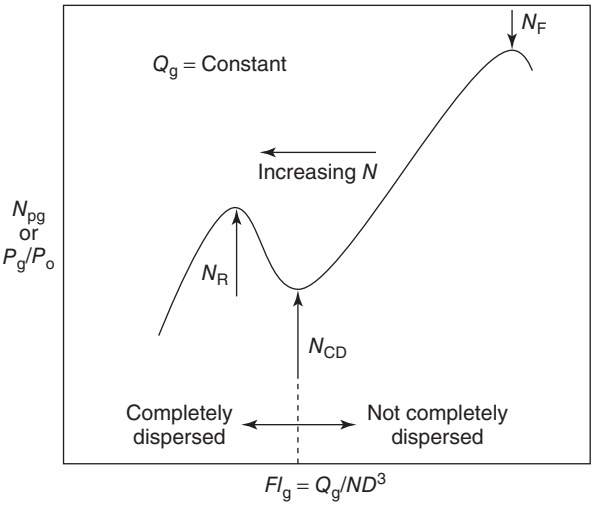

Figure 6.6 Generic transition plot (Kapic, 2005).

where Q_G, N, and D_i are the volumetric flow rate, impeller speed, and impeller diameter, respectively. Generic and experimental examples are shown in Figures 6.6 and 6.7, respectively. Flooding occurs at a local maximum of this graph represented by a flooding transition impeller speed N_F. It has also been defined as the transition point from regime (3) to regime (2) in Figure 6.4 (by decreasing N). The local minimum for the graph holds a special place. It represents the minimum power

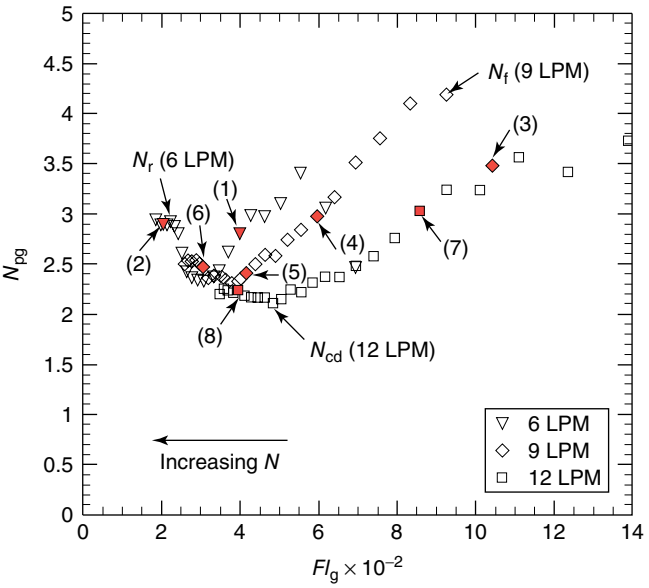

Figure 6.7 Experimental transition plot. The numbered data points represent specific conditions tested by Ford et al. (2008).

input required to achieve bulk flow regime (4), also known as complete dispersion or recirculation. The reactor should be operated such that $N > N_{CD}$; this represents the most economical operation in terms of power usage and gas utilization. Mixing time, which is defined as the time required to mix incoming fluid homogeneously into the existing liquid volume, is also optimized, but it is still higher than in an unaerated system (Hadjiev et al., 2006). If the impeller speed is increased beyond the complete dispersion impeller speed, the power use increases (Nienow et al., 1985; Smith and Warmoeskerken, 1985).

A second local maximum that follows represents the transition to the gross recirculation flow regime. This impeller speed, identified by N_R, should be avoided because it leads to inefficient gas utilization and gas entrainment. If an oxygen probe were to be positioned near the entrained gas, oxygen depletion would be a matter of time and a reduction in $k_L a$ would be recorded. In other words, the impeller should be operated between N_{CD} and N_R to achieve maximum efficiency. The transition between these flow regimes and their representative impeller speeds has been shown to be a function of impeller type, D_i/T, and scale. Given a D_i/T and an impeller type, the transition impeller speeds are scale independent, but the rate at which the transitions occur is not independent. Larger vessels have a gradual transition while smaller vessels experience transition over a limited flow number range (Nienow et al., 1985; Smith and Warmoeskerken, 1985). As shown in Figure 6.7, increasing the gas flow rate leads to smoother and delayed transitions.

6.2.2 Axial Flow Impellers

Axial flow impellers direct the fluid flow within the STR along the axis of the rotating shaft. Propeller-type impellers offer a simple example. In down-pumping axial flow impellers, the fluid is pumped downward while the gas is introduced below the impeller. The cavity propagation of axial flow impellers (Figure 6.8) is similar to the Rushton-type turbine, but gas dispersion differs in that pulsation forces gas to leave the impeller zone via the cavity tail (McFarlane et al., 1995). As shown in Figure 6.8, low impeller speeds and gas flow rates form vortex cavities at the impeller blade tip. Increasing the gas flow rate leads to the creation of a clinging cavity. The creation of larger cavities on axial flow impellers requires an increase in the gas flow rate and the impeller speed. A minimum impeller speed is needed to support larger cavities. If this minimum is not met, axial flow impellers experience vortex shedding such that the vortex detaches from the blade, leading to the next vortex creation cycle. This shedding can cause variations in torque and power draw, but usually do not cause any problems (McFarlane et al., 1995).

Incipient large cavities are formed in axial flow impellers if the gas flow rate is increased and the minimum impeller speed requirement is met. This cavity type occupies more space than the clinging cavity but disperses gas in a similar pulsating fashion. At a higher gas flow rate, large, fully developed cavities form, which occupy almost the entire blade area, but they do not extend beyond the impeller blade edge. When large cavities are present, the liquid and gas are discharged predominately in a radial direction from the impeller zone. Prior to flooding, the large cavity loses its defined boundary and blends into the flow. Once the impeller is flooded, the cavity structure is completely lost and gas simply passes through the impeller zone without any breakage or dispersion (McFarlane et al., 1995).

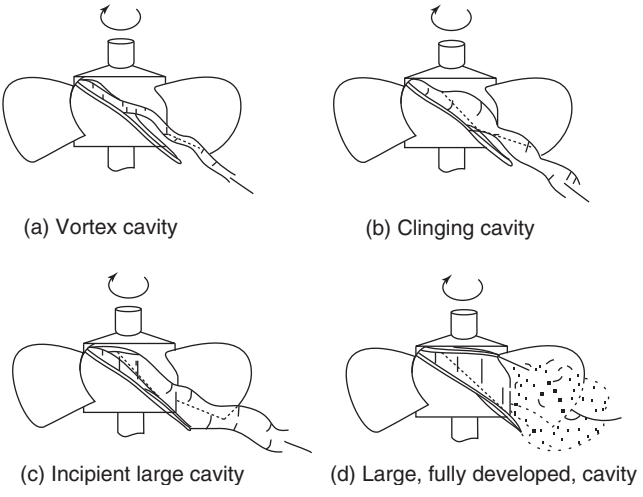

Figure 6.8 Cavity types for axial flow impellers (McFarlane et al., 1995).

Unlike the Rushton-type turbine, cavities on axial flow impellers are rarely stable and frequently change shape, size, and identity, which can induce different gas loading regimes as well as torque and power draw variations. If gas enters the impeller zone via the impeller-induced liquid flow, the impeller is said to be loaded indirectly. In contrast, direct loading is defined by sparged gas-controlled flow into the impeller zone. In other words, the impeller-generated flow is not able to deflect the sparged gas. The transition leads to changes in the cavity size, shape, and identity, which are significant for large cavities (McFarlane et al., 1995).

Down-pumping axial flow impellers exhibit different bulk flow regimes at low and high gas flow rates due to the effects of large cavities; this phenomenon differentiates axial flow impellers from radial flow impellers; however, the major regimes (flooding, loading, and complete dispersion) have similar characteristics. McFarlane et al. (1995) used an A-315 (axial flow impeller) for visualization purposes and noted that other down-pumping axial flow impellers exhibit similar behavior. Figure 6.9 depicts A-315 behavior as described by McFarlane et al. (1995) for low gas flow rates (relative to scale and power draw). The figures progress from (a) to (d) in terms of increasing impeller speeds. In (a), the impeller is flooded at a low impeller speed. Gas rises easily through the impeller zone and behaves similar to flooded radial flow impellers. Increasing impeller speed induces minor recirculation

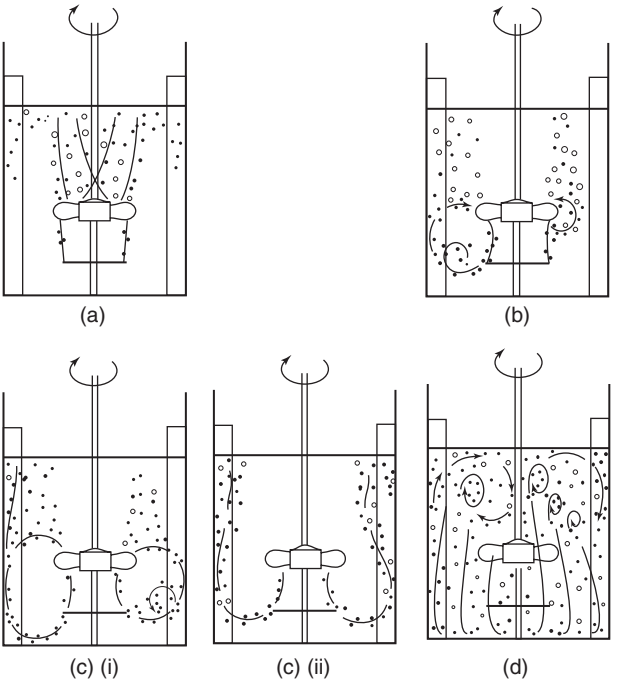

Figure 6.9 Bulk flow regimes generated by down-pumping A-315 at low gas flow rates (McFarlane et al., 1995).

loops in the impeller vicinity, and the impeller is said to be directly loaded. The transition between (b) and (c) signals the direct–indirect transition such that the impeller is partially directly and indirectly loaded. Increasing the impeller speed further leads to indirect loading (c). Cavity oscillations cause the bulk flow to vary between asymmetric (i) and occasional symmetric (ii) flow patterns. Variations in cavity type and loading are not damaging to the motor and gearbox because the flow remains mostly axial throughout the process such that the torque and power draw variations are limited. Further increase in impeller speed leads to complete dispersion as shown in (d) (McFarlane et al., 1995).

McFarlane et al. (1995) describe different flow patterns when relatively high gas flow rates are present (Figure 6.10). At higher gas flow rates and beyond a minimum impeller speed, large cavities form and have a significant impact on flow stability and bulk flow regimes. Flooding occurs in the same manner as with low gas flow rates (a). If the impeller speed is above a threshold, large cavities form causing a significant loss in pumping capacity; this is accompanied by direct loading and a significant radial and axisymmetric flow pattern as shown in (b). The impeller cavity distribution is also axisymmetric. The transition from direct to indirect loading is shown in (c). An increase in the impeller speed induces oscillations between predominantly radial (i) and axial (ii) flow. Occasional cavity shedding induces

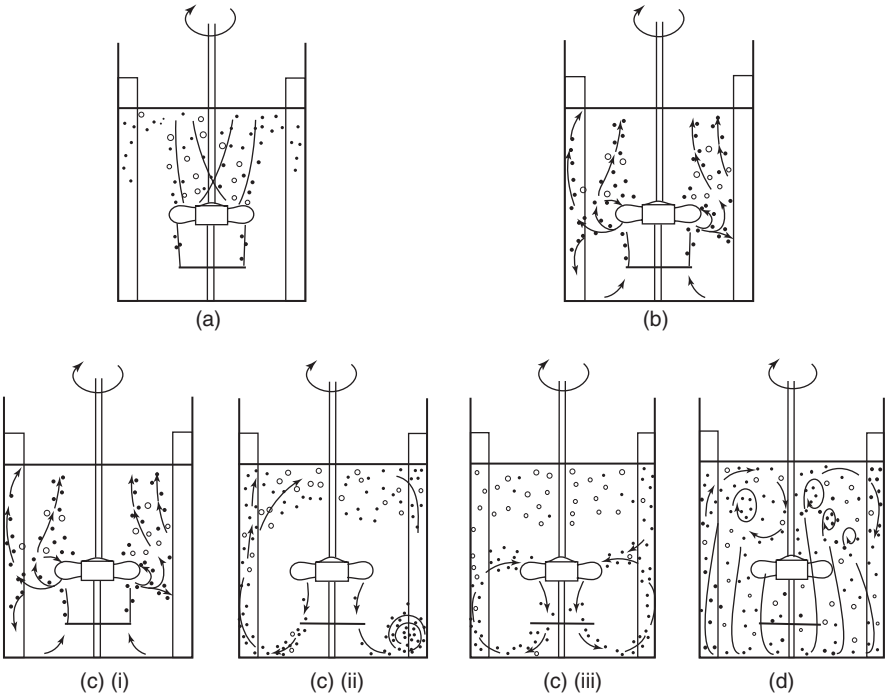

Figure 6.10 Bulk flow regimes generated by down-pumping A-315 at high gas flow rates (McFarlane et al., 1995).

impeller dominance which would force gas to the tank bottom (iii); however, this event is temporary, and flow eventually reverts back to radial or oscillating dominance. This series of events occurs over a very short impeller speed range and a subsequent increase results in proper loading and dispersion (d).

The oscillation in cavity size and flow direction (Figure 6.10c) can produce large and significant variations in power draw and torque such that the power number for the down-pumping A-315, for example, can vary between 0.84 and 1.48 at a frequency of 1–2 min. The variations in torque and power draw can have damaging effects on the motor and gear assembly (Tatterson, 1994) and can lead to vessel vibration (Sardeing et al., 2004b). In addition, large cavities tend to create asymmetric flow that can produce a significant bending moment on the impeller shaft, resulting in shaft damage. Smaller impellers at low power concentrations experience these problems much earlier because large cavities are able to form with a smaller amount of gas at these scales. Up-pumping axial flow impellers have a more stable oscillation because the sparged gas enters the impeller zone in the same direction as the fluid (McFarlane et al., 1995).

The detrimental effects of large cavity formations can be minimized by increasing the impeller speed. Reactor design improvements can be made such that large cavities require more gas or that the minimum impeller speed for large cavity formation is reduced. The goal is to reduce the impact on the normal operating range such that the event is outside normal parameters or induces fluctuations that are within the design specifications for the motor and gear assembly (McFarlane et al., 1995).

6.3 EFFECTS OF IMPELLER DESIGN AND ARRANGEMENT

The impeller provides mechanical agitation and gas dispersion. It is responsible for bubble breakup in gas-sparged STRs and for solid suspension in gas–liquid–solid STRs. Numerous impeller designs exist to meet various needs, and the economic success of a project depends on the evaluation and selection of a proper impeller in concert with reactor geometry (Ungerman and Heindel, 2007). A few standard impellers in gas–liquid dispersion are documented. Normal impeller-to-tank diameter ratio, D_i/T, is typically between 1/4 and 2/3 (Harnby et al., 1992) with the standard ratio being 1/3 (based on industrial experience) and rarely going above 1/2 (Tatterson, 1991). This geometry minimizes cost and is capable of providing a well-mixed state for the liquid phase and complete dispersion of the gas phase. An impeller with a larger D_i/T ratio proves inefficient and unnecessary. The impeller power draw is proportional to the impeller speed to the third power and the impeller diameter raised to the fifth power. It is, therefore, cheaper to operate an impeller at a faster speed than a larger diameter if more dispersion or blending is needed. Impeller clearance, defined as the distance between the impeller and tank bottom, is typically in the range $T/6$–$T/2$ (Tatterson, 1994) depending on the liquid viscosity, impeller type, sparger–impeller separation, and number of impellers.

Impellers usually enter the vessel from the top; however, very large or novel vessels find it useful for the impeller to enter from the bottom or side (Harnby et al.,

1992) because it can minimize the amount of structural steel needed to support the shaft and impeller (Aden et al., 2002). Impeller shafts usually have a circular cross-section and are oriented perpendicular to the reactor bottom and placed along the tank centerline. Other impeller shaft placement relative to the centerline, known as impeller eccentricity, has been practiced (Tatterson, 1991). Off-centering the impeller shaft has been shown to improve mixing, minimize the appearance of vortices (Oldshue, 1983), and produce smaller bubbles in the turbulent regime (Cabaret et al., 2008). Shaft eccentricity (changing the cross-sectional shape) minimizes vortices and can be used in place of baffles. In these applications, mixing time decreases while power input increases. Industrial applications may find this configuration undesirable due to construction and maintenance costs (Cabaret et al., 2008).

Impellers can be classified into groups based on the liquid viscosity used in the reactor (Harnby et al., 1992). Propellers, turbines, and paddles have a higher tip speed relative to other impeller types and are used for low viscosity Newtonian liquids that are encountered in most processes (Ogut and Hatch, 1988). Propellers are usually operated faster and paddles are operated slower than turbines. The standard three-bladed propeller has poor gas–liquid dispersion and contacting characteristics and will be excluded from further discussion.

6.3.1 Radial Flow Impellers

A more common impeller classification is by flow leaving the impeller zone. Impellers can be classified into radial or axial flow impellers. Some examples of radial flow impellers are the Narcissus impeller (NS), concave blade disc turbine (Figure 6.11), (Chemineer) BT-6, and the multibladed disc turbine. A six-bladed disc turbine, shown in Figure 6.12, is often referred to as a Rushton-type turbine (RT) (Ulbrecht and Patterson, 1985). The standard blade is $D_i/4$ long and $D_i/5$

Figure 6.11 Concave impeller.

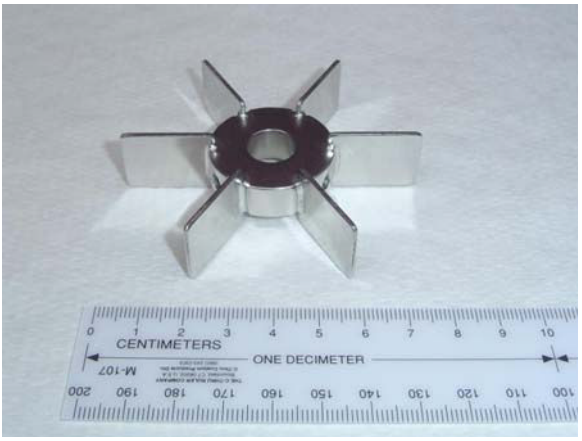

Figure 6.12 Rushton-type turbine.

wide (Oldshue, 1983). Increasing the number of blades (12 or 18) produces similar recirculation as the standard RT, but reduces the power draw drop upon gassing (Smith et al., 1977). Increasing the number of blades, however, increases the ungassed power number from ~5 to 8–9 (Nienow, 1996), which diminishes the use of a disc turbine with higher blade numbers as a mixing device (Nienow et al., 1995). Turbine designs using retreating, angled, or hollow-faced blades are in existence, but have not been able to compete with the Rushton-type turbine for gas–liquid dispersion tasks (Harnby et al., 1992; Williams, 2002).

The Rushton-type turbine has been the most popular impeller for gas–liquid dispersion since the 1950s (Nienow, 1996). It has very good bubble breakup and gas dispersion capabilities leading to good mass transfer characteristics (Cabaret et al., 2008; Williams, 2002). It is the measuring stick to which other gas–liquid impellers are compared. The high power number of the Rushton-type turbine, which is a disadvantage for mixing purposes, is an advantage for gas–liquid dispersion. The RT is capable of creating higher maximum shear zones and produce smaller bubbles. Smaller bubbles lead to a higher interfacial area, which in turn increases the mass transfer capacity. In addition, the disc feature of the RT prevents gas bubbles from passing through the lower shear region and forces the gas flow through the high shear impeller tip region (Oldshue, 1983; Tatterson, 1991). These features give the Rushton-type turbine $k_L a$ values that are an average of 50% higher than other impellers operating under similar conditions (Sardeing et al., 2004a).

Although commonly used, Rushton-type turbines exhibit several negative traits. Some are design specific, but others are shared by all radial flow impellers. This is mainly due to the fact that newer radial impellers were designed with the goal of improving on a small number of disadvantages (Nienow, 1996). The RT experiences a power draw drop of 50–65% upon gassing (McFarlane and Nienow, 1996b). This weakness is purely operational, but forces the reactor to have a complicated gearbox design (Ulbrecht and Patterson, 1985), which adds to the installation

and maintenance costs. Concave (hollow) and 12- or 18-blade disc turbines can be used to minimize this effect. They form smaller cavities on the blade backside relative to the standard RT (Smith et al., 1977). The smaller cavities lead to much smoother power curves and less variation in power draw upon gassing (Ungerman and Heindel, 2007), and hence lead to simpler gearbox designs (Ulbrecht and Patterson, 1985).

Concave blade disc turbines are of interest in gas–liquid dispersion because they are able to handle more gas than Rushton-type turbines before flooding (Smith et al., 1977; Vasconcelos et al., 2000). The mass transfer capacity for the concave blade disc turbine is very similar to the Rushton-type turbine, but Chen and Chen (1999) found that the blade curvature could be optimized for a certain power input to produce higher gas–liquid mass transfer coefficients. Unlike the Rushton-type turbine, the concave blade disc turbine requires the cup orientation to be in the direction of impeller rotation (Tatterson, 1994).

Vasconcelos et al. (2000) investigated the influence of the impeller blade shape, shown in Figure 6.13, on gas–liquid mass transfer. They concluded that the importance of blade shape was negligible for disc turbines as long as the power number, power draw drop upon gassing, and gas flow rate were similar. Other authors have come to a similar conclusion, but also stipulated that the process has to be in the turbulent regime (Nienow, 1996). Angled, concave, and lancelet blade disc turbines not only provided lower impeller power numbers but also offered smaller power draw drops upon gassing and smaller, if any, gas cavities. Hence, they are more efficient and capable of handling gas. Increasing the impeller diameter could discount the power draw disparity while allowing retrofitting to be easily accomplished. As such, the retrofitted system would provide similar gas–liquid mass transfer performance and would handle more gas, potentially allowing for an increased operational range and gas–liquid mass transfer.

Another major weakness for radial flow impellers stems from one of the strengths: the high shear rates. The power dissipation (or shear) rates are concentrated at the blade tips (Gagnon et al., 1998) and are not uniformly distributed throughout the reactor (Fujasova et al., 2007; Ungerman and Heindel, 2007). This unbalanced shear distribution can lead to stagnant zones in the outer reactor region (Bellgardt, 2000b) and higher mass transfer in the impeller stream relative to the working volume (Stenberg and Andersson, 1988a, 1988b). According to Stenberg and Andersson (1988b), 50% of the energy is dissipated in the impeller stream, 20% is dissipated in the immediate impeller vicinity, and 30% is dissipated through the rest of the reactor. This disparity leads to radial flow impellers, especially the RT, providing very poor top-to-bottom mixing (McFarlane and Nienow, 1995), particularly in more viscous fluids.

If a constant impeller speed scale-up rule is used, the impeller tip energy dissipation rate will increase due to its connection to the impeller diameter (Bliem and Katinger, 1988b). The power decay is more pronounced in larger vessels and contributes to scale-up issues (Figueiredo and Calderbank, 1979). This concentration leads to the local energy dissipation rate in the impeller vicinity being up to 270 times higher than the average. Furthermore, the local rate experiences large

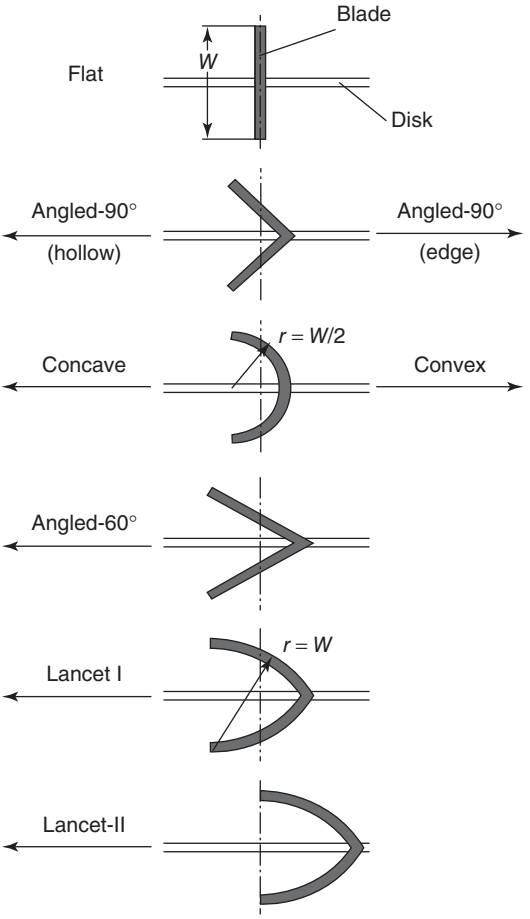

Figure 6.13 Possible blade shapes for use with disc turbines (Vasconcelos et al., 2000).

fluctuations creating problems in scale-up and reactor design comparisons. These high shear fluctuations can be harmful to some bioreactor microorganisms (Bliem and Katinger, 1988a, 1988b; Bredwell and Worden, 1998).

Finally, the fluid can experience low bulk circulation leading to low gas holdup in the bottom reactor section (Fujasova et al., 2007; Ungerman and Heindel, 2007) and gas compartmentalization (Moucha et al., 2003). Gas compartmentalization is to be avoided since it poses the danger of spent gas entrainment or gas starvation. Spent gas is inactive in production and limits the practical working volume (Fujasova et al., 2007) while gas starvation can limit the effectiveness of the microorganisms (Pollack et al., 2008).

As scale increases, a proper mixing state gains in importance that can lead to radial flow impellers, providing very poor mixing conditions in a significant portion of the reactor volume (McFarlane and Nienow, 1995). The solution has been to

simply operate the impeller at a faster speed that can have detrimental effects on microorganisms, power usage, and impeller characteristics. Retrofitting a system with a larger radial flow impeller to resolve some of these problems is not usually possible because different turbine diameters produce very different torques. The higher torque of a larger diameter turbine can be damaging for the motor and drive train to the point that this practice is seen as high risk–low reward and rarely implemented (McFarlane and Nienow, 1995). The smoother power curves of the concave blade turbine are very promising for this purpose and should be seriously considered.

Chen and Chen (1999) investigated the possible replacement of the RT. The comb blade and perforated blade disc turbine were found to have higher $k_L a$ values than the standard RT at similar power inputs. They came to the conclusion that bubble breakup was not only a function of the shear-gradient magnitudes, but also the amount of time the gas phase remained in the shear field. By spatially increasing the shear field, bubbles spent longer time periods in this region and decreased the probability that larger bubbles would pass through this region without significant breakup. The results were that the comb and perforated blade disc turbine produced $k_L a$ values that were almost 12% and 30%, respectively, higher than the Rushton-type turbine at the same power input and superficial gas velocity while producing lower shear-gradient magnitudes. Currently, there is no available information of these impellers being used in processes involving microorganisms.

6.3.2 Axial Flow Impellers

Many attempts have been made to replace radial flow impellers with axial flow impellers. Examples of axial flow impellers include the Lightnin A-310 (Figure 6.14), Lightnin A-315 (Figure 6.15), pitched blade turbine (PBT) (Figure 6.16), Techmix 335 (TX), Prochem Maxflo T, SuperMIG (EKATO), marine propeller, A-3 impeller, or a multibladed paddle. The PBT and hydrofoil impellers, such as the Lightnin A-315, are the most commonly used axial flow impellers. These devices have a much lower power number than radial flow impellers that make them ideal for mixing purposes. Their blending prowess is due to the fact that the mixing time is independent of the impeller type (Nienow, 1996). Hence, the operation can be accomplished at a lower cost with axial flow impellers; however, as shown in Figure 6.17, axial flow impellers are usually inferior to radial flow impellers for mass transfer purposes. They usually produce flow in the axial direction, but can create some radial flow if $D_i/T > 0.5$ (Tatterson, 1991). This situation is usually avoided since the standard low viscosity impellers have a D_i/T ratio of about 1/3 (Harnby et al., 1992).

Axial flow impellers used in low bottom clearance tanks can also create radial flow if the direction of the flow is downward. In this case, the flow can leave the impeller zone only by flowing in the radial direction (Tatterson, 1991). This phenomenon is usually not observed since the standard bottom clearance for low viscosity impellers in gas–liquid dispersions is between one impeller diameter and one half the tank diameter (Ulbrecht and Patterson, 1985). The hydrofoil impeller

Figure 6.14 Lightnin A-310 axial flow impeller.

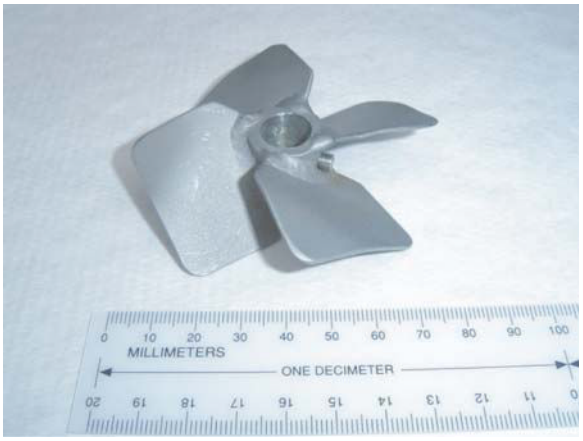

Figure 6.15 Lightnin A-315 axial flow impeller.

discharge is affected by the impeller Reynolds number.[1] If the system is operated with a viscosity such that *Re* is about 5000, the flow becomes more and more radial. This change could have a significant impact on mixing and gas dispersion and would be especially important for viscous non-Newtonian bioprocesses (McFarlane and Nienow, 1995).

The PBT discharges fluid from the impeller zone at an angle of 45–60°. The standard design has flat blades that are 45° from the horizontal and have a 1/5 blade width-to-diameter ratio. This discharge angle causes a significant radial component

[1]Reynolds number is defined in Eq. (3.11) in Section 3—Gas–Liquid Mass Transfer Models.

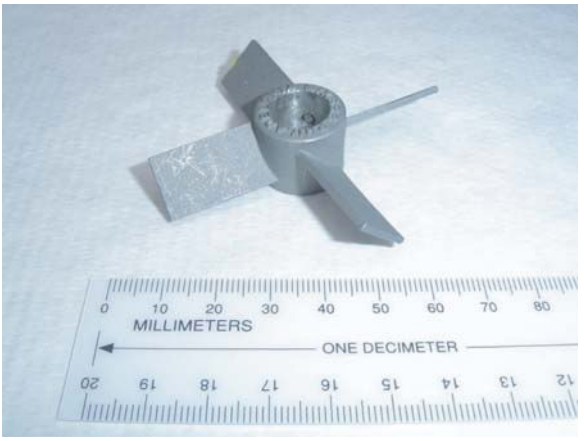

Figure 6.16 Pitched axial flow impeller.

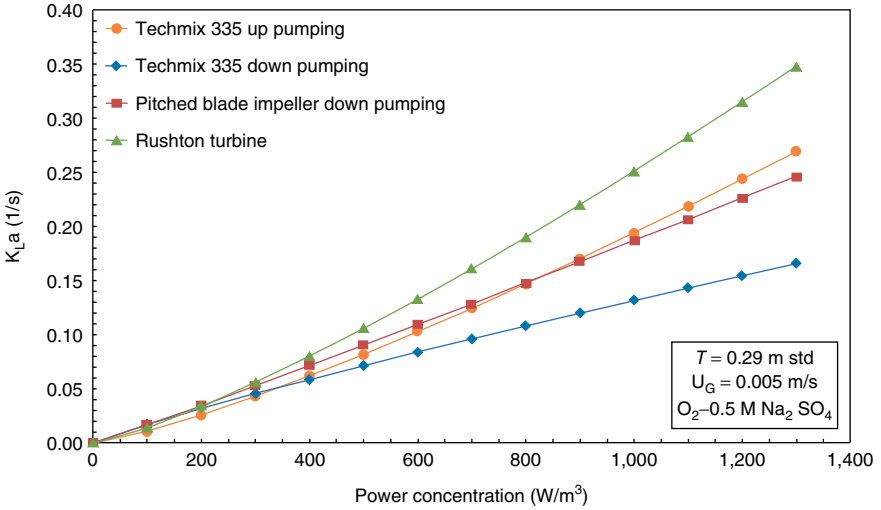

Figure 6.17 Gas–liquid mass transfer for various impeller types. Adapted from Moucha et al (2003).

regardless of the impeller size or position, which has led to the PBT to being classified as a mixed impeller in the axial family (McFarlane and Nienow, 1995). These features make the PBT an excellent mixing device. The mixing (blending) time is reduced and heat transfer is improved; however, the PBT makes a bad impeller for gas breakup. Gas bubbles are led to the blade tip where they are sliced apart, but the blade shape does not accumulate bubbles in a sufficient manner. Therefore, a large number of bubbles pass through the impeller zone without interacting with the breakup mechanism (Martín et al., 2008b). The solidity ratio, which relates the

impeller blade area to the impeller swept area, is about 0.43 for the PBT (Oldshue, 1983). Low solidity ratio impellers flood before radial flow impellers and high solidity ratio impellers, so their use in gas–liquid processes in single impeller systems is atypical (Ungerman and Heindel, 2007).

In order to reduce flooding, high efficiency hydrofoil impellers, distinguished by their profiled blades (McFarlane and Nienow, 1995), were introduced. These impellers, such as the Lightnin A-315 (see, e.g., Figure 6.15), have a much higher solidity ratio of about 0.87, have a smaller power draw drop upon gassing (30–50%) (McFarlane and Nienow, 1996b), and flood later (Ungerman, 2006) than radial flow impellers. It is therefore capable of handling more gas than the radial or PBT impellers (Chen and Chen, 1999). In fact, it can handle 86% more gas than a Rushton-type turbine before flooding (Yawalkar et al., 2002b) and 40% more gas than the PBT before the onset of gas loading transition (described in Section 6.2.2) (McFarlane and Nienow, 1996b). However, the A-315 is still an axial flow impeller and produces lower shear gradients relative to the Rushton-type turbine. The advantage of using the A-315 over an RT depends upon the gas flow rates and shear sensitivity of the microorganisms. If neither of these situations is important, the RT is still the better choice. If the gas flow rates are of importance but shear sensitivity is not, the concave blade disc turbine is the more effective impeller.

The axial flow direction makes particulate suspension easier relative to radial flow impellers (Tatterson, 1991). Axial flow impellers are also better blending devices because they have a lower power number—hence power usage—and shorter blending times; however, results for gas–liquid contact have been unimpressive relative to the Rushton-type turbine, and axial flow impellers tend to have smaller gas–liquid mass transfer coefficients. In addition, large reactors using axial flow impellers have shown highly asymmetric and oscillating gas holdup distributions with periods of up to several minutes (Bakker and Oshinowo, 2004). Therefore, their use has been limited to mixing and shear normalizing in multiple impeller gas–liquid systems (Bouaifi et al., 2001) and mixing and solid suspension in single impeller systems (Oldshue, 1983).

The direction of the flow, up or down, depends on the geometry and rotation of the axial flow impeller. In general, up-pumping impellers push the gas to the surface faster (lower gas holdup) while down-pumping impellers induce recirculation and longer residence times, defined as the time a particle spends in the reactor, which leads to higher gas holdup (Moucha et al., 2003). These circulation loops are important with respect to gas holdup and contribute to multiple impeller systems offering 30% higher gas holdup values than single impeller systems (Bouaifi et al., 2001). The down-pumping impeller also offers shorter mixing times, which can lead to lower operational costs in systems where mixing is important (Gogate and Pandit, 1999a).

Some researchers, on the other hand, do not find a preference for up- or down-pumping axial flow impellers (Fujasova et al., 2007), or find that the up-pumping configuration produces more macromixing than down-pumping systems, which can lead to smaller bubble diameters (Majirova et al., 2004; Sardeing et al., 2004b). Sardeing et al. (2004b) observed that gas holdup in

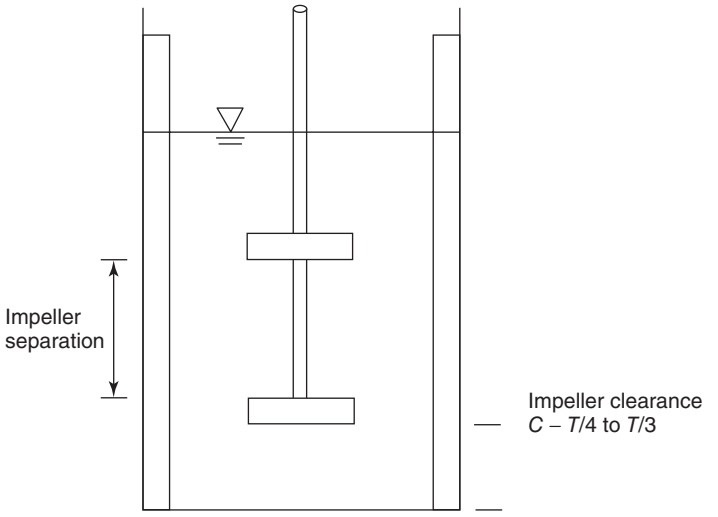

Figure 6.18 Standard multiple impeller stirred-tank reactor design.

the up-pumping configuration was determined to be 10–25% higher than the down-pumping orientation. The gas holdup conclusions were drawn based on constant impeller speed data. Down-pumping axial flow impellers also have significant stability and hydrodynamic problems in certain operating ranges, which may have contributed to the up-pumping axial flow impeller's superior gas holdup performance (McFarlane and Nienow, 1995; McFarlane et al., 1995). Sardeing et al. (2004b) focused on power concentration, which they indicated to be more relevant, and the down-pumping PBT was determined to be more efficient than the up-pumping PBT, confirming similar conclusions made by others (Bouaifi and Roustan, 2001; Gogate and Pandit, 1999a; Moucha et al., 2003).

6.3.3 Multiple Impeller Systems

Multiple impeller STR designs, schematically represented in Figure 6.18, are very popular in practice (Nocentini et al., 1998) and were implemented due to shortcomings of the single impeller system and industrial requirements. For example, when a single impeller system is used in an industrial-scale reactor, it may not provide proper agitation and gas dispersion in large reactors. In addition, viscous or non-Newtonian liquids do not mix well in a single impeller system. Large gas-filled cavities on the back of the impeller blades also limit the amount of gas that can be properly dispersed in a single impeller STR (Cabaret et al., 2008).

Multiple impeller systems are able to distribute energy throughout the reactor more efficiently, which leads to a more homogeneous shear rate distribution. Liquid circulation and gas dispersion are also improved, leading to longer gas-phase residence times. These factors lead to better gas utilization, higher gas–liquid mass transfer coefficients (Bouaifi and Roustan, 2001; Cabaret et al., 2008; Fujasova

et al., 2007; Moucha et al., 2003; Nocentini et al., 1998), longer gas-phase residence times, better bulk flow characteristics (Shewale and Pandit, 2006), and higher gas holdup (Bouaifi et al., 2001; Bouaifi and Roustan, 2001; Shewale and Pandit, 2006) relative to single impeller systems. The industrial implementation of multiple impellers can be made to single impeller systems with minimal retrofitting and without changes to the motor and gearbox (Lines, 2000), especially if the addition is an axial flow impeller (McFarlane and Nienow, 1995).

In order to achieve a proper working condition, however, proper impeller placement has to be considered. The bottom clearance for most multiple impeller designs is between $T/4$ and $T/3$. If the impellers are too close to each other, impeller–impeller interference can lead to inefficient operation and an inability to separate operational inputs; this would add complications without enhancing efficiency. Interference also provides limited, if any, increase in $k_L a$ (Nishikawa et al., 1984). The power draw for a multiple impeller configuration will be normal upon start-up, but may decrease by about 70% of the initial value and remain at those levels throughout the process when the impellers are too close. The flow patterns of interfering impellers may also exhibit characteristics of a single impeller system (Mishra and Joshi, 1994), leading to negligible improvements and increased costs (Oldshue, 1983). For example, a second RT has been reported to increase $k_L a$ by 74% if placed correctly, but would provide no improvement if interference occurred (Nishikawa et al., 1984).

The separation between impellers depends on the impeller type, but should be a minimum of $1D_i$ (Linek et al., 1996b). The Rushton-type turbine, for example, requires a separation of $1.5D_i$, but $2D_i$ would be preferred to ensure independence (Fujasova et al., 2007). Linek et al. (1996b) found that if the impellers were acting independently, each impeller's mass transfer characteristics could be evaluated as a single impeller system. The overall mass transfer coefficient could be calculated using a weighted average, with the lower and upper sections having weights of 0.25 and 0.75, respectively (Linek et al., 1996a). However, this approach failed using non-coalescing media and was not proven at larger scales (Linek et al., 1996b).

Although common shafts are standard, dual-shaft systems have been investigated. Dual shafts allow the impellers to spin at independent speeds and directions. Although this configuration adds to setup and maintenance costs, it provides operational flexibility. Since the amount of gas that passes through each impeller zone differs, independent controls allow optimal operation for each impeller. Cabaret et al. (2008) found that the upper impeller needs to run 20% faster for homogeneous gas distribution. Dual shafts can also accommodate counter-rotation. Cabaret et al. (2008) claim that counter-rotating Rushton-type impellers in unbaffled tanks is just as efficient as standard, baffled operation. The costs of implementing dual shafts would usually be expected to outweigh any gains made using dual impellers in low viscosity liquids.

The impeller is the key component for proper STR operation, especially for multiple impeller systems. A proper selection procedure has to consider numerous options and their applicability to the particular process of interest. A mixed

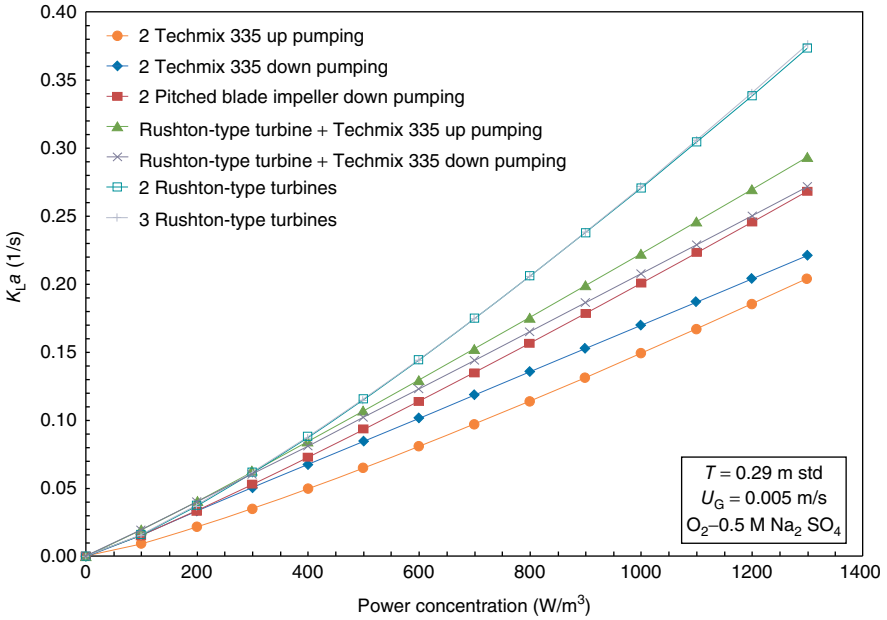

Figure 6.19 Effects of multiple impellers on gas–liquid mass transfer in an STR. Adapted from Moucha et al. (2003).

configuration using a radial and axial flow impeller is assumed to be more efficient for gas dispersion and mixing in a low viscosity Newtonian fluid than in a dual axial or radial configuration, even though the Rushton-type turbine combination provides better $k_L a$ (see, e.g., Figure 6.19). Efficiency, in this case, is defined as the capability to maximize gas–liquid mass transfer while minimizing power input (Gagnon et al., 1998). It is often advantageous to use a Rushton-type or concave blade turbine as the bottom impeller. This impeller would provide optimal bubble breakage. The upper impeller can be a down-pumping axial flow impeller to enhance gas–liquid circulation (Puthli et al., 2005).

Experiments using a radial setup are often performed to set the bar for mass transfer comparisons. Gagnon et al. (1998) contributed to this discussion by investigating the effect of adding impellers to the same reactor. A second Rushton-type turbine increased gas holdup, gas residence time, and the gas–liquid mass transfer coefficient. The addition of a third Rushton-type turbine increased these further, but at a much lower amount. They came to the conclusion that gas holdup and, subsequently, gas–liquid mass transfer does not increase linearly with the number of impellers and power drawn. Moucha et al. (2003) came to a similar conclusion when going from 1RT to 2RT but, as shown in Figure 6.19, the additional mass transfer was insignificant when the increase was made from 2RT to 3RT.

The mixed configuration efficiency and the declining increase in $k_L a$ with increasing number of turbines are determined by the impeller loading. The bottom

impeller is loaded directly (by sparged gas) while the other impeller(s) are loaded indirectly (by impeller-generated flow loops). Direct loading enhances gas dispersion capabilities of the Rushton-type turbine, while indirect loading puts more emphases on liquid mixing efficacy. Impeller loading is a more important consideration in experimental-scale reactors. Larger industrial-scale reactors require more effective blending and top-to-bottom mixing than the Rushton-type turbine can provide (Bouaifi and Roustan, 2001; Fujasova et al., 2007). The Rushton-type turbine is oftentimes limited in this regard, and the conditions created in these impeller zones (cells) are more geared toward axial flow impellers (McFarlane and Nienow, 1995).

Furthermore, radial flow impellers' discharge divides the reactor volume into well-mixed systems with minimal interchange (Nienow, 1996). As a result, radial flow impellers in large-scale systems may produce compartmentalization, caverns (impeller is encased by its flow field while most of the reactor is stagnant), higher gas recirculation, and low volumetric exchange zones (Nocentini et al., 1998). For large STRs, the combination of a radial flow impeller on the bottom and a down-pumping axial flow impeller on the top enhances the reactor fluid mixing such that the reactor volume contact is maximized with minimal power input (Fujasova et al., 2007; Vasconcelos et al., 2000).

Some discrepancies and opposing suggestions in the literature can be explained by using the studies of Linek et al. (1996a) and Nocentini et al. (1998). They found unequal amounts of gas pass through each impeller section regardless of loading type, resulting in gas distribution nonuniformity that can lead to the bottom impeller being flooded far earlier than the others. Since the bottom impeller contacts the most gas and is responsible for initial bubble breakup, flooding of this impeller is severely detrimental to system operation (Nocentini et al., 1998).

Linek et al. (1996a) concluded that the bottom impeller section had gas holdup and mass transfer values that were 15% and 45%, respectively, lower than the upper section when the STR was filled with non-coalescing media (0.5 M Na_2SO_4). Similar conclusions were reached when using water, with the upper section producing higher $k_L a$ values by 15%. This also implies that impeller power consumption was not balanced, that is, one of the impellers consumed more power and created higher shear gradients than the other, producing higher k_L and a values for the upper reactor section. The problem is made worse due to the fact that gas tends to coalesce faster and easier in regions of low power (relatively speaking), creating larger bubbles that reduce the interfacial surface area and possibly lowers k_L. Coalescence, however, would be far less likely in non-coalescing media, which should explain the results of Linek et al. (1996a).

Bouaifi et al. (2001) found that the average bubble diameter was larger in the bottom section of the reactor than the upper section. They concluded that bubbles formed a distribution such that the larger bubbles were in a region outside the impeller stream and were up to four times larger than the bubbles entrained in the impeller stream. More specifically, gas in these setups would concentrate about the impeller shaft, impeller tip, and within the radial area between the impeller and reactor walls (Boden et al., 2008; McFarlane and Nienow, 1996a).

These observations were made for an axial system, but are very similar to those made by Stenberg and Andersson (1988b) for a 1RT setup, which produced a similar qualitative mass transfer behavior for these impeller types.

Bouaifi et al. (2001) also observed that a "very heterogeneous bubble distribution" would form in a dual axial flow impeller system once the bottom impeller was flooded. If the impeller was properly loaded and complete dispersion occurred, 50–60% of the bubbles had a diameter of 1–3 mm. Thus, it was more effective to operate in the loaded and completely dispersed regimes. These experiences confirm and explain the unbalanced mass transfer performance observed by Linek et al. (1996a, 1996b) and Gagnon et al. (1998) in multiple impeller systems, and by Bellgardt (2000b), Moilanen et al. (2008), and Stenberg and Andersson (1988a, 1988b) in single impeller systems.

The impeller choice in multiple impeller reactors is therefore vital. A proper selection requires a minor power increase by about 15% to produce similar $k_L a$ of a Rushton-type setup but with a much friendlier environment for microorganisms and larger scales (Fujasova et al., 2007). The required radial and axial flow impeller often depends on the operational conditions. The simplest configuration includes a Rushton-type turbine for the lower impeller and a down-pumping PBT for the upper turbine(s). Since these impellers tend to flood relatively early, it has been proposed to replace the Rushton-type turbine and down-pumping PBT to extend the operational use. For example, Pinelli et al. (2003) did not find an advantage of using two Rushton-type turbines over two BT-6 impellers (asymmetric concave blade impellers designed by Chemineer). Gas holdup and macromixing were observed to be very similar, which would imply that the concave blade disc turbine could replace a Rushton-type turbine in a single or multiple impeller system without major hydrodynamic implications while providing more gas handling capacity (Vasconcelos et al., 2000). While holding power concentration and superficial gas velocity constant, Chen and Chen (1999) observed much higher mass transfer potential and smaller bubbles by replacing the RT with a comb and perforated blade disc turbine. The A-315 could replace the down-pumping PBT if a higher gas capacity is necessary. A more homogeneous environment is also expected with this replacement at larger scales because the A-315 (e.g., Figure 6.15) provides better recirculation exchange and interaction with the other impeller(s) (Bouaifi et al., 2001).

It is common to use multiple impeller systems in operations that are expected to undergo significant changes in viscosity and rheology. These processes are operated in the laminar regime that puts more emphases on the viscous behavior of the fluid. Multiple impellers have been determined to produce better gas–liquid mass transfer in viscous fluids than the commonly used helical ribbon impeller. Most researchers, however, spend time investigating low viscosity impeller combinations for viscous non-Newtonian applications (Tecante and Choplin, 1993). These low clearance impellers can require large amounts of power, making their operation impractical, especially for very viscous non-Newtonian liquids (Gagnon et al., 1998). In these cases, the operation is simply shut down if the impellers are not capable of providing proper conditions (Ogut and Hatch, 1988).

Cabaret et al. (2008) and Gagnon et al. (1998) concluded that better mixing and higher product conversion can be achieved if a close clearance impeller, such as the helical ribbon, is used in conjunction with a radial flow impeller such as the RT in a highly viscous system. The Rushton-type turbine provides proper gas dispersion, while the close clearance impeller attempts to contact most of the reactor volume and provides proper bulk mixing, shear distribution, lower apparent viscosity, and minimal stagnant zones (Tecante and Choplin, 1993). These effects also lead to higher reactor utilization and can decrease power requirements.

6.3.4 Surface Aeration

STRs are highly turbulent mixers which can induce a high degree of surface turbulence. Although the effects of turbulence in the reactor volume are known, the interaction at the gas–liquid surface can be complicated. Unbaffled vessels can experience flow destructive vortices and solid body motion at normal operating impeller speeds. If the vessel is baffled, these vortices tend to be minor, but their influence on mass transfer can be important. Highly turbulent surfaces allow the STR to entrain head space gas, effectively adding to the sparged gas flow rate. This phenomenon is referred to as surface aeration. Therefore, direct sparging, which has been the only option discussed so far, is not required. However, this form of indirect sparging affects impeller performance and reactor hydrodynamics in the same fashion as direct sparging (Patwardhan and Joshi, 1998).

Surface aeration is used in wastewater treatment, water aeration (e.g., fishing ponds), and processes requiring the gas-phase conversion to be maximized (toxic or highly valuable gases). If the system requires the gas phase to be recycled, surface aeration allows the reactor to be capped creating a dead-end system. Hence, a recycle gas compressor is not necessary, which minimizes fixed costs (Patwardhan and Joshi, 1999). Such reactor designs limit potentially toxic exposure, increase work reliably, and have limited maintenance costs. The lack of a sparger can further extend these benefits for processes containing an excessive amount of a solid phase such as wastewater treatment (Patwardhan and Joshi, 1998).

Surface aeration is most common in multiple impeller systems and/or semibatch and batch processes (Lines, 1999). Multiple impeller designs place an impeller relatively close to the surface that can induce surface aeration at relatively low impeller speeds. Most authors do not check for this phenomenon, and it is often unclear as to which models are used for the mass balance in the gas phase. The exclusion of a dynamic gas holdup term (assuming dynamic conditions) does not affect the results if surface aeration is limited; however, if surface aeration is significant, experimental errors could be large (Figueiredo and Calderbank, 1979).

The critical impeller speed for surface aeration (N_{CSA}) can be identified using indirect sparging. A simple $k_L a$ versus N graph produces a sharp increase in $k_L a$ at N_{CSA}. Direct sparging makes this identification more difficult. Although gas may be entrained, additional gas dispersion does not occur until the impeller speed is increased by about 20% above the initial entrainment speed. Other factors

controlling the surface aeration are impeller type and diameter, tank diameter, impeller clearance and submergence, baffling, and gas and liquid properties (Patwardhan and Joshi, 1998).

Surface aerators are, however, highly limited by impeller submergence and require an impeller to be very close to the surface in order to be effective. Furthermore, the operation becomes hampered with scale-up such that dead zones are common (Lines, 1999; Patwardhan and Joshi, 1998). Design and scale-up for surface aerated systems are even more challenging than a standard STR (Lines, 1999). As such, this reactor design is not capable of competing with conventional designs. However, surface aeration is an important phenomenon that occurs in STRs (Patwardhan and Joshi, 1998). Although it may not have a significant impact on gas–liquid mass transfer, it should be kept in mind especially if comparisons are to be made between competing designs. Many experimental reactors include an operating range that is much higher than traditional industrial applications (Benz, 2008). These designs may induce surface aeration and artificially increase mass transfer performance.

6.3.5 Self-Inducing Impellers

Self-inducing impellers are also used for indirect sparging purposes. The spinning action of the impeller creates a low pressure region at the impeller intake. Orifice holes are exposed to this low pressure region and connected by a hollow shaft to the atmosphere or head space (for dead-end systems) (Patwardhan and Joshi, 1999; Vesselinov et al., 2008). As such, the gas flow rate is a function of the impeller speed. The "atmospheric" pressure can be adjusted by pressurizing the shaft entrance such that additional gas is pumped into the system (Patwardhan and Joshi, 1999).

Self-inducing impellers are classified by the flow in and out of the impeller zone. Type 11 impellers are shown in Figure 6.20a and are defined by the gas being the only phase at the inlet and the outlet. The most common and simplest design is a hollow pipe with orifice holes at the ends. The hollow pipe impeller induces gas flow through Bernoulli's equation. Gas induction occurs once the pressure differential is large enough to overpower the liquid hydrostatic head. Type 12 impellers (Figure 6.20b) have a gas phase at the inlet and a gas–liquid flow at the outlet. Gas induction occurs in a similar manner to Type 11, but Type 12 impellers mix the phases in the impeller zone through some intricate designs. Type 22 impellers (Figure 6.20c) are intricate devices that have a two-phase inlet and outlet composition. The impeller induces a large vortex until the impeller is able to induce phase interface ("surface") aeration. The design calls for an axial gas–liquid inlet and radial outlet. An optional impeller hood prevents gas outlet in the axial direction, inducing a pressure differential so that the liquid is pumped into the impeller zone from the bottom reactor section (Patwardhan and Joshi, 1999).

These impellers have both advantages and disadvantages. Type 12 and 22 impellers force the gas phase to travel through a high shear volume, creating smaller average bubble diameters and higher interfacial area in the outlet flow.

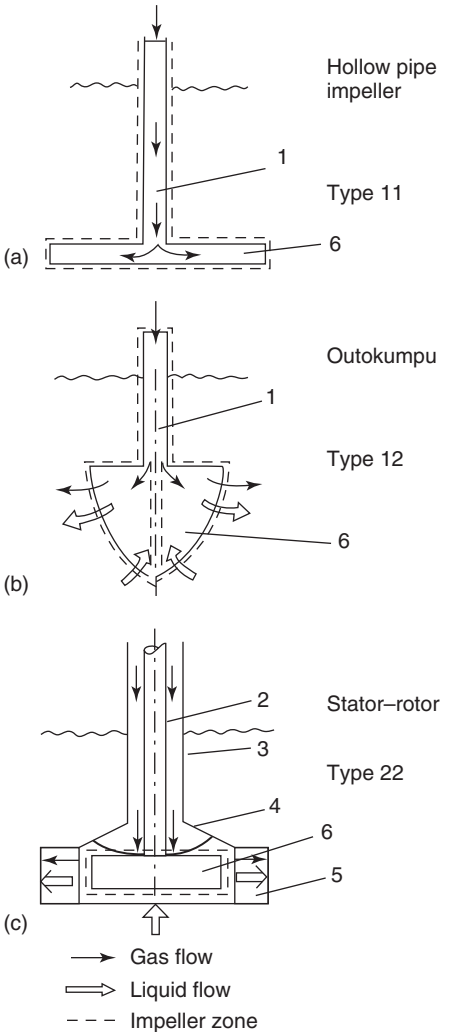

Figure 6.20 Self-inducing impeller types (Patwardhan and Joshi, 1999).

These designs also allow for a reduction in power usage, but this usually comes at a cost of reduced residence time that can have a negative impact on conversion. Since dead-end zones are feasible, this design provides similar advantages to surface aerators. The disadvantages of self-inducing impellers are usually their complicated designs, diminished control (with power input often being the only control variable), and gas–liquid mass transfer performance comparable to "standard" STRs. Unless the gas phase is highly toxic or the gas recycling system is too expensive, self-inducing impellers have little to offer in microorganism systems.

6.4 SUPERFICIAL GAS VELOCITY

The superficial gas velocity U_G is a description of the amount of gas present in the reactor volume and is defined as the volumetric gas flow rate per unit cross-sectional area of the reactor. This definition is easily quantifiable and has been used by many researchers as a correlation parameter for gas holdup and gas–liquid mass transfer. Most researchers cited in this chapter, with the exception of Linek et al. (2005a), have proposed a positive correlation of superficial gas velocity with gas–liquid mass transfer; however, its specific influence on mass transfer is often confusing.

If the impeller is operated below a minimum tip speed (2.25 m/s for RT), the reactor hydrodynamics are dominated by the gas flow and the reactor acts as a bubble column. At this point, gas–liquid mass transfer has an exclusive dependence on the superficial gas velocity (Charpentier, 1981). Since the intent of the STR is to provide agitation that would be superior to gas sparging alone, STRs are operated such that impeller agitation dominates the hydrodynamics (Nishikawa et al., 1981).

The superficial gas velocity is often recognized to influence gas–liquid mass transfer through gas holdup (Nocentini et al., 1993) and its influence on the interfacial surface area (Garcia-Ochoa and Gomez, 2004). It is generally assumed that the interfacial surface area can be increased by entraining more gas in the reactor, and this results in increased gas dispersion and gas–liquid mass transfer.

Bubble–bubble interaction and coalescence have to be considered when the superficial gas velocity is increased. Coalescence occurs through a three-step process. First, bubbles collide and form a liquid layer (typically 10^{-3}–10^{-4} cm thick). Second, the film drains assuming that the collision force is sufficient to deform the bubble interface and that the bubbles spend enough time in contact for the film to drain. Third, assuming that a critical film layer thickness ($\sim 10^{-6}$ cm) is achieved, the film breaks and the bubbles combine (Martín et al., 2008b; Tse et al., 1998). The entire sequence of events is completed in milliseconds for coalescing liquids (Tse et al., 1998), but may take up to 15 s for liquids containing surface-active agents (Laari and Turunen, 2005). Coalescence is, therefore, influenced by the collision frequency, collision force, bubble deformation, and coalescence efficiency (Bredwell et al., 1999; Martín et al., 2008b), and is controlled by the film drainage rate (Tse et al., 1998).

Superficial gas velocity has an influence over the collision frequency. If more gas is present, there is a higher probability of collision (Martín et al., 2008b). Coalescence efficiency and drainage rate depend on the film properties which are a function of the liquid properties. The collision force, however, is the controlling factor because the bubble diameter is a function of the power input (Bouaifi et al., 2001; Nocentini et al., 1993).

Thus, increasing the superficial gas velocity may initially increase $k_L a$ because there will be more gas bubbles and a larger gas–liquid interfacial area. However, further increasing superficial gas velocity could lead to bubble coalescence, which would increase the average bubble diameter and bubble rise velocity and lower the gas residence time (Moilanen et al., 2008). All of these factors would lower

gas–liquid mass transfer (Charpentier, 1981). Under these conditions, the impeller fails to disperse the gas properly, and bubbles form a heterogeneous distribution (Bouaifi et al., 2001) and rise easily (Ford et al., 2008). Even if a higher $k_L a$ is achieved by increasing U_G, a lower residence time can still lead to lower fermentation conversion levels (Bredwell et al., 1999).

The effect of increasing gas holdup on the gas–liquid interfacial area (a) is often ambiguous. This is a special situation for the STR because the power input determines the bubble diameter and hydrodynamics (Bouaifi et al., 2001; Nocentini et al., 1993), while the gas flow rate has a driving influence on bubble dynamics in other reactor designs (to be discussed in other chapters). In other words, gas holdup information does not necessarily contain any (quantitative or qualitative) information about bubble diameter and interfacial surface area for STRs such that an increase in gas holdup does not necessarily increase a (Moilanen et al., 2008). However, gas holdup is still reported as an indicator of hydrodynamic performance, gas distribution (Boden et al., 2008), and gas–liquid contacting (Garcia-Ochoa and Gomez, 2004).

Gas–liquid mass transfer correlations, however, typically fail to reflect STR hydrodynamics and predict an increase in mass transfer with an increase in the superficial gas velocity. If these correlations are used improperly, such as during scale-up or outside their representative size and operating conditions, inaccurate $k_L a$ estimates will result. In other words, the correlation form is simply incapable of representing the hydrodynamic situation and fails to decouple events occurring due to the superficial gas velocity and those occurring due to the power concentration. The current state-of-the-art $k_L a$ correlations with respect to STR conditions will be described in detail in Section 6.9, but it is important to realize that a correlation that is capable of communicating a more complete hydrodynamic picture still remains elusive.

6.5 POWER INPUT

Power dissipation has a direct impact on the gas–liquid mass transfer in STRs. As the power dissipation increases, the bubble diameter decreases (Bouaifi et al., 2001; Nocentini et al., 1993), which, in turn, increases the interfacial surface area. Bubbles break apart because the surface tension force is overcome by a higher power density. Coalescence behavior is reduced because bubbles are not allowed enough contact time for film drainage between adjacent bubbles. At the same time, however, a higher power density implies that the collision force is also increased that would enhance coalescing. Thus, an equilibrium point is reached. As the bubble diameter is reduced to $d_B < 1$ mm, the effect of increased power concentration is decreased. These small bubbles tend to have immobile interfaces that are more resistant to mass and energy transfer. These diminishing returns cause low viscosity Newtonian fluids to have an optimal bubble diameter distribution of 1–3 mm (Bouaifi et al., 2001) unless surfactant stabilized microbubbles are produced (Bredwell and Worden, 1998; Worden and Bredwell, 1998).

The power dissipation influence on the liquid-phase mass transfer coefficient (k_L) is highly debated in STRs, especially at higher power densities. The slip velocity model and eddy turbulence model have been used to explain mass transfer, but they come to different conclusions with respect to power. The slip velocity model predicts a decrease in mass transfer with increasing power dissipation while the eddy turbulence model predicts an increase. Linek et al. (2004) postulate that the main reason for the confusion stems from the miscalculation of k_L. They investigated different measurement methods and models used by others and concluded that the slip velocity models were underestimating $k_L a$ and, hence, k_L.

It was recognized that both models represent parallel mass transfer processes, but that STRs were prone to induce higher rates of eddy diffusion and turbulence (rather than molecular diffusion and surface rigidity control) over surface renewal and mass transfer. Hence, shear rates in STRs regulate surface renewal during normal operating conditions. A similar conclusion could be drawn from the border diffusion layer model (Azbel, 1981). It stipulates, for example, that the eddy diffusion coefficient is three orders of magnitude higher than the molecular diffusivity in the viscous sublayer. If power rates were increased, the viscous sublayer would decrease, which in turn would limit the effect of molecular diffusion on mass transfer, and the liquid-phase mass transfer coefficient would increase.

Other researchers have taken an engineering approach. Nocentini et al. (1993) concluded that k_L changes relatively little with power dissipation with respect to a. Thus, any changes in $k_L a$ during an operation are dominated by changes in a and k_L is of little interest (Hoffmann et al., 2007; Stenberg and Andersson, 1988b). STR flow patterns should also be considered and neglecting them can lead to a fivefold underestimation in gas–liquid mass transfer (Linek et al., 2004).

One may conclude that power dissipation is the only variable that definitely and directly influences gas–liquid mass transfer in STRs. It has direct control over bubble diameter (interfacial area) and the liquid-phase mass transfer coefficient; however, increasing the impeller speed to achieve higher gas–liquid mass transfer rates can be inefficient. STRs also operate under an economical constraint. The impeller speed is related to the power draw by an exponential factor of 3. Along with operational limitations such as the motor and gearbox assembly and microorganism shear constraint, most gas–liquid mass transfer processes operate in the power dissipation range of 3000–4000 W/m^3 (Bredwell and Worden, 1998; Oldshue, 1983). Certain specialized processes require extreme power dissipations of 40,000–100,000 W/m^3 (Gezork et al., 2000, 2001). Operation below 30 W/m^3 is not practical with an STR (Gagnon et al., 1998).

Superficial gas velocity does not necessarily control the interfacial area or liquid-phase mass transfer in STRs directly, but influences the gas dispersion efficiency and power dissipation rate. It is very difficult to disconnect the superficial gas velocity from the power concentration in STRs, even under experimental settings. Thus, most $k_L a$ correlations include the power concentration and superficial gas velocity as variables with the power concentration having a larger role than the superficial gas velocity; this will be discussed in more detail in Section 6.9.

6.6 BAFFLE DESIGN

Whirlpool effects are often troublesome for STR operation with low viscosity liquids because they diminish mixing and dispersion (Williams, 2002). Multiphase systems that are mixed with impellers can experience a central vortex that causes recirculation, low power consumption, minimal mixing (Patwardhan and Joshi, 1998), and phase separation (Tatterson, 1994). If the impeller speed is increased even further, this vortex can reach the impeller (Patwardhan and Joshi, 1998). Baffles are often used to alleviate these effects in low viscosity Newtonian liquids, but are avoided with viscous and/or non-Newtonian liquids (Cabaret et al., 2008; Harnby et al., 1992; Williams, 2002). A secondary advantage is that baffles reduce the liquid velocity forcing a larger differential with the impeller velocity. The consequence is that the ungassed power draw is higher in baffled than in unbaffled vessels, potentially increasing eddy turbulence and gas–liquid mass transfer. These events are exclusive to turbulent operation, and baffles are unnecessary in the laminar regime (Tatterson, 1994). Gassed power draw can be expected to be similar in baffled and unbaffled vessels while the impeller is loaded (Gagnon et al., 1998). A less common application for baffles in gas–liquid processes is as fins for heat transfer purposes or as gas- or liquid-feeding device.

Baffle designs are quite numerous and include half, finger, triangle, partition, and bottom baffles with vertical, horizontal, or spiral direction and a wide array of cross-sectional shapes. The basic design, however, is by far the most common because the advantages of non-standard designs are often limited and because the standard design has been widely researched with easily accessible information, scale-up data, and design specs (Ungerman, 2006). The standard design specifies four to eight equally spaced, vertical plates (Williams, 2002) with a width between $T/12$ to $T/10$ (Oldshue, 1983; Tatterson, 1991, 1994). Baffles are often offset from the reactor wall to discourage dead zones. The standard wall clearance is about 1.5% T (Paul et al., 2004). Baffles are either welded or bolted to the vessel (Bakker and Oshinowo, 2004). If the vessel is made from or lined by a fragile material, baffles can be supported by a ring placed on top of the tank. The mounting limits these vessels to one or two baffles (Torré et al., 2007).

Prefixes are often used to describe the length or shape. For example, full baffles describe standard baffles having a length equal to the reactor height, half baffles have a length equal to half the height, etc. The shape is often distinguished by a prefix affiliated with a common object. For example, beavertail baffles have a shape that looks like a beavertail (wide in the bottom and tappers off at the top) and C-baffles have a semi-circular cross-sectional shape.

Several STR baffle arrangements have been tested to optimize gas–liquid mass transfer or process time. Surface baffles, which are half baffles located in the upper half of the reactor, limit vortex formation while increasing surface turbulence (Patwardhan and Joshi, 1998). This baffle design induces small vortices which entrain gas more effectively, increasing gas holdup and $k_L a$. The limitation of baffle usage in the lower portion of the reactor volume allows for higher turbulence

and enhances sparged gas and power utilization (Gagnon et al., 1998); however, Sivashanmugam and Prabhakaran (2008) noted that such nonstandard baffles also lead to lower impeller power draw, which may decrease mass transfer in that portion of the tank. Regardless, this setup has limited application for batch and semibatch operations.

Lines (2000), however, came to a different conclusion in addressing similar goals of enhanced operation for batch and semibatch modes. He concluded that half baffles in the lower portion of the reactor volume allow for more efficient operation that would induce surface aeration without allowing large vortices to reach deep into the vessel and influence the impeller. The limitation, of course, is the liquid height. The baffles break even at a liquid height-to-reactor diameter ratio of 1.1 for single impeller systems. A two-beavertail baffle system can be used to extend the range to a ratio of 1.5 and any further increase in reactor height relative to its diameter negates this advantage.

These two examples help to point to a common occurrence: the prescription of opposing systems. Both researchers are correct, and their suggestions are useful for their particular task, but they are not universal. Each system and process has an optimal design—including baffles—that may differ from the standard. It is recommended that a proper baffle design be investigated in the initial design stages and should be compared to the standard option; however, most prefer to avoid this situation and use full baffles due to their simplicity, reduced design costs, and known operation compared to nonstandard designs (Oldshue, 1983; Tatterson, 1991, 1994).

6.7 SPARGER DESIGN

Spargers are used to input gas into the reactor and affect impeller power consumption (Ni et al., 1995), critical impeller speed for complete dispersion, and critical impeller speed for suspension (Murthy et al., 2007). Spargers are typically located underneath the impeller with the distance and size being dependent on impeller type. The most common placement is $1D_i$ below the impeller. The sparger diameter is usually smaller than the impeller diameter (Birch and Ahmed, 1997). The orifice holes are usually placed on the sparger bottom. This placement prevents the holes from getting plugged during processes that use high viscosity fluids, a solid phase, or fine particles (Patwardhan and Joshi, 1998). The conditions in the sparger orifice have to be such that the gas flow Reynolds number is in excess of 2100 to ensure that all holes are operational (Rewatkar and Joshi, 1993).

Standard sparger designs include ring, single orifice (point), pipe, porous, and membrane spargers. A ring sparger with equally spaced holes is the most commonly used design for STRs since it provides the most consistent results, uses less power, causes a smaller power drop upon gassing, and is thought to provide higher gas holdup and gas–liquid mass transfer coefficients than other sparger types. To be more exact, a small ring sparger is preferred because it produces higher $k_L a$ values than the large ring sparger or quadruple pipe sparger (Bakker, 1992).

6.7.1 Axial Flow Impellers

The selection of the sparger design has to include a discussion of the accompanying impeller type. An improper selection is often used to explain inconsistencies in published data (Ungerman and Heindel, 2007). The most common source of error is to simply use the standard ring sparger design for all impeller types. This may lead to problems with the down-pumping axial flow impellers (Birch and Ahmed, 1996, 1997; McFarlane and Nienow, 1995; McFarlane et al., 1995; Sardeing et al., 2004b). The standard ring sparger forces gas to flow in the opposite direction of the impeller flow field and induces direct loading such that variations in torque and power draw are easily realized. Larger orifice diameters exasperate this problem by increasing the rate at which cavities are allowed to grow on the impeller blades (Murthy et al., 2007). Replacement of a ring sparger with a pipe sparger can reduce gas holdup by 25% (Rewatkar et al., 1993) and does not address the flow issue since gas is sparged in a similar manner. A single orifice sparger enhances the problem since most of the gas is sent into the impeller center promoting cavity formation (McFarlane et al., 1995).

The influence on axial flow impellers can, however, be negated by using a large ring sparger such that gas exhausts in the impeller periphery. Direct loading is avoided and power draw and torque variations are reduced (McFarlane and Nienow, 1996a) because the gas is sparged into a strong downward stream such that the probability of indirect loading is increased. This regime provides the down-pumping axial flow impeller with steady operation (McFarlane et al., 1995), a lower critical impeller speed for complete dispersion and suspension, while flooding is avoided. Particle suspension is achieved with less power and gas is distributed more uniformly for this arrangement (Murthy et al., 2007). Increasing the impeller diameter has also proven to increase stability (Birch and Ahmed, 1996) and suspension efficiency (Sardeing et al., 2004a). Large axial flow impellers solve the problem due to their stable vortex formations and inherent "periodic vortex shedding" (McFarlane and Nienow, 1995).

Another solution for the loading problem, which is not always practical, is to increase the distance between the sparger and impeller, which makes it more likely that the gas is diverted away from the axial flow impeller by the flow stream, leading to more indirect loading (McFarlane et al., 1995). Increasing the distance also tends to delay the power drop upon gassing, making the separation distance an important design parameter (Garcia-Ochoa and Gomez, 1998). The advantage, however, decreases with increasing viscosity (McFarlane and Nienow, 1996a).

Sparger placement for down-pumping axial flow impellers is suggested to be $0.8D_i$ below the impeller. Larger distances increase the flow instabilities and affect the operating range (McFarlane et al., 1995), whereas smaller distances increase the frequency at which impeller loading fluctuates (McFarlane and Nienow, 1996a). The exact sparger position is often determined by other equipment and the impeller position requirement such that most designs place the sparger $1D_i$ below the impeller and optimize the proper sparger size and type to provide maximum gas holdup and minimum power drop upon gassing (Birch and Ahmed, 1996; Ungerman, 2006).

6.7.2 Radial Flow Impellers

One may think that sparger design may have an important role in the initial bubble diameter and, as such, will influence the interfacial surface area and gas–liquid mass transfer coefficient (Bouaifi et al., 2001; Garcia-Ochoa and Gomez, 1998). Designers should choose a sparger that would offer a smaller initial bubble diameter to increase the efficiency of the operation. However, it has been shown that Rushton-type impellers control the bubble diameter and dispersion such that the sparger choice is noncritical (Garcia-Ochoa and Gomez, 1998). Even if the bubble diameter originating from the sparger is very large, the bubbles are broken apart by the time they reach the impeller and do not affect cavity size, impeller loading, gas–liquid interfacial area, and gas–liquid mass transfer. However, in order to ensure that bubbles pass through the high shear impeller zone, the sparger diameter is suggested to be smaller than the impeller diameter with a standard of $0.8D_i$ (McFarlane et al., 1995; Tatterson, 1991).

This discussion sheds light into the superior performance of a multiple impeller system with a radial–axial flow impeller combination, with a radial flow impeller in the lower position and an axial flow impeller in the upper position. The radial flow impeller is not affected by the sparger type and is able to efficiently disperse small bubbles. The upper impeller is loaded indirectly by the flow field, which it generates, and is able to provide proper mixing conditions. As such, the sparger choice does not affect the performance of the other impellers. If the impellers operate independently, impellers are optimally loaded for gas dispersion and liquid mixing such that progressive reduction in $k_L a$ is minimized and the desired process time can be reduced by >30% (Lines, 2000).

6.8 MICROBIAL CULTURES

Microbial cultures are used as catalysts in bioreactors. Bacteria are the most commonly used culture, but animal, plant, or insect cells have also been implemented (Bliem and Katinger, 1988a). STRs are popular with microorganisms (Vazquez et al., 1997) because STRs enhance feedstock contact, provide pH and temperature uniformity, and maximize mixing (Hoffmann et al., 2008). Their impact on reactor hydrodynamics is mostly indirect. Occasionally, microorganisms retard turbulence if the organic holdup is above 11–15% depending on the species. The other possibility is that the microorganisms produce surface-active agents (van der Meer et al., 1992); however, their most common impact on hydrodynamics is that reaction kinetics may be limited by the environment such that the operational range (power concentration, superficial gas velocity, etc.) may be reduced. As such, it is more constructive to concentrate on the impact that hydrodynamics have on microorganisms.

The most influential sensitivity is for shear gradients that most commonly hinders productivity regardless of the mass transfer situation (Bliem and Katinger, 1988a, 1988b; Hoffmann et al., 2008). Shear gradients damage microorganisms using several mechanisms. The simplest one is cell wall (physical) damage.

This mechanism also separates animal and plant cell applications from the bacterial applications. Bacteria are usually smaller and have stronger cell walls relative to their size than animal or plant cells such that bacterial processes use a power range of 1–5 W/kg (comparable to chemical processes) while cellular processes use 0.0005–0.1 W/kg (Bliem and Katinger, 1988a). In other words, smaller cultures are usually able to withstand higher shear gradients because the most damaging eddies have to be on the order of the cell size. As such, animal cell growth rate has been found to reduce with eddies smaller than 130 μm (Bliem and Katinger, 1988b).

Shear gradients may also interfere with cell-to-cell interaction, cell-to-substrate adhesion, and microbial competition. In addition, certain microorganisms prefer to flocculate. Hoffmann et al. (2008)[2] concluded that bacteria, which tended to form elongated filaments, were more prone to shear-induced damage than those which formed cocci (spherical formations). Although the elongated filaments were more advantageous for food collection during calmer operation, the introduction of strong turbulence provided a competitive advantage for cocci-forming bacteria such that those dominated the population at the end of the experiment.

The bacteria's spatial juxtaposition (awareness relative to other bacteria) may also be hindered by turbulence. In the worst-case scenario, the bacteria are not able to make significant contact and are not able to achieve the necessary cell density for optimal operation (Bliem and Katinger, 1988b) or are not able to make syntropic relationships with other bacterial cultures (Hoffmann et al., 2008). The result is that start-up performance is very poor with minimal or insignificant conversion while long-term performance is not hindered in a bacterial mixture that allows competition and has at least one shear-tolerant species. Conditioning with feast and famine cycles improved recovery time and tolerance to feed and shear shocks (Hoffmann et al., 2008).

Thus, bioreactors using shear-sensitive microorganisms have to minimize cellular damage, maximize feedstock transfer to microorganisms, and maximize mixing. The latter requirements are important because the bacterial structure may change during starvation mode to make the culture even more susceptible to cell wall degradation. This situation is true for mycelia (fungi) and may be applicable to other branching bacteria. A healthy specimen, shown in Figure 6.21a, has relatively thick branches without vacuoles (empty pockets). As the bacteria starves (Figure 6.21b), it reduces the number of branches and starts to consume its internal reserves, which leads to the formation of vacuoles. As the number and size of vacuoles increases, the cell wall strengthens and its ability to resist environmental stresses decrease. As starvation is extended, the specimen will consume as much of its own mass as it can (which depends on the species) and vacuoles will dominate its structure, as can be seen in Figure 6.21c. At this point, the microorganism is easily and significantly

[2]The conclusions are based on a particular set of microbial species and have not been verified by other researchers. According to their published article, Hoffmann et al. (2008) experimented with the same sized vessels at a different impeller speed. Since turbulence and power concentration grow nonlinearly with impeller speed, their results and conclusions may not be universally applicable or practical at larger scale.

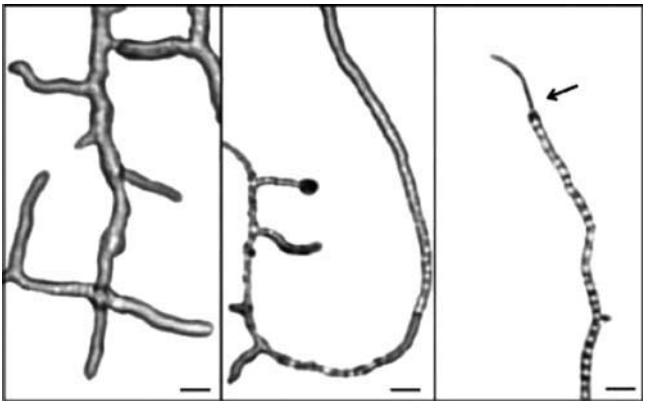

Figure 6.21 Bacteria starvation; (a) a healthy specimen, (b) a bacterium under starvation conditions, and (c) extensive starvation with the formation of many vacuoles (empty pockets) (Pollack et al., 2008).

damaged by shear gradients (Hoffmann et al., 2008). Energy and mass are diverted to the tip, as pointed out in Figure 6.23c, in order to search for a food source. This tip is of solid construction relative to the main body. Insufficient mixing can have similar effects in that the reactor volume is partially in starvation mode and not producing an optimal amount (if any) of product in those regions (Shewale and Pandit, 2006).

Microorganisms and their reaction kinetics may start out being gas–liquid mass transfer limited, but the process and changing environment may change the limiting factor to temperature or pH level. Bacteria are classified by their temperature preference into mesophilic or thermophilic families. Mesophilic bacteria operate optimally at about 30 °C with a sharp drop-off in efficiency as temperature approaches 50 °C. These cultures are used more widely because they are easier to control and produce a more consistent product, but are generally able to convert only 40% of the biological matter in 30–40 days. Thermophilic bacteria, on the other hand, prefer temperatures of about 60 °C and have proven conversion rates up to 48% in just 10 days (Demirel and Yenigün, 2002; Ros and Zupancic, 2002). Acidity is quite variable (although not for a specific bacterial culture) and can range from pH 4.3 to pH 7.9 for anaerobic bacteria (Demirel and Yenigün, 2002). Output can be maximized for acid-sensitive processes using syntropic relationships (i.e., volatile fatty acid-oxidizing bacteria and hydrogen-utilizing methanogens) (Hoffmann et al., 2008).

Furthermore, microorganism production and conversion processes often introduce unwanted by-products or create products that negatively affect bioreactor operation. For example, protein-producing microorganisms, which are often used in pharmacokinetics, produce a mixture over time that is damaging to the bacteria aside from the surface-active agent properties of the protein. Shear is tolerated by the microorganisms in this mixture, but air–liquid interfaces, which are naturally

very common in gas–liquid processes, can lead to denaturation (Titchener-Hooker and Hoare, 2008). Batch and semibatch stirred-tank bioreactors are also influenced by the accumulation of products in the volume, which can significantly change liquid-phase properties. Although the production is certainly welcome, it can lead to the process being tail dominated (e.g., process time controlled by last 20%) or creating an extremely viscous liquid phase, which, in most cases, forces the operation to cease.

Many industries, in which the stirred-tank bioreactors are being implemented, require production to be very consistent and/or the design phase to be completed quickly. For example, it is common in the biopharmaceutical industry to start the design phase once approval of a drug has been secured; however, the design process requires a significant amount of time during which the patent clock is ticking. Hence, expensive delays are very common (Titchener-Hooker and Hoare, 2008).

The need for better results has led to the implementation of process and genetic engineering. Process engineering is described throughout this section. Its goal is to optimize the conditions such that production and/or conversion are increased; however, it can be difficult to predict hydrodynamic effects on microorganisms. The answer has been to carefully test microorganism on the micro (experimental) scale and implement genetic engineering techniques to create more shear-resistant strains (Zeng and Deckwer, 1996). Process engineering, however, prevails in practice as genetic engineering has not been able to produce very resistive strains (although productivity has been increased) such that stirred-tank bioreactors are limited in their power dissipation rates.

Impellers and their arrangements also need to be modified for solid suspension. Impellers used in single impeller configurations for solid suspension are preferred to have a bottom clearance up to $D_i/3$. This clearance is dependent on the process and impeller type. In order to provide proper mixing, the tanks are shorter than standard gas–liquid designs with an aspect ratio (H/T) about 0.6–0.7, and a second impeller is warranted for a ratio above 1. Solids will settle and stack around the wall if the reactor has a diameter that is too large or an impeller that is too small relative to the tank diameter (Tatterson, 1994). The bottom impeller in a multiple impeller arrangement is more important for solid suspension because the upper impeller can only suspend as much as is fed by its partner (Oldshue, 1983); however, an improper spacing can cause the upper impeller to interfere with the bottom impeller, usually degrading suspension (Tatterson, 1994).

Certain impellers create flow patterns that induce suspension at lower impeller speeds. For example, the down-pumping PBT is more efficient at solid suspension due to its axial bottom-lifting flow than radial impellers or the up-pumping PBT. Radial impellers, such as the Rushton-type turbines, are not efficient suspension impellers (Tatterson, 1994) because the particle lifting occurs through axial flow impeller suction which usually uses about half the impeller flow. Therefore, the Rushton-type turbine (RT) requires as much as three times the power for the same level of suspension as the down-pumping PBT (Oldshue, 1983). The advantage and the use of down-pumping axial flow impellers for solid suspension places

more relevance on the selection and performance of the sparger design, which is explained in Section 6.7.

Operators are potentially presented with an awkward choice of achieving better gas breakage with a radial flow impeller or better suspension with an axial flow impeller. The decision really comes down to the gas flow rate. Since most biological processes require a significant amount of gas to proceed efficiently, the potential instabilities present in the down-pumping PBT and necessary gas–liquid mass transfer have led to a close clearance Rushton-type turbine (clearance of $H/4$ and $D_i = T/2$), the safest impeller choice for three-phase systems if the impeller is operated under complete dispersion conditions (Ulbrecht and Patterson, 1985). The close clearance RT has a significant axial component while still preserving some of its gas-breakage capabilities (Harnby et al., 1992).

Baffle designs for gas–liquid stirred-tank bioreactors can be used with solids that have a similar density as the liquid. If the solid phase is denser than the liquid, baffles should be much thinner if they are used at all. This is due to the fact that the decreased level of turbulence may lead to stratification, dead zones, and/or recirculation loops near the baffles. These occurrences can cause excessive buildup of solid material and poor performance. Therefore, baffles used for this purpose may have a plate thickness as small as $T/24$ (Oldshue, 1983).

6.9 CORRELATION FORMS

The mass transfer theories from Chapter 3 have been used to define operational boundaries for STRs. The hydrodynamic complexity of gas–liquid flows in STRs has curbed the practical application of theoretical models. Currently, a universal model or correlation has not been successfully developed and applied over a wide range of system configurations, scales, operating conditions, or inputs (Garcia-Ochoa and Gomez, 2004; Kawase and Moo-Young, 1988), which is a major disadvantage of STRs. The situation is even worse in gas–liquid–solid processes due to lack of relevant data and increased hydrodynamic complexity (Garcia-Ochoa and Gomez, 2004; Murthy et al., 2007). Design and scale-up are implemented using an iterative method, where previous works are used as the first step in a trial-and-error process (Benz, 2008), which continues until the reactor produces the desired conditions (Bliem and Katinger, 1988a).

In order to streamline the process, empirical, semi-empirical, or dimensionless group correlations have been proposed of which empirical correlations are the most commonly used (Bliem and Katinger, 1988a; Garcia-Ochoa and Gomez, 2004; Kawase and Moo-Young, 1988). Variables are chosen based on a gas–liquid mass transfer model believed to dominate the process as well as practical considerations. These correlations have been used in design and scale-up, but are only valid for the particular system and operating range (Benz, 2008; Garcia-Ochoa and Gomez, 2004) and have an accuracy of about $\pm 30\%$ at best (Benz, 2008) even if they are in dimensionless form (Bliem and Katinger, 1988a).

In general, STR correlations lack the ability to account for reactor variations and the specific hydrodynamic state; however, they can be used as an estimate if the

corresponding systems have geometric, hydrodynamic, and flow pattern similarity. Industrial designs based on experimental setups should be referenced to systems that properly reflect the desired industrial settings and circumstances (Bliem and Katinger, 1988b; Kapic and Heindel, 2006; Kapic et al., 2006). For example, most experimental setups are operated in a Reynolds range of 5000–10,000 while large industrial units operate in the range 10,000–100,000 (Bliem and Katinger, 1988b). The disconnect becomes more obvious when we consider that a significant number of experiments include data in a power range of 5–10 kW/m^3, while industrial units are rarely operated beyond 3 kW/m^3 (Benz, 2008) or below 500 W/m^3 (Bliem and Katinger, 1988b). This is mainly due to the theoretical models' requirement of a well-mixed state for the liquid phase while industrial units require minimal costs. Hence, mixing and process time often grows much quicker with scale than anticipated and often leads to production difficulties (Nienow, 1996).

A simple approach for finding an appropriate gas–liquid mass transfer correlation is to break $k_L a$ down into its components (a and k_L) and find separate correlations for each, after which those components would be combined to generate a $k_L a$ correlation. It is very convenient to start with the interfacial area since an applicable theoretical correlation is readily available (Figueiredo and Calderbank, 1979)

$$a = \frac{6\epsilon}{d_{SM}} \tag{6.2}$$

where ϵ is the gas holdup and d_{SM} is the Sauter mean bubble diameter.

Next, an assumption is made on the mass transfer model, and the two terms are combined. If a film model is used, k_L is assumed to be inversely proportional to d_B. Therefore,

$$k_L a = \frac{\beta\epsilon}{d_B^n} \tag{6.3}$$

where d_B is the mean bubble diameter and β and n are the fitted constants. If a penetration model is used, k_L is correlated with a power concentration, usually defined in terms of P_G/V_L:

$$k_L a = \frac{C\epsilon(P_g/\forall_L)^A}{d_B} \tag{6.4}$$

where A and C are fitted values, P_g represents the gassed power, and $\forall_L$ is the liquid volume within the STR. It should be noted that Eqs (6.3) and (6.4) fall in the semiempirical family of correlations. Gas holdup correlations, which are presented in Table 6.1, could be substituted into Eq. (6.4) to obtain the gas–liquid mass transfer approximations.

Some researchers have found a better statistical fit by using the total power, P_{tot}, defined as the gassed impeller power plus the buoyancy power of the sparged gas (Moucha et al., 2003). This has been done because the sparged gas power has been shown to impact gas–liquid mass transfer in a similar manner to impeller power (Stenberg and Andersson, 1988b). On the other hand, Gagnon et al. (1998) came to the conclusion that the impeller transfers energy to the fluid in the impeller zone and

TABLE 6.1 Gas Holdup Correlations for Stirred-Tank Reactors

$\varepsilon_G = C(P_G/V)^a UG^b$

Researchers	C	a	b	U_G Range (mm/s)	P_G/V Range (W/m^3)	Gas	Liquid	Impeller Configuration	H (m)	T (m)
Bouaifi et al. (2001)	22.4	0.24	0.65	3.7–18.1	0–1000	Air	Tap water	2 (PBT, A310, A315)	0.86	0.43
	24.8	0.24	0.65					2 (RT, PBT, A310, A315)		
Figueiredo and Calderbank (1979)	0.34	0.25	0.75	n/a	n/a	n/a	n/a	n/a	n/a	n/a
Linek et al. (1994)	0.23	0.31	0.73	n/a	n/a	n/a	Water	2 (RT)	n/a	n/a
	0.05	0.49	0.58				0.5 M Na_2SO_4			
Linek et al. (1996)	0.07	0.36	0.54	0–0.00848	0–4000	Nitrogen and oxygen	Water	4 (RT)	0.19, 0.38, 0.57, 0.76	0.19
	0.29	0.30	0.73							
	0.02	0.59	0.44				0.5 M Na_2SO_4			
	0.05	0.46	0.52							
Moucha et al. (2003)	0.02	0.63	0.52					1 (TXU)		
	0.05	0.49	0.57					2 (TXU)		
	0.17	0.42	0.75					3 (TXU)		
	0.05	0.42	0.53					1 (TXD)		
	0.14	0.32	0.59					2 (TXD)		
	0.26	0.36	0.74					3 (TXD)		

	0.05	0.47	0.58	2.12, 4.24, 8.48	0–1300	Oxygen	0.5 M Na_2SO_4	1 (PBD)	0.29, 0.58, 0.87	0.29
	0.08	0.52	0.71					2 (PBD)		
	0.35	0.29	0.80					3 (PBD)		
	0.19	0.44	0.75					3 (RT, 2TXU)		
	0.24	0.45	0.82					3 (RT, 2TXD)		
	0.10	0.52	0.71					3 (RT, 2PBD)		
	0.03	0.51	0.50					2 (RT, TXU)		
	0.11	0.42	0.66					2 (RT, TXD)		
	0.05	0.50	0.57					2 (RT, PBD)		
	0.02	0.62	0.57					1 (RT)		
	0.05	0.49	0.58					2 (RT)		
	0.04	0.54	0.58					3 (RT)		
Pinelli et al. (2003)	0.10	0.28	0.48	7.0–14.0	200–2,600	Air	Water	2 (BT-6)	0.96, 1.44	0.48
	0.25	0.24	0.65							
Vasconcelos et al. (2000)	0.10	0.37	0.65	n/a	n/a	n/a	Water	2 (RT)	n/a	n/a
Whitton and Nienow (1993)	1.28	0.26	0.66	11.8–33.1	1.4–1.7 rps	n/a	n/a	1 (RT)	n/a	0.61, 2.67
Yawalker et al. (2002)	0.56	0.25	0.41	4.0–15.7	0.7–8.3 rps	Air	Water	1 (PBD)	0.57	0.57
	0.52	0.25	0.40							

Note the correlation by Whitton and Nienow (1993) is as cited by Yawalkar et al. (2002b).

that the gas phase does not influence this energy transfer directly. Most researchers, therefore, ignore the effect of the buoyancy force and the gas expansion energy in STRs. The power dependence can also be accomplished by using the impeller speed N or a combination of the impeller diameter D_i and N. Correlations based on D_i and N are more scale dependent than the power concentration. Therefore, correlations will be compared on a power concentration basis.

Equation (6.2) has two control and measurement difficulties: gas holdup and bubble diameter. Gas holdup can have dynamic features and its measurement may be difficult to implement in a reactor control scheme. The bubble diameter, especially in heterogeneous flow, is not uniform and its measurement requires visual inspection, which is troublesome in industrial or large-scale experimental units. Therefore, the representative control inputs (power concentration and superficial gas velocity) for the bubble diameter and gas holdup can be used (Moo-Young and Blanch, 1981). The two inputs represent forces acting on the bubbles such as the drag, buoyancy, inertial, and the surface tension forces. These substitutions have led to the most widely used empirical correlation form:

$$k_L a = C\left(\frac{P_g}{\forall_L}\right)^A U_G^B \tag{6.5}$$

where A, B, and C are fitted constants and U_G is the superficial gas velocity. Correlations based on Eq. (6.5) are presented in Table 6.2.

Although Eq. (6.5) has been widely used in practice (Kawase and Moo-Young, 1988), it conveys very little information about the particular system and mass transfer mechanism (Moucha et al., 2003). For example, impeller-operating regimes, flow patterns, forces, and liquid and gas properties are not accounted for in this correlation. The particular results are global representations of the system and have little hope of representing microscale effects that are vital in gas–liquid mass transfer (Bouaifi et al., 2001). As shown in Figure 6.22, these issues have caused a wide variability in the available gas–liquid mass transfer (and gas holdup) correlations and their dependence on power concentration and superficial velocity (Yawalkar et al., 2002b). For example, the power concentration exponent ranges from 0.32 (Gagnon et al., 1998) to 1.32 (Linek et al., 1996a), and the U_G exponent ranges from 0 (Linek et al., 2005a) to 0.77 (Moucha et al., 2003). Hence, depending on the particular correlation, estimated $k_L a$ values may vary by a factor of 2 or more for a fixed power concentration.

It would be fair to conclude that the choice of fitted variables is based on statistical methods with little thought to implications on mass transfer models and forces acting on the system, thus reducing the usefulness outside the experimental range. For example, the exponents depend on the reactor size (Stenberg and Andersson, 1988b), system geometry, experimental range, and experimental method (Figueiredo and Calderbank, 1979). Therefore, one may conclude that Eq. (6.5) is leaving out major variables.

A second problem with Eq. (6.5) is that the two measured variables, power concentration and superficial gas velocity, are inherently connected through hydrodynamics. Their experimental and statistical separation is a very difficult task and is

TABLE 6.2 Standard Gas–Liquid Mass Transfer Correlations Based on Eq. (6.5)

$k_La=C(P_G/V)^A U_G{}^B$

Researchers	C	A	B	U_G Range (mm/s)	P_G/V Range (W/m^3)	Gas	Liquid	Impeller Configuration	H (m)	T (m)
Bouaifi et al. (2001)	0.022	0.50	0.60	3.72–18.10	0–1,000	Air	Tap water	2 (RT, PBT, A310, A315)	0.86	0.43
Fujasova et al. (2007)	0.006	0.74	0.53	2.12, 4.24, 8.48	0–1,200	Air	Water	3 (RT in bottom; PBD, PBU, TXD, LTN, NS)	0.29, 0.58, 0.87	0.29
	0.001	1.22	0.51				0.5 M Na_2SO_4			
	0.002	0.95	0.58				Sokrat 44			
	0.006	0.69	0.53				Water			
	0.001	1.25	0.57				0.5 M Na_2SO_4			
	0.001	1.00	0.50				Sokrat 44			
	0.006	0.69	0.53				Water			
	0.001	1.20	0.58				0.5 M Na_2SO_4			
	0.001	0.95	0.53				Sokrat 44			
	0.005	0.72	0.50				Water			
	0.000	1.22	0.45				0.5 M Na_2SO_4			
	0.002	0.95	0.57				Sokrat 44			

(*continued*)

TABLE 6.2 (*Continued*)

$k_La=C(P_G/V)^A U_G{}^B$										
Researchers	*C*	*A*	*B*	U_G Range (mm/s)	P_G/V Range (W/m^3)	Gas	Liquid	Impeller Configuration	*H* (m)	*T* (m)
Gagnon et al. (1998)	0.5	0.01	0.86	0–1.2	0.001–30	Air	Water	1 (RT)	0.55	0.23
	0.8	0.02	0.92					2 (RT)		
	0.2	0.02	0.72					2 (RT)		
	0.3	0.03	0.79					3 (RT)		
	0.4	0.01	0.87		0.001–100			HR		
	0.5	0.06	0.88					HRB		
	12.2	0.57	0.47		30–10,000			1 (RT)		
	2.9	0.83	0.50					2 (RT)		
	3.2	0.79	0.48					2 (RT)		
	9.2	0.60	0.50					3 (RT)		
	15.4	0.32	0.50		100–10,000			HR		
	31.1	0.38	0.65					HRB		
Gezork et al. (2001)	0.005	0.59	0.27	0–130000	0–100,000	Air	Water	1 or 2 (RT)	0.29	0.29
	0.004	0.70	0.18				0.2M Na_2SO_4			

Hickman (1988)	0.043	0.40	0.57	2–17	50–3500	Air	Water	1 (RT)	n/a	0.6
	0.027	0.54	0.68							2
Kapic and Heindel (2006)	0.040	0.47	0.60	0.5–7.2	6.7–13.3 rps	Air	Tap water	1 (RT)	0.21	0.21
Kapic et al. (2006)	0.026	0.61	0.61	0.5–7.2	6.7–13.3 rps	CO	Water	1 (RT)	0.21	0.21
	0.001	1.23	0.55			Air	0.5 M Na_2SO_4	2 (RT)		
Linek et al. (1987)	0.005	0.59	0.40	2.12, 4.24	100–3500	Air	Water	1 (RT)	n/a	0.29
	0.001	0.95	0.40				0.5 M Na_2SO_4			
Linek et al. (1990)	0.000	1.24	0.40	n/a	n/a	Air	Water	n/a	n/a	n/a
Linek et al. (1994)	0.000	1.21	0.40	n/a	n/a	Air	0.3 M Na_2SO_4	3 (RT)	n/a	n/a
Linek et al. (1996)	0.009	0.63	0.54	0–8.48	0–4,000	Nitrogen and oxygen	Water	4 (RT)	0.19, 0.38, 0.57, 0.76	0.19
	0.006	0.68	0.50							
	0.001	1.17	0.46				0.5 M Na_2SO_4			
	0.001	1.32	0.33							

(*continued*)

TABLE 6.2 (*Continued*)

$k_La=C(P_G/V)^A U_G{}^B$										
Researchers	C	A	B	U_G Range (mm/s)	P_G/V Range (W/m^3)	Gas	Liquid	Impeller Configuration	H (m)	T (m)
Linek et al. (2005)	0.00003	1.18	0.00	1.8, 3.6, 5.4	10–1,500	Pure oxygen or air	0.8 M Na_2SO_4	1 (RT)	0.12	0.12
	0.00003	1.16	0.00				0.8 M Na_2SO_4 and Sokrat 44 (3% vol)			
	0.00004	1.08	0.00				0.8 M Na_2SO_4 and CMC TS.5 (0.2wt%)			
	0.00022	0.77	0.00				0.8 M Na_2SO_4 and CMC TS.5 (0.6 wt%)			
	0.00013	0.73	0.00				0.8 M Na_2SO_4 and Ocenol (3 ppm by volume)			
	0.00003	1.15	0.00				0.8 M Na_2SO_4 and PEG 1000 (100 ppm by mass)			

Moucha et al. (2003)	0.001	1.25	0.63	2.12, 4.24,8.48	0–1,300	Oxygen	0.5 MNa_2SO_4	1 (TXU)	0.29, 0.58, 0.87	0.29
	0.002	1.20	0.74					2 (TXU)		
	0.002	1.20	0.70					3 (TXU)		
	0.018	0.88	0.77					1 (TXD)		
	0.006	1.01	0.69					2 (TXD)		
	0.009	1.01	0.75					3 (TXD)		
	0.002	1.05	0.46					1 (PBD)		
	0.001	1.11	0.39					2 (PBD)		
	0.001	1.15	0.51					3 (PBD)		
	0.003	1.01	0.54					3 (RT, 2TXU)		
	0.003	1.04	0.51					3 (RT, 2TXD)		
	0.001	1.14	0.46					3 (RT, 2PBD)		
	0.001	1.06	0.36					2 (RT, TXU)		
	0.002	1.02	0.47					2 (RT, TXD)		
	0.001	1.13	0.43					2 (RT, PBD)		
	0.000	1.24	0.34					1 (RT)		
	0.001	1.23	0.56					2 (RT)		
	0.001	1.24	0.47					3 (RT)		
	0.001	1.19	0.55					All Data		

(*continued*)

TABLE 6.2 (*Continued*)

$k_La=C(P_G/V)^A U_G{}^B$										
Researchers	C	A	B	U_G Range (mm/s)	P_G/V Range (W/m^3)	Gas	Liquid	Impeller Configuration	H (m)	T (m)
Ni et al. (1995)	1.645	0.50	0.64	0.5 vvm	0–10,000	Air	Yeast and feed	2 (RT)	0.195 0.37	0.12 0.24 3
Nocentini et al. (1993)	0.015	0.59	0.55	0.1–0.7 vvm	100–10,000	Air	Water and glycerol	4 (RT)	0.70, 0.93	0.23
Pinelli et al. (2003)	0.018	0.37	0.29	7.0–14.0	200–2,600	Air	Water	2 (BT-6)	0.96, 1.44	0.48
	0.005	0.59	0.40							
Puthli et al. (2003)	0.0001	0.58	0.43	1.7–6.4	300–600 rpm	Air	Water	1 (RT)	0.22	0.13
	0.0001	0.61	0.43					2 (RT, PBT)		
	0.0002	0.67	0.53					3 (RT, 2PBT)		
	0.0001	0.68	0.53				0.25% (w/v)CMC	3 (RT, 2PBT)		
	0.0001	0.66	0.54				0.375% (w/v)CMC			
	0.0022	0.36	0.56				0.50% (w/v)CMC			

Riggs and Heindel (2006)	0.051	0.51	0.65	0.5–2.88	200–600 rpm	CO	Water	1 (RT)	0.21	0.21
Smith et al. (1977)	0.010	0.48	0.40	4.0–20.0	20–5,000	Air	Water	1 (RT)	0.60 0.61	0.44 0.61
	0.020	4.75	0.40	4.0–46.0	0–700	Air	0.11 Na_2SO_4		0.91 1.63	0.91 1.83
Van't Riet (1979)	0.026	0.40	0.50	n/a	n/a	n/a	Coalescent	1 (RT)	n/a	n/a
	0.020	0.70	0.20				Non-coalescent			
Vasconcelos et al. (2000)	0.006	0.66	0.51	n/a	n/a	n/a	Water	2 (RT)	n/a	n/a
Zhu et al. (2001)	0.031	0.40	0.50	1.0–7.5	100–1,500	Air	Water	1 (RT)	n/a	0.39

Note: The correlations by Hickman (1988), Linek et al. (1987), Van't Riet (1979), and Zhu et al. (2001) are as cited by Yawalkar et al. (2002a).

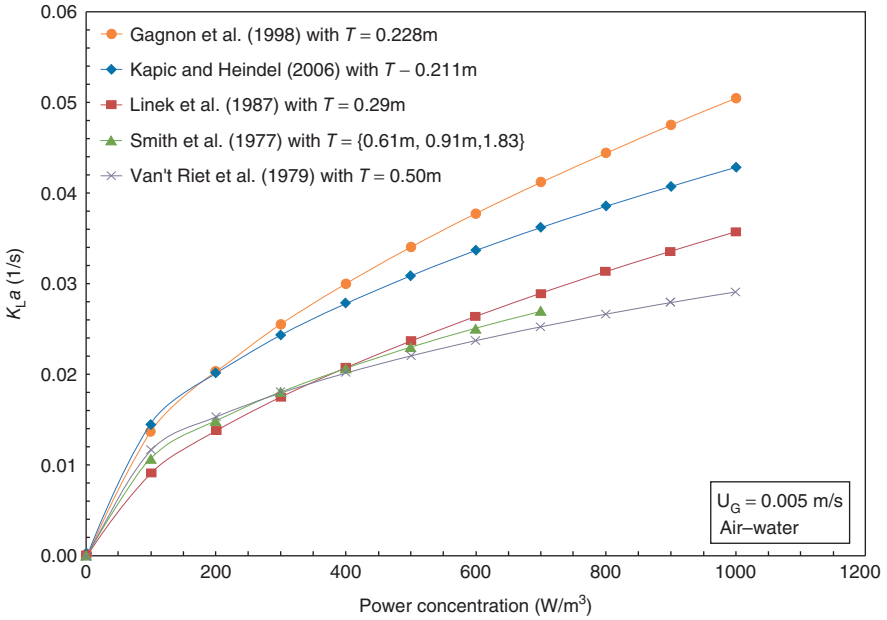

Figure 6.22 Sample mass transfer results for an STR with a single Rushton-type impeller from the correlation based on Eq. (6.5).

rarely achieved (Garcia-Ochoa and Gomez, 2004; Stenberg and Andersson, 1988b). As stated in the STR literature, questionable measurement techniques (Linek et al., 1996a) and experimental assumptions (Nocentini, 1990) make a large number of the STR correlations inadequate and conflicting (Nishikawa et al., 1984).

The need to define the system more accurately has led to several improvements on Eq. (6.5). Fujasova et al. (2007), and Moucha et al. (2003) have added a gassed power term N_{Pg} to account for the impeller type:

$$k_L a = C\left(\frac{P_{tot}}{\forall_L}\right)^A U_G^B N_{Pg}^D \tag{6.6}$$

where A, B, C, and D are fitted constants. The (gassed) power number is defined as

$$N_{Pg} = \frac{P_g}{\rho N^3 D_i} \tag{6.7}$$

where ρ is the liquid density and P_g is the gassed impeller power draw. Cavity effects are reflected by a decrease in the gassed power draw and hence the gassed power number. Although the power number helps to identify the particular impeller type, it does not identify the flow regime in which the impeller is operating.

Fujasova et al. (2007) and Linek et al. (1996a, 1996b) went further and attempted to account for multiple impellers. Linek et al. (1996a, 1996b) pointed to the fact that

different amounts of gas pass through each impeller zone. It was suggested that one correlation should be formulated for the bottom section while the other impellers were packaged into a separate correlation. Linek et al. (1996a) presented a weighted power term that could be used in Eq. (6.5). The bottom impeller would account for 25% of the power draw while the other impellers accounted for 75%. Fujasova et al. (2007) added a gassed-to-ungassed power ratio term that would account for the different amounts of gas passing through each impeller and communicate the impeller performance upon gassing relative to its ungassed state (McFarlane and Nienow, 1996b). Hence, the total mass transfer coefficient was determined from an average of the mass transfer coefficients of each impeller section, which was calculated using

$$k_{\mathrm{L}}a = CP_{\mathrm{tot}}^{A}U_{\mathrm{G}}^{B}(P_{\mathrm{g}}/P_0)^{D}N_{\mathrm{P}}^{E} \tag{6.8}$$

where A, B, C, D, and E are the fitted constants and P_0 is the ungassed power.

The previous equations assume that liquid properties do not change throughout the process or hope that any viscosity changes or liquid type is reflected in the power concentration term (Ni et al., 1995). These circumstances lead Eq. (6.5) to fail when the fluid viscosity changes during the process or when the fluid exhibits non-Newtonian behavior. Several authors have suggested the inclusion of a viscosity term to account for these effects (Garcia-Ochoa and Gomez, 1998, 2004; Linek et al., 2005a; Ogut and Hatch, 1988; Tecante and Choplin, 1993):

$$k_{\mathrm{L}}a = C\left(\frac{P_{\mathrm{g}}}{\forall_{\mathrm{L}}}\right)^{A}U_{\mathrm{G}}^{B}\mu_{\mathrm{a}}^{C} \tag{6.9}$$

where A, B, C, and D are fitted constants and μ_{a} is the apparent viscosity based on the Ostwald–de Waele model. A Casson viscosity (Garcia-Ochoa and Gomez, 1998, 2004) and a liquid-to-water viscosity ratio (Nocentini et al., 1993) have also been used successfully. Unfortunately, Eq. (6.9) also shares the same disadvantages as Eq. (6.5)—it is limited to similar systems operating over similar ranges.

Flow patterns and impeller loading conditions have not been considered thus far. They are important characteristics of a system, but are identified through indirect and inefficient means. Yawalkar et al. (2002a, 2002b) and Kapic et al. (Kapic, 2005; Kapic and Heindel, 2006; Kapic et al., 2006) have attacked this prospect using a correlation based on a complete dispersion impeller speed N_{CD}. It defines the point at which complete gas dispersion is achieved at the minimal power input (e.g., see Figures 6.6 and 6.7). Yawalkar et al. (2002a) proposed

$$k_{\mathrm{L}}a = C\left(\frac{N}{N_{\mathrm{CD}}}\right)^{A}U_{\mathrm{G}}^{B} \tag{6.10}$$

where A, B, and C are fitted constants. Various correlations of this form are summarized in Table 6.3. It was noted that this $k_{\mathrm{L}}a$ correlation was independent of reactor geometry, impeller type, position of the impeller, and sparger if operated at the

TABLE 6.3 Gas–Liquid Mass Transfer Correlations Based on Eq. (6.17)

$k_La=C(N/N_{CD})^A U_G{}^B$										
Researchers	C	A	B	U_G Range (mm/s)	N/N_{CD}	Gas	Liquid	Impeller Configuration	H (m)	T (m)
Chandrasekharan and Calderbank (1981)	2.7	1.15	0.96	3.5–18	0.85–1.56	Air	Water	1 (RT)	n/a	1.22
Calderbank (1958), van't Riet (1979)	2.8	1.14	0.97	5–36	0.67–2.65	Air	Water	1 (RT)	n/a	0.5
Hickman (1988)	4.3	1.35	1.04	2–17	066–1.61	Air	Water	1 (RT)	n/a	0.60, 2
Linek et al. (1987)	5.2	1.69	1.09	2.12–4.24	1.4–3.8	Air	Water	1 (RT)	n/a	0.29
Smith et al. (1977)	2.4	1.38	0.96	4.4–46	0.25–2.44	Air	Water	1 (RT)	0.61 0.91 1.63	0.61 0.91 1.83
Smith (1991)	6.5	1.44	1.12	n/a	n/a	Air	Water	1 (RT)	n/a	0.6, 2.7, 2.7
Smith and Warmoeskerken (1985)	12.6	1.54	1.27	n/a	n/a	Air	Water	1 (RT)	n/a	0.44
Whitton and Nienow (1993)	3.5	1.17	1.00	n/a	n/a	Air	Water	1 (RT)	n/a	0.61, 2.67
Yawalkar et al. (2002)	3.4	1.46	1.00	n/a	n/a	Air	Water	1 (RT)	n/a	
Zhu et al. (2001)	3.3	1.14	0.97	1.0-7.5	n/a	Air	Water	1 (RT)	n/a	0.69

Adapted from Yawalkar et al. (2002a)

Note: The correlations by Calderbank (1958), Linek et al. (1987), Smith and Warmoeskerken (1985), Van't Riet (1979), and Zhu et al. (2001) are as cited by Yawalkar et al. (2002a).

same N/N_{CD} ratio. For example, Kapic and Heindel (2006) correlated data from several different sources and STR sizes into a single correlation[3]:

$$\frac{k_L a}{U_G^A} = C\left(\frac{N}{N_{CD}}\right)^B \left(\frac{D_i}{T}\right)^D \tag{6.11}$$

where A, B, C, and D are fitted constants. These results are shown in Figure 6.23. This correlation does a good job of fitting the experimental data for a variety of tank sizes. However, the correlation is valid only for STRs with Rushton-type impellers operating in the completely dispersed flow regime.

In order to achieve more consistent scale-up success, full-scale and pilot reactors should have geometric and hydrodynamic similarities. The pilot reactor used for preliminary design should have operational relevance to the full-scale unit especially with respect to the impeller speed (Kapic and Heindel, 2006). Yawalkar et al. (2002a) went further to address the question of scale-up by defining Eq. (6.10) in terms of gas volume per unit liquid volume per minute (vvm):

$$k_L a = C\left(\frac{N}{N_{CD}}\right)^A (\text{vvm})(T)^B \tag{6.12}$$

where A, B, and C are fitted constants. Equation (6.12) proved more effective at predicting $k_L a$ for larger volumes. This scaling approach is, however, limited because it requires the pilot reactor to provide a vvm 10 to 20 times higher than the full-scale version (Benz, 2008).

A much simpler approach can be taken with systems having geometric and hydrodynamic similarities. It is often thought the gas–liquid mass transfer coefficient could be increased by increasing the amount of gas in the reactor volume. This idea has been in extensive use in multiple impeller systems because of the difficulty in determining k_L (Moucha et al., 2003). Total gas holdup ϵ was used to represent this concept (Moucha et al., 2003) and is defined as

$$\epsilon = \frac{\forall_g}{\forall_g + \forall_L} \tag{6.13}$$

where $\forall_g$ and $\forall_L$ are the gas and liquid volumes, respectively. A very simple form of the gas–liquid mass transfer coefficient proposed by Stenberg and Andersson (1988b) is

$$k_L a = C\epsilon \tag{6.14}$$

where C is a fitted value.

Stenberg and Andersson (1988b) found that Eq. (6.14) accounted for over 93% of their data. It was concluded that the gas–liquid mass transfer coefficient variations in a system are explained by changes in the interfacial area due to its connection to gas holdup by Eq. (6.2). They also found that a large error

[3]The original correlation in Kapic and Heindel (2006) inadvertently transposed the D_i/T fraction.

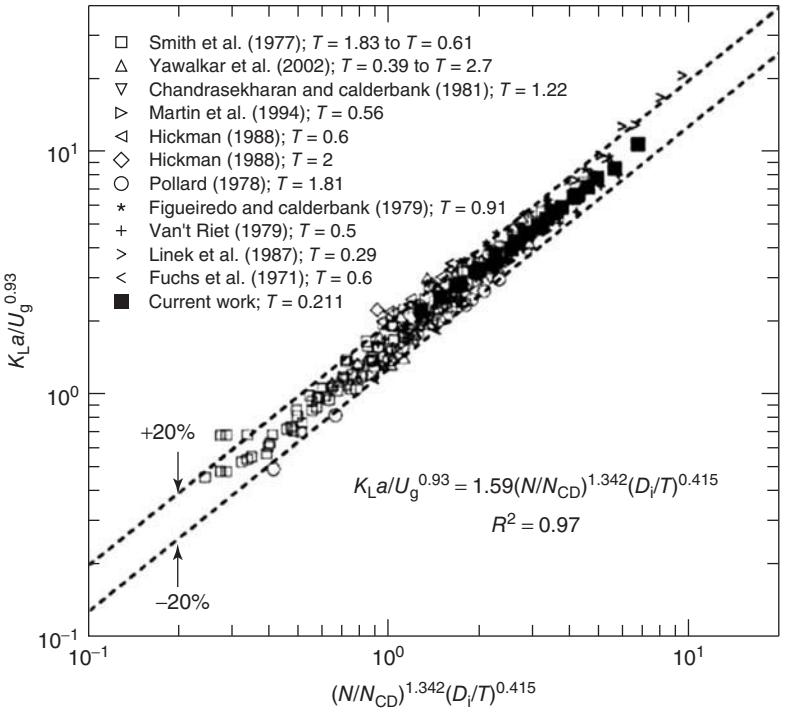

Figure 6.23 Scale-up correlations developed by Kapic and Heindel (2006). Note the original correlation by Kapic and Heindel inadvertently transposed the D_i/T fraction and has been corrected here.

in the bubble diameter would create a relatively small error in k_La, which was shown using Eq. (6.3). Unfortunately, the correlation does not communicate any information regarding the mass transfer process, hydrodynamics, or fluid properties and is somewhat unconventional since no other authors have presented their work in this form. The reactor design and operational uniqueness are not accounted for with Eq. (6.14). In addition, Moucha et al. (2003) found that axial flow impellers, which could provide higher gas holdup, would still underperform radial flow impellers in terms of mass transfer due to their inability to provide smaller bubble diameters. Therefore, Eq. (6.14) will fail during scale-up, but could be used as a first approximation for a similar design and size.

The scale-up problems arise from the fact that all STR gas–liquid mass transfer correlations are empirical. They are, for the most part, unable to account for hydrodynamic or liquid property changes with scale and time. Extensive attempts have been made in using nondimensional groups, especially toward solving gas–liquid processes involving non-Newtonian liquids. These correlations tend to be more complicated and require numerous static, but only few dynamic, inputs. One of the simplest correlations is presented by Ogut and Hatch (1988), which involves four dimensionless groups and requires six inputs. One of the more complicated forms,

proposed by Nishikawa et al. (1981), uses 12 dimensionless groups because the model tries to explain operation during low power input leading to the STR behaving like a bubble column. A general word of warning would be that if a correlation is based on statistical fitting, it runs the risk that the fit is achieved by probability rather than causality. The result could be that the correlation predicts improbable outcomes when extended beyond the operating range (Stenberg and Andersson, 1988b).

6.10 SUMMARY

STRs are one of the standard bioreactor designs used in biological applications because gas–liquid mass transfer can be easily increased through faster impeller speed and higher gas flow rates. STRs come in many different flavors and scales. Small and experimental scale STRs can be serviced by a single impeller while most industrial applications use multiple impellers. The best choice for single impeller STRs is a radial disc impeller, but other designs may be more advantageous depending on the application. For example, retrofitting with some radial flow impeller, such as the Rushton-type turbine, may be difficult due to its high torque; however, replacement or addition of an axial flow impeller, such as the A-315, is easily achieved without further stress on the motor and gearbox. Therefore, a multiple impeller design with a non-interfering radial flow impeller (bottom) and axial flow impeller(s) is preferred.

Theoretical models explaining mass transfer are in place, but a $k_L a$ equation, which is applicable over a wide array of designs and operational range, is still not available. The interaction between the impeller and the gas and liquid phases is very complicated and a lot of ambiguity and controversy exists. Literature is often filled with contradictory suggestions and explanations. Hence, practical design procedures, such as scale-up or retrofitting, can be very complicated and results are often hard to predict correctly. Furthermore, microorganisms add another level of complication because they may be sensitive to the reactor conditions so that production declines even if gas–liquid mass transfer, the supposed limiting factor, increases. These interactions in turn have led to industrial applications often being dominated (in terms of time) by the last 10–20% of conversion (relative).

Therefore, great care has to be used in designing, operating, or retrofitting STRs for biological applications. Scale-up may be more successful if the experimental and industrial scale designs have hydrodynamic and geometric similarities because the probability of similar conditions is increased. In such a case, it is expected that production would also meet predicted values. In addition, the implemented scale-up strategy has to account for increased turbulence with scale. A common error is to use a constant impeller speed scale-up strategy, which leads to much higher levels of turbulence and power costs at the industrial scale. In fact, a global scale-up strategy does not exist, and any designs and modifications have to be thoroughly tested. The trial-and-error method cannot be avoided, but hydrodynamic and geometric similarities reduce the time and cost required to achieve satisfactory results.

7 Bubble Column Bioreactors

7.1 INTRODUCTION

Bubble columns (BCs) belong to a family of pneumatic bioreactors. These bioreactors do not have any mechanical or otherwise moving parts. Compressed air, which is used for mixing purposes, is injected into the base of a cylindrical vessel. This approach provides a cheap and simple method to contact and mix different phases (Díaz et al., 2008). The liquid phase is delivered in batch or continuous mode, which can be either countercurrent or cocurrent. The batch BC is the more common form, but the cocurrent version, shown in Figure 7.1, is also encountered. Countercurrent liquid flow is rarely used in industry as it provides minor, if any, advantages and multiple complications (Deckwer, 1992), with separation by evaporation being one of the few exceptions (Ribeiro Jr. and Lage, 2005).

The gas throughput has a significant impact on the column design. Superficial gas velocity in BCs is limited to $U_G = 0.03-1\,m/s$ with most applications operating at the lower end. The exact value is scale and flow regime dependent and only large industrial projects would use $U_G \approx 1\,m/s$. Such flow rates lead to very fast-rising bubbles (Deckwer, 1992; Krishna et al., 2001).

BCs tend to be tall vessels with a large aspect ratio (H/D_R). The height is an important design variable because of its influence on the process and residence times, especially for batch and semibatch operations (Roy and Joshi, 2008). Biochemical processes require an aspect ratio between 2 and 5 even for experimental work. Industrial applications require much taller vessels with an aspect ratio of at least 5 (Kantarci et al., 2005), and it is fairly common to have vessels with an aspect ratio greater than 10 (Bellgardt, 2000b). An aspect ratio greater than 5 is also preferred because it does not influence BC hydrodynamics (Ribeiro Jr., 2008). It also allows for the breakup and coalescence mechanism to stabilize and reach steady state.

The upper section of the BC is often widened to encourage gas separation. BC volume is dependent on the application. The chemical production industry uses columns with volumes on the order of $100-200\,m^3$, whereas the biotechnology industry and wastewater treatment use columns that may be up to 3000 and $20{,}000\,m^3$, respectively (Deckwer, 1992).

An Introduction to Bioreactor Hydrodynamics and Gas-Liquid Mass Transfer, First Edition.
Enes Kadic and Theodore J. Heindel.

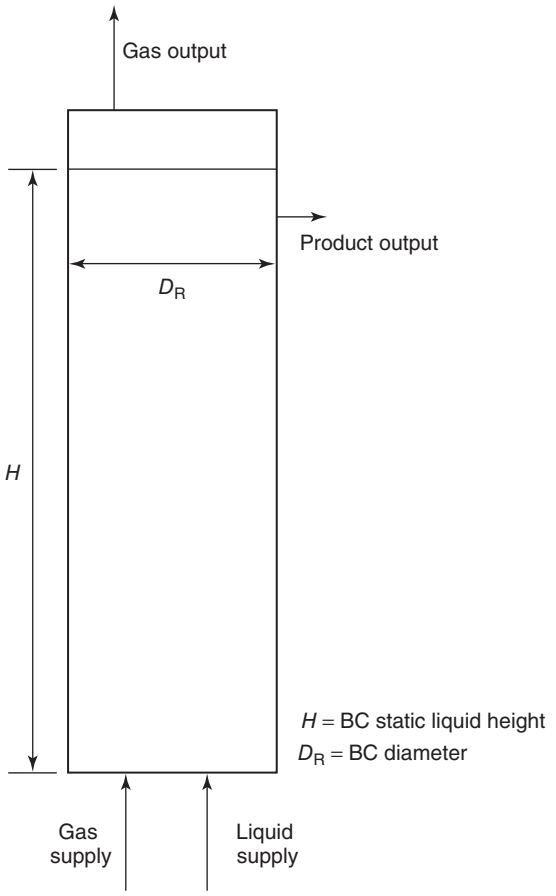

Figure 7.1 Bubble column schematic; if the liquid is also flowing continuously, the bubble column would be identified as cocurrent.

BCs require very little maintenance or floor space and have low operating costs compared to other reactor types (Ribeiro Jr., 2008). The low operating and maintenance costs are due to the lack of moving parts. Compressed gas is capable of producing a friendlier and uniform environment, which is important for processes involving shear-sensitive microorganisms or pressure-sensitive catalysts (Kantarci et al., 2005). Compressed gas is also a more effective power source for very large reactor volumes (up to 500 m^3) (Bellgardt, 2000b). The pneumatic power source typically produces lower energy dissipation rates compared to stirred-tank bioreactors. Furthermore, BC designs allow for online modification of microorganism concentrations (Kantarci et al., 2005) and handling of materials that may cause erosion or plugging (Ribeiro Jr., 2008).

The above advantages make BCs ideally suited for a variety of process industries including the chemical, petrochemical, biochemical, pharmaceutical, food,

environmental, and metallurgical industries, and are used in operations such as oxidation, chlorination, alkylation, polymerization, and hydrogenation. BCs are also widely used for the treatment of wastewater and manufacture of synthetic fuels (through fermentation), enzymes, proteins, and antibiotics (Kantarci et al., 2005).

Ultimately, the BC is preferred by many because it is easily applied to problems and applications; however, the BC has innate complexities (Huang and Cheng, 2011). The major disadvantage is the difficulty in controlling the complex hydrodynamics found in the reactor, which have a controlling effect on the transport and mass transfer characteristics (Kantarci et al., 2005). The flow patterns, which are not well defined (Bellgardt, 2000b), create considerable backmixing and a large pressure drop through the column. These phenomena are due to the complex bubble interactions and their coalescence behavior (Martín et al., 2008a), which limit the designer's ability to control reactor performance (Dhaouadi et al., 2008; Roy and Joshi, 2008; Vial et al., 2001). The result is that BC behavior is fairly unknown, especially if reactor geometries, liquid properties, or operating ranges are varied in parallel (Godbole and Shah, 1986; Vial et al., 2001). Hence, design and scale-up are difficult (Ribeiro Jr., 2008; Vial et al., 2001) and require a tedious and iterative process (Godbole and Shah, 1986). Additional information on BCs is provided in the literature (Beenackers and Van Swaaij, 1993; Deckwer, 1992; Godbole and Shah, 1986; Han and Al-Dahhan, 2007; Kantarci et al., 2005; Lau et al., 2004; Ribeiro Jr. and Lage, 2005).

7.2 FLOW REGIMES

Gas–liquid mass transfer behavior in BCs is closely tied to gas holdup through the various flow regimes identified in Figure 7.2. The two principal and industrially useful flow regimes are the homogeneous and heterogeneous flow regimes (Mena et al., 2005). At low gas flow rates, the bubbly or homogeneous flow regime develops (Figure 7.2a). The regime is characterized by small bubbles that are a few

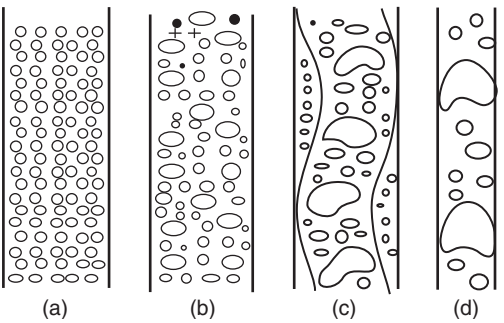

Figure 7.2 (a) Homogeneous, (b) transition, (c) heterogeneous, and (d) slug flow regimes (Kantarci et al., 2005).

millimeters in diameter and uniformly distributed in the radial direction and, therefore, rise uniformly. The bubble diameter in the homogeneous regime tends to be controlled by the sparger design and liquid properties. Bubble–bubble interaction is limited in this regime, and bubble coalescence and breakup are negligible. So, if the sparger is capable of producing smaller bubbles, these bubbles tend to stay stable at the smaller diameter.

As the gas flow rate increases, more bubbles are created without affecting the bubble diameter or distribution significantly. Hence, the interfacial area and gas holdup increase almost linearly (Kantarci et al., 2005). Mixing is minimal, which leads to very fast average bubble rise velocity (20–30 cm/s) and short residence times, even in very tall BCs (Deckwer, 1992). Therefore, better performance can be achieved at the subsequent flow regimes, which have much better mixing features; however, a significant amount of research has been directed towards the stability of the homogeneous flow regime because certain biochemical processes require the calm environment experienced in this regime. The size of most industrial units makes it difficult for the homogeneous flow regime to be used because the amount of gas throughput and mixing is often inadequate (Kantarci et al., 2005). Additional geometric restraints exist for reactors using the homogeneous flow regime. These restrictions will be discussed in Section 7.3.

As the gas flow rate is increased, the flow evolves into an unstable structure, referred to as the transition regime (Figure 7.2b). The flow regime transition in terms of gas holdup as a function of superficial gas velocity is shown in Figure 7.3. Bubbles collide and distinct bubble classes are formed. The nature of the transition can occur through two different paths. The first is described by line "a" in Figure 7.3. The gas holdup and interfacial area are still increasing within the transition regime up to a local maximum. This effect is mainly due to the balancing act between more gas being present in the reactor and coalescence phenomenon, which lead to larger bubbles and faster bubble rise velocities, leading to a local gas

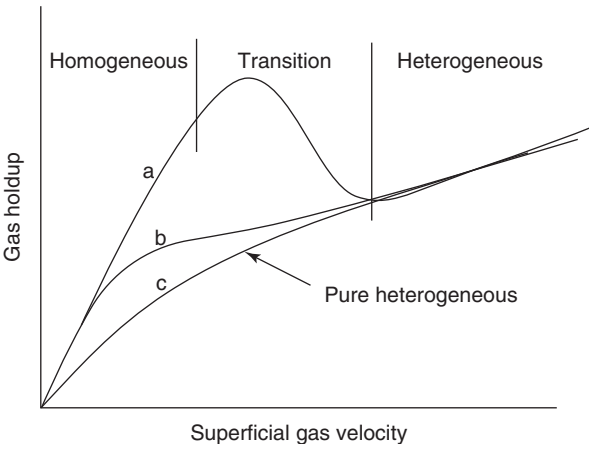

Figure 7.3 Flow regime progression (Su and Heindel, 2005b).

holdup maximum (Kantarci et al., 2005). Another reason for the increase is that the larger bubbles tend to breakup and coalesce frequently, adding to turbulence (Dhaouadi et al., 2008).

After the maximum has been reached, gas holdup and interfacial area decrease as the larger bubbles start to take control of gas holdup behavior (Kantarci et al., 2005). The second path, described by line "b" in Figure 7.3, occurs much faster and is identified by a continuous increase in gas holdup, albeit at a smaller rate, once the flow reaches the heterogeneous flow regime. Line "c" in Figure 7.3 represents a pure heterogeneous flow regime, which may occur with viscous liquids, large orifices, and/or small BC diameters (Ruzicka et al., 2003; Ruzicka et al., 2001b).

The instability that triggers the flow regime transition is mainly due to the bubble size and shape—smaller bubbles with rigid interfaces stabilize the flow because these bubbles have an inherent aversion to coalescence and breakup (León-Becerril and Liné, 2001). If the colliding bubbles are deformable, the collision is inelastic and will have an easier time forming a liquid channel to drain the liquid film, which separates the two bubbles. If, on the other hand, the colliding bubbles are nondeformable (rigid), the bubbles have a higher probability of simply bouncing off each other or separating quickly (Martín et al., 2008a). Hence, experimental results show that spherical bubbles correlate to a transition from homogeneous flow at about $U_G = 5\,cm/s$ while ellipsoidal bubbles have a transition at a lower superficial gas velocity of $U_G = 3\,cm/s$. Therefore, the moment of transition is dependent on bubble behavior in the homogeneous regime. If the homogeneous flow regime is more stable, the transition regime will be more defined, shorter, and occur at a higher superficial gas velocity (León-Becerril et al., 2002), which are beneficial side effects for industrial applications. In practice, the transition superficial gas velocity also tends to deviate with the column dimensions, sparger design, and liquid properties (Kantarci et al., 2005). In general, coalescence starts to occur at $U_G \sim 2\,cm/s$ while the actual transition to heterogeneous flow occurs at $U_G = 4–5\,cm/s$ (Deckwer, 1992).

Even though the transition regime may offer a maximum for the gas holdup and interfacial area, it is not desired for industrial processes due to its unstable and erratic nature. The instability has made the exact identification of the transition point nearly impossible. Although computational fluid dynamics and other methods are capable of predicting the other flow regimes, these methods usually have a difficult time predicting the transition point or the hydrodynamic behavior near it (Olmos et al., 2003). Hence, even if the operator wanted to work with the transition regime, it would be nearly impossible to achieve consistent results.

The evolution to the next flow regime, the churn-turbulent or heterogeneous flow regime (Figure 7.2c), is signaled by an increase in gas holdup and interfacial area with increasing gas flow rate. This growth is fairly small (less than linear) and tends to trail off. The mean bubble diameter, which tends to be on the order of a few centimeters, is controlled by coalescence and breakup mechanisms in the center section of the BC. Even though the gas–liquid mass transfer coefficient is lower in the heterogeneous regime than in the homogeneous regime, most industrial units

operate in this flow regime (Ruzicka et al., 2001a) because it offers significantly better mixing and acceptable gas holdup and interfacial area values. Furthermore, selectivity and productivity requirements force a large number of industrial operations to be highly turbulent, which is an advantage of the heterogeneous regime (Jakobsen et al., 2005b).

Phase backmixing is a characteristic of the heterogeneous flow regime and represents a major disadvantage for certain types of operations. It causes very complex hydrodynamic behavior, which leads to significant problems for the design and scale-up of BCs. The backmixing and recirculation are induced by a differential static pressure between the central and wall regions (Zahradnik et al., 1997). The basic description of backmixing and circulation has changed significantly over the decades. The view was that circulation in BCs occurred mainly in upward moving cells; however, more recent studies have shed light into stationary or periodic cell behavior (Huang and Cheng, 2011).

As the flow transitions to the heterogeneous flow regime, two different bubble classes emerge, small and large, and behave differently with a unique influence on gas holdup. In the transition regime, the gas holdup for large bubbles increases much faster than the gas holdup contribution due to the small bubbles. This trend continues until the coalescence rate of smaller bubbles increases so that the growth in gas holdup and interfacial area caused by large bubbles cannot account for the decrease caused by the shrinking number of small bubbles.

As the heterogeneous flow regime is entered, the gas holdup due to the large bubble classes consistently increases, but at ever decreasing rates while the gas holdup due to small bubble classes is relatively constant (Kantarci et al., 2005). This progression can be seen in Figure 7.4; it is due to the very high bubble rise velocity of the large bubble class ($U_R \approx 160\,\mathrm{cm/s}$ at $U_G = 20\,\mathrm{cm/s}$) while the rise velocity for the small bubble class remains relatively unchanged ($U_R \approx 21\,\mathrm{cm/s}$ at $U_G = 20\,\mathrm{cm/s}$) (Schumpe and Grund, 1986).

For small column diameters ($D_R < 0.15\,\mathrm{m}$), a fourth flow regime is feasible: slug flow (Figure 7.2d). It is characterized by a train of large bubbles, which spans the entire column diameter, dominating the flow. This flow regime is not practical and is not achieved in industrial units. Another flow regime that is not often encountered is the foaming flow regime, which is present under high superficial gas velocities, viscosity, and pressure (Kantarci et al., 2005; van der Schaaf et al., 2007).

Since most industrial processes are performed in the heterogeneous flow regime, studies have been directed towards its macroscopic flow patterns. Tzeng et al. (1993) classified these macroscopic flow structures into four regions using a 2D BC: descending flow, vortical flow, fast bubble flow, and central plume. The central region of the BC is made up of a central plume through which relatively small bubbles ascended. This central plume is surrounded by a fast bubble flow that is made of larger bubbles. At the edge of this motion, vortices form that trap bubbles and liquid to form the vortical flow region. These vortices direct bubbles near the column wall to descend (descending flow region). Chen et al. (1994) arrived at similar macroscopic structures using a 3D BC. The fast and descending

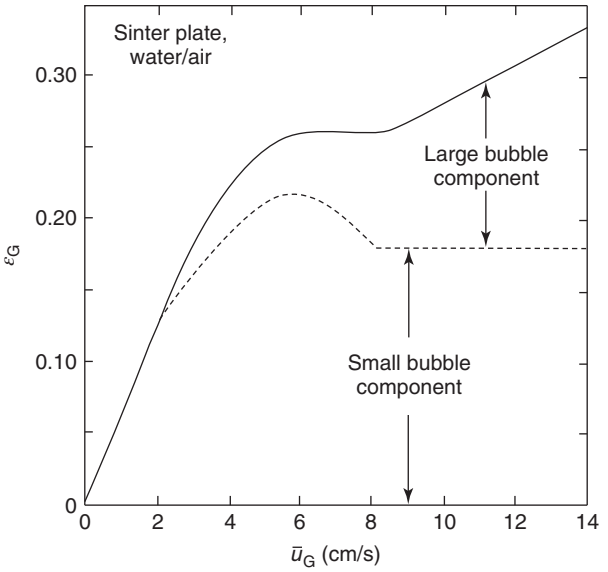

Figure 7.4 Bubble class contributions to gas holdup (Deckwer, 1992).

bubble flows, however, flowed in a spiral pattern. In addition, the homogeneous flow regime also displayed a descending flow structure near the wall region. A graphic depiction of the heterogeneous flow regime described by Chen et al. (1994) is presented in Figure 7.5.

The progression and behavior of these flow regimes is often quite complicated and depends on the superficial gas velocity, liquid properties, column dimensions, operating temperature and pressure, sparger design, and the solid phase properties (if present) (Kantarci et al., 2005). This dependence is derived from the controlling factors determining the bubble diameter.

Gas holdup and superficial gas velocity effects on gas–liquid mass transfer are analyzed based on the previously mentioned bubble interactions and flow regime progression. Global gas holdup is assumed to be directly correlated with the gas–liquid mass transfer coefficient because local variations in the interfacial area and gas holdup coincide. Having reviewed the flow regimes, it can be concluded that the transition regime offers a dilemma. Its hydrodynamics are not linear and do not follow general behavior in the homogeneous and heterogeneous flow regimes (Chaumat et al., 2005). Therefore, errors in the gas–liquid mass transfer coefficient are expected to be greater around the transition region, and better approximations are expected for correlations that take into account the regime identification.

Flow regime identification is often assumed to be based on the superficial gas velocity (all else being equal). If a correlation is based on a certain design with a specific process in mind, adjustments could be incorporated into operation while

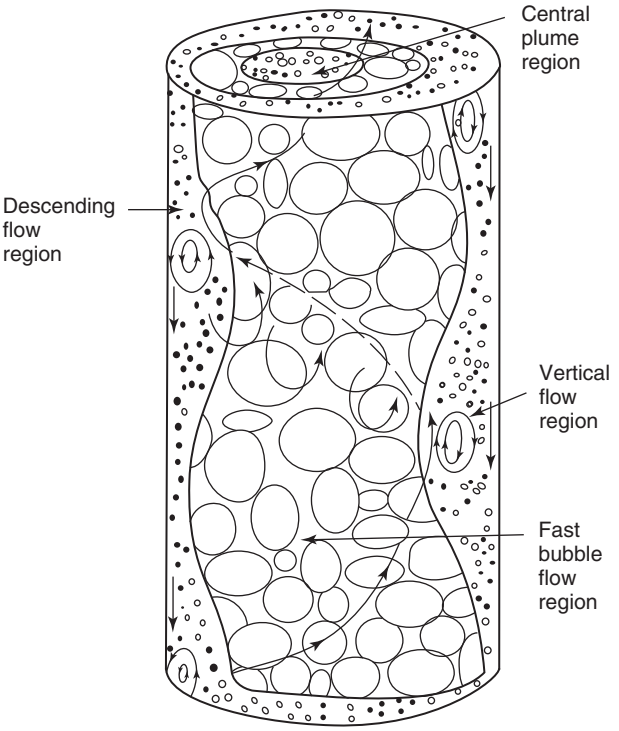

Figure 7.5 Macroscopic flow structure in the heterogeneous flow regime (Chen et al., 1994).

assuming that the results will be close to the predicted values. At the same time, most correlations neglect any changes in the liquid-phase mass transfer coefficient. If operation is expected to include rheological changes, which may have a significant effect on the liquid-phase film resistance, the correlation could fail. It would produce additional variations in the gas–liquid mass transfer correlation that could not be accounted for by variations in the interfacial area and its codependent variations in gas holdup. Therefore, a proper gas–liquid mass transfer study should attempt to separate the approximation of the liquid-phase mass transfer coefficient and the interfacial area under such circumstances.

7.3 COLUMN GEOMETRY

7.3.1 Column Diameter

The gas–liquid mass transfer coefficient and gas holdup tend to decrease with increasing BC diameter in the homogeneous and transition flow regime (Zahradnik et al., 1997) up to a critical value (Deckwer, 1992; Shah et al., 1982; Zahradnik et al., 1997), which is usually cited to be $D_R = 0.15\,m$ (Kantarci et al., 2005);

however, gas holdup has been influenced by column diameters greater than 0.15 m in the homogeneous and heterogeneous flow regimes (Ruzicka et al., 2001a; Vandu and Krishna, 2004), and the critical diameter is more accurately described to lie in the range of 0.1–0.2 m (Zahradnik et al., 1997).

The diameter dependence is created by several factors such as wall effects (Lau et al., 2004), which are negligible for water-filled columns larger than 0.10 m (Kantarci et al., 2005; Lau et al., 2004), and the flow and mixing conditions (Krishna et al., 2001; Zehner, 1989). The wall effect on gas holdup is summarized in Figure 7.6. Figure 7.6a and 7.6c represent radial gas holdup profiles in small BCs ($D_R \leq 0.060$ m), while Figure 7.6b and 7.6d represent more realistic effects in larger BCs. Hence, smaller BCs distort gas holdup behavior and may also misrepresent bubble diameter measurements (if done visually). Column diameter also has a strong influence on flow stability, defined by a critical gas holdup and gas flow rate at which the onset of the transition flow regime occurs. A larger diameter causes instability and earlier transition while a smaller diameter would induce the opposite behavior (Ruzicka et al., 2001a).

Although the slug flow regime is defined by low gas holdup and is observed in small BCs, small BCs do not necessarily have low gas holdup. The smaller BC diameter may limit the bubble size distribution, which can lead to smaller bubbles, increase stability, and sustain a higher gas holdup. Once the column diameter is

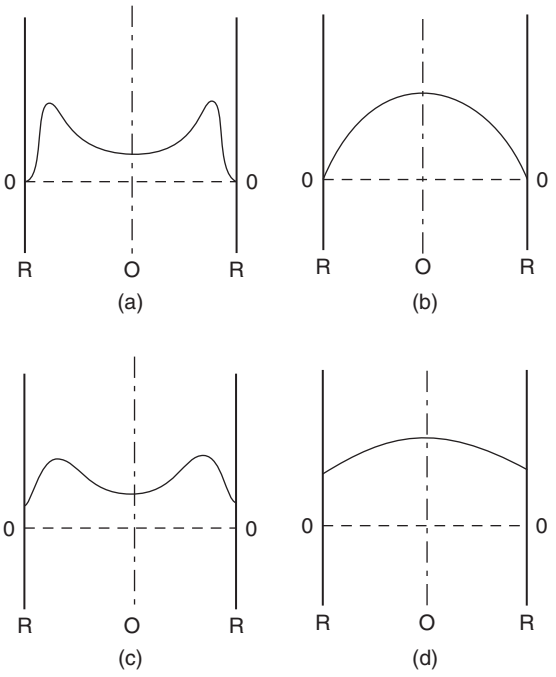

Figure 7.6 Radial gas holdup profiles for small (a and c) and large (b and d) bubble column diameters (Veera and Joshi, 1999).

larger than 0.10–0.15 m, the bubble size distribution is controlled by the coalescence and breakup mechanisms (Lau et al., 2004). This effect has been confirmed by Bouaifi et al. (2001) who investigated different gas distributors and column sizes; their results are shown in Figure 7.7.

It is often observed that the smaller bubble class is not affected by BC diameter while the larger one is (Kantarci et al., 2005; Li and Prakash, 2000). Larger BCs experience a larger degree of recirculation, which may lead to a higher degree of coalescence, higher bubble rise velocities, and lower gas holdup values (Krishna et al., 2001; Zehner, 1989). It is also feasible to observe lower gas holdup values in a smaller BC if it is operated in the slug flow regime, which is dominated by very large and fast-rising bubbles. Larger columns cannot maintain this mode of operation so that a direct comparison at a higher gas flow rate may lead to the conclusion that larger columns have larger gas holdup values (Daly et al., 1992). This effect can be seen in Figure 7.8 where the BC with the largest diameter shows the best gas holdup performance. A fairer comparison would be made on a gas flow rate per unaerated liquid volume basis.

Research work by Krishna et al. (2001) and Zehner (1989) concluded that most studies did not account for the flow regime dependence. For example, the heterogeneous flow regime, for which significant column geometry research exists, has a positive effect due to the higher degree of liquid recirculation. The homogeneous flow regime, on the other hand, has limited liquid recirculation by design. Instead, the larger BC diameter leads to faster bubble rise velocities, especially in the central region, which leads to lower gas holdup and gas–liquid mass transfer. Unfortunately, a significant number of gas holdup and gas–liquid mass transfer studies fail

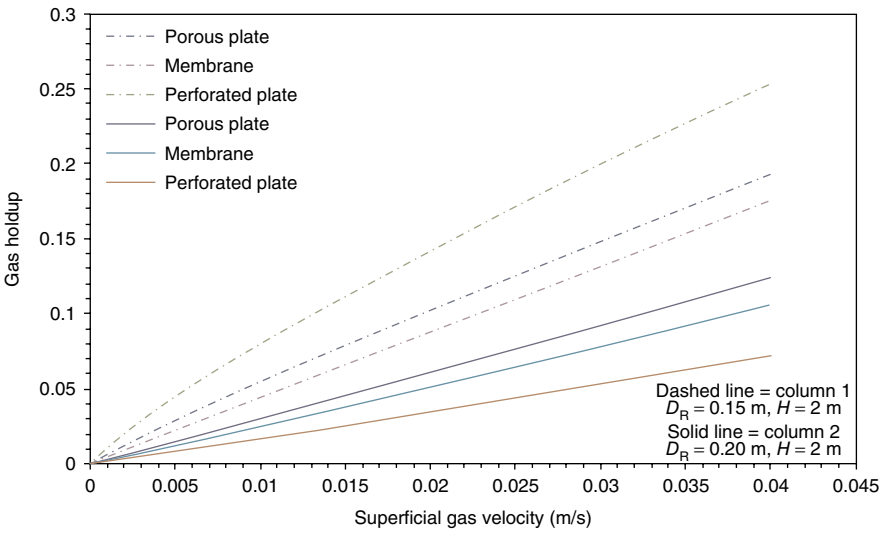

Figure 7.7 Gas holdup dependence on column diameter and gas distributor. Adapted from Bouaifi et al. (2001).

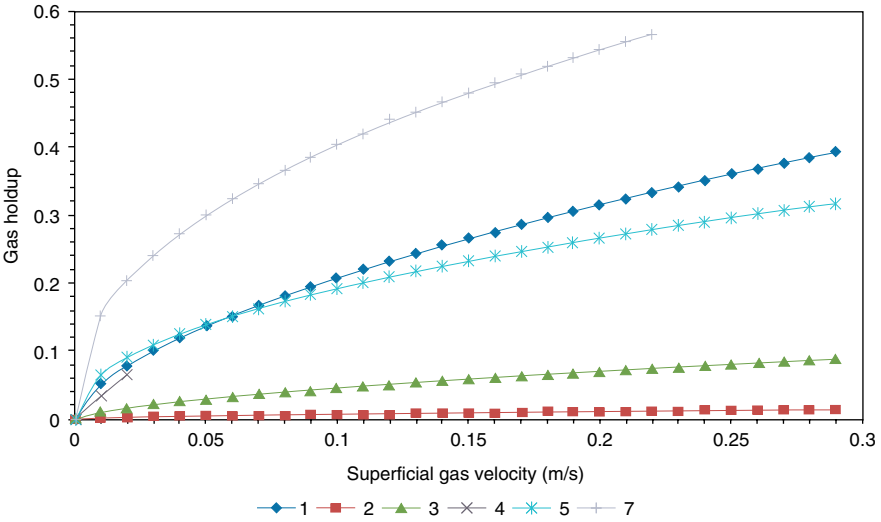

Figure 7.8 Gas holdup correlation sample using tap water at 15 °C as liquid phase: (1) Anabtawi et al. (2003) ($H = 0.60$, $D_R = 0.074$ m), (2) Deckwer (1992) ($D_R = 0.14$ m), (3) Godbole et al. (1982), (4) Hammer (1984), (5) Hikita and Kikukawa (1974) ($D_R = 0.10$ m), (6) Hughmark (1967) ($D_R = 0.0254–0.10$ m), and (7) Reilley et al. (1986) ($D_R = 0.30$ m).

to identify the flow regime in which the BC is operating, which makes meaningful comparisons often difficult.

The effect of column diameter on bubble size and flow regime has led to the introduction of flow regime maps, such as the one presented in Figure 7.9. These maps plot the regimes depending on the superficial gas velocity and BC diameter and attempt to predict the gas holdup; however, the maps are only examples and cannot be applied universally. Flow regimes and bubble behavior are also influenced by the gas distributor design and physiochemical properties of the liquid phase. Changes in these factors bring about significant variations, which are not accounted for by flow regime maps. Nonetheless, these maps may be used as operating instructions for a reactor design that has been extensively studied.

7.3.2 Unaerated Liquid Height

The BC height, defined by the static liquid level, regulates the residence time over which the bubbles are allowed to go through the coalescence and breakup process. In other words, the column height may allow enough time for equilibrium to be reached. Hence, shorter columns often experience smaller bubble size distributions and higher gas holdup values (Kantarci et al., 2005; Wilkinson, 1991; Zahradnik et al., 1997). A height greater than 1–3 m or an aspect ratio greater than 5 usually ensures that equilibrium has been established. Even though the gas holdup behavior indicates that operation with shorter BCs is more effective (Kantarci et al.,

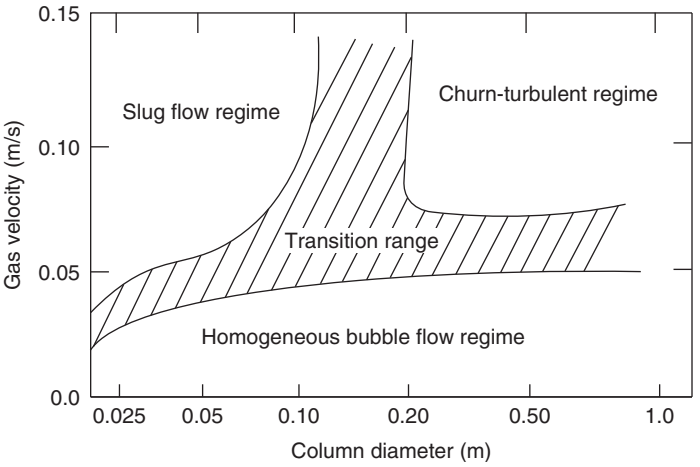

Figure 7.9 Flow regime dependence on column diameter (Kantarci et al., 2005).

2005), the practical application is limited. The residence time is simply too short and would require extensive gas recycle and a very large column footprint for meaningful BC volumes; however, the idea can be advantageous and has been applied to microreactors.

The column height may lead to bubble behavior stratification. For example, the top of the BC may experience high gas holdup due to foaming. The volume surrounding the sparger behaves differently depending on the gas distributor design. If the gas distributor is capable of producing smaller bubbles, the gas holdup is higher; however, this effect is limited only to the immediate area. The reactor bulk (middle section) usually behaves according to coalescence and breakup principles and the prevailing flow regime. Hence, the bulk region would be expected to have smaller gas holdup values (Ruzicka et al., 2001a). If the column is tall enough, such as a height greater than 1–3 m or an aspect ratio greater than 5, the sparger and foaming effects on gas holdup become negligible and the bulk region dominates reactor hydrodynamics (Veera and Joshi, 1999; Wilkinson et al., 1992; Zahradnik et al., 1997); however, foaming should still be avoided since it may damage any microorganisms and block gas disengagement.

7.3.3 Aspect Ratio

BCs are assumed to decrease gas holdup with an increase in size, but an aspect ratio above 5 does not seem to affect hydrodynamics significantly and is usually ignored. Comparisons based on aspect ratio have failed in the past due to large gas holdup data scatter. A good fit could not be obtained such that scale-up rules still need to be based on column diameter and height individually (Ruzicka et al., 2001a). Aspect ratios below 5 are rarely used in industry and are often ignored in experimental settings.

7.4 OTHER OPERATING CONDITIONS

7.4.1 Pressure

Pressure affects bubble dynamics and, therefore, has an important influence on gas holdup and gas–liquid mass transfer. It should be noted that correlations often fail to account for pressure and provide poor predictions if pressurized systems are used, as is the case in industrial applications (Dhaouadi et al., 2008). Generally, an increase in pressure is accompanied by a decrease in the bubble surface tension and an increase in bubble inertia (Kantarci et al., 2005; Luo et al., 1999) and gas solubility (Dhaouadi et al., 2008). These factors decrease the average bubble diameter, which allows for higher interfacial area and gas holdup values (Kojima et al., 1997). Thus, the higher interfacial area leads to higher gas–liquid mass transfer coefficients (Lau et al., 2004). In addition, as the bubble diameter decreases with increasing pressure, the bubble rise velocity also decreases, leading to an increased gas residence time and a more efficient gas–liquid mass transfer performance.

The effect on the liquid-phase mass transfer coefficient is most likely neutral to positive. Past experience has been that the liquid-phase mass transfer coefficient is only dependent on the phase data (Gestrich et al., 1978), but current research efforts have presented contradictory evidence (Han and Al-Dahhan, 2007), most likely due to the method used in calculating the liquid-phase mass transfer. It is probable that the effect is negligible at lower pressures due to the much more important changes in the bubble diameter and interfacial area; however, the solubility dependence on pressure could be significant, especially at higher pressure (Kojima et al., 1997).

The extent of the effect often depends on the pressure increase, liquid properties, and gas flow rates. It is often cited that pressures below 1 MPa have a negligible impact on bubble size and gas holdup; however, the references usually point to older articles that used stirred-tank reactors and have significantly different power characteristics than BCs (Stegeman et al., 1995). More recent work, on the other hand, suggests that pressure, even below 1 MPa, has a significant impact on gas holdup and the interfacial area. Furthermore, pressurization has been determined to have a more significant impact on viscous liquids, slurries, and the heterogeneous flow regime (Lau et al., 2004).

As the liquid becomes more viscous, bubbles have a tendency to coalesce more readily. The increased pressure serves as a detriment to coalescence and decreases the average bubble diameter. Hence, systems with a slurry phase benefit from pressurization (Luo et al., 1999). Bubble characteristics in the heterogeneous flow regime are defined by bubble breakage and coalescence frequencies. Once again, higher pressure tends to suppress coalescence and decrease the average bubble diameter. For example, Lau et al. (2004) varied pressure and gas flow rate in their study and found that increasing the pressure from 0.1 to 2.86 MPa led to an increase in $k_L a$ of 130% at a gas flow rate of 10 cm/s. When the same pressure increase was implemented at a gas flow rate of 20 cm/s, an increase by 187% was observed. These results can be seen in Figure 7.10. It should be noted that the gas holdup failed to predict gas–liquid mass transfer increase as pressure increased.

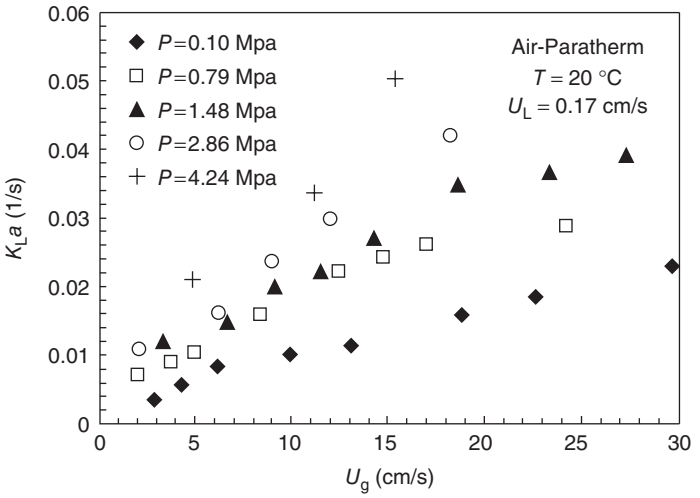

Figure 7.10 Pressure effects on gas–liquid mass transfer in a 10.16 cm bubble column with a single-nozzle gas distributor (Lau et al., 2004).

This effect can be clearly seen when a comparison is made between Figures 7.10 and 7.11, which related gas holdup to pressure.

The gas holdup data of Lau et al. (2004) are basically parallel while the gas–liquid mass transfer data have different slopes. Furthermore, the gas holdup

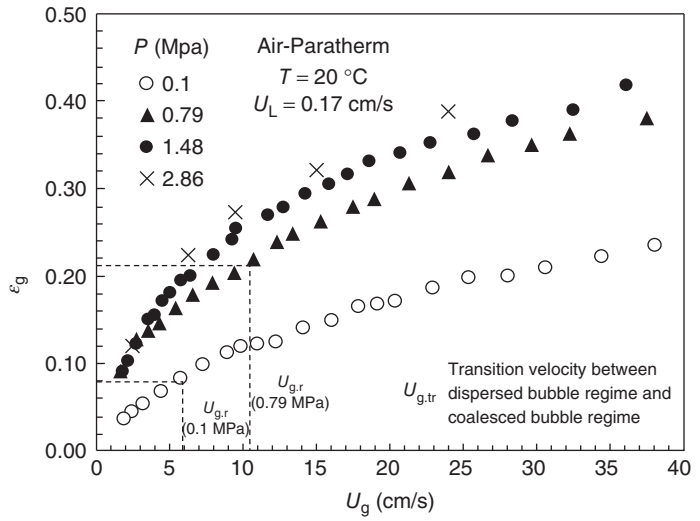

Figure 7.11 Pressure effects on gas holdup in a 10.16 cm bubble column with a single-nozzle gas distributor (Lau et al., 2004).

increase at a pressure of 1.48 MPa versus 2.86 MPa is modest at about 10% (assuming minimal experimental error) while the gas–liquid mass transfer is more impressive, especially at higher gas flow rates. These observations would lead to the conclusion that the interfacial area increased significantly from 0.1 to 1.48 MPa while the liquid-phase mass transfer coefficient had a stronger influence in the increase from 1.48 MPa to 2.86 MPa. More data points for gas–liquid mass transfer would give a larger resolution and more confidence in this conclusion.

Even more surprising was the increase in $k_L a$ with liquid velocity at high pressures observed by Lau et al. (2004). Usually, the superficial liquid velocity is ignored and is cited as having an insignificant or negative effect on gas–liquid mass transfer because a higher superficial liquid velocity is thought to decrease the gas residence time and, therefore, $k_L a$ (Chaumat et al., 2005). At a pressure of 2.86 MPa, Lau et al. (2004) observed a $k_L a$ increase by 30% when the superficial liquid velocity was increased from $U_L = 0.17$ to 0.26 cm/s.

Vibrations within the liquid phase could be introduced to improve gas holdup and gas–liquid mass transfer performance. This goal has been accomplished using mechanical vibration devices, but an easier solution would be to introduce sinusoidal pressure variations at a frequency on the order of 100 Hz and amplitude of 0.0025–0.01 mm, which lead to a reduction in the bubble diameter by 40–50% and an increase by 100–300% in gas holdup and 200% in the gas–liquid mass transfer coefficient. These variations reduced the bubble rise velocity, destabilized the bubble surface, and reduced surface tension forces, which improved the liquid-phase mass transfer coefficient (Ellenberger and Krishna, 2002).

7.4.2 Temperature

Temperature is a much more contentious issue. Generally, it is thought that higher temperatures reduce the liquid viscosity and surface tension, which would lead to a higher stability of the small bubble population and lead to higher interfacial area. In addition, the liquid-phase mass transfer (k_L) is, therefore, thought to increase with an increase in temperature due to the lower viscosity according to Calderbank's slip velocity model. At the same time, liquid-phase mass transfer coefficient is thought to decrease due to lower surface tension and turbulence. Hence, the liquid-phase mass transfer coefficient could go in either direction according to a balancing act between the two forces with increasing temperature.

Lau et al. (2004) also varied temperature with the gas flow rate and concluded that higher temperatures lead to higher gas–liquid mass transfer coefficients at constant gas flow rates. For example, an increase in temperature from 25 to 92 °C at a superficial gas velocity of 20 cm/s led to an increase in the gas–liquid mass transfer coefficient by 470% while gas holdup increased by only 25%. Although this temperature increase is huge, Lau et al. (2004) noticed a significant increase in the gas–liquid mass transfer coefficient with even a few degree Celsius change in temperature. At the same time, gas holdup did not show any significant variation.

A secondary effect could be that the rate of reaction is often directly correlated to temperature and (partial) pressure. Most rates of reaction are expected to increase

with an increase in temperature or pressure. Hence, a similar assumption is made with bioreactors. This assumption can be used as a rule of thumb, but it cannot be applied generally. The microorganism and its metabolism are the ultimate judge of the rule's applicability.

The introduction of higher temperatures and pressures leads to a potential problem. The control schema for bioreactors is generally tied to the gas flow rate. The idea is that the gas flow rate would impact gas holdup, which would, in turn, control gas–liquid mass transfer. Significant temperature changes, however, decouple gas–liquid mass transfer from gas holdup and add new operational variables. Most correlations do not include temperature and pressure effects directly, but instead attempt to quantify these effects by altering or introducing effective liquid properties, which are much harder to cost-effectively measure in an industrial setting.

The biological reaction, which may occur at the interface, is often ignored during experimental measurements and correlation formulations as these are not apparent in pure liquids without the presence of bacteria; however, industrial processes may experience a significant degree of interfacial reaction. Therefore, industrial processes would be expected to perform better than experiments might suggest due to the application of higher temperatures and pressures. In effect, the use of pure liquids may provide an additional engineering factor. Alternatively, microorganisms have to play an important role as they may limit the operating range.

7.4.3 Viscosity

The liquid viscosity determines the degree to which bubbles can deform. As the viscosity increases, bubbles become more deformable and the steady-state bubble diameter increases (Martín et al., 2008a), while bubble breakup is suppressed (Zahradnik et al., 1997). Deformable bubbles allow for the bubble interface to drain much easier and allow for coalescence to occur in a shorter amount of time. First, the bubble breakup is suppressed because the higher viscosity tends to reduce turbulence. A second negative effect is that the larger bubbles have a higher rise velocity and lead to a shorter residence time for the gas phase (Zahradnik et al., 1997). Hence, higher viscosity liquids are observed to have larger bubbles and smaller gas holdups and interfacial areas (Li and Prakash, 1997; Zahradnik et al., 1997).

Viscosity also affects the liquid-phase mass transfer coefficient through the Stokes–Einstein effect. Einstein proposed that the diffusion coefficient could be expressed as

$$D_{\mathrm{L}} = \frac{RT}{N_{\mathrm{A}}} \frac{1}{6\pi \mu_{\mathrm{L}} r_{\mathrm{B}}} \tag{7.1}$$

where R, T, N_{A}, μ_{L}, and r_{B} are the gas constant, temperature, Avogadro's constant, viscosity, and bubble radius, respectively (Sharma and Yashonath, 2006). Hence, a higher viscosity could significantly reduce the diffusivity, which in turn would decrease the liquid-phase mass transfer coefficient (Chaumat et al., 2005; Lau et al., 2004; Sharma and Yashonath, 2006; Waghmare et al., 2008); however, the decrease

in the interfacial area is expected to dominate the decrease in the liquid-phase mass transfer coefficient.

7.4.4 Surface Tension and Additives

Surface tension is a liquid property that tends to counter bubble deformation and encourages bubble breakup (Akita and Yoshida, 1974; Mehrnia et al., 2005; Walter and Blanch, 1986). The result is a more stable bubble interface that leads to smaller bubble diameters, a more stable flow regime (Lau et al., 2004; Schäfer et al., 2002), and higher gas holdups and interfacial areas (Kluytmans et al., 2001). It is also thought that a lower surface tension leads to a higher contact time because the liquid flow over the bubble surface is slowed (Lau et al., 2004).

Surface tension is influenced by the presence of surfactants (Kantarci et al., 2005). Surfactants attach themselves to the bubble interface and form a hydrophilic boundary at the bubble surface. The result is a much smaller bubble size and a more rigid surface. This surface, in turn, lowers the bubble surface tension and further reduces the bubble rise velocity.

Electrolytes have been shown to increase gas holdup and decrease bubble diameter (Kantarci et al., 2005) even at high concentrations where they result in a surface tension higher than that of pure water (Levin and Flores-Mena, 2001). At relatively low concentrations, electrolytes decrease surface tension and reduce the film drainage speed, leading to higher gas holdup (Kluytmans et al., 2001). Antifoam agents, on the other hand, cause a decrease in gas holdup due to higher surface tension and enhance coalescence leading to larger bubble diameters (Veera et al., 2004). Other impurities, especially of organic origin, tend to increase gas holdup and create immobile bubble interfaces; however, most research has been conducted using inorganic mixtures or pure liquids (Chaumat et al., 2005).

Alcohols create smaller bubbles and higher gas holdups because they are either amphiphilic or have a lower surface tension so that the aqueous mixture supports smaller bubbles. This behavior has been observed for a large number of alcohols in an aqueous saccharose solution. The only exception was proved to be methanol. The theory, which was successfully tested by Zahradnik et al. (1999b), is that the longer carbon chains increase the effectiveness (of alcohols as coalescence suppressants) and cause methanol, the simplest alcohol, to lose its usefulness at a much lower concentration relative to the other alcohols (Zahradnik et al., 1999a; Zahradnik et al., 1999b).

7.5 GAS DISTRIBUTOR DESIGN

Gas distributors used in BCs include (i) sintered, perforated, or porous plates; (ii) membrane or ring-type distributors; (iii) arm spargers; or (iv) single-orifice nozzles. The sintered plate (Figure 7.12a), which is usually made out of glass

or metal, produces very small bubbles. Comparative experimental works are expected to find the sintered plate to perform the best using gas holdup as the criteria due to its effectiveness of creating small bubble populations; however, it is rarely used for industrial applications because it can plug very easily and requires cocurrent operation and significant maintenance. Perforated plates (Figure 7.12b), which are normally made out of rubber or metal, usually have holes 1–5 mm in diameter and are the most common gas distributor for BCs. The total aeration open area is usually maintained between 0.5% and 5% of the cross-sectional area of the reactor. Single-orifice nozzles (Figure 7.12c) are simple tubes, which are able to produce uniform gas flow far from the injection point. The flow, however, tends to be somewhat unstable. BCs may also use ring spargers (Figure 7.12d). Ring spargers are able to produce uniform and stable flow, but are usually unable to produce small bubbles (Deckwer, 1992) and lead to an earlier transition to the heterogeneous flow regime than the perforated plate (Schumpe and Grund, 1986).

The effects of gas distributor design and its extent depend on the superficial gas velocity and flow regime in which the BC operates. In the case of heterogeneous flow, the sparger has a negligible influence on the bubble size and gas–liquid mass transfer because the bubble dynamics are determined by the rate of coalescence and breakup, which are controlled by the liquid properties and the nature and frequency of bubble collisions (Chaumat et al., 2005). Hence, the sparger effect is more pronounced at lower superficial gas velocities ($U_G < 0.15\,m/s$) while it is much less important at $U_G > 0.20$ m/s and nonexistent at $U_G > 0.30\,m/s$ (Han and Al-Dahhan, 2007). Viscous liquids are also not affected by the gas distributor design if the column is sufficiently tall (Zahradnik et al., 1997).

Furthermore, the mechanisms that dominate gas holdup (e.g., surface tension, particle wettability, ionic force of surfactant, viscosity, and density) require consideration. If the liquid undergoes viscosity or density changes through, for example, particle addition, the initial bubble diameter does not affect gas holdup in the heterogeneous flow regime. If, on the other hand, the other mechanisms are affected

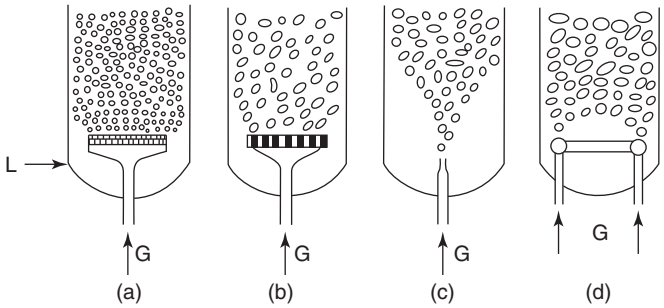

Figure 7.12 Sample bubble column aerators: (a) sintered plate, (b) perforated plate, (c) orifice nozzle, and (d) ring sparger (Deckwer, 1992).

or adjusted, such as by the addition of surfactants or electrolytes, the heterogeneous flow regime is affected by the initial bubble diameter up to a relatively high superficial gas velocity (of about 0.5 m/s), and hence, gas distributor design is important. Once a high enough superficial gas velocity is reached, the probability and frequency of bubble collision increases greatly and a precipitous decrease in gas holdup is observed (Kluytmans et al., 2001).

The homogeneous and transition regimes are highly influenced by the gas distributor design. A sparger, which is able to produce smaller initial bubble diameters, is able to produce a higher number of bubbles at the same flow rate and a more stable homogeneous flow regime (Álvarez et al., 2008). If the sparger is able to produce smaller bubbles in the homogeneous regime, the sparger would also be able to produce higher gas holdups and interfacial areas (Bouaifi et al., 2001). Hence, these spargers are also able to produce higher gas–liquid mass transfer coefficients under the homogeneous flow regime (Verma and Rai, 2003).

The distributor effect can be quite significant such that the gas–liquid mass transfer correlation can vary by up to a factor of 2 (Lau et al., 2004). The extent to which the gas distributor affects gas holdup and bubble dynamics depends on the BC geometry and superficial gas velocity. The taller the column is, the smaller the influence of the initial bubble diameter will be on the global gas holdup. A higher superficial gas velocity increases the probability and frequency of bubble collisions and decreases the effect of the initial bubble diameter and gas distributor design.

The assumption made up to this point is that all spargers are indeed capable of producing the entire range of flow regimes; however, Wilkinson (1991) noted that the discussion was irrelevant if the orifice diameter was larger than 1–2 mm because it would create bubbles that are too large and would be affected by the macroscopic flow pattern alone. In order to create significant influence, the aeration holes have to be smaller than 1 mm. Zahradnik et al. (1997), however, investigated the performance of a perforated plate and concluded that the hole diameter has to be smaller than 0.5 mm for a significant effect. A perforated plate with an orifice diameter of even 0.6 mm only created the heterogeneous flow regime using a variety of liquids.

The open area ratio, defined as the total aeration orifice area divided by the column cross-sectional area, was investigated and led to many conflicting conclusions. Different researchers approached the subject from different directions. One camp has chosen to adjust the number of holes while keeping the orifice diameter constant, whereas the other camp increases the orifice diameter while keeping the number of holes equal. Both approaches are potentially troublesome. If the open area ratio is increased by increasing the number of holes and keeping the orifice diameter constant, the holes could be spaced too close such that neighboring orifices start acting as a single sparger hole at higher gas flow rates. This sparger behavior is caused by immediate coalescence from neighboring bubbles as they are created and prior to their disengagement from the sparger orifice (Martín et al., 2008a; Su and Heindel, 2005a). If the holes are made larger while the number is held constant, the homogeneous flow regime could be skipped entirely (Zahradnik et al., 1997). Regardless, the agreement exists that if the open area ratio decreases, gas

holdup increases, but the homogeneous flow regime stability may not necessarily be affected (Su and Heindel, 2005a). Logically, the open area ratio does not affect gas holdup in the fully developed heterogeneous flow regime (Kantarci et al., 2005; Su and Heindel, 2005a).

Bubble formation and orifice activity are two important factors determining stability. Synchronous bubble formation, where almost all holes are active instantaneously, tends to produce a uniform bubble and gas holdup distribution. The uniform bubble distribution leads to a more stable homogeneous flow regime, less liquid recirculation, and higher gas holdup and gas–liquid mass transfer. Asynchronous orifice operation is often accompanied by alternating or oscillating orifice activity, which leads to flow instability. The instability creates more bubble–bubble interaction and leads to lower gas holdup and gas–liquid mass transfer. Hence, the gas distributor affects the critical superficial gas velocity at which the transition regime is detected.

Perforated plates are defined by a critical flow rate above which the orifice operation is asynchronous and the liquid flow in the sparger region is relatively unstable. As the hole spacing decreases, the critical flow rate decreases as well. At the same time, perforated plates require a minimum pressure drop in order to achieve uniform orifice activity. In other words, a critical flow rate is also created at the lower end such that a lower flow rate would lead to instability as well (Kang et al., 1999; Ruzicka et al., 2003; Su and Heindel, 2005a). This effect would produce additional complications in making comparative analysis between research works using different open area ratio adjustment methods.

Vial et al. (2001) compared different gas distributor designs and made several interesting observations. The single-orifice nozzle tended to produce highly nonuniform flow while the porous plate and multiple-orifice sparger produced a fairly uniform flow pattern. This led the single-orifice sparger to always operate in the heterogeneous flow regime. Furthermore, the multiple-orifice sparger proved to be the most dependable. It produced the homogeneous flow regime until the superficial gas velocity reached about 4 cm/s. The heterogeneous flow regime would fully develop at 11–12 cm/s. The porous plate, on the other hand, was sensitive and provided different results depending on the start-up procedure.

Kluytmans et al. (2001) compared initial bubble diameters produced by different gas distributors and found that a 30-μm porous plate produced much smaller bubble diameters (0.2–0.5 mm) than the 0.5 mm perforated plate (1–2 mm). The higher gas holdup performance of the porous plate was attributed to the creation of these smaller bubbles.

Bouaifi et al. (2001) used two different columns (Column 1 with $D_R = 0.15\,\text{m}$; Column 2 with $D_R = 0.20\,\text{m}$; $H = 2\,\text{m}$) and found that the porous plate generally produced higher gas holdup, followed by the membrane distributor and perforated plate. They agreed that smaller bubbles would lead to higher gas holdup values, and also concluded that the power consumption can vary significantly. For example, the membrane gas distributor would create very small bubbles with 80% of the bubble population being in the 3.5–4.5 mm range, which compared well with the results of the porous plate and its range of 2.5–4.5 mm. The membrane

gas sparger, however, used much more power to obtain similar results. This is usually not a concern in an experimental setting, but may be of concern in (larger) industrial operations. Bouaifi et al. (2001) are the only researchers to account for the power usage of the different gas distributor designs. This is most likely due to the often ignored or relatively minor cost of compressed gas for experimental vessels.

7.6 CORRELATIONS

Correlations attempt to reflect the reactor environment as closely as possible. This goal is most often achieved through empirical data fitting (Martín et al., 2009). Analytical expressions are rarely used because they are burdensome with regard to the required data (Dhaouadi et al., 2008). A single correlation based on first principles does not exist for BCs due to the complexities discussed above. For example, Tang and Heindel (2006b) described what is needed to develop a dimensionless correlation for gas holdup in a BC based on the Buckingham-Pi Theorem, and they identified nine dimensionless parameters containing 13 variables representing three basic dimensions:

$$\epsilon = f\left\{ R_A, \frac{H}{D_R}, \frac{d_0}{D_R}, \frac{\rho_G}{\rho_L}, \frac{\mu_G}{\mu_L}, \frac{U_G}{U_L}, Re_L, Fr, We \right\} \tag{7.2}$$

where $R_A, H, D_R, d_0, \rho_G, \rho_L, \mu_G, \mu_L, Re_L, Fr$, and We are the gas distributor open area ratio, BC height, BC diameter, gas distributor orifice diameter, gas- and liquid-phase densities, gas- and liquid-phase viscosities, gas- and liquid-phase superficial velocities, liquid-phase Reynolds number, Froude number, and Weber number, respectively.

Unfortunately for industrial settings, a majority of gas holdup and gas–liquid mass transfer correlations require inputs that are not easily collected for large tanks used in mass production settings. For example, commonly used inputs for gas holdup are the average bubble diameter and superficial gas velocity. Although superficial gas velocity is easily estimated, real-time average bubble diameter data are very hard to obtain. Large reactors have a great deal of spatial variation. In addition, industrial tanks are made out of steel and include nontransparent liquids. Visual bubble diameter observations, which are commonly used in experimental settings, would be unlikely to yield appropriate bubble size approximations. The changing environment would also provide many problems for process automation. Hence, it is rarely used in industrial-sized reactors.

Furthermore, many of the inputs are interdependent. The superficial gas velocity cannot be changed without impacting the average bubble diameter. This leads to the requirement of either a second data stream or an approximation for the bubble diameter, which could be built into the model from the very beginning. Another example would be that a significant number of correlations include the diffusivity and liquid properties as inputs. If the liquid is expected to change rheologically,

which often occurs in biological processes, measurement or approximation of these inputs would be needed. Once again, this is information that is not easily obtained, even in an experimental setting.

A minor inconvenience is that many BC review, and a few original articles, do not include proper classification of variables and units, which is particularly troublesome when the correlation is not dimensionless. The inputs are not categorized as being in English or SI units. Moreover, some correlations use standard units, such as Pascal-second, while others use nonstandard units, such as milliPascal-second, without acknowledgement. Many review articles also do not define the reactor or the phases involved. The classification and definition of variables are made more difficult if the correlation is based on a theoretical derivation. These correlations often include terms that are left as constants, and further work is required to define these more accurately for practical applications. Temperature or pressure readings are usually not included as parameters, but are significant in industrial practice.

These problems can be dealt with if the correlation is selected and fit for the process in question. For example, one could easily use a gas holdup correlation such as (Guy et al., 1986)

$$\epsilon = 0.386 N_o \left(\frac{g D_R^3}{\nu_L^2} \right)^{0.025} \left(\frac{U_o}{\sqrt{g d_o}} \right)^{0.84} \left(\frac{d_o}{D_R} \right)^{2.075} \tag{7.3}$$

where $\epsilon, N_o, g, D_R, \nu_L, U_o$, and d_o are gas holdup, a sparger-dependent constant, gravitational acceleration, BC diameter, liquid viscosity (kinematic), gas velocity in the sparger orifice, and sparger orifice diameter, respectively. A separate gas–liquid mass transfer correlation may then be used, such as (Jordan and Schumpe, 2001)

$$\frac{k_L a d_B^2}{D_L} = A \left(\frac{\nu_L}{D_L} \right)^{0.5} \left(\frac{g \rho_L d_B^2}{\sigma} \right)^{0.34} \left(\frac{g d_B^3}{\nu_L^2} \right)^{0.27} \left(\frac{U_G}{\sqrt{g d_B}} \right)^{0.72} \left[1 + 13.2 \left(\frac{U_G}{\sqrt{g d_B}} \right)^{0.37} \left(\frac{\rho_G}{\rho_L} \right)^{0.49} \right] \tag{7.4}$$

where $k_L a, d_B, D_L, A, \nu_L, g, \rho_L, \rho_G, \sigma$, and U_G are gas–liquid mass transfer coefficient, average bubble diameter, liquid-phase diffusion coefficient, sparger-dependent coefficient, liquid viscosity (kinematic), gravitational acceleration, liquid-phase density, gas-phase density, surface tension, and superficial gas velocity, respectively. These correlations include almost all required information to define the reactor environment except pressure and temperature.

In contrast, an industrial design has several choices. First and most complicated would be to use the experimental approach, which would be very intensive and costly. Second, a simplified correlation for gas holdup and gas–liquid mass transfer coefficient could be used:

$$\epsilon = C_2 U_G^x \tag{7.5}$$

$$k_L a = 0.467 U_G^{0.82} \tag{7.6}$$

where ϵ is the gas holdup, $k_L a$ is the gas–liquid mass transfer coefficient, U_G is the superficial gas velocity, and C_2 and x are the constants. Equations (7.5) and (7.6) were obtained by Bouaifi et al. (2001) and Shah et al. (1982), respectively. The effect of system-specific variables would have to be included in the constants. This approach would be not only highly practical and simple, but also nontransferable or limited, especially if rheological changes occur.

Lastly, a cook book approach could be used. As such, a simplified correlation would be used and time adjusted based on experience and parameter variables such as concentrations and temperature/pressure. This approach has a high upfront cost for correlation development, but would not require many data inputs and would have a low variable cost. It would represent a compromise between industrial practicality and scientific reality.

Ultimately, these problems have led to a large degree of variation in results and correlations that can be seen in Table 7.1 for gas holdup, Table 7.2 for the liquid-phase mass transfer coefficient, and Table 7.3 for the volumetric gas–liquid mass transfer correlation. The presented correlations, for example, show a wide degree and range of dependencies and variables. The result, as seen in Figure 7.13, is that some systems have anemic performance while others seem to be superstars of efficiency. Hence, the end user and designer have a great deal of work to ensure logical application of existing data and proper design constraints.

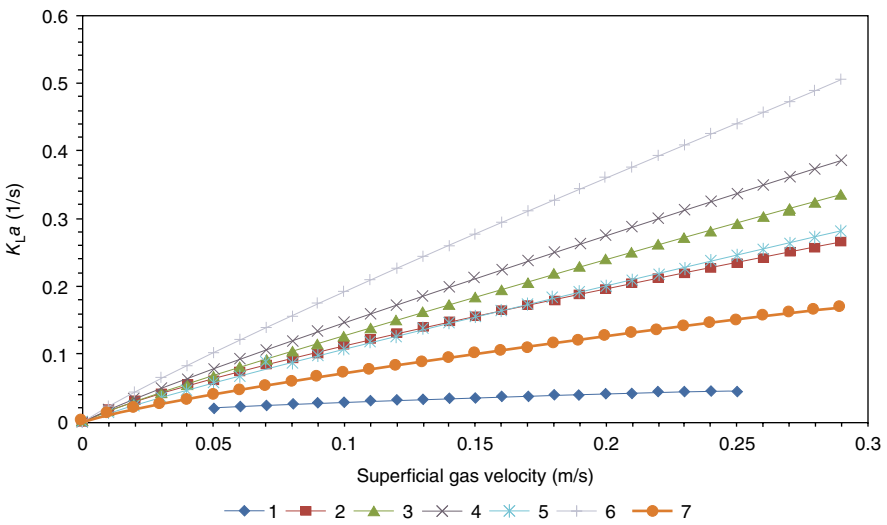

Figure 7.13 Gas–liquid mass transfer by (1) Behkish et al. (2002) (CO–hexane mixture without solids, $D_R = 0.316$ m), (2) Cho and Wakao (1988) (air–aqueous solutions, porous plate; $D_R = 0.115$ m), (3) water, (4) ethanol (96%), (5) 1-butanol, (6) toluene from Jordan et al. (2002) ($D_R = 0.115$ m), and (7) Shah et al. (1982).

TABLE 7.1 Gas Holdup Correlations for Bubble Columns

Reference	System	Conditions	Correlation
Akita and Yoshida (1973)[a]	Air–H_2O, O_2–H_2O, He–H_2O, CO_2–H_2O, air–glycol, air–aqueous glycol solution, Air-methanol	α = 0.2 for pure liquids, 0.25 for salt solutions D_R = 0.152 m H = 4.0 m d_0 = 0.5 mm (SO) U_G = 0.5–33 cm/s P up to 0.1 MPa T up to 293K	$\frac{\varepsilon_G}{(1-\varepsilon_G)^4} = \alpha \left(\frac{D_R^2 \rho_L g}{\sigma}\right)^{1/8} \left(\frac{D_R^3 \rho_L^2 g}{\mu_L^2}\right)^{1/12} \frac{U_G}{\sqrt{g D_R}}$
Anabtawi et al. (2003)[b]	Air–(light oil, machine oil, five different engine oils)	D_R = 74 mm d_0 = 10 mm H = 0.12–0.60 m U_G = 0.18–29 cm/s ρ_L = 906–928 kg/m^3 μ_L = 63–320 mPa-s σ = 24.8–35 mN/m	$\varepsilon_G = 0.362 \frac{U_G^{0.60}}{H^{0.38} \mu_L^{0.24}}$
Bach and Pilhofer (1978)[c]	Air–(water, butandiol–1,3, ethylene glycol, *n*-octanol, tetrabromomethane, cyclohexane, cyclohexanol, ethanol, propanol, ethyl acetate)	D_R = 0.10 m d_0 = 5 mm (PP) U_G = 1–20 cm/s ρ_L = 0.8–2.98 g/cm^3 ν_L = (0.7–124)×10^2 cm^2/s, σ = 21.7–72 mN/m	$\frac{\varepsilon_G}{1-\varepsilon_G} = 0.115 \left(\frac{U_G^3}{\nu_L g \Delta\rho / \rho_L}\right)^{0.23}$
Bouaifi et al. (2001)	Air–water	U_G = 0.25–4.0 cm/s Column 1 D_R = 0.15 m H = 2 m Column 2 D_R = 0.20 m H = 2 m	$\varepsilon_G = C_2 U_G^x$

	Porous Plate		Membrane		Perforated Plate	
	C2	x	C2	x	C2	x
Column1	3.62	0.91	4.25	0.99	3.66	0.83
Column2	3.43	1.03	3.12	1.05	2.2	1.06

(*continued*)

TABLE 7.1 (*Continued*)

Reference	System	Conditions	Correlation
Deckwer (1992)	Air-CMC concentration 0.8–1.8% wt	$D_R = 0.14$ m $d_0 = 2$ mm (PP) and 0.15 or 0.2 mm (SP) $\mu_L > 50$ mPa-s	$\varepsilon_G = 0.0322 U_G^{0.674}$ for slug flow regime ($U_G > 3$ cm/s) $\varepsilon_G = 0.0908 U_G^{0.85}$ for homogeneous flow regime ($U_G < 2$ cm/s)
Gestrich and Rahse (1975)[b]	Air–organic liquids (methanol, ethanol, *n*-butanol, ethyl acetate, glycol, methylethylketone, $C_2H_4Cl_2$)	$H/D_R = 0.26$–20 $U_G = 1$–8 cm/s $\frac{\rho_L \sigma^3}{g\mu_L^4}$ 8×10^4–5×10^{10}	$\varepsilon_G = 0.89 \left(\frac{H}{D_R}\right)^{0.035(-15.7+\log K)} \left(\frac{d_B}{D_R}\right)^{0.3} \left(\frac{U_G^2}{g d_B}\right)^{0.025(2.6+\log K)} K^{0.047} - 0.05$ $K = \frac{\rho_L \sigma^3}{g\mu_L^4}$ and $d_B = 3$ mm
Godbole et al. (1982)[a]	Air–viscous media		$\varepsilon_G = 0.239 U_G^{0.634} D_R^{-0.5}$
Grover et al. (1986)[a]	$D_R = 0.10$ m $d_0 = 100$–120 µm $U_G = 0.1$–4.5 cm/s $T = 303$–353K		$\varepsilon_G = \left(\frac{1 + b_1 P_V}{b_2 P_V}\right) \left(\frac{U_G \mu_L}{\sigma}\right)^{0.76} \left(\frac{\mu_L^4 g}{\rho_L \sigma^3}\right)^{-0.27} \left(\frac{\rho_G}{\rho_L}\right)^{0.09} \left(\frac{\mu_G}{\mu_L}\right)^{0.35}$ $b_1 = 1.1\times10^{-4}$ and $b_2 = 5$–10^{-4}
Guy et al. (1986)[b]	Air–water Air–aqueous solutions (glycerol, carboxyl-methyl cellulose)	$D_R = 0.254$ m $d_0 = 1$ mm $U_G = 1$–8 cm/s $\frac{U_{b\infty} d_e}{\nu_L} > 4.02 \frac{g\mu_L^4}{\rho_L \sigma^3}$ $\frac{g d_e^2 \rho_L}{\sigma} >> 8$	$\varepsilon_G = 0.386 N_0 \left(\frac{g D_R^3}{\nu_L^2}\right)^{0.025} \left(\frac{U_0}{\sqrt{g d_0}}\right)^{0.84} \left(\frac{d_0}{D_R}\right)^{2.075}$

Hammer (1984)[b]	N_2–organic liquids (methanol, cyclohexane, cyclehexanol, *n*-octanol, $C_2H_4Cl_2$)	d_0 = 0.15–2 mm U_G = 0.5–2 cm/s ρ_L = 780–1250 kg/m^3 μ_L = 0.31–22 mPa-s σ = 21.8–31.9 mN/m	$\varepsilon_G = 0.20 \left(\frac{U_G^2}{gD_R}\right)^{0.46} \left(\frac{D_R^3 g}{\nu_L^2}\right)^{0.08} \left(\frac{d_0}{D_R}\right)^{-0.17}$
Haque et al. (1986)[b]	Air–aqueous carboxy methyl cellulose solutions	D_R = 0.10–1.0 m d_0 = 0.3–2.0 mm U_G > 3 cm/s	$\varepsilon_G = 0.171 U_G^{0.6} \left[K(5000U_G)^{n-1}\right]^{-0.22} D_R^{-0.15}$ (SI)
Hikita and Kikukawa (1974)[b]	Air–water Air–aqueous solutions (methanol, sucrose)	D_R = 0.10 and 0.19 m d_0 = 13.0–36.2 mm U_G = 4.3–33.8 cm/s ρ_L = 911–1233 kg/m^3 μ_L = 1–19.2 mPa-s σ = 38.2–75.5 mN/m	$\varepsilon_G = 0.505 U_G^{0.47} \left(\frac{\sigma_w}{\sigma}\right)^{2/3} \left(\frac{\mu_w}{\mu_L}\right)^{0.05}$ (SI)
Hikita et al. (1980)[c]	D_R = [0.10,0.19] m H = [1.5,2.4] m d_0 = 1.1 cm (SO) U_G = 4.2–39 cm/s P up to 0.1 MPa T = 283-303K Non-electrolytes ρ_L = 0.79–1.24 g/cm^3 $\rho_G = (0.0837–1.84)\times10^{-3}$ g/cm^3 μ_L = 0.66–17.8 mPa-s $\mu_G = (0.8–1.81)\times10^{-2}$ mPa-s σ = 30–76 mN/m Electrolytes ρ_L = 1.01–1.17 g/cm^3 μ_L = 0.9–1.87 mPa-s σ = 71.9–79.6 mN/m	$\varepsilon_G = 0.672 f \left(\frac{U_G \mu_L}{\sigma}\right)^{0.578} \left(\frac{\mu_L^4 g}{\rho_L \sigma^3}\right)^{-0.131} \left(\frac{\rho_G}{\rho_L}\right)^{0.062} \left(\frac{\mu_G}{\mu_L}\right)^{0.107}$ where: f = 1 for electrolytes, $10^{0.0414I}$ for ion strength I <1 g-ion/L, 1.1 for I >1 g-ion/L

(*continued*)

TABLE 7.1 (*Continued*)

Reference	System	Conditions	Correlation
Hughmark (1967)[a]	Air–(water, Na_2CO_3 solution, light oil, glycerol, $ZnCl_2$ and Na_2SO_3 solution)	D_R = 0.0254–1.07m (PP) U_G = 0.4–45 cm/s U_L = 0–12 cm/s ρ_L = 777–1698 kg/m^3 μ_L = 0.9–152 mPa-s σ = 25–76 mN/m	$\varepsilon_G = \dfrac{1}{2 + \left(\dfrac{0.35}{U_G}\right)\left[\rho_L \dfrac{\sigma}{72}\right]^{1/3}}$
Idogawa et al. (1987)[b]	(Air, H_2, He)–water Air–organic liquids (acetone, ethanol, methanol) Air–aqueous solutions (ethanol, isoamyl alcohol)	D_R = 0.05 m d_0 = 1 mm U_G = 0.5–5 cm/s ρ_L = 791–1000 kg/m^3 ρ_G = 0.084–120.8 kg/m^3 μ_L = 0.35–3.0 mPa-s σ = 22.6–72.1 mN/m	$\dfrac{\varepsilon_G}{1-\varepsilon_G} = 0.059 U_G^{0.8} \rho_G^{0.17} \left(\dfrac{\sigma}{\sigma_w}\right)^{-0.22\exp(-P)}$
Ityokumbul et al. (1994)[b]	Air–water	D_R = 0.06 m d_0 = 134 μm U_G = 0–2.5 cm/s	$\varepsilon_G = 5.9 U_G$ (SI)
Jean and Fan (1987)[b]	Air–water	D_R = 0.0762 (PP) U_G = 0–12.08 cm/s U_L = 3.27–32.18 cm/s	$\varepsilon_G = 0.00164 U_G^{0.988} (28.821 + 0.564 U_L - 0.221\times10^5 U_L^2)$ for $U_G \le 5.19$ cm/s $\varepsilon_G = \dfrac{0.2933 U_G^{0.34}}{\exp(-0.248 U_L U_G^{-0.648}) + \exp(-0.243 U_L U_G^{-0.648})}$ for $U_G \ge 5.19$ cm/s

Jordan and Schumpe (2001)[a]	(Air, N_2, He, CO_2, H_2)–23 different organic liquids	D_R = 0.095–0.115 m d_0 = 1.0–4.3 mm U_G = 1–21 cm/s $\frac{g\rho_L d_b^2}{\sigma}$ = 825–1.55×10^6 $\frac{U_G}{\sqrt{gd_b}}$ = 0.06–1.22 $\frac{\rho_G}{\rho_L}$ = 9.3×10^{-5}–0.059	$\frac{\varepsilon_G}{1-\varepsilon_G} = B\left(\frac{g\rho_L d_b^2}{\sigma}\right)^{0.16}\left(\frac{gd_b^3}{\nu_L^2}\right)^{0.04}\left(\frac{U_G}{\sqrt{gd_b}}\right)^{0.70}$ $\left[1+27.0\left(\frac{U_G}{\sqrt{gd_b}}\right)^{0.52}\left(\frac{\rho_G}{\rho_L}\right)^{0.58}\right]$ B is sparger dependent
Jordan et al. (2002)	(Air, N_2)–(water, ethanol (96%), 1-butanol, toluene)	D_R = 0.115 m H = 1.370 m U_G = 0.01–0.15 m/s ρ_L = 759–884 kg/m^3 μ_L = 0.58–2.94 mPa-s σ = 19.9–32.5 mN/m D_L (10^{-9} m^2/s) = 1.60–4.38 P = 1–10 bar T = 293K	$\varepsilon_G = B(U_G)^{0.86}(\rho_G)^{0.24}$ Values for B Water = 1.69 Ethanol (96%) = 1.62 1-Butanol = 1.34 Toluene = 1.95
Joshi and Sharma (1979)[a]	$\varepsilon_G = \frac{U_G}{0.3+2U_G}$		
Kang et al. (1999)	Air–(water, aqueous solutions of carboxy methyl cellulose)	D_R = 0.152 m d_0 = 1.0 mm U_G = 2–20 cm/s μ_L = 1–38 mPa-s P = 0.1–0.6 MPa	$\varepsilon_G = 0.910\times10^{-2.10}\left(\frac{D_R U_G \rho_G}{\mu_L}\right)^{0.254}$
Kato and Nishiwaki (1972)[b]	Air–water	D_R = 0.066–0.214 m d_0 = 1.0–3.0 mm U_G = 0–30 cm/s U_L = 0–1.5 cm/s	$\varepsilon_G = \frac{U_G}{31+\beta U_G^{0.8}(1-\exp(\gamma))}$ where: $\beta = 4.5–3.5\exp(-0.064D_R^{1.8})$ $\gamma = -0.18U_G^{1.8}\beta^{-1}$

(*continued*)

TABLE 7.1 (*Continued*)

Kawase and Moo-Young (1987)[a]	$\varepsilon_G = 1.07\, Fr^{1/3}$ where: $Fr = \dfrac{U_G}{\sqrt{gD_R}}$		
Kawase et al. (1992)[a]	$\dfrac{\varepsilon_G}{1-\varepsilon_G} = 0.0625 \left(\dfrac{U_G}{\nu_L g}\right)^{1/4}$		
Kim et al. (1972)[b]	$D_R = 0.049$ m $d_0 = 3.175$ mm $U_G = 0$–26 cm/s $U_L = 1.4$–10.2 cm/s	$1-\varepsilon_G = 1.02 \left(\dfrac{\mu_L{}^2 \rho_G}{D_R g \rho_L}\right)^{-0.009} \left(\dfrac{U_G \rho_L}{D_R g \rho_G}\right)^{-0.036} \left(\dfrac{U_G U_L D_R{}^2}{\nu_G \nu_L}\right)^{-0.015}$	
Koide et al. (1979)[a]	$\varepsilon_G = \dfrac{U_G}{31+\beta(1-e)\sqrt{U_G}}$ where: $\beta = 4.5-3.5 \exp(-0.064 D_R{}^{1.3})$ and $e = \dfrac{-0.18 U_G{}^{1.8}}{\beta}$		
Koide et al. (1984)[a]	Air–water Air–aqueous solutions (electrolytes, glycol, glycerol)	$D_R = 0.10$–0.30 m $d_0 = 0.5$–2.5 mm (MO) $U_G = 1$–18 cm/s $\rho_L = 997$–1178 kg/m^3 $\rho_S = 2500$ and 8700 kg/m^3 $\mu_L = 0.894$–17.6 mPa-s $\sigma = 51.5$–73 mN/m $c_S = 0$–200 kg/m^3 $d_S = 47.5$–192 µm	$\dfrac{\varepsilon_G}{(1-\varepsilon_G)^4} = \dfrac{A \left(\dfrac{U_G \mu_L}{\sigma}\right)^{0.918} \left(\dfrac{g \mu_L{}^4}{\rho_L \sigma^3}\right)^{-0.252}}{1+4.35 \left(\dfrac{C_S}{\rho_s}\right)^{0.748} \left[\dfrac{\rho_s-\rho_L}{\rho_L}\right]^{0.88} \left(\dfrac{U_G D_R}{\nu_L}\right)^{-0.168}}$ where: $A = 0.277$ for water and non-electrolyte solutions, $A = 0.364$ for electrolyte solutions

Kojima et al. (1997)[b]	(N_2, O_2)–water (N_2, O_2)–aqueous solutions (enzyme, Na_2HPO_4, citric acid)	D_R = 0.045 m d_0 = 1.38–4.03 mm U_G = 0.5–15 cm/s ρ_L = 1000–1025 kg/m^3 μ_L = 0.890–1.075 mPa-s σ = 63.36–71.96 mN/m P = 0.1–1.1 MPa	$\varepsilon_G = \varepsilon_0 = 1.18 U_G^{0.679} \left(\frac{\sigma}{0.076}\right)^{-0.546}$ for P = 101 kPa $\varepsilon_G = \varepsilon_0 = \exp\left[A\left(\frac{\pi D_R^4 \rho_L U_G^2}{16 d_0^3 \sigma}\right)\left(\frac{P}{P_{atm}}\right)^B\right]$ for P > 101 kPa where: $A = 1.27\times10^{-4}$ and B = 1.0
Kumar et al. (1976)[a]	Air–H_2O Air–kerosene Air–40% glycerol Air-2M NaOH solution	D_R = 0.05–0.10 m d_0 = 0.087–0.309 cm (PP) U_G = 0.2–14 cm/s ρ_L = 0.78–1.11 g/cm^3 μ_L = 0.88–11.5 mPa-s σ = 31.2–74.5 mN/m	$\varepsilon_G = 0.728 U_G^* - 0.485 U_G^{*2} + 0.0975 U_G^{*3}$ $U_G^* = U_G \left(\frac{\sigma \Delta\rho g}{\rho_L}\right)^{1/4}$ where:
Lau et al. (2004)	D_R = 0.045–0.45 m H/D_R > 5 d_0 = 1.5 mm U_G = 2.8–67.8 cm/s U_L = 0–0.089 cm/s P up to 22 MPa T up to 250°C ρ_L = 790–1580 kg/m^3 ρ_G = 0.97–33.4 kg/m^3 μ_L = 0.36–38.3 mPa-s σ = 23.3–72.6 mN/m	$\frac{\varepsilon_G}{(1-\varepsilon_G)^4} = \frac{2.9\left(\frac{U_G^4 \rho_G}{\sigma_G}\right)^{\alpha}\left(\frac{\rho_G}{\rho_m}\right)^{\beta}}{\left[\cosh(Mo_m^{0.054})\right]^{4.1}}$ Where: $\alpha = 0.21 Mo_m^{0.0079}$, $\beta = 0.096 Mo_m^{-0.011}$, $Mo_m = \frac{(\xi\mu_L)^4 g}{\rho_m \sigma^3}$, $\ln \xi = 4.6\varepsilon_s \left\{5.7\, \varepsilon_s^{0.58} \sinh\left[-0.71 \exp(-5.8\varepsilon_s) \ln Mo^{0.22}\right] + 1\right\}$, and $Mo = \frac{g\mu_L^4}{\rho_L \sigma^3}$	
Lee et al. (2000)[b]	Air–water	D_R = 0.083–0.15 m d_0 = 4 mm U_G = 0–270 cm/s U_L = 0–23 cm/s	$\frac{\varepsilon_G}{1-\varepsilon_G} = 0.759 U_G^{0.685} U_L^{-0.116}$ (SI)

(*continued*)

TABLE 7.1 (*Continued*)

Lockett and Kirkpatrick (1975)[a]	$U_G(1-\varepsilon_G)+U_L\varepsilon_G = V_B\varepsilon_G(1-\varepsilon_G)^{2.39}\,(1+2.55\varepsilon_G{}^3)$		
Luo et al. (1999)[b]	D_R = 0.1–0.61 m U_G = 5–69 cm/s U_L = 0 m/s ρ_L = 668–2965 kg/m^3 ρ_s = 2200–5730 kg/m^3 ρ_G = 0.2–90 kg/m^3 μ_L = 0.29–30.0 mPa-s σ = 19.0–73.0 mN/m φ_s = 0, 0.081,0.181 T = 301K, 351K P = 0.1–5.62 MPa	(Air, He, CO_2, N_2)–water Air–organic liquids (methanol, glycol, glycerol, $C_2H_3Br_3$, *n*-octanol, heptanes, *n*-butanol, 1,3-butanediol, trichloroethylene) Air–Isopar G, Paratherm F liquids with and without suspended solids	
		$\frac{\varepsilon_G}{(1-\varepsilon_G)} = 2.9\left(\frac{U_G{}^4\rho_G}{\sigma_G}\right)^{\alpha}\left(\frac{\rho_G}{\rho_L}\right)^{\beta}\left[\cosh(Mo_s{}^{0.054})\right]^{-4.1}$ Where: $\alpha = 0.21Mo_s{}^{0.079}$, $\beta = 0.096Mo_s{}^{-0.011}$, $\rho_s = \varphi_s\rho_s+\varphi_L\rho_L$, $Mo_s = \frac{(\xi\mu_L)^4 g}{\rho_s{}^1\sigma^3}$, $\ln\xi = 4.6\varphi_s\left\{5.7\,\varphi_s{}^{0.58}\sinh\left[-0.1562\exp(-5.8\varphi_s)\ln\frac{g\mu_L}{\rho_L\sigma^3}\right]+1\right\}$	
Mashelkar (1970)[b]	Air–water Air–electrolyte aqueous solutions	$\varepsilon_G = \frac{U_G}{\rho_L(30+2U_G)}\left(\frac{\sigma_w}{\sigma}\right)^{-1/3}$	
Mersmann (1977)[b]		$\varepsilon_G(1-\varepsilon_G)^n = 0.14U_G\left[\frac{\rho_L{}^2}{\sigma(\rho_L-\rho_G)g}\right]^{1/4}\left(\frac{\rho_L}{\rho_G}\right)^{5/72}\left[\frac{\rho_L}{\rho_L-\rho_G}\right]^{1/3}\left[\frac{\sigma^3\rho_L{}^2}{\mu_L{}^4(\rho_L-\rho_G)g}\right]^{1/24}$	
Mok et al. (1990)[b]	Air–water Air–CMC aqueous solutions	D_R = 0.14 m d_0 = 0.3 mm U_G = 0.96–5.04 cm/s ρ_L = 997.1–998.2 kg/m^3 σ = 70.5–72 mN/m	$\varepsilon_G = 1.07\times10^{-5}\left(\frac{D_RU_G}{\nu_G}\right)^{1.09}\left(\frac{gD_R{}^3}{\nu_L{}^2}\right)^{0.096}\left(\frac{d_0}{D_R}\right)^{-0.19}$

Mouza et al. (2005)[b]	Air–water Air–aqueous solutions (glycerin, *n*-butanol)	Square column with Width = 0.10 m d_0 = 20 and 40 μm $U_G < U_{trans}$ ρ_L = 991–1173 kg/m^3 μ_L = 0.9–22.5 mPa-s σ = 48.0–72 mN/m	$\varepsilon_G = 0.001 \left[\frac{U_G}{\sqrt{gD_R}} \left(\frac{D_R{}^3 \rho_L{}^2 g}{\mu_L{}^2} \right)^{0.1} \left(\frac{D_R{}^2 \rho_L g}{\sigma} \right)^{2.2} \frac{D_d}{D_R} \right]^{2/3}$
Reilley et al. (1986)[a]	D_R = 0.30 m d_0 = 1.5 mm U_G = 0.77–21.7 cm/s ρ_L = 771–1482 kg/m^3 μ_L = 0.489–1.29 mPa-s σ = 28.3–72 mN/m ρ_G = 0.185–1.48 kg/m^3		$\varepsilon_G = 0.009+296 U_G{}^{0.44} \rho_L{}^{-0.98} \sigma_L{}^{-0.16} \rho_G{}^{0.19}$ can replace ρ_L with ρ_s
Roy et al. (1963)[a]	$\varepsilon_G = 3.88\times10^{-3} \left[Re_T \left(\frac{\sigma_w}{\sigma_L} \right)^{1/3} (1-\nu_s)^3 \right]^{0.44}$ for $Re_T > 500$ $\nu_s = \frac{W_s/\rho_s}{(W_s/\rho_s)+(W_L/\rho_L)}$ where:		
Sada et al. (1984)[a]	(N_2, He)–(Water, molten $NaNO_3$, molten LiCl-KCl) N_2–Methanol N_2–Aqueous solutions (glycerol, Na_2SO_4)	D_R = 0.073 m d_0 = 1.5–5.7 mm U_G = 0.56–8.3 cm/s ρ_L = 788–1888 kg/m^3 μ_L = 0.45–3.658 mPa-s σ = 21.5–130 mN/m	$\varepsilon_G = 0.32\ (1-\varepsilon_G)^4\ Bo^{0.21}\ Ga^{0.086}\ Fr \left(\frac{\rho_G}{\rho_L} \right)^{0.068}$ Where: $Bo = \frac{\rho_L g D_R{}^2}{\sigma}$, $Ga = \frac{g D_R{}^3}{\nu_L{}^2}$, *and* $Fr = \frac{U_G}{\sqrt{gD_R}}$ $\frac{\varepsilon_G}{(1-\varepsilon_G)^3} = 0.019 U_\infty{}^{1/16}\ \nu_s{}^{-0.215 U_\infty{}^{-0.16}} U_G$

(*continued*)

TABLE 7.1 (*Continued*)

Salvacion et al. (1995)[b]	D_R = 0.14–0.30 m d_0 = 0.5–2.5 mm U_G = 2–15 cm/s ρ_L = 995–997 kg/m^3 ρ_s = 1000–1087 kg/m^3 φ_s = 0–0.20 μ_L = 0.863–0.894 mPa-s σ = 55.6–72.0 mN/m		$\frac{\varepsilon_G}{(1-\varepsilon_G)^4} = \varepsilon_0 \left[\frac{1+0.00468\,(D_R{}^2 g\rho_L\sigma^{-1})^{0.465} f(A)}{1+2.34\varphi_s{}^{0.799}\,(D_R{}^2 g\rho_L\sigma^{-1})^{-0.0464}}\right]$ where: $A = 0$, $\varepsilon_0 = 0.277\left(\frac{U_G\mu_L}{\sigma}\right)^{0.918}\left(\frac{g\mu_L}{\rho_L\sigma^3}\right)^{-0.252}$ $f(A) = A^{0.223}(1+0.0143A^{0.466})^{-1}$
Schumpe and Deckwer (1987)[a]	$Bo = 1.4\times10^3$–1.4×10^5 $Ga = 1.2\times10^7$–6.5×10^{10} $Fr = 3\times10^{-3}$–2.2×10^{-1}		$\varepsilon_G = 0.2Bo^{-0.13}\,Ga^{0.11}\,Fr^{0.54}$ For highly viscous media
Smith et al. (1983)[a]	$\varepsilon_G = \left[2.25+\frac{0.379}{U_G}\left(\frac{\rho_L}{72}\right)^{0.31}\mu_L{}^{0.016}\right]^{-1}$ μ_L can be replaced with μ_s, except $\mu_s = \mu_L\, exp\left[\frac{(5/3)\nu_s}{1-\nu_s}\right]$		
Sotelo et al. (1994)[b]	(Air, CO_2)–water (Air, CO_2)–aqueous solutions (sucrose, ethanol glycerin)	D_R = 0.04-0.08 m d_0 = 30–150 μm U_G = 0.64–4.9 cm/s ρ_L = 928–1147 kg/m^3 ρ_G = 1.18–1.83 kg/m^3 μ_L = 1.0–4.17 mPa-s μ_G = 0.0148–0.0191 mPa-s σ = 29.8–73.4 mN/m	$\varepsilon_G = 129\left(\frac{U_G\mu_L}{\sigma}\right)^{0.99}\left(\frac{\mu_L{}^4 g}{\rho_L\sigma^3}\right)^{-0.123}\left(\frac{\rho_G}{\rho_L}\right)^{0.187}\left(\frac{\mu_G}{\mu_L}\right)^{0.343}\left(\frac{d_0}{D_R}\right)^{-0.089}$
Syeda et al. (2002)[b]	Air–(Water, methanol, glycerol, i-propanol)	D_R = 0.09 m d_0 = 5 mm	$\varepsilon_G = 1.1855\left(\frac{\rho_L d_b}{\sigma}\right)^{0.016}\left(\frac{U_G\mu_L}{\sigma}\right)^{0.578}\left(\frac{\mu_L g}{\rho_L\sigma^3}\right)^{-0.131}\left(\frac{\rho_G}{\rho_L}\right)^{0.062}\left(\frac{\mu_G}{\mu_L}\right)^{0.107}$

Ulbrecht and Patterson (1985)[b]	N_2–(Tellus oil, aqueous glucose solution)	D_R = 0.15 and 0.23 m d_0 = 0.5–1.5 mm U_G = 0–25 cm/s ρ_L = 867–1380 kg/m^3 μ_L = 70–550 mPa-s σ = 31.0–76.0 mN/m P = 0.1–1.0 MPa	$\varepsilon_G = 0.21 \frac{U_G^{0.58} \rho_G^{0.3\exp(-9\mu_L)}}{D_R^{0.18} \mu_L^{0.12}}$
Zahradnik and Kastanek (1979)[b]	Air–water	D_R = 0.152 and 0.292 m d_0 = 0.87–3 mm U_G = 3.1–27.6 cm/s	$\varepsilon_G = \frac{U_G}{0.3+2.0U_G}$ (SI)
Zahradnik et al. (1997)	Air–water	D_R = 0.29 m H_0 = 1.5 m U_G = 0.4–16.6 cm/s	$\varepsilon_G = 2.81 U_G^{0.9}$
Zehner (1989)	$\varepsilon_G = \frac{U_G/\alpha}{\sqrt{1+4\left(U_G/\alpha\right)^{2/3} \frac{V_L(0)}{\alpha}}}$ where $\alpha = 1.4 \left(\frac{\sigma}{\rho_L} \frac{\rho_L - \rho_G}{\rho_L} g\right)^{1/4}$ and $V(0) = \left(\frac{1}{2.5} \frac{\rho_L - \rho_G}{\rho_L} U_G g D_R\right)^{1/2}$		
Zou et al. (1988)[a]	D_R = 0.10 m d_0 = 10 mm ρ_L = 748.3–997.1 kg/m^3 ρ_G = 1.833–2.161 kg/m^3 μ_L = 0.295–0.894 mPa-s σ = 18.77–71.97 mN/m T = 298.15–369.65K		$\varepsilon_G = 0.17283 \left(\frac{\mu_L^4 g}{\rho_L \sigma_L^3}\right)^{-0.15} \left(\frac{U_G \mu_L}{\sigma_L}\right)^{0.15} \left(\frac{P+P_{sat}}{P}\right)^{1.61}$

[a]As cited by Kantarci et al. (2005)

[b]As cited by Ribeiro Jr. and Lage (2005)

[c]As cited by Deckwer (1992)

TABLE 7.2 Liquid-Phase Mass Transfer Correlations for Bubble Column

Reference	System	Conditions	Correlation
Akita and Yoshida (1974)[a]	(Air, O_2, He, CO_2)–water Air–organic liquids (glycol, methanol) Air–aqueous solutions (glycol, methanol, glycerol, electrolyte)	D_R = 0.07–0.600 m d_0 = 0.01–5.0 mm U_G = 4.0–33 cm/s ρ_L = 790–1165 kg/m^3 μ_L = 0.58–21.14 mPa-s σ = 22.3–74.2 mN/m D_L (10^{-9} m^2/s) = 0.26–4.22	$\frac{k_L d_b}{D_L} = 0.5 \left(\frac{\nu_L}{D_L}\right)^{1/2} \left(\frac{d_b^3 g}{\nu_L^2}\right)^{1/4} \left(\frac{g d_b^2 \rho_L}{\sigma}\right)^{3/8}$
Calderbank and Moo-Young (1961)[a]	ρ_L = 698–1260 kg/m^3 μ_L = 0.371–8.7 mPa-s λ_L = 0.60–27.92 W/(mK) D_L (10^{-4} m^2/s) = 1.9×10^{-6}–0.26		$\frac{k_L d_b}{D_L} = 2.0+0.31 \left(\frac{d_b^2(\rho_L-\rho_G)g}{\mu_L D_L}\right)^{1/3}$ for $d_b < 2.5$ mm $k_L \left(\frac{\nu_L}{D_L}\right)^{1/2} = 0.42 \left[\frac{(\rho_L-\rho_G)\mu_L g}{\rho_L^2}\right]^{1/3}$ for $d_b > 2.5$ mm
Cockx et al. (1995)[a]	$\frac{k_L}{U_G} = \frac{4.47\times10^{-2}}{\varepsilon_G} \left(\frac{\nu_L}{D_L}\right)^{-1/2}$		
Fair (1967)[a]	$\frac{k_L d_b}{D_L} = 2.0 \left[1+0.276 \left(\frac{d_b U_b}{\nu_L}\right)^{1/2} \left(\frac{\nu_L}{D_L}\right)^{1/3}\right]$		
Fukuma et al. (1987)[a]	U_G = 0.30–1.5 cm/s $\frac{g d_b^3}{\nu_L} = 3.2\times10^{-5}$–$2.6\times10^{8}$ $\frac{g\rho_L d_b^2}{\sigma}$ = 1.4–120 $\frac{\nu_L}{D_L}$ = 480–1600		$\frac{k_L d_b}{D_L} = 4.5\times10^{-4} \left(\frac{\nu_L}{D_L}\right)^{1/2} \left(\frac{g\rho_L d_b^2}{\sigma}\right)^{-0.2} \left(\frac{g d_b^3}{\nu_L^2}\right)^{0.8}$

Gestrich et al. (1978)[a]	(CO_2, O_2)–water (CO_2, O_2)–aqueous solutions (glycerine, glycerol, electrolyte)		$k_L = 2.23\times10^{-4}\left(\frac{g\mu_L^4}{\rho_L\sigma^3}\right)^{-0.180} + 3.85\times10^{-3}\left(\frac{H_0}{D_R}\right)^{-0.605} U_G^{0.65+0.0335\frac{H_0}{D_R}}$
Gestrich et al. (1978)[a]	(CO_2, O_2)–water (CO_2, O_2)–aqueous solutions (glycerine, glycerol, electrolyte)		$k_L = 2.23\times10^{-4}\left(\frac{g\mu_L^4}{\rho_L\sigma^3}\right)^{-0.180} + 3.85\times10^{-3}\left(\frac{H_0}{D_R}\right)^{-0.605} U_G^{0.65+0.0335\frac{H_0}{D_R}}$
Hughmark (1967)[a]	Air–(water, Na_2CO_3 solution, light oil, glycerol, $ZnCl_2$ and Na_2SO_3 solution)	D_R = 0.0254–1.07 m U_G = 0.4–45 cm/s U_L = 0–12 cm/s ρ_L = 777–1698 kg/m^3 μ_L = 0.9–152 mPa-s σ = 25–76 mN/m	$\frac{k_L d_b}{D_L} = 2.0+0.0187\left[\left(\frac{U_G d_b}{\varepsilon_G \nu_L}\right)^{0.484}\left(\frac{\nu_L}{D_L}\right)^{0.339}\left(\frac{d_b g^{1/3}}{D_L^{2/3}}\right)^{0.072}\right]^{1.61}$
Kawase et al. (1987)[a]	$k_L = \frac{2}{\sqrt{\pi}}\sqrt{D_L}\left(\frac{U_G g}{\nu_L}\right)^{1/4}$		
Kawase and Moo–Young (1992)[a]	$k_L = \frac{0.28 D_L^{2/3} g^{1/3}}{\nu_L^{1/3}}$ for small bubbles $k_L = \frac{0.47 D_L^{1/2} g^{1/3}}{\nu_L^{1/6}}$ for large bubbles		
Linek et al. (2005a)	O_2–water O_2–aqueous solutions (Na_2SO_3 pure and with the addition of Sokrat 44 and carboxy–methyl–cellulose)	D_R = 0.19 m U_G = 0.18–0.54 cm/s ρ_L = 1000–1093 kg/m^3 μ_L = 1.11–3.14 mPa-s	$k_L = 0.463(gU_G\nu_L)^{1/4}\left(\frac{D_L}{\nu_L}\right)^{1/2}$

(*continued*)

TABLE 7.2 (*Continued*)

Reference	System	Conditions	Correlation
Miller (1974)[a]	Air–water	$D_R = 0.152–0.686$ m $d_0 = 1.6–6.4$ mm $U_G = 0.762–15.2$ cm/s	$k_L = 1366 d_b^{1.376} \sqrt{\frac{D_L U_b}{\pi d_b}}$
Nedeltchev (2003)[a]	N_2–gasoline, toluene	$D_R = 0.316$ m $U_G = 5–25$ cm/s $\rho_L = 692–866$ kg/m^3 $\mu_L = 0.46–0.59$ mPa-s	$k_L = 2.43\times10^7 d_b^{2.928} \sqrt{\frac{D_L U_b}{\pi d_b}}$ (SI)
Ruckenstein (1964)[a]	$\frac{k_L d_b}{D_L} = 1.252 \left[\frac{(1-\varepsilon_G)^{5/3}}{2+3(\varepsilon_G{}^{5/3}-\varepsilon_G{}^{1/3}-2\varepsilon_G{}^2)}\right]^{1/3} \left(\frac{U_b d_b}{D_L}\right)^{1/3}$		
Sokolov and Aksenova (1983)[a]	(Air, CO_2)–water (Air, CO_2)–aqueous solutions (sucrose, carbonate–bicarbonate buffer)	$D_R = 0.05–0.60$ m $d_0 = 2.25–40$ mm $U_G = 0.05–4.0$ cm/s $\frac{\nu_L}{D_L} = 310–8320$ $\frac{U_L}{\mu_L\sqrt{\rho_L\sigma/g}} = 5–740$	$\frac{k_L\sigma}{D_L\rho_L g} = 0.05 \left(\frac{\nu_L}{D_L}\right)^{0.5} \frac{U_G}{U_L} \left(\frac{\rho_L\sigma}{g}\right)^{0.5}$
Vázquez et al. (2000)	$D_R = 0.113$ m $d_0 = 0.04–0.20$ mm (MO) $U_G = 0.085–0.181$ cm/s $\nu_L = 1.22\times10^{-6}$ m^2/s $\sigma = 66.00–75.01$ mN/m	$k_L = A\sigma^{1.35} U_G{}^{0.5}$ (SI) where:	

Equivalent pore diameter (10^6 m)	A
150–200	0.17587
90–150	0.18233
40–90	0.18689

[a]As cited by Kantarci et al. (2005)
[b]As cited by Ribeiro Jr. and Lage (2005)
[c]As cited by Deckwer (1992)

TABLE 7.3 Gas–Liquid Mass Transfer Correlations for Bubble Columns

Reference	System	Conditions	Correlation
Akita and Yoshida (1973)[a]	Air–H_2O O_2–H_2O He–H_2O CO_2–H_2O Air-glycol Air-aqueous glycol solution Air-methanol	D_R = 0.15–0.600 m H = 4.0 m d_0 = 0.5 mm U_G = 0.4–32.8 cm/s P up to 0.1 MPa T up to 293 K $\frac{U_G}{\sqrt{gD_R}}$ = 0.0024–0.135 $\frac{gD_R^2\rho_L}{\sigma}$ = 3050–0.45×10^4 $\frac{\nu_L}{D_L}\frac{\sigma}{}$ = 173–7.25×10^3	$\frac{k_L a D_R^2}{D_L} = 0.6\left(\frac{\upsilon_L}{D_L}\right)^{0.5}\left(\frac{gD_R^2\rho_L}{\sigma}\right)^{0.62}\left(\frac{gD_R^3}{\nu_L^2}\right)\varepsilon_G^{1.1}$
Álvarez et al. (2000)	CO_2–water CO_2–aqueous solutions (sucrose, sodium lauryl sulfate)	D_R = 0.113 m d_0 = 0.04–0.20 mm (MO) U_G = 0.085–0.150 cm/s ρ_L = 997–1030 kg/m^3 μ_L = 0.896–1.135 mPa-s σ = 65.20–72.49 mN/m D_L (10^{-9} m^2/s) = 1.549–1.897	$k_L a = A\,\frac{U_G^{2/3}\sigma^{3/4}\rho_L^{3/2}}{\mu_L^{3/4}}$ Where: Equivalent pore diameter (10^6 m) / A (10^7) 150–200 / 1.924 90–150 / 1.969 40–90 / 2.079
Behkish et al. (2002)	(H_2, CO, N_2, CH_4)-(hexane mixture, Isopar-M) with and without solids (iron oxides catalyst and glass beads)	D_R = 0.316 m U_G = 5–25 cm/s ρ_L = 680–783 kg/m^3 μ_L = 0.32–2.7 mPa-s σ = 27.0–230 mN/m D_L (10^{-9} m^2/s) = 1.33–9. 40φ_s = 0–0.36	$k_L a = 0.18\left(\frac{\nu_L}{D_L}\right)^{0.16}\left(\frac{\rho_L}{\rho_G}\right)^{2.84}(\rho_G U_G)^{0.49}\exp(-266\varphi_s)$
Cho and Wakao (1988)[b]	N_2–aqueous solutions (benzene, CCl_4, $CHCl_3$, $C_2H_4Cl_2$, $C_2H_3Cl_2$)	D_R = 0.11 m U_G = 0.71–5.0 cm/s D_L (10^{-9} m^2/s) = 0.99–2.42	$k_L a = A D_L^{0.5} U_G^{0.81}$ where: A = 6500 for single nozzle sparger or A = 23000 for porous plate

(*continued*)

TABLE 7.3 (*Continued*)

Hikita et al. (1981)[c]	D_R = [0.10,0.19] m H = [1.5,2.4] m d_0 = 1.1 cm (SO) U_G = 4.2–39 cm/s P up to 0.1 MPa T = 283–303 K Nonelectrolytes ρ_L = 0.79–1.24 g/cm^3 ρ_G = (0.0837–1.84)*10^{-3} g/cm^3 μ_L = 0.66–17.8 mPa-s μ_G = (0.821.81)*10^{-2} mPa-s σ = 30–76 mN/m Electrolytes ρ_L = 1.01–1.17 g/cm^3 μ_L = 0.9–1.87 mPa-s σ = 71.9–79.6 mN/m	$k_L a = \frac{14.9gf}{U_G}\left(\frac{U_G\mu_L}{\sigma}\right)^{1.76}\left(\frac{g\mu_L^4}{\sigma^3}\right)^{-0.284}\left(\frac{\mu_G}{\mu_L}\right)^{0.243}\left(\frac{\mu_L}{\rho_L D_L}\right)^{-0.604}$ where f = 1 for electrolytes, $10^{0.0414I}$ for ion strength I<1 g-ion/L, 1.1 for I>1 g-ion/L
Jordan and Schumpe (2001)	D_R = 0.095–0.115 m d_0 = 1.0–4.3 mm (SO, MO) U_G = 0.80–21 cm/s $\frac{g\rho_L d_b^2}{\sigma}$ = 1.21–5.39 $\frac{gd_b^3}{\nu_L^2}$ 825–1.55×10^6 $\frac{U_G}{\sqrt{gd_b}}$ = 0.06–1.22 $\frac{\rho_G}{\rho_L}$ = 9.3×10^{-5}–0.059 $\frac{\nu_L}{D_L}$ = 71–6.89×10^4	$\frac{k_L a d_b^2}{D_L} = A\left(\frac{\nu_L}{D_L}\right)^{0.5}\left(\frac{g\rho_L d_b^2}{\sigma}\right)^{0.34}\left(\frac{gd_b^3}{\nu_L^2}\right)^{0.27}\left(\frac{U_G}{gd_b}\right)^{0.72}\left[1+13.2\left(\frac{U_G}{\sqrt{gd_b}}\right)^{0.37}\left(\frac{\rho_G}{\rho_L}\right)^{0.49}\right]$ where A is sparger dependent

<table>
<tr><td>Jordan et al. (2002)</td><td>(Air, N_2)–(water, ethanol (96%), 1-butanol, toluene)</td><td>$D_R = 0.115$ m
$H = 1.370$ m
$U_G = 0.01$–0.15 m/s
$\rho_L = 759$–884 kg/m^3
$\mu_L = 0.58$–2.94 mPa-s
$\sigma = 19.9$–32.5 mN/m
D_L (10^{-9} m^2/s) = 1.60–4.38
$P = 1$–10 bar
$T = 293$K</td><td>$k_La = C(U_G)^{0.91}\,(\rho_G)^{0.24}$
$k_La = D(\varepsilon_G)^{1.06}$<table><tr><th>Liquid</th><th>C</th><th>D</th></tr><tr><td>Water</td><td>0.99</td><td>0.56</td></tr><tr><td>Ethanol (96%)</td><td>1.14</td><td>0.67</td></tr><tr><td>1-Butanol</td><td>0.83</td><td>0.60</td></tr><tr><td>Toluene</td><td>1.49</td><td>0.72</td></tr></table></td></tr>
<tr><td>Kang et al. (1999)</td><td>Air–(water, aqueous solutions of carboxymethyl cellulose)</td><td>$D_R = 0.152$ m
$d_0 = 1.0$ mm
$U_G = 2$–20 cm/s
$\mu_L = 1$–38 mPa-s
$P = 0.1$–0.6 MPa</td><td>$k_La = 0.930\times10^{-3.08}\left(\frac{D_R U_G \rho_G}{\mu_L}\right)^{0.254}$</td></tr>
<tr><td>Kawase and Moo-Young (1987)[a]</td><td colspan="3">$\frac{k_L a D_R^2}{D_L} = 0.452\left(\frac{\nu_L}{D_L}\right)^{1/2}\left(\frac{D_R U_G}{\nu_L}\right)^{3/4}\left(\frac{g D_R^2 \rho_L}{\sigma}\right)^{-3/5}\left(\frac{U_G^2}{D_R g}\right)^{7/60}$</td></tr>
<tr><td>Khudenko and Shpirt (1986)[b]</td><td>Air–water</td><td>$R_{dt} = 0.125$–1
$\frac{H_0}{H_b} = 0.25$–1
$U_G = 0.055$–2.1 cm/s
$T = 17$–24 °C</td><td>$k_La = 0.041 R_{dt}^{0.18}\left(\frac{U_G}{H_b}\right)^{0.67}$</td></tr>
<tr><td>Koide et al. (1984)[b]</td><td>Air–water
Air–aqueous solutions (electrolytes, glycol, glycerol)</td><td>$D_R = 0.10$–0.30 m
$d_0 = 0.5$–2.5 mm (MO)
$U_G = 1$–18 cm/s
$\rho_L = 997$–1178 kg/m^3
$\rho_s = 2500$ and 8770 kg/m^3
$\mu_L = 0.894$–17.6 mPa-s
$\sigma = 51.5$–73 mN/m
$c_s = 0$–200 kg/m^3
$d_s = 47.5$–192 μm</td><td>$\frac{k_L a \sigma}{\rho_L D_L g} = \frac{211\left(\frac{\nu_L}{D_L}\right)^{0.5}\left(\frac{g\mu_L}{\rho_L \sigma^3}\right)^{0.5}\varepsilon_G^{1.18}}{1+1.47\times10^4\left(\frac{C_s}{\rho_s}\right)^{0.612}\left(\frac{U_P}{\sqrt{D_R g}}\right)^{0.612}\left(\frac{\rho_L g D_R^2}{\sigma}\right)^{-0.477}\left(\frac{\rho_L U_G D_R}{\mu_L}\right)^{-0.345}}$</td></tr>
</table>

(*continued*)

TABLE 7.3 (*Continued*)

Lau et al. (2004)	(Air, N_2)-(water, Paratherm NF heat-transfer fluid) (Air, N_2, CO, He, H_2)-9 different organic liquids	$D_R = 0.045–0.45$ m $H/D_R > 5$ $d_0 = 1.5$ mm (PP) $U_G = 2.8–67.8$ cm/s $U_L = 0–0.089$ cm/s $\rho_L = 790–1580$ kg/m^3 $\rho_G = 0.97–33.4$ kg/m^3 $\mu_L = 0.36–38.3$ mPa-s $\sigma = 23.3–72.6$ mN/m P up to 22 MPa T up to 250 °C	$k_L a = 1.77\,\sigma^{-0.22}\exp(1.65U_L - 65.3\mu_L)\varepsilon_G^{1.2}$
Nakanoh and Yoshida (1980)[b]	Air–water Air–aqueous solutions	$D_R = 0.14$ m $d_0 = 4$ mm $U_G < 10$ cm/s $\rho_L = 995–1230$ kg/m^3 ν_L (10^{-6} m^2/s) = 0.804–8.82 D_L (10^{-9} m^2/s) = 1.06–2.6	$\frac{k_L a D_R^2}{D_L} = 0.09\left(\frac{\nu_L}{D_L}\right)^{1/2}\left(\frac{D_R^3 g}{\nu_L^2}\right)^{0.39}\left(\frac{gD_R\rho_L}{\sigma}\right)^{0.75}\frac{U_G}{\sqrt{gD_R}}$
Ozturk et al. (1987)[b]	(Air, N_2, CO_2, He, H_2)-organic liquids	$D_R = 0.095$ m $d_0 = 3$ mm (SO) $U_G = 0.80–10$ cm/s $\frac{g\rho_L d_b^2}{\sigma} = 1.2–5.4$ $\frac{g d_b^3}{\nu_L^2} = 830–1.5\times10^6$ $\frac{U_G}{\sqrt{g d_b}} = 0.043–0.6$ $\frac{\rho_G}{\rho_L} = 9.3\times10^{-5}–2.0\times10^{-3}$ $\frac{\nu_L}{D_L} = 32–1.5\times10^5$ $P = 0.1$ MPa $T = 293$ K	$\frac{k_L a d_B^2}{D_L} = 0.62\left(\frac{\mu_L}{\rho_L D_L}\right)^{0.5}\left(\frac{g\rho_L d_B^2}{\sigma}\right)^{0.33}\left(\frac{g\rho_L^2 d_B^3}{\mu_L^2}\right)\left(\frac{U_G}{\sqrt{g d_B}}\right)^{0.68}\left(\frac{\rho_G}{\rho_L}\right)^{0.04}$

Salvacion et al. (1995)[b]	Air-water Air-aqueous solutions (methanol, ethanol, *n*-butanol, *n*-hexanol, *n*-octanol)	D_R = 0.14–0.30 m d_0 = 0.5–2.5 mm (MO) U_G = 2–15 cm/s ρ_L = 995–997 kg/m^3 ρ_s = 1000–1087 kg/m^3 φ_s = 0–0.20 μ_L = 0.863–0.894 mPa-s σ = 55.6–72.0 mN/m	$\frac{k_L a\sigma}{\rho_L D_L g} = 12.9 \left(\frac{\nu_L}{D_L}\right)^{1/2} \left(\frac{g\mu_L^2}{\rho_L\sigma^3}\right)^{-0.159} \left(\frac{g\rho_L D_R^2}{\sigma}\right) (1 + 0.62\varphi_s) f(B)$ $f(B) = 0.47 + 0.53 \exp\left(-41.4 \frac{B\varepsilon_G}{U_G}\sqrt{\frac{\varepsilon_G}{d_b\mu_L\rho_L U_G}}\right)$ Where: $B = 0$ for water
Schumpe and Grund (1986)[a]	Air-water	D_R = 0.30 m H = 4.4 m d_0 = 1 mm U_G< 20 cm/s T = 20 °C	$k_L a = K U_G^{0.82} \mu_{eff}^{-0.39}$ where: K = 0.063 (water/salt solution) or 0.042 (water/0.8M Na_2SO_4 solution)
Shah et al. (1982)[c]	$k_L a = 0.467 U_G^{0.82}$		
Shpirt (1981)[b]	Air–aqueous solutions of NH_4Cl	D_R = 0.107 m H_0 = 0.30–1.0 m U_G = 0.094–0.75 cm/s T = 20 °C	$\frac{k_L a d_b^2}{D_L} = A \left(\frac{U_G d_b}{\nu_L}\right)^{0.45} \left(\frac{H_0}{d_b}\right)^{-0.30}$ where: A = 0.007 for heterogeneous flow regime or A = 0.0136 for homogeneous flow regime
Sotelo et al. (1994)[b]	CO_2–water CO_2–aqueous solutions (sucrose, ethanol, glycerin)	D_R = 0.04–0.08 m d_0 = 30–150 µm (MO) U_G = 0.064–0.49 cm/s ρ_L = 998–1147 kg/m^3 μ_L = 1.00–4.17 mPa-s μ_G = 1.48–1.53 mPa-s σ = 29.8–73.4 mN/m D_L (10^{-9} m^2/s) = 0.51–1.78	$\frac{k_L a U_G}{g} = 16.9 \left(\frac{U_G\mu_L}{\sigma}\right)^{2.14} \left(\frac{\mu_L^4 g}{\rho_L\sigma^3}\right)^{-0.518} \left(\frac{\mu_G}{\mu_L}\right)^{0.074} \left(\frac{\nu_L}{D_L}\right)^{-0.038} \left(\frac{d_0}{D_R}\right)^{-0.98}$
Vasquez et al. (1993)[b]	CO_2–water CO_2–aqueous solutions (glycerin, glucose, sucrose)	ρ_L = 997–1151 kg/m^3 μ_L = 0.896–6.42 mPa-s σ = 66.9–73.4 mN/m D_L (10^{-9} m^2/s) = 0.40–1.92	$k_L a = 0.779 D_L^{0.5} \mu_L^{-0.2} F l_G^{1/6}$ (SI)

[a]As cited by Kantarci et al. (2005)
[b]As cited by Ribeiro Jr. and Lage (2005)
[c]As cited by Deckwer (1992)

7.7 NEEDED BUBBLE COLUMN RESEARCH

Although a lot of research exists on BC gas holdup and gas–liquid mass transfer, little focuses specifically on bioreactors when microorganisms are present. Controlled experiments containing actual microorganisms as well as materials able to mimic microorganism behavior, such as fiber suspensions or other liquid additives, need to be incorporated into more comprehensive studies. For example, microorganism flocculation and its effects on hydrodynamics are not commonly studied or simulated, but obviously have serious consequences on bioreactor performance. The goal would be twofold. The first would be to quantify possible surface reactions and other phenomena when microorganisms are present in the reactor environment. The second goal would be to quantify the quality of currently used substitutes to simulate microorganisms and attempt to identify newer organic possibilities. In connection to these goals, more study is needed on the effect of higher temperature, pressure, and viscosity on microorganisms as well as bioreactor hydrodynamics.

A major study should be attempted to compare the different bioreactor performance characteristics. Comparisons between BCs and airlift reactors are available, but a wider array is lacking, but needed. Research towards this end, such as Bouaifi et al. (2001) who compared stirred-tank reactors and BCs, is sparse. Different bioreactor designs have quite unique scaling abilities and associated costs, and the economic benefits and decisions would be better understood if such studies would be more common.

7.8 SUMMARY

Bubble interactions are tightly connected to hydrodynamics so that gas holdup is usually capable of representing gas–liquid mass transfer trends fairly accurately and, more importantly, predicting reactor hydrodynamics. Thus, any BC experiment (or series of experiments) starts with a gas holdup study. The literature provides a wide array of gas holdup information; however, the more detailed experiments, especially those that investigate gas–liquid mass transfer, are much fewer in number and smaller in scope.

Most studies, for example, are based on air–water interaction in an isothermal setting, even though most industrial bioprocesses have thermal interactions and complex fluid properties. It is also common for industrial processes to be performed at relatively high temperatures and/or pressure. These settings still lack experimental coverage (Lau et al., 2004). Furthermore, gas holdup and gas–liquid mass transfer are decoupled under thermal operation, and pressure variances are rarely accounted for in currently available correlations.

Gas–liquid mass transfer correlations and their design applications have to be handled very carefully. Bubble–bubble interactions are very complicated processes, which still have not been mastered and are not easily represented with the current set of tools. Although a change in gas holdup can predict the direction of the change in gas–liquid mass transfer, it cannot predict the amount

due to the hydrodynamic complexity (Chaumat et al., 2005). Scale-up, design, and application require patience and due diligence. Since most gas–liquid mass transfer correlations use gas holdup data, hydrodynamic and geometric similarities should be attempted in order to maximize the probability of successful prediction. Approximation of gas–liquid mass transfer using third-party gas holdup correlations or data has a low probability of success and should be used as a first iteration for scale-up or design. Follow-up investigations are then strongly advised.

8 Airlift Bioreactors

8.1 INTRODUCTION

The airlift reactor (ALR) is a pneumatic device that attempts to reconcile bubble column shortcomings and provide more control to the operator. The term *ALR* is also used to identify an airlift bioreactor. Two general families of airlift bioreactors exist: internal-loop airlift bioreactors and external-loop airlift bioreactors (ILALRs and ELALRs, respectively). The internal-loop variant is sectioned by a baffle (Figure 8.1a) or draught tube (Figure 8.1b), which allows for internal liquid recirculation. The external-loop airlift bioreactor (Figure 8.2) connects the up- and down-flowing regions with additional piping, thereby separating the flow paths. These two designs make up the basic idea, and extensive modification can be implemented to create a wide array of application-specific flow conditions (Ribeiro Jr. and Lage, 2005).

Airlift bioreactor construction is very simple and similar to that of a bubble column (Al-Masry, 1999; Blazej et al., 2004c). There are four basic sections: riser, gas separator, downcomer, and base. The riser is the up-flowing section of the airlift bioreactor. The gas sparger is oriented such that gas is injected into the riser causing upward fluid motion. The gas sparger location may be within the riser or the base, which is simply the region that connects the downcomer to the riser. The gas separator is located at the top of the bioreactor where gas is allowed to disengage from the liquid phase (or slurry). The downcomer is defined as the region in which down-flowing phases are present.

Airlift bioreactors tend to be larger vessels. Industrial units may have a height and diameter up to 10–40 m and 2–10 m, respectively. The specific dimensions are a function of process requirements. For example, industrial scale units may operate with a liquid circulation velocity up to 1 m/s and gas residence time of approximately 1 min (Giovannettone et al., 2009; van Benthum et al., 1999a; van Benthum et al., 1999b). The liquid circulation is a function of the gas flow rate and disengagement properties of the separator. Hence, the height is used to adjust the gas residence time to achieve the necessary conversion (van Benthum et al., 1999b). Pilot-scale bioreactors tend to have volumes of 0.05–0.30 m^3. Biological applications use industrial volumes of approximately 10 m^3, but certain applications, such

An Introduction to Bioreactor Hydrodynamics and Gas-Liquid Mass Transfer, First Edition.
Enes Kadic and Theodore J. Heindel.

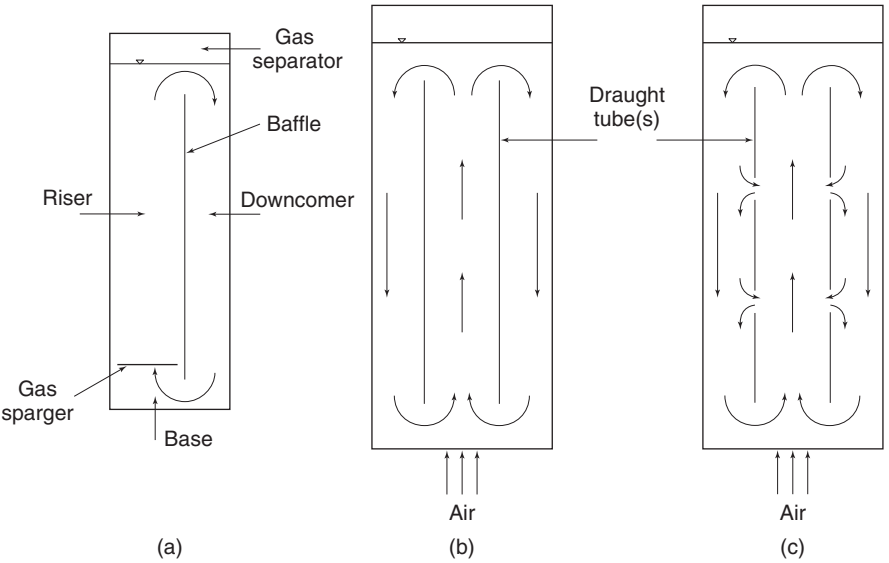

Figure 8.1 Internal-loop airlift bioreactor with (a) a baffle separating the riser and downcomer, (b) a continuous draught tube separating the riser and downcomer, and (c) a sectioned draught tube separating the riser and downcomer.

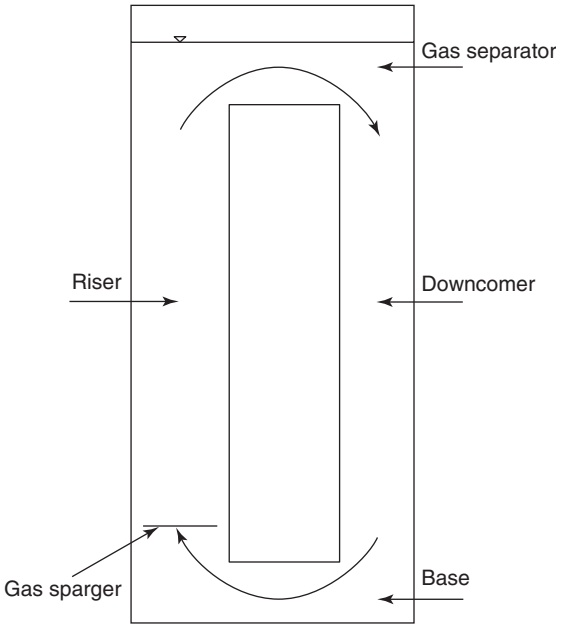

Figure 8.2 External-loop airlift bioreactor schematic.

as wastewater treatment, may use bioreactors up to 1000 m^3 in size (Joshi et al., 1990).

Biological applications use smaller scale vessels because turbulence increases with scale, which leads to an increase in shear stresses as well. Airlift bioreactors have become popular in mammalian cell suspension applications for which shear stresses become important. Increasing the bioreactor size leads to an increase in the mechanical damage and lower cell densities (Martin and Vermette, 2005).

Airlift bioreactors can be viewed from two different perspectives. One is that the airlift bioreactors are variations of the bubble column. The bubble–bubble interactions, forces, construction, and bioreactor applications are very similar to those of the bubble column. On the other hand, airlift bioreactor hydrodynamics are strongly biased on the interactions between the riser and downcomer gas holdup. The gas separator, in conjunction with gas injection in the riser section, generally leads to the gas holdup in the riser section being larger than in the downcomer. This effect creates a hydrodynamic pressure difference, which leads to the liquid–gas mixture circulating in a fairly controlled manner. This mechanism is a source of many advantages unique to the airlift bioreactor.

Another advantage is that the liquid- and gas-phase flow rates may be controlled independently of each other if a control valve is placed in the downcomer (Williams, 2002). This ability introduces much more control, making the airlift bioreactor ideal for fine-tuning industrial applications. The phases are circulated by design, which allows much higher gas and liquid flow rates over that of bubble columns (Figure 8.3) without the requirement of a complicated recycle system. The difference between Figure 8.3a and b is that Figure 8.3a can be achieved through a throttling device. In other words, mixing, heat transfer, and residence time can be optimized while providing the ability to protect any microorganism or catalyst.

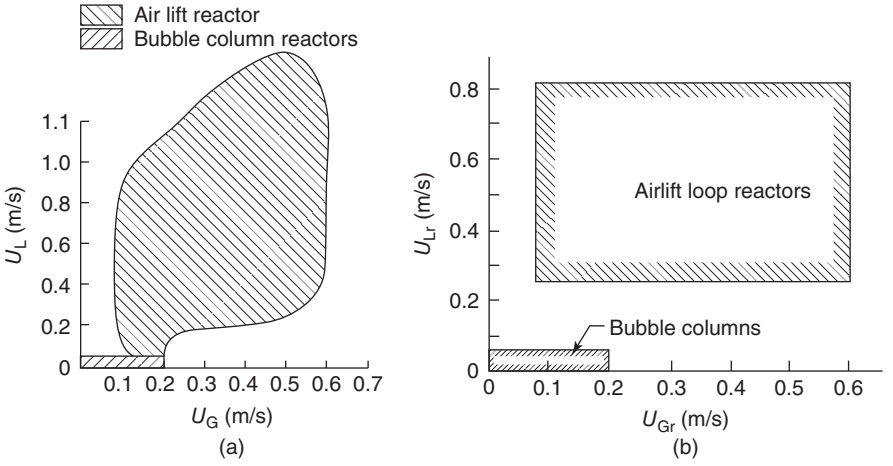

Figure 8.3 Comparison between superficial liquid and gas velocities in bubble columns and airlift bioreactors from (a) Merchuk (1986) and (b) Chisti (1989).

Dead or high shear zones are limited in airlift bioreactors because the influence of sparged gas is limited and the gas-phase distribution tends to be practically homogeneous throughout the riser volume, although a nonuniform phase distribution may be observed for approximately the first meter in the riser, which introduces variability in relatively short columns ($h_R < 4$ m) (Giovannettone et al., 2009). The only possible high shear areas are caused by turns (Merchuk and Gluz, 1999), but these can be eliminated or minimized.

The price for the advantages of ALRs is that the capital investment is usually larger relative to bubble columns. The higher costs can be offset with a liquid and/or gas input increase that is not feasible in a bubble column, which would lead to higher output; however, operation at larger flow rates in airlift bioreactors can lead to increased variable costs associated with additional gas throughput and pressurization. Foaming also becomes more likely at high gas and liquid flow rates, which leads to inefficient gas separation and recirculation of spent gas bubbles (Wei et al., 2000; Williams, 2002). Complete mixing typically requires four to nine cycles (the number of times that the liquid circulates in the ALR) (Karamanev et al., 1996), which would cause further problems if continuous operation is required. Luckily, external-loop airlift bioreactors can be designed to have much better mixing performance.

8.2 CIRCULATION REGIMES

The airlift bioreactor and bubble column have very similar bubble–bubble interactions and behavior, which leads to almost identical gas flow regimes and progression. These have been covered in detail in Section 7.2; however, more attention is placed on liquid flow behavior in airlift bioreactors since the liquid phase is a significant source of momentum and gas recirculation.

The process of gas entrainment and circulation is complicated and not easily quantified. Problems arise from an abstract relationship between the liquid and gas phases. On the one hand, the gas flow rate affects the liquid flow rate through the gas holdup and hydraulic pressure differential relationship. As the gas flow rate increases, larger bubbles rise faster and increase the circulation velocity. A higher circulation velocity, in turn, would decrease the slip velocity and make entrainment easier. On the other hand, if the liquid velocity is higher than the bubble rise velocity, bubbles would experience a drag (lift) force, which would aid entrainment.

Quantification of this process becomes complex very quickly, and a theoretical measure or technique does not exist. Researchers, instead, have to rely on empirical techniques. Nevertheless, a rough understanding of the circulation process exists and is very helpful in the empirical understanding of airlift bioreactors. Airlift bioreactor circulation can be sectioned into three general regimes, as shown in Figure 8.4. At very low gas flow rates, which correspond to $U_{Gr} < 0.012$ m/s, the induced liquid circulation velocity is not strong enough to entrain gas bubbles into the downcomer. Note that U_{Gr} is the superficial gas velocity in the riser. The gas phase is able to almost completely disengage from the liquid phase (regime 1). This

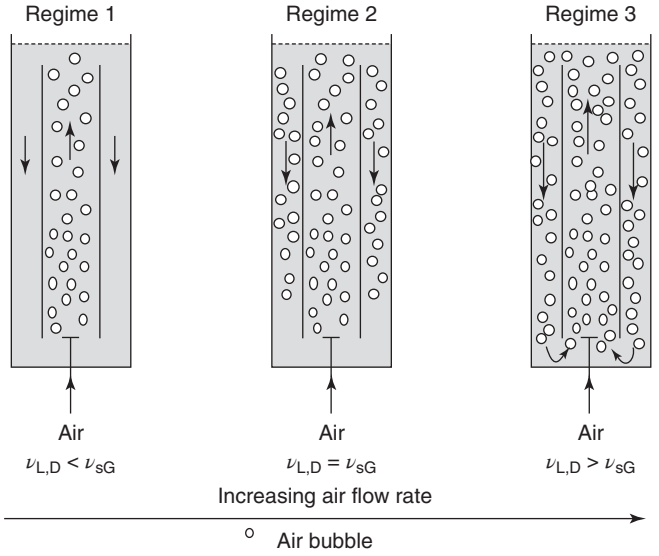

Figure 8.4 Circulation regime progression in a draught tube internal-loop airlift bioreactor (van Benthum et al., 1999b), where $v_{L,D}$ is the downcomer liquid velocity and v_{sG} is the gas slip velocity.

regime, referred to as the bubble-free regime, is usually not significantly influenced by the liquid properties simply because the amount of gas present in the system is still fairly low. In order for the liquid properties to become more important, a higher degree of bubble–bubble interaction is needed.

The liquid is capable of entraining only very small bubbles ($d_B < 1$ mm) in regime 1. The resulting downcomer gas holdup is usually small with a maximum of about 3%. Once these small bubbles are entrained in the downcomer, they are not transported far and are expected to reach depths up to 30% of the downcomer height (Albijanic et al., 2007). Any increase in the superficial gas velocity leads to a significant increase in the liquid circulation velocity (Blazej et al., 2004c; van Benthum et al., 1999b). The basic guideline is that the bubble-free regime exists as long as the downcomer superficial liquid velocity is lower than the average slip velocity (van Benthum et al., 1999a).

Once the gas is in the downcomer, the liquid has to flow even faster to cause circulation. Gas bubbles are still lighter than the liquid and have a buoyant force, which propels them to rise against the flow. The liquid-phase momentum has to provide the power to overcome the buoyant force and create a net downward force in order to cause forward motion and eventual circulation. In effect, a superficial liquid velocity exists at which gas bubbles can be suspended or are stagnant in the downcomer (regime 2 in Figure 8.4). Hence, this circulation regime is referred to as the transition regime.

When the liquid velocity in the downcomer is approximately equal to the average slip velocity, an approximate stationary bubble behavior can be observed. In addition, bubble–bubble interactions become more frequent, and liquid properties start to have more influence on bioreactor performance (Albijanic et al., 2007). Unlike regime 1, the liquid velocity does not deviate significantly and stays approximately constant in regime 2, but the transition regime is not very stable and minor variations in the superficial gas velocity can lead to regime transition. Unfortunately, a theoretical prediction of gas holdup is very challenging and experimental values vary over a wide range (van Benthum et al., 1999b). Regime 1 and the beginning of regime 2 can be described as homogeneous, while the later portion of regime 2 occurs in the transition flow regime described in Section 7.2 (Merchuk et al., 1998; van Benthum et al., 1999b).

If the downcomer liquid velocity is larger in magnitude than the bubble rise velocity, the bubble will circulate with the liquid (Albijanic et al., 2007). This minimum superficial liquid velocity usually occurs at $U_{\mathrm{Gr}} = 3.5 - 5.0\,\mathrm{cm/s}$ (Jones, 2007; Wei et al., 2008) and is described by thorough gas bubble circulation (complete bubble circulation regime—regime 3 in Figure 8.4). It should be noted that regime 3 is by far the most commonly used circulation regime. The required gas flow rate for pilot and industrial scale bioreactors requires very high superficial gas velocities, which all but guarantee circulation (Blazej et al., 2004c; Chisti, 1989). Bubble-free (regime 1) and transition (regime 2) regimes are usually avoided because they have poor phase contacting, mixing, and selectivity (Wei et al., 2008). In addition, special attention and effort are required to keep the flow in bubble-free and transition regimes for an industrial-scale bioreactor.

Bioreactors operating in the bubble-free or possibly early transition regimes are usually found when cultivating mammalian cell structures or highly shear-sensitive microorganisms for which shear stress becomes the limiting operational factor; however, designers have found it easier to operate in nonstandard designs, which at least partially circulate (see, e.g., van Benthum et al. (1999a)).

The transition from regime 2 to regime 3 is not well understood. It is suspected that the transition is initiated by the gas phase entering the heterogeneous or transition flow regime, which is synonymous to bubble column flow regimes. These flow regimes would produce larger bubbles with faster bubble rise velocities, which disengage easier, decrease the downcomer gas holdup, and increase the circulation driving force. This behavior is often confirmed with circulation starting and flow entering the transition flow regime at a superficial riser gas velocity of 0.045 m/s (Joshi et al., 1990; Merchuk et al., 1998). The faster liquid circulation velocity eventually surpasses the gas slip velocity in the downcomer, and gas bubbles are entrained in the downcomer flow. The circulating gas adds to the riser gas holdup, potentially reinforcing the trend.

Complications arise when/if the gas disengagement leads to a smaller riser gas holdup, such that the driving force is not heavily influenced. The gas disengagement process has some geometric influences that cause the transition to regime 3 to occur relatively early in the transition flow regime or well into the heterogeneous flow regime. A second complication is that the recirculated gas can lead to

more frequent bubble collisions and coalescence so that the riser gas holdup may decrease early in regime 3 until the flow structure stabilizes. This case requires the downcomer gas holdup to decrease at a faster rate than the riser gas holdup. Otherwise, the circulation would stay in regime 2. This behavior makes circulation regime transition highly variable. Interestingly, the transition to regime 3 occurs at a gas holdup of 10–12% regardless of the bubble flow regime, and for reasons and through mechanisms that are not well understood at this time (van Benthum et al., 1999b). The liquid circulation velocity resumes its relationship in regime 3 and increases with the riser superficial gas velocity. In general, the maximum downcomer gas holdup can be as high as ~20% (van Benthum et al., 1999b).

The riser superficial gas velocity at which transition occurs depends significantly on liquid properties. Generally, liquids containing surfactants or alcohols tend to experience circulation relatively early ($U_{Gr} \approx 0.035\,m/s$) while water experiences it later ($U_{Gr} \approx 0.045\,m/s$) (Albijanic et al., 2007; Jones, 2007; van Benthum et al., 1999b). Large bubbles, 3–5 mm in diameter, are not entrained in the downcomer in a water system until $U_{Gr} \approx 0.20\,m/s$. Large, ellipsoidal bubbles at these velocities also form significant wakes that limit the effective interfacial area. This factor is almost always ignored in theoretical gas–liquid mass transfer coefficient correlations or models (Talvy et al., 2007).

A simple measure to correlate liquid circulation velocity with the superficial gas velocity would be through a power law such as (Bello et al., 1984; Merchuk, 1986):

$$U_{Lr} = \alpha U_{Gr}^{\beta} \tag{8.1}$$

where U_{Lr} and U_{Gr} are the riser superficial liquid and gas velocities, and α and β are the fitted constants. The coefficient α depends on the bioreactor geometry and liquid properties while the exponent β is a function of the flow regime and bioreactor geometry. This base equation can be further enhanced, and terms can be added to account for specific properties or bioreactor design (Chisti, 1989). The fitted terms are usually positive, implying that the liquid circulation velocity increases with increasing superficial gas velocity; however, if slugging, choking, or throttling occurs, the liquid circulation velocity can actually decrease with an increase in superficial gas velocity (Jones, 2007).

A more detailed correlation could be arrived at by accounting for each force. For example, one would balance the hydrostatic pressure difference with bioreactor-specific pressure drops (e.g., head losses due to wall friction, elbows, and bends). This approach would be based on a theoretical foundation, but attempts have not been very successful due to the specific geometric dependence, and empirical correlations are still the most practical approach (Albijanic et al., 2007; Chisti, 1989).

Analysis could be skewed to favor riser versus downcomer data due to the riser cross-sectional area usually being larger than that of the downcomer. A better strategy would be to analyze each section separately. One approach is to assume a large degree of independence, which would work relatively well if the controlling factors in each section are independent of the other. A large effective riser diameter would

not impact the riser gas holdup and would cause the riser gas holdup behavior to be a function of just the gas flow rate and liquid properties. A small downcomer diameter, on the other hand, could cause the downcomer to enter the slug flow regime, which would limit circulation. Even larger downcomer diameters can be affected by trapped gas, which can grow with superficial gas velocity. The effect could be a reduction in the effective downcomer cross-sectional area and possible flow choking (Chisti, 1989; Jones, 2007). A single correlation does not take these interactions into account.

8.3 CONFIGURATION

The specific bioreactor configuration has a significant effect on gas holdup and gas–liquid mass transfer performance, as can be seen in Figure 8.5. Other factors, such as downcomer-to-riser cross-sectional area ratio or the gas separator design, can also play significant roles. For example, external-loop airlift bioreactors use gas separators that allow more time for the gas phase to disengage than in internal-loop airlift bioreactors. Hence, the downcomer in ELALRs has a negative effect on global or total gas holdup and gas–liquid mass transfer.

Furthermore, airlift bioreactor studies often use an effective riser diameter that is less than 0.15 m, which has been shown to influence the bubble size distribution in bubble columns (Kantarci et al., 2005). Not surprisingly, research work that compares ALR designs based on the bioreactor diameter uses smaller riser and downcomer columns and finds a strong bioreactor diameter dependence, noting

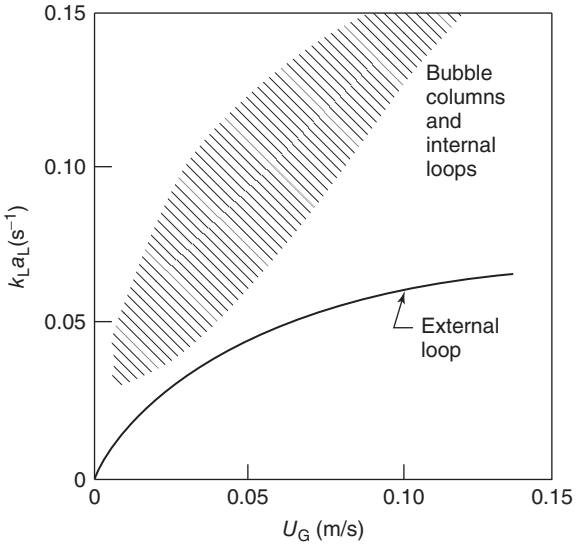

Figure 8.5 Achievable gas–liquid mass transfer in bubble columns and internal loops versus external loops (Chisti, 1989).

that bubble diameters increase with an increase in bioreactor size (Ruen-ngam et al., 2008). The bioreactor (riser) diameter effect is expected to be very similar to that of bubble columns, which has been reviewed in Section 7.3.1.

The influence of the bioreactor base is usually not discussed. The understanding is that as long as the base does not interfere with flow and increase frictional losses, one does not pay attention to it; however, some evidence exists that curved or filled bottoms may promote this limited impact (Chisti, 1989). With this in mind, the base height has a minimal impact on ALR operation as well. The only restriction is that a short base height can cause a large pressure drop, which would increase the operational cost. In such a case, gas holdup is expected to increase with an increase in bottom clearance (Al-Masry, 1999). Luckily, for designers, a restrictive bottom clearance in the experimental scale is often self-corrected during scale-up such that minimal problems are encountered in the pilot or industrial stage. None of the presented correlations at the end of this chapter attempt to reflect the bottom designs in any form.

8.3.1 Bioreactor Height

The bioreactor height can be defined in two ways. The first definition is often termed the effective bioreactor height and is defined as the distance between the base and the bottom of the gas separator. The second is the unaerated liquid height, which is defined as the distance from the base to the fluid surface prior to aeration. These definitions are shown in Figure 8.6 for the internal-loop and external-loop airlift bioreactors.

The effective bioreactor height influences the circulation path, which has many hydrodynamic implications as implied by the liquid circulation velocity defined by Blenke (1979):

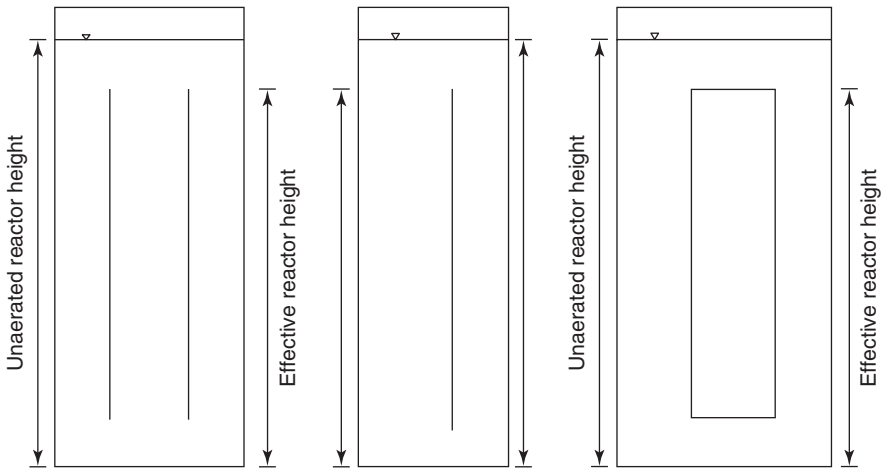

Figure 8.6 Airlift bioreactor component definitions.

$$U_{Lc} = \frac{x_c}{t_c} \tag{8.2}$$

where U_{Lc}, x_c, and t_c are the liquid circulation velocity, the circulation path length, and the circulation time, respectively. By changing the bioreactor height, the circulation path length also changes. The circulation path length influences the liquid circulation velocity, gas disengagement, and the hydraulic pressure difference, which drives the circulation flow. As the circulation path length increases, the liquid circulation velocity is expected to increase. The result would be an increase in gas disengagement and a decrease in gas holdup and gas–liquid mass transfer. At the same time, a long circulation path or time could be dangerous because it could lead to spent gas or minimal surface renewal in the downcomer (Talvy et al., 2007), possibly leading to microorganism starvation. It should be noted that the circulation time is largely influenced by the riser and downcomer residence times, while the separator and base residence times are oftentimes ignored (Joshi et al., 1990).

Bentifraouine et al. (1997a) varied the effective bioreactor height from 1 to 1.6 m and observed a significant increase in the superficial liquid velocity, which was attributed to an increase in the hydrostatic pressure differential. They also concluded that the increase in superficial gas velocity caused a decrease in the gas-phase residence time and, hence, gas holdup; however, the other possibility is that the faster liquid velocity is able to prevent the gas from disengaging and may lead to higher gas residence time. This was observed by Snape et al. (1995) who concluded that gas holdup increased and superficial liquid velocity varied minimally with an increase in bioreactor height. In other words, the effective bioreactor height's influence is dependent on the liquid flow regime and liquid velocities; however, gas–liquid mass transfer is usually seen as increasing with the effective bioreactor height (Siegel and Merchuk, 1988) unless gas holdup decreases significantly as well. It should be noted that the risk of recirculating used gas increases with higher liquid circulation velocity.

The effect of the unaerated liquid height is more complicated. If the unaerated liquid height was less than the effective bioreactor height, an increase in the unaerated liquid height would lead to an increase in the superficial liquid velocity and a decrease in gas holdup (Bentifraouine et al., 1997a, 1997b; Wei et al., 2008). If, on the other hand, the unaerated liquid height was equal to or greater than the effective bioreactor height, gas holdup, superficial liquid velocity, and, hence, ALR operation are not affected (Bentifraouine et al., 1997a, 1997b; Snape et al., 1995).

Wei et al. (2008) concluded that the unaerated liquid height had a negligible influence in the transition from the bubble-free (regime 1) to the transition regime (regime 2), but had a very important influence in the shift from the transition to complete bubble circulation regime (regime 3). Bubbles were entrained into the downcomer at approximately the same superficial gas velocity, regardless of unaerated liquid height; however, the flow resistance decreased with increased unaerated liquid height such that bubble penetration also increased, which led to an earlier transition into the complete bubble circulation regime.

The bioreactor height is often presented in the form of the riser aspect ratio (h_R/d_R). The effect of riser aspect ratio is expected to depend on the gas flow and gas circulation rate. An increase in the riser aspect ratio does not significantly change the liquid circulation velocity. Therefore, the circulation path length and circulation time increases with increasing riser aspect ratio, which allows the gas phase to achieve its equilibrium bubble diameter more efficiently.

If the superficial gas velocity and gas circulation rate are low, such that bubble–bubble interaction is low as well, an increase in the riser aspect ratio is expected to increase the average bubble diameter, decrease the gas holdup, and decrease the gas–liquid mass transfer coefficient. This effect occurs until the bioreactor is tall enough to achieve equilibrium. Bubble columns achieve this at an aspect ratio of approximately 5 and height of 1–3 m. The airlift bioreactor, especially the external-loop variant, is expected to require a higher riser aspect ratio due to the limited axial velocity variations. Evidence suggests that the superficial gas velocity is an important variable in this determination and a decrease in gas holdup may be observed up to a riser aspect ratio of 20–40. Therefore, it is fairly common to observe bubble size variations with bioreactor height in both the draught tube and external-loop airlift bioreactor (Ruen-ngam et al., 2008). If, on the other hand, the superficial gas velocity and gas circulation rate are relatively fast, a riser aspect ratio much less than 20 shows a negligible influence (Joshi et al., 1990).

8.3.2 Area Ratio

The area ratio is defined as the ratio of downcomer-to-riser cross-sectional area, but can also be represented by a downcomer-to-riser hydraulic diameter ratio. It is a simple representation of the flow restriction that exists in the bioreactor design since wall friction is of little importance unless viscosity is significantly increased (Chisti, 1989).

The area ratio influences the liquid circulation rate by adjusting the flow restriction. If the downcomer diameter or area ratio is reduced too much, the liquid flow becomes restricted and the liquid circulation velocity is expected to decrease. According to Eq. (8.2), the gas phase could follow for the same circulation path length (x_c) but the circulation time (t_c) could increase, which would lead to higher gas–liquid mass transfer (Blenke, 1979). Mere scale can have a perceived influence as well, and studies using area ratios higher than 0.25 on the pilot and industrial scales do not observe any restrictive effects. In general, frictional losses decrease with increasing scale such that the losses in a 10.5-l ILALR are four times higher than those observed in a geometrically similar 200-l ILALR (Blazej et al., 2004c). Generally, correlations model the area ratio with a negative exponent, meaning that an increase in the downcomer-to-riser area ratio leads to a decrease in gas holdup and the gas–liquid mass transfer coefficient (Garcia-Ochoa and Gomez, 2009); however, very large or very small area ratios often do not follow this rule.

An excessive reduction in the downcomer diameter (very low area ratio) would be too restrictive and reduce the liquid velocity such that the gas phase could

easily disengage, which would reduce the amount of available gas (gas holdup), the driving force, and gas–liquid mass transfer. In other words, a restrained system would decrease the liquid circulation velocity, driving force, gas holdup, and gas–liquid mass transfer by decreasing the area ratio. In general, research work has not focused on area ratios below 0.10 with the exception of Jones (2007) who used an ELALR with an area ratio of 0.063. Popovic and Robinson (1984) confirmed this by increasing the area ratio from 0.11 to 0.44, which increased the superficial liquid velocity about fourfold. Airlift bioreactors are defined by the riser and very large area ratios result in bubble column-like performance; hence, area ratios beyond 4.0 are rarely used.

Valves are occasionally used to adjust the area ratio for experimentation, such as the research by Bendjaballah et al. (1999). They closed the valve from fully to 40% open without major effects on gas holdup. This would lead to the conclusion that an optimum area ratio exists, which does not impact gas holdup and also minimizes cost. The optimum ratio may not be easily determined since it depends on the scale and operating range, and the installation of a restrictive valve in the downcomer (assuming the optimum area ratio is below the valve-free area ratio) would provide the necessary flexibility and means to get there (Weiland, 1984). Additional losses and dynamics would be introduced by the valve and must also be addressed.

If circulation is a major design goal, Joshi et al. (1990) concluded that an area ratio of about 1 maximizes the liquid circulation rate in a 10 m^3 volume bioreactor regardless of sparger location. If the bioreactor volume is increased to 100 m^3, the optimum area ratio increases by 2. When the area ratio is adjusted, the circulation velocity monotonically decreases with increasing area ratio. In Joshi's work, a bioreactor with $V_L = 10\,m^3$, $h_R/d_R = 40$, and $P/V_L = 0.3\,kW/m^3$ experienced a liquid circulation velocity decrease from 3.0 to 0.5 m/s when the area ratio increased from 0.25 to 4.0. The higher liquid velocities at lower area ratio also introduced circulation instabilities, which disappeared at $A_d/A_r = 0.3$ at 10 m^3 and $A_d/A_r = 0.5$ at 100 m^3. Hence, a stable and optimum area ratio can be achieved with a riser-to-downcomer diameter ratio of about 1.41 (Joshi et al., 1990). Variations exist for the draught tube and external-loop airlift bioreactor, which depend on the maximizing characteristic and are presented in Sections 8.3.4 and 8.3.5, respectively.

8.3.3 Gas Separator

The gas separator is an important design feature that is often ignored. The simple reason is that internal-loop airlift bioreactors have only a few options, and the design is essentially the same: a vented headspace, which is similar to the tank separator shown in Figure 8.7c. The external-loop airlift bioreactor, however, is presented with additional design options (shown in Figure 8.7a and b), which provides the external-loop airlift bioreactor with some advantages for certain processes.

The tank separator (Figure 8.7c) is the simplest and most common design and is used for both the ELALR and ILALR. It is usually a simple, rectangular vented

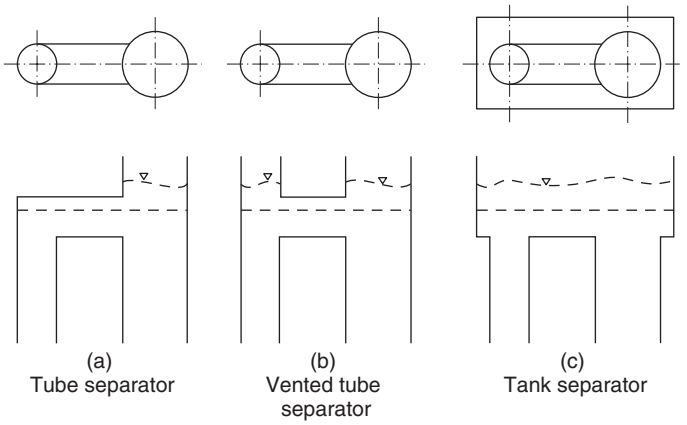

Figure 8.7 Common gas separator designs for external-loop airlift bioreactors (Jones, 2007).

box that connects the riser to the downcomer. The tank separator, however, has a negative effect in the ELALR. It increases the available gas separation area and gas separator residence time relative to a comparable ILALR design. If a comparison is made between an ELALR and ILALR on the basis of unaerated liquid height, the ELALR will have a shallower separator liquid height and higher rate of gas disengagement. Hence, the ELALR is often cited to have not only lower gas holdup and gas–liquid mass transfer performance, as shown in Figure 8.5, but also higher liquid circulation velocity (Chisti, 1989).

The unaerated liquid level is an important feature. Liquid circulation can usually be achieved by injecting more gas and ensuring a sufficiently high aerated fluid level; however, in some extreme cases, additional gas would not cause additional circulation or could actually suppress circulation to the point of no liquid circulation. This may occur when the aerated liquid level is too shallow in the gas separator such that complete gas disengagement is promoted. Therefore, increasing the liquid level to a minimal operational level would allow gas-phase circulation (Merchuk and Gluz, 1999). The operator is expected to have the ability to add enough liquid to have control, and, naturally, research has not gone toward quantifying the necessary unaerated liquid height.

More importantly for operation, the gas residence time in the separator controls disengagement such that decreasing the gas residence time in this region would lead to an increase in the downcomer gas holdup, which could decrease the hydraulic pressure differential and liquid circulation velocity (Siegel et al., 1986). The negative effect would be if the gas residence time in the separator is too long such that gas easily disengages and causes a decrease in gas holdup and gas–liquid mass transfer (Al-Masry, 1999).

One cannot easily quantify the critical fluid level since it is highly dependent on liquid properties, but a simple guideline can be used. If the gas separator residence time is longer than the minimum separation time (time required for the average

bubble to rise from the top of the riser to the liquid surface), gas disengagement is encouraged (Al-Masry, 1999). In other words, the separator would encourage gas detachment if bubbles are allowed to spend enough time in the gas separator to rise to the surface given their bubble rise velocity. Hence, increasing the superficial gas velocity could increase the bubble rise velocity and decrease the minimum separation time. Luckily, for ELALR operators, this design allows liquid circulation velocity adjustments (Chisti, 1989) so that the described situation may be offset. The gas separator, however, is sometimes designed to decrease the liquid velocity such that spent gas disengages more readily. Such a system might require a second sparger in the downcomer in order to provide sufficient gas for microorganism viability (Merchuk and Gluz, 1999).

A system-specific operational rule could be introduced based on a ratio between tank separator volume and the total bioreactor volume. An optimum volume ratio is expected to minimize power input without affecting downcomer gas holdup, which would lower operational cost and optimize output. Al-Masry (1999) varied separator volume in air–water and air–glycerol systems from 0–37%. He found that the optimum ratio, based on hydrodynamics and power input, was 11% for the air–water system. Increasing the volume ratio did not lead to significantly higher riser or downcomer gas holdup. Decreasing the volume ratio produced higher gas holdup, but it also led to much lower liquid circulation velocity. The air–glycerol system proved more difficult due to coalescence, and a volume ratio of 0% failed to lead to circulation until $U_{Gr} = 0.08\,m/s$. Hence, the airlift bioreactor acted as a bubble column. Increasing the volume ratio beyond 7% would cause negative effects such that gas holdup was minimal at 37%. The liquid circulation velocity in the air–glycerol system was much lower than in the air–water system, which made the air–water system hydrodynamically superior.

The other gas separator designs offer an alternative such that the gas separator residence time is limited. The (closed) tube (Figure 8.7a) and vented tube (Figure 8.7b) represent the same idea. The tube separator is a simple design that basically increases the separator liquid height (assuming comparable volume as with a tank separator), which increases the amount of time required for bubbles to reach the surface and disengage from the liquid phase; however, in reality, it works too well. Gas often fails to disengage completely and tends to build in the connector and eventually in the downcomer. This accumulation leads to flow choking and reduces the liquid circulation velocity. Another way to interpret the gas accumulation is that it reduces the effective downcomer-to-riser area ratio. Making the situation worse, the downcomer can enter the plug flow regime. Gas holdup increases, but the representative bubbles are very large and gas–liquid mass transfer suffers greatly. Ultimately, the connector and downcomer could be completely choked, at which point the airlift bioreactor acts just like a bubble column (Jones, 2007).

The vented tube connector minimizes the problem of gas accumulation, and gas is allowed to separate fairly efficiently. Unfortunately for some processes, the additional separator volume increases the gas separation efficiency relative to an internal-loop airlift bioreactor for the same reasons as for the tank separator;

however, the liquid circulation velocity keeps increasing with superficial gas velocity without a local maximum (Bentifraouine et al., 1997a; Choi, 2001), which may be advantageous for some processes. The vented tube separator is also susceptible to the risk of operating in the slug flow regime and the formation of very large bubbles, which can choke the downcomer flow (Jones, 2007).

The vented tube separator, in turn, can be improved with the introduction of a valve, which allows the overhead pressure to be varied. The valve would introduce an additional circulation control mechanism. As the valve closes, the overhead pressure would increase, and the gas would not disengage as readily. The assumption is that gas disengages too easily in the vented state, while it almost fails to disengage in the tube separator (Jones, 2007; van Benthum et al., 1999a), which a closed valve would imitate. Hence, the optimum would be somewhere in the middle, and a valve adjustment would allow this operational point to be reached. If the initial assumption does not hold true for the design, the valve addition to the vented tube separator would not improve operation.

The connector length (vented or closed) is expected to decrease the separator liquid height and minimum separation time and increase the separation efficiency (Choi and Lee, 1993). Hence, the liquid circulation velocity increases with a longer connector length, which leads to a decrease in downcomer gas holdup. The gas–liquid mass transfer coefficient also decreases with a decrease in downcomer gas holdup for similar reasons (Choi, 2001). Frictional losses would also increase, but wall losses can be ignored for water-like substances and would only be important in highly viscous liquids (Chisti, 1989).

The flow in the separator is much different than the other airlift components. The riser and downcomer have very well-defined flow without backmixing. The separator, on the other hand, has defined up-flow and down-flow regions. As with the bubble column, the up-flow region was present in the central region while the down-flow region occurs near the wall. The results are that a stagnant region is present between these flow regions, which may lead to bubble coalescence, and a lower liquid velocity in the separator than in the top of the riser (Lo and Hwang, 2003).

8.3.4 Internal-Loop Airlift Bioreactor

The internal-loop airlift bioreactor is a very simple design that presents some advantages for gas–liquid mass transfer. The two basic variants, explained earlier, include a vessel separated by a full baffle and a draught tube internal-loop airlift bioreactor. Regardless of the variant, the internal airlift bioreactor has very similar gas holdup characteristics to that of a bubble column, as long as the comparison is made within the bubble column's feasible superficial gas velocity range. This similarity is due to the fact that the downcomer gas holdup is 80–95% of the riser gas holdup, and the riser gas holdup is comparable to that of the bubble column. Hence, the global or total ILALR gas holdup is very similar to that of the bubble column (Bello et al., 1984; van Benthum et al., 1999b).

The draught tube ILALR (DT-ILALR) is more efficient than the baffled ILALR at gas–liquid mass transfer, and much more research has been directed toward this

variant. This imbalance is due to the advantage that the gas residence time may be up to twice as long in the DT-ILALR than in the baffled ILALR. As a matter of fact, a majority of the correlations for ILALRs, which are presented in Tables 8.1 and 8.2, have been developed using draught tubes. The baffled ILALR is usually used to study hydrodynamic behavior. Industrial application seems to be dominated by draught tube ILALRs as well. Baffled ILALRs are a little cheaper, but the advantages of the draught tube far outweigh the costs.

Since the gas phase spends more time in contact with the liquid phase, gas–liquid mass transfer in the ILALR is usually higher than the ELALR (Shariati et al., 2007). Gas–liquid mass transfer coefficients in DT-ILALRs are even slightly higher than in bubble columns due to higher operating gas flow rates. The draught tube diameter can be optimized to minimize costs and maximize a desired variable. General guidelines have been developed for different applications using a draught tube to column diameter ratio (d_D/d_R). A ratio of 0.8–0.9 maximizes mixing and mass transfer. A range of 0.5–0.6 maximizes circulation while a range of 0.6–1.0 minimizes the mixing time (Chisti, 1989). The problem for microorganism applications and the mass transfer guideline ($d_D/d_R = 0.8 - 0.9$) is that the downcomer provides minimal contribution to global gas–liquid mass transfer or gas holdup, which runs the risk of starving the microorganisms. If microorganism gas consumption in the downcomer is important, the operator has basically two solutions. First, circulation has to become more important. A tradeoff would have to be struck and the diameter ratio (d_D/d_R) be reduced. The result would be that the microorganisms could spend less time in the oxygen-deprived environment or the circulation could be designed to entrain more gas in the downcomer. Second, the microorganisms could be suspended. If the microorganisms are sensitive to shear, they can be suspended in the downcomer. If, on the other hand, the microorganisms require lots of gas, they could be suspended in the riser. Suspension could involve packed particles, porous media, and so on.

8.3.5 External-Loop Airlift Bioreactor

The external-loop airlift bioreactor has a wide array of variants ranging from the fairly simple, shown in Figure 8.2, to quite complex multistage designs. An important advantage is that the design allows access to all major bioreactor components, which is a great benefit for troubleshooting bioreactor performance or visualization (Merchuk and Gluz, 1999); however, this advantage is often not enough, and the ELALR is typically limited for use with shear-sensitive cells, photosynthetic microorganisms like algae, or processes requiring fluid recirculation. For example, mammalian cell structure can usually tolerate shear stresses in the range of $0.05 - 500\,\mathrm{N/m^2}$ (Chisti, 1989), but the sensitivity is highly variable with cell structure and density such that cells could be highly shear sensitive at low cell density and somewhat resistant at higher densities (Martin and Vermette, 2005). Hence, the bioreactor operating conditions need to be flexible enough to adjust from very low shear conditions and still potentially operate with a high degree of turbulence (high shear stress).

Stirred-tank bioreactors (discussed in Chapter 6) usually create shear stresses much larger than those that can be tolerated by mammalian cells, and bubble column bioreactors (discussed in Chapter 7) and ILALRs may reach the high end of the mammalian cell spectrum at best. Bubble–bubble interactions, especially bubble bursts or breakup, create high local shear stresses, which have a negative impact on mammalian cell growth. ELALRs, on the other hand, can maintain low shear rates while still providing a respectable oxygen transfer of 0.6–1.0 mmol/(l min) (Chisti, 1989), which is sufficient even for human skin (0.0011 mmol/(l min) at 10^6 cells/ml) and liver cells (0.005 mmol/(l min) at 10^6 cells/ml) (Martin and Vermette, 2005). This is doable using minimal circulation in the downcomer and cell suspension on packed material in the lower portion of the downcomer. The cells have minimal bubble–bubble interactions and usually have enough oxygen for growth and liquid flow for waste disposal.

Nonetheless, cell density can become a major problem. For example, mammalian cells are usually 100 μm within a blood capillary for oxygen transfer. Therefore, nature has provided a design limitation. Cells can only be 150–200 μm away from an oxygen source, such as dissolved oxygen in a liquid, because oxygen has a maximum diffusion depth of about 240 μm for cellular material. This may limit the cell density and, in turn, the operational gas flow or local shear rate. Some production problems of critical cells are mitigated by cellular design. Connective tissue cells are elongated and form low density cell structures, while some critical ones, such as liver or kidney cells, operate at high density, and also form many more blood capillaries (Martin and Vermette, 2005). In other words, the external-loop airlift bioreactor provides the possible production of a wide array of mammalian cell structures as well as shear-sensitive microorganism by-products.

The ELALR can be used for these processes because gas disengagement is very efficient. The bubbles have a relatively fast rise velocity and slow radial velocity. Hence, bubble–bubble interactions are diminished in the external-loop variant relative to the bubble column or stirred-tank bioreactor, which, in turn, leads to higher gas holdup sensitivity to liquid property variations in bubble columns than in ELALRs (Chisti, 1989; Joshi et al., 1990; Shariati et al., 2007). In other words, the bubble–bubble collision frequency is lower in ELALRs, which makes coalescence-adjusting liquid properties, such as viscosity, surface tension, or ionic strength, less important. So, while bubble column and internal-loop airlift bioreactor gas holdup are usually similar, the downcomer gas holdup in an external-loop airlift bioreactor is only 0–50% of the riser gas holdup (Bello et al., 1984), which leads to much lower global gas holdup in ELALRs.

The bioreactor geometry effects in an ELALR can be quite complex and dynamic. As the area ratio increases, the liquid circulation velocity decreases. Hence, the gas-phase circulation time decreases and gas holdup increases. The increase in gas holdup leads to an increase in the interfacial area. Some bubble dynamics are reflected in the growth, but, due to the lower bubble–bubble interactions in ELALRs, the increase is fairly continuous, but at a relatively slow rate. For example, Joshi et al. (1990) showed that by increasing the area ratio from 0.25 to 1.0 using a 10-m^3 ELALR at 0.3 kW/m^3 yielded a negligible increase

in the interfacial area while a further increase in area ratio to 4.0 increased the interfacial area by about 30%.

The area ratio effects on the liquid-phase mass transfer coefficient are more difficult to predict. Area ratio effects are usually studied by keeping the bioreactor volume equal, which requires the effective bioreactor height to be adjusted. As the height is increased, the interfacial solute gas concentration increases as well, which decreases the gas solubility and, in turn, the liquid-phase mass transfer coefficient. In addition, an increase in the area ratio decreases the liquid circulation rate, which increases gas holdup, but may decrease surface renewal. The greater height also raises the pressure drop and power consumption, which increases surface renewal and the liquid-phase mass transfer coefficient. The extent of these effects is dependent on the operational scale and power level, and it is hard to predict which will dominate.

For example, at a power consumption of $0.3\,kW/m^3$ in an ELARL, Joshi et al. (1990) observed a local maximum when $V_L = 10\,m^3$; this led to the conclusion that the decrease in gas solubility and surface renewal due to the liquid circulation velocity decline was not dominant until the area ratio was increased by about 0.5. The decline, though, was somewhat gradual. At a power consumption of $0.6\,kW/m^3$, a local maximum was not observed, which suggested the solubility effect was stronger; however, the gas–liquid mass transfer coefficient was about 50% higher at $0.6\,kW/m^3$ than at $0.3\,kW/m^3$, which was attributed to a doubling of the interfacial area. Hence, Joshi et al. (1990) concluded that the solubility decrease must have played a more significant role.

An increase in viscosity has a much stronger effect on external-loop airlift bioreactors than internal-loop airlift or bubble column bioreactors. At higher viscosities, the lower gas holdup in an internal-loop airlift bioreactor is attributed to the lower bubble rise velocity, which causes the bubbles to have a longer circulation time. At lower increases in viscosity, gas entrapment into the downcomer actually becomes easier and may increase gas holdup slightly. This behavior has been observed with a 25% glycerol concentration (Hallaile, 1993). It has also been reported that a viscosity increase in the range of 1.54–19.5 mPa-s has a minimal effect on liquid circulation rate and mixing time inside a draught tube airlift bioreactor (Molina et al., 1999). The experience in the external-loop airlift bioreactor, however, is opposite. The bubble disengagement efficiency increases because the bubble residence time in the gas separator increases significantly. The result is that if the viscosity is increased to 14 mPa-s by the addition of glycerol, the bioreactor experiences a severe gas holdup decrease (McManamey and Wase, 1986; Shariati et al., 2007).

8.4 SPARGER DESIGN

Gas distributors used in airlift bioreactors are very similar to those used in bubble columns and include sintered, perforated, or porous plates, membrane or ring-type distributors, arm spargers, and single-orifice nozzles (Figure 7.12). The sintered

plate (Figure 7.12a) is usually made out of glass or metal and produces very small bubbles. However, sintered plates are rarely used for industrial applications because they can easily plug and require cocurrent operation; they are preferred for laboratory use. Porous plates experience a similar fate. In addition, porous plates suffer from hysteresis and start-up dependent behavior, although some of this has been attributed to liquid impurities buildup (Merchuk et al., 1998). Perforated plates (Figure 7.12b), which are normally made out of rubber or metal, usually have holes 1–5 mm in diameter and are the most common gas distributor for bubble columns and airlift bioreactors. The total aeration open area is usually maintained between 0.5% and 5% of the cross-sectional area of the bioreactor. Single-orifice nozzles (Figure 7.12c) are simple tubes, which are able to produce uniform gas flow far from the injection point. The flow, however, tends to be somewhat unstable. Airlift bioreactors may also use ring spargers (Figure 7.12d) that are used with stirred-tank bioreactors and bubble columns. Ring spargers are able to produce uniform and stable flow, but are usually unable to produce small bubbles (Deckwer, 1992) and lead to an early transition to heterogeneous flow regime when compared to perforated plates (Schumpe and Grund, 1986). If the sparger is placed within the riser in an airlift bioreactor, the sparger is often a perforated tube or ring that attempts to mimic the perforated plate performance.

The sparger effect is more pronounced for $U_G < 0.15$ m/s while it is much less important at $U_G > 0.20$ m/s and nonexistent at $U_G > 0.30$ m/s (Han and Al-Dahhan, 2007). Hence, in the case of heterogeneous flow, the sparger has a negligible influence on the bubble size, gas holdup, or gas–liquid mass transfer because the bubble dynamics are determined by the rate of coalescence and breakup, which are controlled by the liquid properties and the nature and frequency of bubble collisions (Chaumat et al., 2005; Merchuk et al., 1998). Since airlift bioreactors are operated most commonly above 0.15–0.20 m/s, as seen in Figure 8.3, and using rheologically complex fluids, most research work ignores the sparger effect (Merchuk et al., 1998). Of the reviewed work in Tables 8.1 and 8.2, almost all (with very few exceptions) use perforated plate or tube spargers.

The commonly observed high gas flow rates result in correlations that can be fitted across data sets without accounting for sparger design (Kawase and Moo-Young, 1986b). Even a correlation for the liquid circulation velocity can be formed without regard to the sparger, and the results are still within 10%, even for very short vessels (Miyahara et al., 1986). The gas spargers usually do not provide enough kinetic energy from the gas jets to influence the liquid circulation rates (Chisti and Moo-Young, 1987). Hence, the preference and selection for spargers is based on operational restrictions. The perforated plates and tubes provide the cheapest and most reliable operation, while the others have major drawbacks (Chisti, 1989).

Merchuk et al. (1998) investigated the use of different sparger designs in a draught tube airlift bioreactor using $U_{Gr} = 0 - 0.20$ m/s. Their results concurred with the bubble column experience. If a sparger created a smaller initial bubble diameter, it would lead to higher gas holdup in the homogeneous and transition flow regime and longer mixing times. This dependence diminished with gas flow

rate and practically disappeared when $U_{Gr} > 0.15$ m/s, which was determined to correspond to the transition into the heterogeneous flow regime. A cylindrical perforated-pipe sparger created additional mixing due to a more radial bubble distribution, which interfered with bubble detachment and led to a higher rate of coalescence, especially in the sparger zone, and easier transition to the heterogeneous flow regime. The sparger zone in airlift bioreactors is defined as the liquid volume up to one column diameter above the sparger location (Giovannettone et al., 2009).

Although the sparger type does not appear to significantly affect ALR performance, sparger position is important and can be optimized. If the gas sparger is left at the bottom of the bioreactor, the incoming flow tends to interfere and cause a flow imbalance, which in turn leads to accumulation of gas and possible coalescence, as shown in Figure 8.8a and b. If the sparger is placed just within the riser, the incoming fluid flow does not interfere with the incoming gas flow, and the sparged gas is not affected. Elimination of dead zones in the aeration region, as shown by the shaded regions in Figure 8.8c and d, would also be beneficial. Moving the sparger too close to the surface, however, could lead to surface aeration and a higher rate of gas separation such that gas recirculation could be in troublesome. Thus, placing the sparger too far beyond the downcomer inlet does not provide additional benefits.

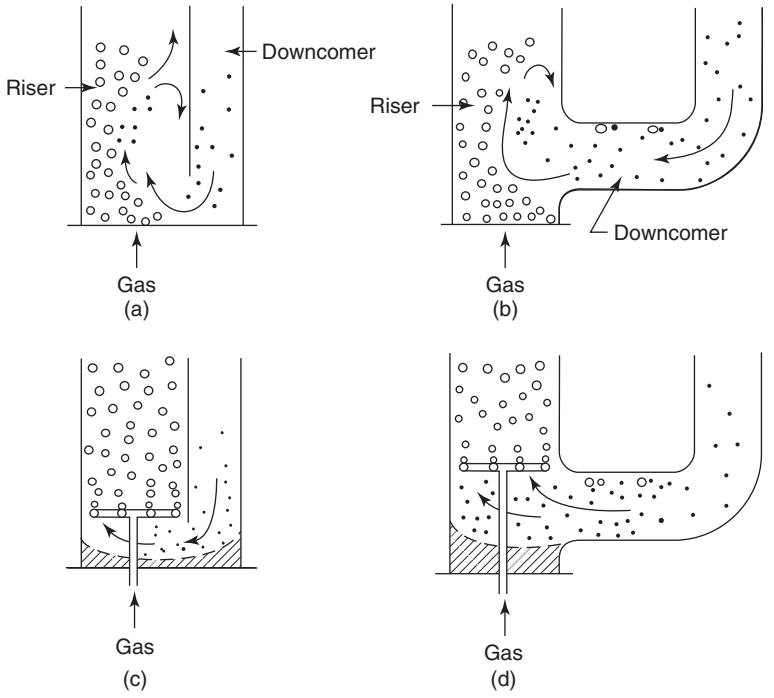

Figure 8.8 Location behavior of gas spargers in airlift bioreactors (Chisti, 1989).

Placing a sparger in the downcomer can alleviate some problems with oxygen suffocation of microorganisms and circulation, improve control, and reduce energy usage (Merchuk and Gluz, 1999). In effect, the complete bubble circulation regime could be induced earlier and with finer bubbles, which could potentially decrease the bubble diameter and increase the interfacial area; however, downcomer sparging introduces circulation instability, which can only be solved by placing the downcomer sparger at a critical height (h_{DC}).

The critical height can also be used to compare the stability between the different designs. The system is more stable if the critical height is higher. The unfortunate aspect of downcomer sparging is that it is also dependent on the riser and downcomer gas flow rates, which makes the location of the critical height highly variable. A higher riser gas flow rate increases the critical height, but the rate of increase decreases with higher downcomer gas flow. Placing the riser sparger farther into the riser may also increase the critical height (Joshi et al., 1990).

According to Joshi et al. (1990), system stability can be optimized by adjusting certain bioreactor geometries (aspect and area ratio) such that the critical height ratio (h_{DC}/h_R) is the highest possible. The area ratio was easily optimized by Joshi et al. (1990) for this purpose with a critical value of approximately 0.75. The sparger location was then dependent on the power consumption such that the critical height ratio was 0.70 at $0.6\,kW/m^3$ and 0.60 at $0.3\,kW/m^3$. In other words, the critical height determined by Joshi et al. (1990) was scale dependent. As a geometrically similar bioreactor gets larger, the critical height will increase as well.

The aspect ratio is a bit more difficult. Joshi et al. (1990) showed that the critical height rose quickly with an aspect ratio up to 10. A change in the aspect ratio from 10 to 40 yielded a relatively minor change in the critical height ratio (from 0.7 to 0.75) with a liquid volume of 10 m^3. In order to achieve $h_{DC}/h_R = 0.80$, the necessary aspect ratio was about 80, which is usually not used for biological applications. A similar trend was observed with bioreactor scale (using an aspect ratio of 40). The critical height ratio increased quickly up to 10 m^3 and changed slightly (from 0.7 to 0.75) with a volume increase from 10 to 100 m^3. A volume of 1000 m^3 was required to achieve $h_{DC}/h_R = 0.80$ (Joshi et al., 1990).

8.5 CORRELATIONS

Approaches used to develop gas–liquid mass transfer correlations in bubble columns have been ported over to airlift bioreactors, and, unfortunately, they have brought some issues along with them. Airlift bioreactor correlations are highly empirical, and a unifying development method does not exist. Some correlations attempt to be very specific and use multiple inputs, which are hard to quantify in an industrial setting, or use inputs that are not independent of each other. The suggestion is similar as with the bubble column: experimental units can use these more complicated correlations, but pilot or industrial scale units will have to depend on empirical and design specific correlations.

Further problems are presented by the downcomer and riser. Conditions in the two different sections can be very different, either by design or operation. Gas

holdup correlations, which are summarized in Table 8.1, often reflect the different conditions, and two different approaches have been developed. The first approach is to develop correlations and models for the riser. The downcomer is then modeled based on the riser. One such approach has been taken by Bello et al. (1985a) by suggesting that

$$\varepsilon_{Gd} = 0.89\varepsilon_{Gr} \tag{8.3}$$

where ε_{Gd} and ε_{Gr} are the downcomer and riser gas holdups, respectively. The other approach is to develop correlations for the riser and downcomer independently. The correlations would use similar inputs such as the riser superficial gas velocity. The assumption is that the downcomer hydrodynamics are ultimately controlled by the riser conditions and its inputs. This approach has been taken by Li et al. (1995)

$$\varepsilon_{Gr} = 0.441 U_{Gr}^{0.841} \mu_a^{-0.135} \tag{8.4}$$

$$\varepsilon_{Gd} = 0.297 U_{Gr}^{0.935} \mu_a^{-0.107} \tag{8.5}$$

where U_{Gr} and μ_a are the riser superficial gas velocity and the apparent viscosity.

Interestingly, gas–liquid mass transfer correlations for ALRs, presented in Table 8.2, do not differentiate between the bioreactor components and are displayed in global form. The situation can get troublesome for processes employing microorganisms. Gas holdup correlations have to be used and relied upon to predict the gas–liquid mass transfer conditions in the downcomer, where the danger of starvation is the highest. Although this relationship oftentimes is intact, industrial processes commonly create surfactants, temperatures, and pressures, which may decouple the relationship.

Gas–liquid mass transfer coefficients follow the same gas holdup trends. As shown in Figure 8.9, the gas–liquid mass transfer coefficient increases monotonically with riser superficial gas velocity. The correlations by Chisti et al. (1988b) (as cited by Murchuk and Gluz (1999) and Popovic and Robinson (1984) were developed using external-loop airlift bioreactors, while the others used the draught tube internal-loop airlift bioreactor. The DT-ILALR has much better performance than the ELALR. It is unfortunate to note that gas–liquid mass transfer correlations are much fewer in number than their gas holdup counterpart.

The gas holdup correlations also have a high degree of variability, as shown in Figure 8.10. Correlations are able to reflect the consensus that the internal-loop airlift bioreactor has better gas holdup performance than the external-loop airlift bioreactor. This advantage is reflected in the power law presented in the correlations in Table 8.1. The internal-loop airlift bioreactors consistently have a higher constant and stronger dependence on the superficial gas velocity. As a matter of fact, the ILALR usually has a superficial gas velocity power close to 1 while the ELALR is usually less than 0.5. A similar observation is made for the gas–liquid mass transfer correlations in Table 8.2. The advantage of the airlift bioreactor relative to the bubble column also comes through. The bubble column correlations show a leveling effect at higher superficial gas velocities. This trend is not present in the airlift bioreactor correlations.

TABLE 8.1 Gas Holdup Correlations for Airlift Bioreactors

Reference	Bioreactor Type(s)	Bioreactor parameters	Correlations
Albijanic et al. (2007)	DT-ILALR	Air-(water, 1 wt% aqueous solutions of methanol, ethanol, *n*-propanol, isopropanol, and *n*-butanol) $U_G = 0$–0.07 m/s	$\varepsilon_G = 1.65 U_G^{0.97} \left[1 + \left(\frac{d\sigma}{dC_A}\right)^{0.20}\right]^{1.52}$
Bello (1981)[a]	ELALR	$\varepsilon_{Gr} = 0.16 \left(\frac{U_G^2}{U_{Lr}}\right)^{0.56} \left(1 + \frac{A_d}{A_r}\right)$ $\varepsilon_{Gd} = 0.89\varepsilon_{Gr}$	
Bello et al. (1985a)[b]	ELALR	Air-(water, NaCl solution) $C_{NaCl} = 0.15$ kmol/m^3 d_R or $d_r = 0.152$ m $h_D = 1.8$ m $U_{Gr} = 0.0137$–0.086 m/s $A_d/A_r = 0.11$–0.69	$\varepsilon_{Gr} = 0.16 \left(\frac{U_{Gr}}{U_L}\right)^{\alpha} \left(1 + \frac{A_d}{A_r}\right)$ $\varepsilon_{Gd} = 0.89\varepsilon_r$ for DT-ILALR $\varepsilon_{Gd} = 0.79\varepsilon_r - 0.057$ for ELALR $\alpha = 0.56$ for water $\alpha = 0.58$ for salt solution
Bello et al. (1985b)[b]	ELALR DT-ILALR BC	Air-(water, NaCl solution) $C_{NaCl} = 0.15$ kmol/m^3 d_R or $d_r = 0.152$ m $h_D = 1.8$ m $U_{Gr} = 0.0137$–0.086 m/s $A_d/A_r = 0.11$–0.69 (ELALR) $A_d/A_r = (0.13, 0.35, 0.56)$ (ILALR) $A_d/A_r = 0$ (BC)	$\varepsilon_G = 3.4\times10^{-3} \left(1 + \frac{A_d}{A_r}\right)^{-1} \left(\frac{P_G}{V_D}\right)^{2/3}$
Bentifraouine et al. (1997a)[c]	?	$U_G = 0.002$–0.06 m/s $U_{Lr} = 0$–0.2 m/s	$\varepsilon_{Gr} = 2U_G^{0.88}(1 - 0.97U_{Lr}^{0.49})$

Blazej et al. (2004c)	ILALR	Air-water For 10.5 l: $d_R = 0.108$ m $d_r = 0.070$ m $h_R = 1.26$ m $h_D = 1.145$ $A_d/A_r = 1.23$ $h_c = 0.030$ m $h_R/d_R = 11$ For 32 l: $d_R = 0.157$ m $d_r = 0.106$ m $h_R = 1.815$ m $h_D = 1.710$ $A_d/A_r = 0.95$ $h_c = 0.046$ m $h_R/d_R = 12$ For 200 l: $d_R = 0.294$ m $d_r = 0.200$ m $h_R = 2.936$ m $h_D = 2.700$ $A_d/A_r = 1.01$ $h_c = 0.061$ m $h_R/d_R = 10$	For 10.5 l: $\varepsilon_{Gr} = 0.829U_{Gr}^{0.505}$ $\varepsilon_{Gd} = 0.857\varepsilon_{Gr} - 0.0095$ in regime 2 $\varepsilon_{Gd} = 0.432\varepsilon_{Gr} - 0.0139$ in regime 3 For 32 l: $\varepsilon_{Gr} = 0.815U_{Gr}^{0.449}$ $\varepsilon_{Gd} = 0.885\varepsilon_{Gr} + 0.0065$ in regime 2 $\varepsilon_{Gd} = 0.670\varepsilon_{Gr} - 0.0037$ in regime 3 For 200 l (only regime 3 was presented): $\varepsilon_{Gr} = 0.792U_{Gr}^{0.427}$ $\varepsilon_{Gd} = 0.967\varepsilon_{Gr} + 0.0068$
Cai et al. (1992)[a]	ILALR	$\varepsilon_{Gr} = 2.47U_{Gr}^{0.97}$	
Chakravarty et al. (1973)[b]	DT-ILALR	Air-(water, sulphate, glycerol, and iso-butyl alcohol solutions) $d_R = 0.10$ m $d_D = (0.074, 0.59, 0.45)$ m $L_D = 0.40$ m $L_c = 0.026$ m	$\varepsilon_{Gr} = \left[(\mu_L - \mu_W)^{2.75} + 161\,\frac{73.3 - \sigma}{79.3 - \sigma}\right] \times 10^{-4} \times U_{Gr}^{0.88}$ $\varepsilon_{Gr} = 1.23 \times 10^{-2} \left[\frac{74.2 - \sigma}{79.3 - \sigma}\right] \mu_L^{0.45} \left(\frac{A_d}{A_r}\right)^{1.08} U_{Gr}^{0.88}$

(*continued*)

TABLE 8.1 (*Continued*)

Chisti and Moo-Young (1986)[b]	ILALR (rectangular)	Air-(water, aqueous salt solution)+1–3 dry wt./vol. % KS-1016 cellulose fiber	Homogeneous flow regime: $\varepsilon_G = (1.488–0.496C_s)U_G^{0.892\pm0.075}$ Heterogeneous flow regime: $\varepsilon_G = (0.371–0.089C_s)U_G^{0.430\pm0.015}$
Chisti et al. (1988a)[a]	ILALR	$\varepsilon_{Gr} = 0.65U_{Gr}^{(0.603+0.078C_0)}\left(1+\frac{A_d}{A_r}\right)^{-0.258}$ $\varepsilon_{Gd} = 0.46\varepsilon_r - 0.0244$	
Chisti (1989)	ILALR	$U_{Gr} = 0.026–0.21$ m/s $A_d/A_r = 0.25–0.44$	$\varepsilon_{Gr} = 0.65\left(1+\frac{A_d}{A_r}\right)^{-0.258}U_{Gr}^{0.603}$ $\varepsilon_{Gr} = 2.4U_G^{0.97}$
Choi (2000)[c]	?	$U_G = 0.02–0.18$ m/s $h_R = 0.04–0.20$ m $A_d/A_r = 0.11–0.53$	$\varepsilon_{Gr} = 0.2447U_G^{0.5616}\left(\frac{A_d}{A_r}\right)^{-0.2779}h_R^{-0.0130}$
Choi (2001)[c]	ELALR	$U_G = 0.02–0.18$ m/s $L_c/L_h = 0.1–0.5$ m $A_d/A_r = 0.11–0.53$	$\varepsilon_{Gr} = 0.431U_G^{0.580}\left(\frac{A_d}{A_r}\right)^{-0.040}\left(\frac{L_c}{L_h}\right)^{-0.042}$
Ghirardini et al. (1992)[a]	ELALR	$\varepsilon_G = 0.55U_{Gr}^{0.78}\left(\frac{U_{Ls}}{U_L}\right)^{0.2}d_r^{0.42}$	
Hills (1976)[c]	?	$U_G = 0.4–3.2$ m/s $U_{Lr} = 0–2.5$ m/s	$\varepsilon_{Gr} = \frac{U_G}{0.21 + 1.35(U_G+U_{Lr})^{0.93}}$

Li et al. (1995)[a]	ILALR	$\varepsilon_{Gr} = 0.441 U_{Gr}^{0.841} \quad \mu_{\alpha}^{-0.135}$ $\varepsilon_{Gd} = 0.297 U_{Gr}^{0.935} \quad \mu_{\alpha}^{-0.107}$	
Kawase et al. (1995)[a]	ILALR	$\dfrac{\varepsilon_{Gr}}{1-\varepsilon_{Gr}} = \dfrac{U_{Gr}^{n+2/2(n+1)}}{2^{3n+1/n+1}\, n^{n+2/2(n+1)} \left(\dfrac{K}{\rho_L}\right)^{1/2(n+1)} g^{n/2(n+1)} \left(1+\dfrac{A_d}{A_r}\right)^{3(n+2)/4(n+1)}}$	
Kawase and Moo-Young (1986a)[a]	ILALR	$\varepsilon_G = 0.24 n^{-0.6} Fr^{0.84-0.14n} Ga$	
Kawase and Moo-Young (1986b)[b]	DT-ILALR BC	Air-(water, pseudoplastic fluids) $U_G = 0.008$–0.285 m/s $d_R = 0.14$–0.35 m $n = 0.28$–1 $K = 0.001$–1.22 Pa–s^n	$\varepsilon_G = 0.24 n^{-0.6} \left(\dfrac{U_G}{\sqrt{g d_R}}\right)^{0.84-0.14n} \left(\dfrac{g d_R^3 \rho_L^2}{\mu_a^2}\right)$
Kawase and Moo-Young (1987)[a]	ELALR	$\varepsilon_{Gr} = 1.07 \left(\dfrac{U_G^2}{g d_r}\right)^{0.333}$	
Kemblowski et al. (1993)[a]	ELALR	$\varepsilon_{Gr} = 0.203 \dfrac{Fr^{0.31}}{Mo^{0.012}} \left(\dfrac{U_{Gr}}{U_{Lr}} \dfrac{A_r}{A_d}\right)^{0.74}$ where: $Mo = \dfrac{g(\rho_L - \rho_G)}{\sigma \rho_L^2} K^4 \left(\dfrac{8 U_{Gr}}{d_r}\right)^{4(n-1)} \left(\dfrac{3n+1}{4n}\right)^{4n}$ $Fr = \dfrac{(U_{Lr} + U_{Gr})^2}{g d_r}$	

(*continued*)

TABLE 8.1 (*Continued*)

Koide et al. (1983a)[a]	ILALR	$\frac{\varepsilon_G}{(1+\varepsilon_G)^4} = 0.16\left(\frac{U_G\mu_L}{\sigma}\right)Mo^{-0.283}\left(\frac{d_r}{d_R}\right)^{-0.222}\left(\frac{\rho_L}{\Delta\rho}\right)^{0.283}\left[1\text{–}1.61\left(1-e^{0.00565Ma}\right)\right]^{-1}$	
Koide et al. (1985)[a]	ILALR	$\frac{\varepsilon_G}{(1+\varepsilon_G)^4} = \frac{0.124\left(\frac{U_G\mu_L}{\sigma}\right)^{0.996}\left(\frac{\rho_L\sigma^3}{g\mu_L^4}\right)^{0.294}\left(\frac{d_r}{d_R}\right)^{0.114}}{1\text{–}0.276\left(1-e^{-0.0368Ma}\right)}$	
Koide et al. (1988)[a]	ILALR	$\varepsilon_{Gr} = \frac{Fr}{0.415+4.27\left(\frac{U_{Gr}+U_{Lr}}{\sqrt{gd_r}}\right)\left(\frac{g\rho_L d_R^2}{\sigma}\right)^{-0.188}+1.13Fr^{1.22}Mo^{0.0386}\left(\frac{\Delta\rho}{\rho_L}\right)^{0.0386}}$	
Merchuk (1986)[c]	?	$U_G = 0.002$–0.5 m/s	$\varepsilon_{Gr} = 0.047U_{Gr}^{0.59}$
Merchuk et al. (1998)	DT-ILALR	Air-seawater from Almeria Bay $U_G = 0$–0.21 m/s $h_R = 2$ m $d_R = 0.096$ m $h_D = 1.5$ m $A_r = 0.00283$ m^2 $A_d = 0.00280$ m^2	$\varepsilon_{Gr} = \alpha\left(\frac{U_{Gr}}{U_{Lr}}\right)^{\beta}$

Sparger	α	β
PP with $30\times d_0 = 1$ mm	0.48	1.03
PP with $30\times d_0 = 0.5$ mm	0.37	0.79
CS with $d_0 = 120$ μm	0.34	0.69
CS with $d_0 = 60$ μm	0.33	0.68
PS with $d_0 = 120$ μm	0.48	1.13
PS with $d_0 = 60$ μm	0.40	0.99
PS with $d_0 = 30$ μm	0.38	0.88

Miyahara et al. (1986)[b]	DT-ILALR	Air-non-Newtonian CMC solutions ρ_L = 952–1168 kg/m^3 μ_L = 1.0–14.9 mPa-s σ = 34.1–72.0 mN/m d_R = 0.148 m L_d = 1.0 m h_R = 1.20 m d_0 = 0.0005–0.0015 m A_d/A_r = 0.128–0.808	$\varepsilon_{Gr} = \dfrac{0.4\sqrt{Fr}}{1 + 0.4\sqrt{Fr}\left(1 + \dfrac{U_L}{U_{Gr}}\right)}$ For : $\varepsilon_{Gr} < 0.0133 \left(\dfrac{A_r}{A_d}\right)^{-1.32}$ $\varepsilon_{Gd} = 4.51 \times 10^6 \, Mo^{0.115} \left(\dfrac{A_r}{A_d}\right)^{4.2} \varepsilon_{Gr}^{4.2}$ For : $\varepsilon_{Gr} > 0.0133 \left(\dfrac{A_r}{A_d}\right)^{-1.32}$ $\varepsilon_{Gd} = 0.05 \, Mo^{-0.22} \left[\left(\dfrac{A_r}{A_d}\right)^{0.5} \varepsilon_{Gr}\right]^{0.31 Mo^{-0.073}}$
Shariati et al. (2007)	DT-ILALR	Air-(distilled water, aqueous isomax diesel) U_G = 0–0.07 m/s d_R = 0.14 m h_D = 1.1 m d_r = 0.1 m h_c = 0.024 m A_d/A_r = 0.906 h_0 = 25×1 mm (PP) ν_L = 46.142×10^{-6} m^2/s	$\varepsilon_G = 4.92 U_{Gr}^{1.066} \nu_L^{-0.355}$ $\varepsilon_{Gd} = 0.788 \varepsilon_{Gr} - 0.004$

(*continued*)

TABLE 8.1 (*Continued*)

Trilleros et al. (2005)	DT-ILALR	Air-water $h_R = 1.25$ m $d_R = 0.42$ m $d_{pg} = 0.25$ and 1 mm $\rho_{pg} = 2.6$ g/cm^3 $d_{pc} = 3$ mm $\rho_{pg} = 1.0$ g/cm^3 $d_0 = 12\times1$ mm (PP) $d_D = (0.044, 0.082, 0.125, 0.240)$ m $h_D = 0.630$ and 1.050 m $\varepsilon_s = 1$–7%	Large glass particles: $\frac{U_{Gr}}{\varepsilon_{Gr}} = \left[0.43\left(U_{Gr} + U_{Lr} + U_{Sr}\right)\right] + 0.26$ $U_{Gr} = 0.02$–0.10 m/s $(U_{Gr} + U_{Lr} + U_{Sr}) = 0.80$–$14.05$ m/s $\varepsilon_{Gr} = 0.013$–0.14 Small glass particles: $\frac{U_{Gr}}{\varepsilon_{Gr}} = \left[0.35\left(U_{Gr} + U_{Lr} + U_{Sr}\right)\right] + 0.15$ $U_{Gr} = 0.006$–0.12 m/s $(U_{Gr} + U_{Lr} + U_{Sr}) = 1.05$–$14.75$ m/s $\varepsilon_{Gr} = 0.005$–0.17 Polystyrene particles: $\frac{U_{Gr}}{\varepsilon_{Gr}} = \left[0.22\left(U_{Gr} + U_{Lr} + U_{Sr}\right)\right] + 0.15$ $U_{Gr} = 0.005$–0.12 m/s $(U_{Gr} + U_{Lr} + U_{Sr}) = 0.50$–$15.20$ m/s $\varepsilon_{Gr} = 0.005$–0.16
Posarac and Petrovic (1988)[a]	ELALR	$\varepsilon_{Gr} = \frac{0.6\,\rho_G^{0.062}\,\rho_L^{0.069}\,\mu_G^{0.107}}{\mu_L^{0.053}\,S_L^{0.185}} \frac{U_{Gr}^{0.936}}{\left(U_{Gr} + U_{Lr}\right)^{0.474}}$	
Popovic and Robinson (1984)[a]	ELALR BC	Air-non-Newtonian CMC solutions $\mu_L = 0.015$–0.5 Pa-s $A_d/A_r = (0, 0.11, 0.25, 0.44)$	$\varepsilon_{Gr} = 0.465 U_{Gr}^{0.65} \left(1 + \frac{A_d}{A_r}\right)^{-1.06} \mu_a^{-0.103}$
Vatai and Tekic (1986)[a]	ILALR	$\varepsilon_{Gr} = \left(0.491 - 0.498\right) U_{Gr}^{0.706} \left(\frac{A_d}{A_r}\right)^{-0.254} d_r \mu_a^{0.0684}$	

[a]As cited by Merchuk and Gluz (Merchuk and Gluz, 1999)
[b]As cited by Chisti (Chisti, 1989)
[c]As cited by Jones (Jones, 2007)

TABLE 8.2 Gas–Liquid Mass Transfer Coefficient Correlations for Airlift Bioreactors

Reference	Bioreactor Type(s)	Bioreactor Parameters	Correlations
Albijanic et al. (2007)	DT-ILALR	Air–(water, 1 wt% aqueous solutions of methanol, ethanol, *n*-propanol, isopropanol, and *n*-butanol) U_G = 0–0.07 m/s	$k_L a = 0.28 U_G^{0.77} \left[1 + \left(\frac{d\sigma}{dC_A}\right)^{0.15}\right]^{0.71}$
Bello et al. (1985a)[a]	ELALR	Air–(water, NaCl solution) d_R or d_r = 0.152 m h_D = 1.8 m U_{Gr} = 0.0137–0.086 m/s A_d/A_r = 0.11–0.69	$\frac{k_L a h_r}{U_L} = 2.28 \left(\frac{U_{Gr}}{U_L}\right)^{0.90} \left(1 + \frac{A_d}{A_r}\right)^{-1}$
Bello et al. (1985b)[a]	ELALR DT-ILALR BC	Air–(water, NaCl solution) d_R or d_r = 0.152 m h_D = 1.8 m U_{Gr} = 0.0137–0.086 m/s A_d/A_r = 0.11–0.69 (ELALR) A_d/A_r = (0.13, 0.35, 0.56) (ILALR) A_d/A_r = 0 (BC)	$k_L a = 0.76 \left(1 + \frac{A_d}{A_r}\right)^{-2} U_{Gr}^{0.8}$ $k_L a = 5.5 \times 10^{-4} \left(1 + \frac{A_d}{A_r}\right)^{-1.2} \left(\frac{P_G}{V_D}\right)^{0.8}$

(*continued*)

TABLE 8.2 (*Continued*)

Reference	Bioreactor Type(s)	Bioreactor Parameters	Correlations
Blazej et al. (2004b)	DT-ILALR	(Air, pure oxygen, nitrogen)–(Na_2SO_3 aqueous solution) $d_R = 0.157$ m $d_D = 0.106$ m $V_L = 40$ dm^3 $d_0 = 25\times1$ mm (PP)	$k_La = 0.91\varepsilon_{Gr}^{1.39}$
Chisti et al. (1988b)[b]	ELALR	$k_La = (0.349-0.102C_s)U_{Gr}^{0.837}\left(1+\frac{A_d}{A_r}\right)^{-1}$	
Freitas and Teixeira (2001)	DT-ILALR	Low density solids: $d_P = 2.131\pm0.102$ mm $\rho_s = 1023\pm1$ kg/m^3 High density solids: $d_P = 2.151\pm0.125$ mm $\rho_s = 1048\pm1$ kg/m^3 $\varepsilon_s = 0$–30% $U_{Gr} = 0.01$–0.5 m/s	Water/low density solids $k_La = (-0.93U_{Gr}^2+1.33U_{Gr}-0.012)(-0.0000016\varepsilon_s^2-0.00099\varepsilon_s+0.054)$ Water/high density solids $k_La = (-0.33U_{Gr}^2+0.43U_{Gr}-0.0064)(-0.000080\varepsilon_s^2-0.0056\varepsilon_s+0.17)$ Ethanol (10 g/l)/low density solids $k_La = (-0.95U_{Gr}^2+1.34U_{Gr}-0.021)(-0.000072\varepsilon_s^2-0.00079\varepsilon_s+0.075)$ Ethanol (10 g/l)/high density solids $k_La = (-0.78U_{Gr}^2+1.20U_{Gr}-0.021)(-0.000074\varepsilon_s^2+0.0035\varepsilon_s+0.081)$

Kawase and Moo-Young (1986a)[b]	ILALR	$Sh = 0.68n^{-0.72}Fr^{0.38n+0.52}Sc^{0.38-0.14n}$	
Kawase and Moo-Young (1986b)[a]	DT-ILALR BC	Air–(water, pseudoplastic fluids) U_G = 0.008–0.084 m/s d_R = 0.14–0.305 m n = 0.543–1 K = 0.00089–2.82 Pa-s^n	$\frac{k_L a d_R^2}{D_L} = 0.68n^{-6.72}\left(\frac{d_R U_G \rho_L}{\mu_a}\right)^{0.38n+0.52}\left(\frac{\mu_a}{D_L \rho_L}\right)^{0.38n-0.14}$
Koide et al. (1983a)[a]	DT-ILALR	Air–Newtonian fluids μ_L = 0.9–13 mPa-s σ = 51–73 mN/m^3 D_L (10^9) = 0.18–2.42 m^2/s U_G = 0.0098–0.156 m/s d_R = 0.10–0.30 m d_D = 0.06–0.19 m L_d = 0.70–2.10 m L = 0.84–2.24 m d_0 = 0.001–0.015 m (SO) d_0 = 7×0.001 m (PP)	$\frac{k_L a d_R^2}{D_L} = 0.477\left(\frac{\mu_L}{\rho_L D_L}\right)^{0.5}\left(\frac{g d_R^2 D_L}{\sigma}\right)^{0.837}\left(\frac{g d_R^3 D_L^2}{\mu_L^2}\right)^{0.257}\left(\frac{d_D}{d_R}\right)^{-0.54}\varepsilon_G{}^{1.36}$ $3.69\times10^2 \le \frac{\mu_L}{\rho_L D_L} \le 5.68\times10^4$ $1.36\times10^3 \le \frac{g d_R^2 D_L}{\sigma} \le 1.22\times10^4$ $2.27\times10^8 \le \frac{g d_R^3 D_L^2}{\mu_L^2} \le 3.32\times10^{11}$ $0.471 \le \frac{d_D}{d_R} \le 0.743$ $0.037 \le \varepsilon_G \le 0.21$

(*continued*)

TABLE 8.2 (*Continued*)

Reference	Bioreactor Type(s)	Bioreactor Parameters	Correlations
Koide et al. (1983b)[a]	DT-ILALR	Air–Newtonian fluids μ_L = 0.9–13 mPa-s σ = 51–73 mN/m^3 D_L (10^9) = 0.18–2.42 m^2/s U_G = 0.0098–0.156 m/s d_R = 0.10–0.30 m d_D = 0.06–0.19 m L_d = 0.70–2.10 m L = 0.84–2.24 m d_0 = 0.001–0.004 m (SO)	$\frac{k_L a\sigma}{D_L g \rho_L} = 2.25 \left(\frac{\mu_L}{\rho_L D_L}\right)^{0.5} \left(\frac{\rho_L \sigma^3}{g\mu_L{}^4}\right)^{0.136} \left(\frac{d_0}{d_R}\right)^{-0.0905} \varepsilon_G{}^{1.26}$ $3.71\times10^2 \le \frac{\mu_L}{\rho_L D_L} \le 6.00\times10^4$ $1.18\times10^6 \le \frac{\rho_L \sigma^3}{g\mu_L{}^4} \le 5.93\times10^4$ $0.471 \le \frac{d_D}{d_R} \le 0.743$ $7.41\times10^{-3} \le \frac{d_0}{d_c} \le 2.86\times10^{-2}$ $0.0302 \le \varepsilon_G \le 0.305$
Koide et al. (1985)[b]	ILALR	$Sh = 2.66 Sc^{0.5} Bo^{0.715} Ga^{0.25} \left(\frac{d_r}{d_R}\right)^{-0.429} \varepsilon_G{}^{1.34}$	
Li et al. (1995)[b]	ILALR	$k_L a = 0.0343 U_{Gr}{}^{0.524} \mu_a{}^{-0.255}$	
Merchuk et al. (1994)[b]	ILALR	$Sh = 30000 Fr^{0.97} M^{-5.4} Ga^{0.045} \left(1+\frac{A_d}{A_r}\right)^{-1}$	

Muthukumar and Velan (2006)	DT- ILALR	Air–(isoamyl alcohol, benzoic acid, propanol, CMC solution) ε_s = 5–20% d_R = 0.19 m d_r/d_R = (0.34, 0.44, 0.49, 0.59, 0.76) h_R = 2 m h_D = 1.22 m h_c = 0.05 m d_0 = 37×1 mm (PP)	
	For three-phase systems that enhance k_La: $\frac{k_L a d_R}{D_L} = 0.7 C_s^{-0.214} \left(\frac{U_G^2}{g d_R}\right)^{0.49} \left(\frac{d_r}{d_R}\right)^{-0.46} \left(\frac{g d_R^3 \rho_L^2}{\mu_L^2}\right)^{-0.209} \left(\frac{g d_R^2 \rho_L}{\sigma}\right)^{2.515} \left(\frac{\rho_p - \rho_L}{\rho_L}\right)^{-0.144} \left(\frac{U_t \mu_L}{\sigma}\right)^{-0.1}$ For three-phase systems that decrease k_La: $\frac{k_L a d_R^2}{D_L} = 0.64 \varepsilon_s^{-0.214} \left(\frac{U_G^2}{g d_R}\right)^{0.49} \left(\frac{d_r}{d_R}\right)^{-0.46} \left(\frac{g d_R^3 \rho_L^2}{\mu_L^2}\right)^{0.576} \left(\frac{U_t \mu_L}{\sigma}\right)^{-0.343}$ $k_La = 0.678 U_G^{0.907} \mu_{eff}^{-0.086}$ where: $\mu_{eff} = (5000 U_G)^{n-1}$		
Nicolella et al. (1998)	DT-ILALR	Air–water–biofilm particles U_G = 0.002–0.027 m/s ε_s = 5, 10, 15% d_s = (0.47, 0.91, 1.67, 1.95) mm d_R = 0.060 m d_r = 0.043 m h_R = 0.700 m h_D = 0.360 m	$k_La = 0.6\varepsilon_G$

(*continued*)

TABLE 8.2 (*Continued*)

Reference	Bioreactor Type(s)	Bioreactor Parameters	Correlations
Popovic and Robinson (1984)[a,b]	ELALR BC	Air–non-Newtonian CMC solutions μ_L = 0.015–0.5 Pa-s A_d/A_r = (0, 0.11, 0.25, 0.44)	$k_La = 1.911\times10^{-4}U_{Gr}^{0.525}\left(1+\frac{A_d}{A_r}\right)^{-0.853}\mu_a^{-0.89}$ $k_La = 0.24U_{Gr}^{0.837}\left(1+\frac{A_d}{A_r}\right)^{-1}$
Ruen-ngam et al. (2008)	DT-ILALR	Air–(tap and sea water) Salinity = (0, 15, 30, 45) ppm U_G = 0.01–0.07 m/s h_R = 1.2 m L_D = 1 m h_c = 0.05 m d_R = 0.137 A_d/A_r = (0.067, 0.443, 0.661, 1.008) V_L= 1.5 l d_0 = 30×1 mm (PR)	When salinity = 0 ppm $Sh = 0.41+1.05Gr^{0.48}$ When salinity = 15–45 ppm $Sh = 0.41+1.04Gr^{0.16}Sc^{0.3}+0.13Re^{0.46}Sc^{0.06}$
Siegel and Merchuk (1988)[b]	ELALR	$k_La = 913\left(\frac{P}{V_Ld_R}\right)^{1.04}U_L^{-0.15}$	

[a]As cited by Chisti (1989).
[b]As cited by Merchuk and Gluz(1999).

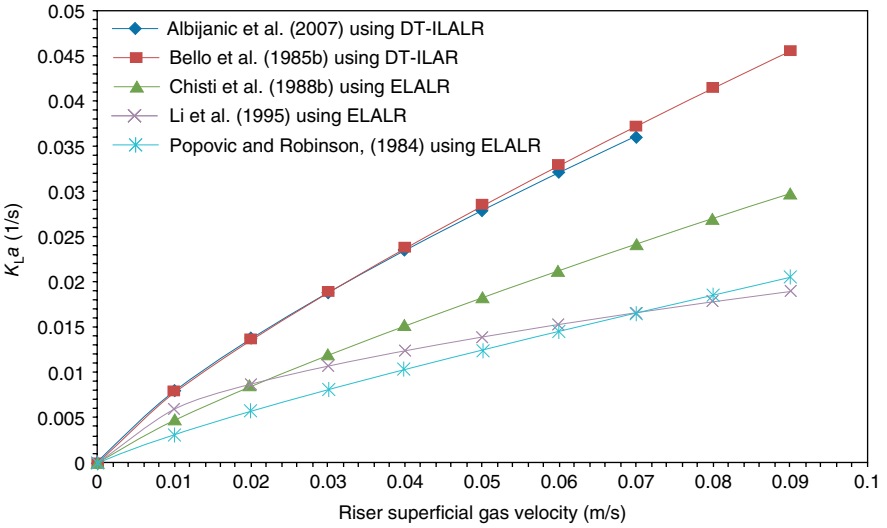

Figure 8.9 Sample gas–liquid mass transfer coefficients for ALRs.

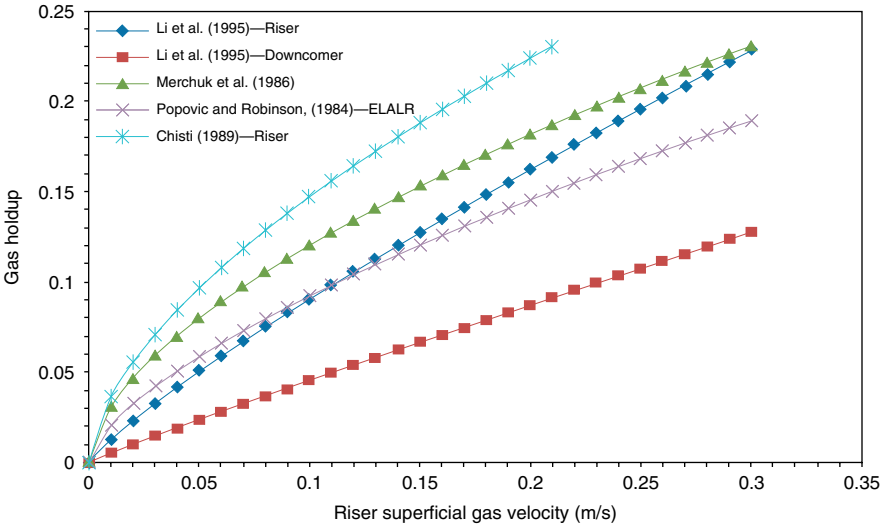

Figure 8.10 Sample gas holdup correlations for the internal-loop airlift bioreactor.

A significant problem with a large number of available correlations is that they require knowledge of the liquid phase behavior. This need is quite logical, but replication often requires a correlation for the liquid velocity, and additional error would be introduced in the generated gas holdup and gas–liquid mass transfer data.

A few measurement and assumption issues are built into the existing correlations. Gas–liquid mass transfer correlations, which are calculated at high gas flow rates, may be 15% lower than the system experiences because an incorrect assumption of ideal phase mixing is often made (Blazej et al., 2004b). A further problem is that a normal bubble size distribution is often assumed in the analysis, but the truth of this or any other assumption has not been thoroughly verified (Fadavi et al., 2008).

8.6 NEEDED RESEARCH

The research on airlift bioreactors is relatively young compared to stirred-tank and bubble column bioreactors (Figures 8.11 and 8.12). The data have been collected using EngineeringVillage2 (EV2), which allows access to several engineering-related databases and services. The search terms used in EV2 are shown in the legends of Figures 8.11 and 8.12. A moving 3-year average was used to smooth the data. This simple search reveals some interesting trends. An equal amount of research is performed in stirred-tank bioreactors and bubble columns, and it is currently preferred to airlift bioreactors. One reason for this is that many experiences from bubble columns are ported to airlift bioreactors. The result has been that the research depth for stirred-tank bioreactors and bubble column bioreactors is great, but specific studies concentrating on airlift bioreactor behavior has waned. Also, there is more mass transfer research performed in bubble

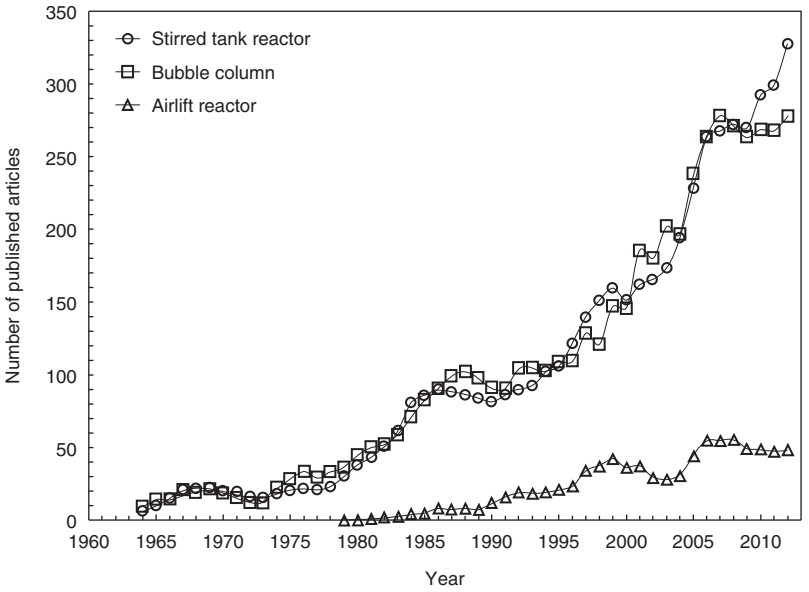

Figure 8.11 General research papers available in the public domain for different bioreactor types. Acquired 07/01/2013.

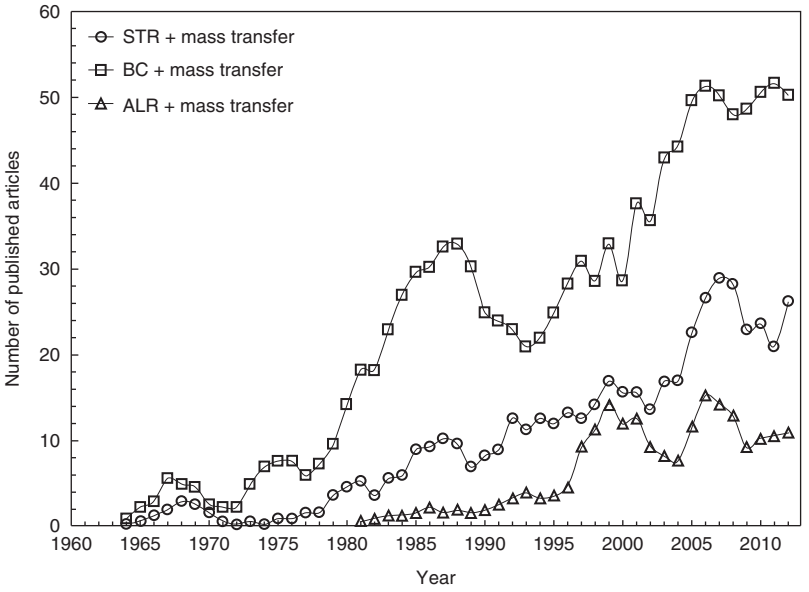

Figure 8.12 Research papers available in the public domain specific to mass transfer for different bioreactor types. Acquired 07/01/2013.

columns than in stirred-tank reactors, which is larger than ALRs. One possible explanation is that gas–liquid mass transfer operations have more applications in bubble columns than in stirred-tank reactors.

A great deal of enthusiasm surrounded airlift bioreactors stemming from the increased attention that the bioreactor had received since the mid-1990s. The progression seemed quite natural. Research in stirred-tank bioreactors had made that bioreactor's shortcomings were obvious and the advent of the bubble column was a natural transition. As research into the bubble column matured, some of its issues also came to light, and the solution, the airlift bioreactor, was seen as the next stage. It may also be concluded that the number of papers related to airlift bioreactors has been suppressed because research in bubble columns has been successfully ported to the airlift bioreactor even though major flow differences exist.

A secondary force in airlift bioreactor research development has been bioreactor design procedure. The question is not which microorganism fits the bioreactor, but which bioreactor fits the microorganism. So, the natural starting point for process research and development is to start with the microorganism and its metabolic production and then select the necessary hardware. Hence, research has become more inclusive of process engineering and biological processes (Zhong, 2010), which can spread resources thin.

One of the potential outcomes is for airlift bioreactor research to slow down for two main reasons. First, bioreactor research seems to be more mature than its biological counterpart. The rate of return on improvements in the metabolic

performance of microorganisms should be higher than the rate of return on bioreactor mass transfer improvements. Second, the continued and successful application of bubble column data to airlift bioreactors should continue to incentivize bubble column researchers to practically undercut new airlift bioreactor research entrants. It is currently easier to make the case that research money serves a multipurpose when applied to bubble columns, whereas research funds on airlift bioreactors offer more specific applications.

That is not to say that airlift bioreactor research is doomed, but bioprocessing could use more specific attention. Research efforts in airlift bioreactors need to go in a direction where they would enable new processes, such as mammalian tissue growth, or incorporate the biological element of bioreactors to a larger degree. For example, current effects of variable local conditions on cellular biochemistry are not understood. As such, cells could be grown to mimic the macroscopic behavior of the desired cells, but still miss the molecular, cellular, and biochemical interactions necessary to mimic the operations of the target cells. Research where bubble column bioreactor similarities break down, such as incorporating a solid phase, are scarce and could also be successful.

Proper start-up procedures, such as initial cell density and distribution, and tracking important or toxic by-products are also troublesome (Martin and Vermette, 2005). Fiber suspensions have not been widely applied in airlift bioreactors, but their application would be of interest for suspended cell growth and density propagation. The incorporation of microorganisms in hydrodynamic studies have not been widely attempted even though microorganisms are known to increase the gas–liquid mass transfer coefficient due to a higher rate of oxygen consumption (Garcia-Ochoa and Gomez, 2009), especially at and near the surface.

More focus on consistent variable testing is needed. Oftentimes, multiple variables are adjusted while the analysis is focused on just one. The conclusions are based on one variable, and the changes in the others are ignored. Particle size comparisons are often done based on scale. One group is often referred to as large with a diameter on the millimeter scale, while the small particles are defined by a diameter less than 1 mm. In addition, these particles are often constructed of differing materials, such that a density variance is introduced, or are used in different concentrations. These facts make hydrodynamic and gas–liquid mass transfer conclusions highly variable in the literature.

This mistake may be made for scale comparison studies as well. Blazej et al. (2004c), for example, compared vessels with volumes of 10.5, 32, and 200 l. The 10.5 and 32 l versions can be classified as experimental scale, while the 200 l ALR may be considered pilot scale (Garcia-Ochoa and Gomez, 2009). Hence, the results, shown in Figure 8.13, could be very helpful for scale-up. Each vessel, however, was geometrically different with varying downcomer-to-riser area and aspect ratio and bottom clearance. Although the differences were not great and comply with the scale-up procedure of Garcia-Ochoa and Gomez (2009), it introduces an additional dilemma. Which effects are related to the scale and which to the downcomer-to-riser area ratio, or is the difference even significant? If a control

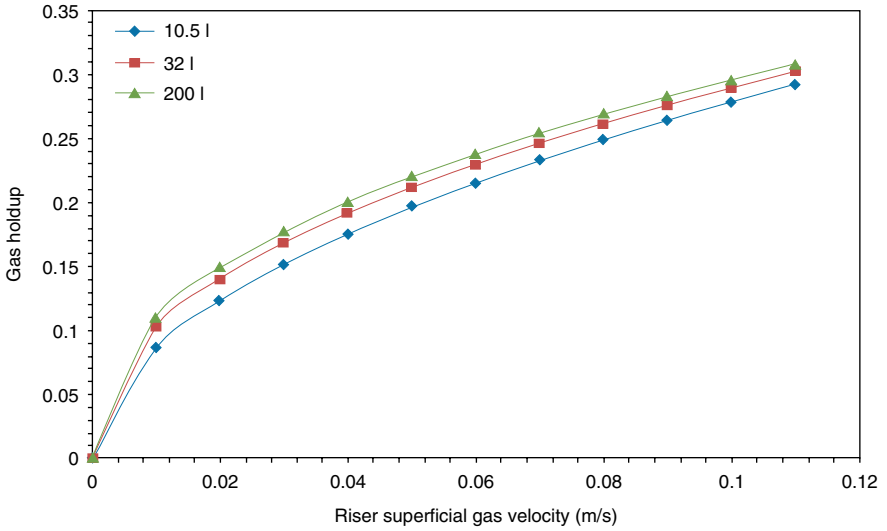

Figure 8.13 Airlift bioreactor scale effects. Adapted from Blazej et al. (2004c).

study with constant ratios is not done, these questions are much harder to answer and conclusions are based on the experimenters' interpretation and inference.

8.7 SUMMARY

Bubble column bioreactors are the main competitor to airlift bioreactors, and deployment decisions are usually based on a competitive basis that excludes the stirred-tank bioreactor. Hence, studies rarely compare the stirred-tank bioreactor, bubble column, and airlift bioreactor in a more comprehensive manner. Usual comparisons are made either between the stirred-tank bioreactor and the bubble column or between the bubble column and the airlift bioreactor. The first stage in identifying a bioreactor usually involves a comparison between the stirred-tank bioreactor and bubble column bioreactor, which clarifies the bioreactor and process requirements. If the bubble column is found to be competitive, the airlift bioreactor is introduced to the discussion.

The airlift bioreactor is often used in cases for which the bubble column lacks the operational flexibility or requirements. In other words, the stirred-tank bioreactor does not have the necessary features, and the bubble column has traits that could have negative effects on the production process. These negative traits often include extensive phase backmixing, undefined flow paths, limited gas flow rates, and potentially damaging shear rates. The airlift bioreactor can successfully address these issues and can provide further control, such as a downcomer sparger, and access to major bioreactor components.

The negative aspect of airlift bioreactors is that research is in its early stages in many respects. A basic hydrodynamic understanding is lacking. For example,

the onset of liquid circulation has been reported to vary between $U_{Gr} = 0.035 - 0.050\,m/s$. It is occasionally reported to coincide with the introduction of the heterogeneous flow regime while the homogeneous flow regime is prevalent in other cases of circulation onset.

Bubble–bubble contacts are regulated by the same forces and interactions as those found in bubble columns, which would imply that the basic behavior should be very similar to bubble columns. This assumption is often invoked, and bubble column research is used in these cases to set expectations and explain outcomes; however, many assumptions have not been tested. The fact that bubble collisions do not occur as frequently in the airlift bioreactor as in the bubble column leads to the conclusion that certain aspects of the bubble column may not be applied to airlift hydrodynamics as easily or at all.

These issues, positive and negative, are reflected in the available correlations. These correlations are both highly useful and also limited. Some are useful because the inputs are easily measured and adjusted as needed; however, correlations are mostly empirical or semi-empirical, which means that they are not widely applicable but, rather, are bioreactor design dependent at best. Hence, geometric similarity is very important. Furthermore, most studies are performed in air–water systems while most industrial processes use much more complicated and time-variant liquids. In other words, the airlift bioreactor correlations have similar problems as those for stirred-tank bioreactors and bubble columns and are due to the fact that they share the "problem" source: bubble–bubble interactions. Bubble–bubble interactions are highly variable and lead to hydrodynamics which, in turn, are difficult to quantify and predict. Hence, the result has been that the airlift bioreactor correlations and models are either system dependent or not adequately constrained.

9 Fixed Bed Bioreactors

9.1 INTRODUCTION

Fixed bed reactors are three-phase systems for which the solid phase is structurally fixed. There are two basic categories of fixed bed reactors that are defined by the phase flow directions. The first class is the packed bed reactors (PBRs), schematically represented in Figure 9.1. PBRs are defined by countercurrent phase flow, which can lead to reactor stability and safety issues during exothermic reactions (Yakhnin and Menzinger, 2008). The liquid phase is sprayed from the top while the gas phase is fed from the bottom. The second class is trickle bed reactors (TBRs), shown in Figure 9.2, which have very similar designs, but each component is adjusted to conform to particular phase flow patterns. TBRs are defined by cocurrent, downward phase flow—the liquid and gas phases are fed from the top (Maiti and Nigam, 2007; Medeiros et al., 2001). The gas phase is pressurized to improve process efficiency. If the flow of the gas and liquid phases occurs upward, the reactor is referred to as flooded bed reactor (FBR). Although the differences may seem minor, the dynamics can be very different. For example, FBRs operate with the packed material being almost or completely submerged while the TBR is usually operated with minimal flooding (Al-Dahhan et al., 1997; Kolev, 2006).

FBRs ensure that the entire packing surface is wetted, which is highly important for liquid-phase limited processes and reactions; however, most biological applications are limited to gas phase, which would make the FBR less useful in its current state (as used by the chemical industry). This reactor design could be useful for biological applications if the microorganisms require significant substrate flow or are sensitive to gas–liquid interfaces; however, FBRs are typically not used in industry because they are difficult to design and manage (Maiti and Nigam, 2007).

The exact reactor choice is highly dependent on the type of reaction required by the process. Since biological applications are not very fast, the choice is going to be more dependent on the microorganism's environmental requirements. For biological applications, fixed bed reactors have traditionally been used for shear-sensitive microbes and cells (especially mammalian). In contrast, shear-resistive strains would be expected to experience better results in a bubble column or airlift reactor since these devices operate at much higher gas and liquid flow rates.

An Introduction to Bioreactor Hydrodynamics and Gas-Liquid Mass Transfer, First Edition.
Enes Kadic and Theodore J. Heindel.

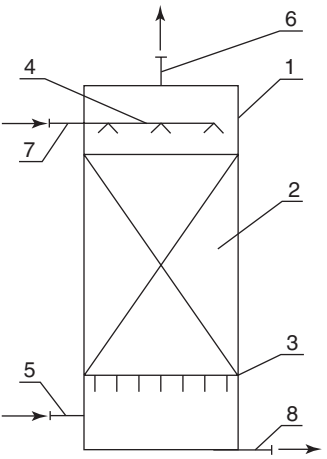

Figure 9.1 Packed bed reactor internals: (1) vessel, (2) packed material, (3) support plate, (4) liquid distributor, (5) gas input, (6) gas output, (7) liquid input, and (8) liquid output (Kolev, 2006).

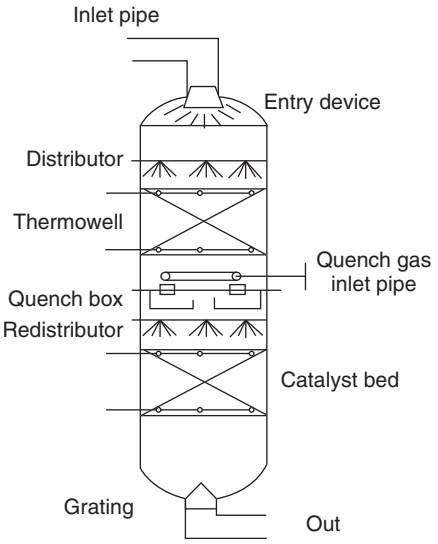

Figure 9.2 Trickle bed reactor schematic (Maiti and Nigam, 2007).

Fixed bed reactors, especially TBRs, are heavily used in industrial practice. They are used by the petroleum, petrochemical, and chemical industries for waste treatment and processing, biochemical and electrochemical processes, and hydrotreatment. Catalysts provide a mechanism to accelerate and channel very complex processes, which would normally require high pressures and/or

temperatures and long processing times, into a more manageable reaction and reactor environment. The fixed bed reactor is the perfect reactor of choice to achieve these goals such that the TBR has been used to process approximately 1.6 billion metric tons of products by the petroleum industry in 1991 alone (Al-Dahhan et al., 1997). Hence, large amounts of research and development have gone, and will continue to go, into these reactors because even marginal improvements can yield significant profitability increases.

The negative aspects of fixed bed reactors are often tied to the performance, behavior of the particular catalyst, and potentially difficult design and scale-up (Nacef et al., 2007). If the catalyst is deactivated or spent fairly quickly, construction of the fixed bed reactors makes the processes impractical. The catalyst would have to be replaced too frequently, leading to high labor and packing costs. One of the main objectives is to ensure that the packing material experiences optimal wetting. Catalysts that do not wet provide inefficient reaction sites. Hence, the flow has to stay within an acceptable pattern. Flow channeling is quite problematic since it can cause inactive catalyst and performance and economic losses (Doan et al., 2008; Maiti and Nigam, 2007). On the extreme, flow channeling can lead to runaway reactions and potentially to combustion/explosion (Al-Dahhan et al., 1997).

A related issue is that identifying flow problems or catalyst utilization is often hard to accomplish in an industrial setting. There are two basic approaches. The first involves measuring pressure drop and/or temperature differentials in the reactor; however, this technique is useful only if flow channeling is significant to cause variations, and it often does not account for wetting problems. The second is to visually inspect the catalyst, but this is often done once the catalyst is spent, which can take up to 2–3 years (Maiti and Nigam, 2007). After the inspection and determination of catalyst inactivity, a plan is made to correct the flow, but the soundness of those corrections cannot be determined until the next inspection, which may be in another 2–3 years. There are other methods to investigate liquid maldistribution, but these can often be complicated or expensive (see, e.g., Llamas et al. (2008)).

Each reactor type has specific operational parameters. TBRs are usually operated adiabatically at high pressure (20–30 MPa) and temperature and employ $U_G < 30$ cm/s and $U_L < 1$ cm/s (Al-Dahhan et al., 1997; Attou et al., 1999; Nigam and Larachi, 2005) although research work is often conducted at atmospheric pressures (Attou et al., 1999). PBRs use similar phase velocity ranges, but those can be increased up to $U_G < 3.5$ m/s and $U_L \sim 0.11$ m/s for some special reactor configurations (Kolev, 2006). Biological operation, however, may call for much lower velocities. If the fixed bed reactor is used as a biofilter, $U_G < 0.001$ m/s and $U_L < 0.005$ m/s are common (Maldonado et al., 2008).

9.2 COLUMN GEOMETRY AND COMPONENTS

The PBRs and TBRs have very similar construction. Both devices are made of a cylindrical vessel, but the internal construction varies greatly between the designs, engineering firm, or even application. The basic components consist of a support

mechanism for the packed material and phase distributors and extractors. The major difference for TBRs is that they tend to use packaged gas–liquid distributors rather than separate units. Other parts are basically the same although the FBR has a different collection system.

The PBRs consist of support plates, hold-down plates, liquid (re)distributors, gas or vapor distributors, gas deflection plates, and screen mesh. The identity and type of the particular parts are dependent largely on reactor scale. The gas deflection plates and screen mesh are used in a cross-flow cascade packed column, which is only useful for chemical processes. The support plates are primarily for structural integrity. They simply hold the packed material in place and allow the gas and liquid to pass through. Since the PBR is sectioned into multiple stages in industrial applications, as shown in Figure 9.1, the support plates also have to prevent phase maldistribution, which is usually accomplished with proper plate leveling. Uneven packing and loading may cause support plate bending and flow maldistribution (Kolev, 2006; Maiti and Nigam, 2007). As with aerated plates in bubble columns, the uniform liquid distribution objective is important, difficult, and often not completely achieved.

The design direction often involves using the lightest and least obstructive support plates in order to achieve packed material and flow stability. Since the PBRs are mainly used by the chemical industry, fouling and erosion are important side effects of the reactants. Hence, the chemical industry requires ready access to the packed material and support plates that are easily removed and changed. This requirement would most likely be necessary for biological applications as well. The support plate is usually fastened to a supporting ring, which is welded to the vessel, due to possible pressure surges, which could potentially lift the support plate and the supported packing.

Support plates are classified according to the type of packing (random or structured) used in the reactor. Support plates used for random packing have inclined walls to support free solid particles and ensure that these stay static. Some examples include the SP 1 (Figure 9.3), 2, and 3 multibeam support plates. The SP 1 is used for packed bed columns with a diameter larger than 1200 mm while the SP 2 and 3 (Figure 9.4) are used for diameters of 100–300 mm and 300–1200 mm, respectively.

The column diameter and geometry of the support plates also impose a minimum packing size. The support plate height is dependent on material construction. For example, carbon and stainless steel call for a height of 265 mm while thermoplastic support plates have a height of 300 mm. Owing to material properties, larger columns (with larger amounts of supported packing) require further strengthening of the support plates.

The downside of these multibeam support plates is that they are plagued by fouling and uncontrolled biological growth, which can lead to improper flow distribution and inefficient reactor operation. Hence, biological processes might find it more advantageous to use a more open support plate such as the hexa-grid (SP-HG) or cross-flow-grid (SP-CF) support plate; however, these plates are usually flat and

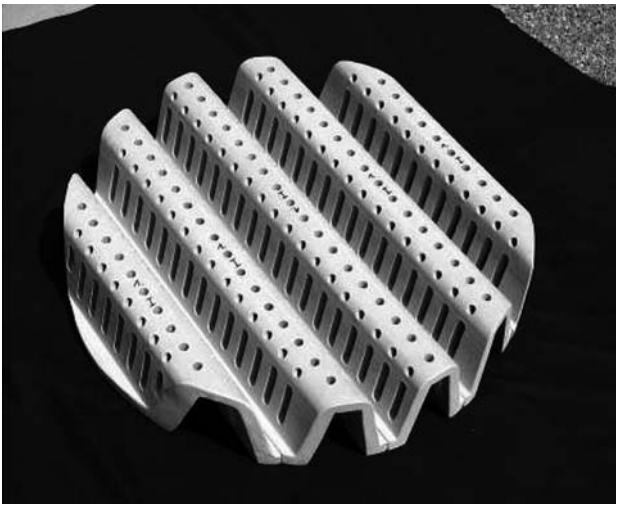

Figure 9.3 SP 1 multibeam support plate used for columns with $D_R > 1200$ mm (Raschig Jaeger Technologies, 2006).

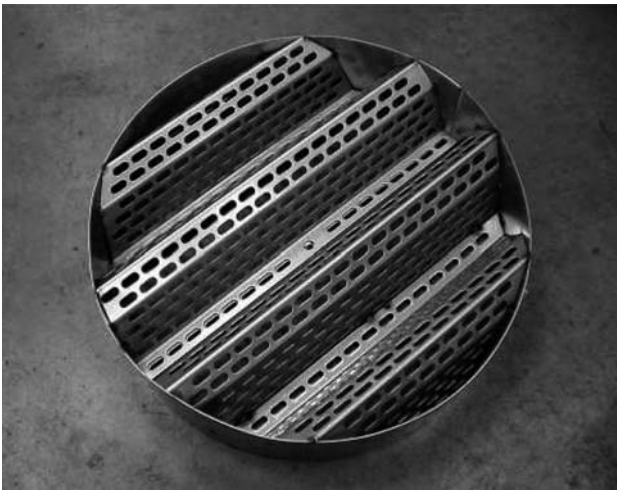

Figure 9.4 SP 2 and 3 multibeam support plates used for $100 < D_R < 300$ mm and $300 < D_R < 1200$ mm, respectively (Raschig Jaeger Technologies, 2006).

are more applicable to structured packings. The SP-HG, shown Figure 9.5, is preferred for mass transfer processes while the SP-CF, as shown in Figure 9.6, ensures a more uniform gas distribution. Other possibilities include the flat bar plate (exclusively for structured packing), vapor distributing packing (used to reduce vapor velocity), or ceramic packing (used for corrosive processes) support plates.

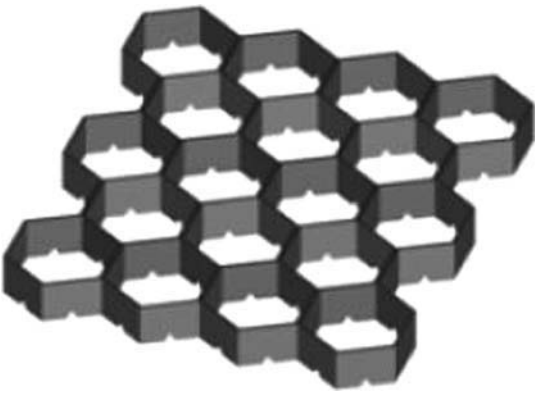

Figure 9.5 SP-HG support plate (Raschig Jaeger Technologies, 2006).

Figure 9.6 SP-CF support plate (Raschig Jaeger Technologies, 2006).

Hold-down plates are used to secure packing in case of flooding or pressure surges. In these situations, it is possible that the packing would wash away and enter the output stream. The standard hold-down plate (HP-1) is constructed from a frame with a metal screen. This hold-down plate is not meant to interfere with the liquid flow, but is also not designed to stabilize the packed material. Hence, more fragile packing, such as ceramics or carbon steel, cannot use the HP-1 plate without a breakage or grinding risk. As such, fragile packing should use the HP-2 hold-down plates, which has a grid-like structure that inhibits packing movement. Structured packing typically utilize hold-down plates (HP-P), which are bolted to the vessel and are designed to prevent movement within the bed or packing washout. An example of the hold-down plate is the grid-like Raschig grid (RG) or HP-1, shown in Figure 9.7. Plates are generally intended for larger vessels ($D_R > 3000\,\text{mm}$), but can also be designed for and installed in smaller vessels ($D_R = 500 - 3000\,\text{mm}$).

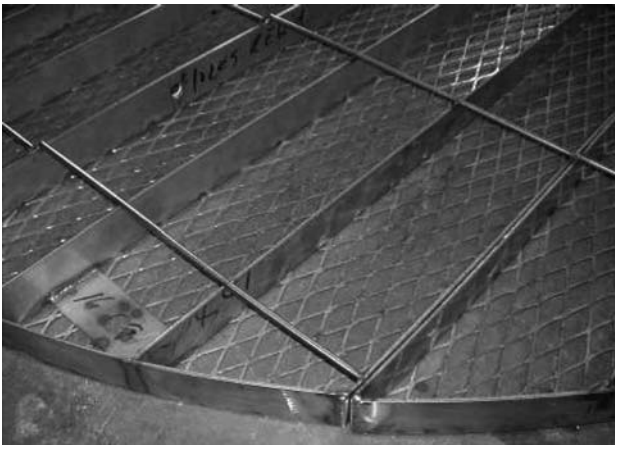

Figure 9.7 HP-1 hold-down plate (Raschig Jaeger Technologies, 2006).

Since packed bed columns are mainly designed for the chemical industry, a lot of attention is paid to liquid-phase distribution, because the liquid distributor design is crucial while gas-phase distribution gets less attention. If the liquid distribution operates or performs poorly, the packing is not going to be wetted effectively, which is important for soluble gases. Nonwetted packing leads to reactor underperformance (Maiti and Nigam, 2007). Although biological systems would also need significant attention, these processes could mostly do with simpler options.

There are two basic options for liquid distribution: single stream and spray distributors. Single stream distributors basically feed the liquid phase through a perforated pipe to channels, which, in turn, distribute the liquid over the cross-sectional area of the reactor, which is shown in Figure 9.8. Some examples of these are the shower-type (perforated) distributor, trough distributor, distributor with weirs, bottom-hole distributor, splash-plate distributor, channel-type distributor, distributor with gas risers, or liquid pipe distributors. Spray distributors are used for processes requiring large amounts of liquid surface, gas cooling, or homogeneous liquid distribution. Since the droplets are smaller, the spray distributors are also better at wetting particles, which produces more efficient packing operation.

Liquid distributors are often used to correct liquid flow to a more uniform pattern and/or to add more liquid to the reactor. Liquid distributors are also often used to redistribute the liquid phase as well, but a simpler option, shown in Figure 9.9, would be a perforated plate with directional facing. Liquid collectors are used to channel the liquid into the liquid outlet in order to prevent converted/used liquid to stay in the column bottom. The hardest portion of designing a collector is to not interfere with gas distribution, and the available designs are quite wide and diverse. TBRs, on the other hand, tend to use liquid collectors, which are only used for collecting and extracting liquid.

Figure 9.8 Example of liquid distributor (Raschig Jaeger Technologies, 2006).

Figure 9.9 Example of a liquid distributor (Raschig Jaeger Technologies, 2006).

Gas distributors are also an important component of packed bed columns and influence phase distribution. The design issue is to ensure a uniform gas flow distribution through the reactor or a necessary gas flow ratio relative to the liquid phase. The liquid–gas ratio is only important if the process requires a chemical reaction of the liquid phase induced by the gas phase. The packing, on the other hand, is responsible for the pressure drop profile and, hence, the downstream gas-phase distribution.

The simplest gas distributor is a perforated pipe. Since the pipe creates a significant amount of flow irregularity in the distributor region, the packed material is usually placed a distance away from the gas inlet to ensure the gas flow becomes more uniformly distributed upon entering the packed region. The separation distance is

dependent on the column diameter such that a column of 1 m requires a distance of about 0.4 m. Columns with $D_R = 1 - 2$ m require a separation distance of 0.7 m while larger columns should have a distance of about 1 m (Kolev, 2006). An actual rule, which is often linear, can be developed to quantify a column diameter to separation distance ratio, but this rule would be dependent on the level of turbulence. This turbulence can be represented by a ratio of inlet to column gas velocity.

Other gas distributor options include more complicated systems such as a guided vane gas distributor, which attempts to create a more uniform gas distribution through higher turbulence, or a liquid collector–gas distributor combination; this design is more appropriate for high pressure reactors, especially if multiple packed beds are necessary. For example, the process may require the product to be extracted and more liquid/gas phase to be input into the reactor. Hence, such a device would be necessary. TBRs share this basic design with PBRs and make more extensive use of combination devices. Examples of combination distributors for the TBRs include perforated plate (Figure 9.10), chimney tray, bubble cap tray, and vapor-assist lift distributors.

A simple choice is the perforated plate while the chimney is useful if vapors are present. If the perforated plate is used and flow uniformity is desired, the number of drip points should be as large and as close together as possible. The problem with most perforated devices is that coking or accumulation of other materials may clog the holes and lead to the initial liquid flow maldistribution. Then the perforated plate requires a certain minimal liquid loading. If the minimal liquid amount is not present, some perforations will stay dry and once again lead to initial liquid maldistribution. The perforated plate cannot be designed for some minimal and universally used value because the pressure drop at nominal operation has to be minimized. Hence, the plate is usually designed for a normal state of operation while off-design conditions may cause operational problems. A quick summary of available devices for TBRs is presented in Table 9.1 (Maiti and Nigam, 2007).

The negative aspects and age of perforated plate distributors have led to improvements over the years. A historical performance summary is presented in Figure 9.11. The chimney-type distributors attempt to improve gas–liquid contacting and prevent clogging issues. The liquid is injected as jets while the air

TABLE 9.1 Distributor Comparison

Type	Spacing Density	Level Sensitivity	Liquid Rangeability	Vapor–Liquid Flexibility	Liquid–Vapor Mixing
Perforated plate	Best	Worst	Worst	Worst	Worst
Chimney	Average	Poor	Poor	Poor	Poor
Multiport chimney	Average	Average	Average	Average	Poor
Bubble cap	Worst	Average	Good	Good	Best
Gas-lift assisted	Best	Best	Best	Best	Best

Adapted from Maiti and Nigam (2007).

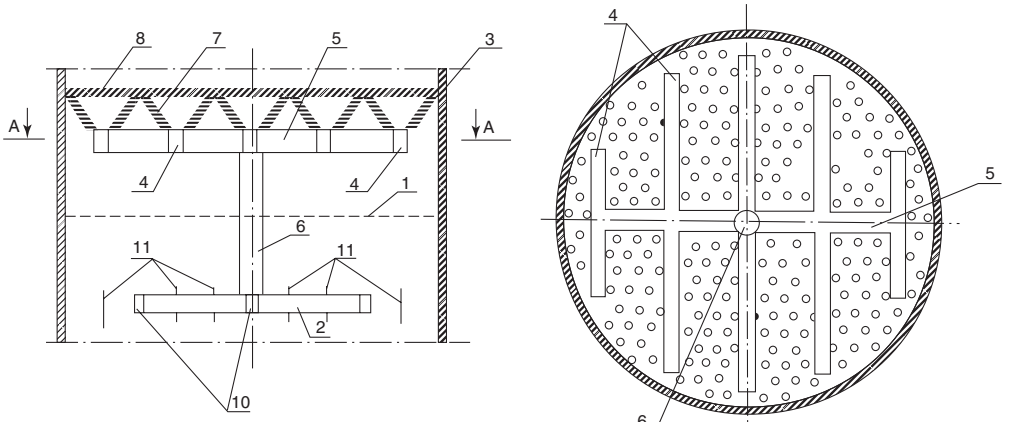

1- perforated plate, 2- liquid distributor, 3- column wall, 4- overflow troughs,
5- collection trough, 6- Join pipe, 7- V separator, 8- separating plate,
9- main distribution trough, 10- distribution trough, 11- reflecting plates.

Figure 9.10 Example of a combination of liquid collector and gas distributor system (Kolev, 2006).

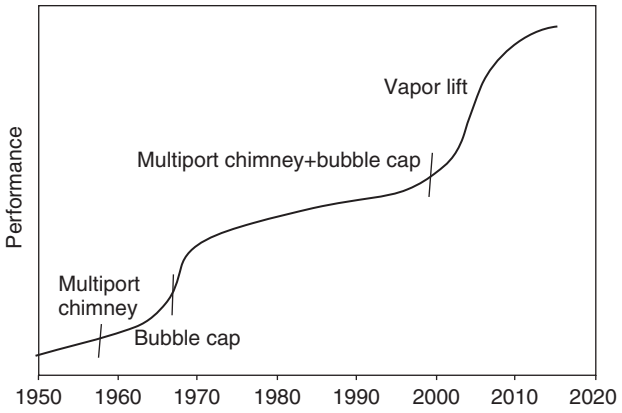

Figure 9.11 Historical distributor performance changes (Maiti and Nigam, 2007).

is used to break up the liquid into smaller droplets. Unfortunately, chimney-type distributors are highly sensitive to the liquid level and have a limited number of liquid entry points. Bubble caps are distributors that do not use the liquid hydraulic head to perform liquid distribution duties. Bubble caps, in turn, use the gas flow to distribute the liquid. Therefore, the bubble cap trays allow much wider liquid flow rates, but the design requires a larger diameter, which leads to even fewer drip points than the chimney-type distributors. Vapor-lift tubes, as the name implies, use the gas phase to push the liquid from an established level through a U-tube and distribute droplets onto the packing. The biggest advantages of the vapor-lift tubes are that they are smaller, simpler, and cheaper to construct; provide more wall coverage; and increase wetting efficiency. Hence, vapor-lift tubes are expected to become dominant for chemical processes, but a perforated plate might be good enough for biological applications. Graphical examples of combination devices for TBRs are shown in Figure 9.12 (Maiti and Nigam, 2007).

9.3 FLOW REGIME

PBRs and TBRs, respectively, share some basic flow characteristics, but major differences exist, which lead to differing reactor performance and application. At very low superficial gas velocity, the superficial liquid velocity has a significant impact on the relative gas velocity for both PBR and TBR operations. Furthermore, liquid holdup is solely a function of the superficial liquid velocity (Alix and Raynal, 2008). Under PBR operation, increasing the superficial liquid velocity causes an increase in the relative gas velocity. This effect, in turn, increases the pressure drop of wetted to dry packing. TBR operation, on the other hand, leads to the opposite effect.

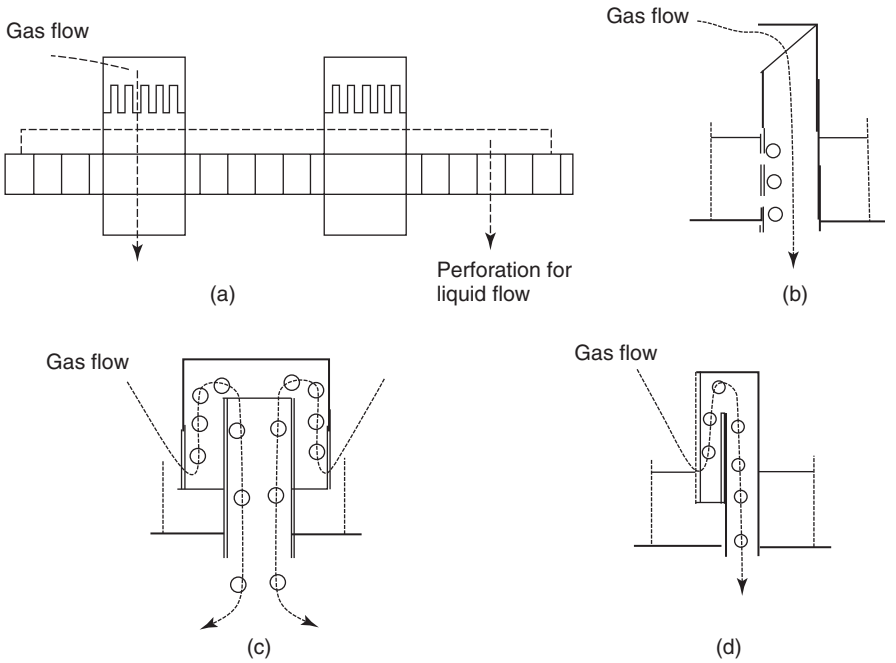

Figure 9.12 Examples of (a) perforated plate, (b) chimney, (c) bubble cap, and (d) vapor-lift tube used in TBRs (Maiti and Nigam, 2007).

By increasing the superficial gas velocity in PBRs, a critical superficial gas velocity is reached at which the friction between the gas and liquid phases leads to an increase in liquid holdup. This critical point also represents the inflection shown in Figure 9.13 and is caused by the emerging and powerful influence of the superficial gas velocity on the liquid holdup. This point is referred to as the loading point.

As the superficial gas velocity is increased, the liquid holdup increases as well until another critical point, the flooding point, is reached. At the flooding point, the slope of the pressure drop versus superficial gas velocity line becomes exponential. The drag force of the gas phase becomes the dominating influence on the pressure drop (Kolev, 2006; Stichlmair et al., 1989). The effect of the loading and flooding points and the transition on the pressure drop and slope can be seen in Figure 9.14. The identification of these boundaries allow for optimal operation, which is observed between the loading and flooding points for most industrial processes, such that mass transfer is maximized while operating costs are minimized.

The operating range between the loading and flooding points is referred to as the loaded regime. The loaded regime is important for mass transfer purposes. One way to judge mass transfer efficiency in fixed bed reactors is with the height equivalent to a theoretical plate (HETP). A theoretical plate is an abstract stage in which two phases are capable of establishing an equilibrium. Thus, having an actual height that

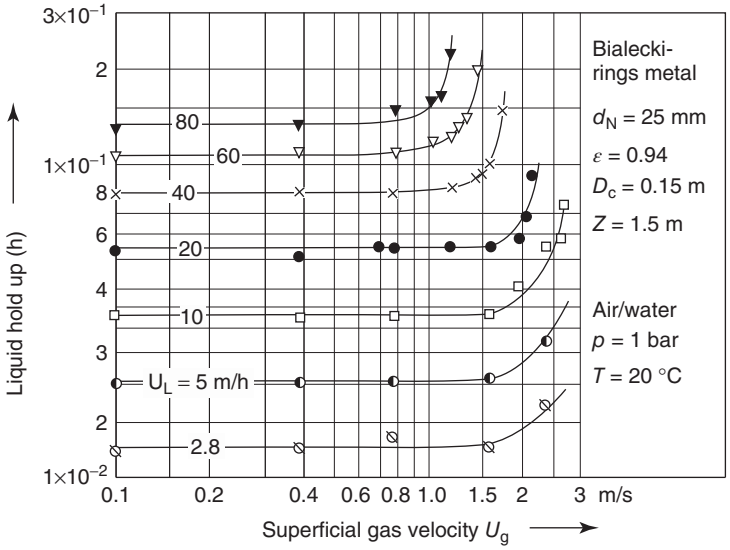

Figure 9.13 Representation of the loading point in packed bed columns (Stichlmair et al., 1989).

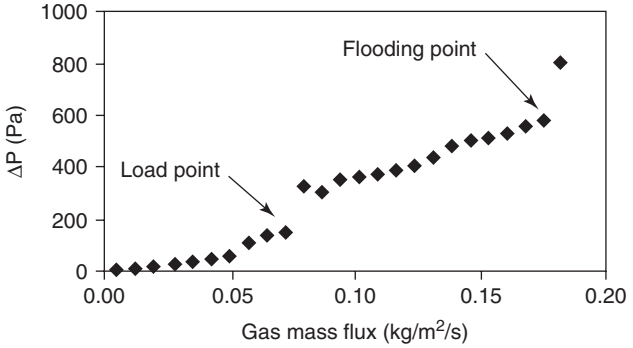

Figure 9.14 Example illustrating loading and flooding points (Breijer et al., 2008).

is lower at the same superficial gas velocity implies a more efficient mass transfer process. In the same line of reasoning, having the same equivalent height with a higher superficial gas velocity implies that more mass has been transferred, and the reaction occurs under more optimal circumstances.

Figure 9.15 represents the effect of increasing the liquid rate in direct proportion with the vapor (gas) rate. The important markers are points C, E, G, and F. Point A illustrates a minimal liquid loading or a minimal liquid and vapor rate at which the column converts the feed. If the vapor rate is lower than the critical value at point A, the HETP increases such that a practical column is not operable. Points C and F

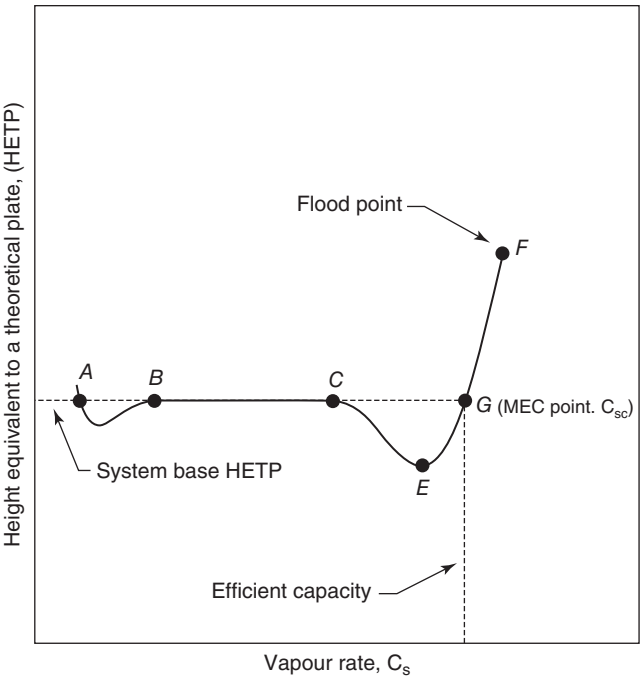

Figure 9.15 Packed bed reactor operating regimes (Kolev, 2006).

represent the loading and flooding points, respectively. The region between points B and C defines the constant separation efficiency region, where the interaction between the liquid and vapor is weak. Point E represents the minimal HETP, which would yield the operating condition for the shortest and smallest reactor; however, a more efficient point can be obtained at point G, which represents the maximal efficiency capacity (MCE). The MCE provides the most stable operations while also maximizing the mass transfer potential. Increasing the vapor rate beyond point G yields an inefficient result such that the column requires larger and larger scale in order to achieve the same result (Kolev, 2006)—not something designers and operators look for.

Another way to define the flow in PBRs is using the Reynolds number, which is defined by the packing diameter and superficial (gas) velocity. Creeping flow is observed at Reynolds numbers <1. This region is defined by a linear pressure drop with increasing interstitial velocity. A steady laminar inertial flow is observed within a Reynolds range of 10–150 where the pressure drop develops a nonlinear relationship with interstitial velocity. An unsteady laminar inertial flow develops at Reynolds numbers of 150–300; this region is defined by laminar wake oscillations in the pores. Furthermore, vortices start developing at a Reynolds number of approximately 250. At Reynolds numbers above 300, the flow becomes unsteady

and resembles turbulent flow. It should be noted that experimental scale vessels experience Reynolds numbers in the creeping and steady laminar inertial flow while industrial scales operate at higher Reynolds numbers (Schuurman, 2008).

In trickle bed operation, the frictional force acts in the flow direction, decreasing the liquid holdup. For TBR operation, the flooding point does not exist in the same sense as in a PBR. Instead, the same critical ("flooding") point in the trickle flow regime is defined by a decreasing slope relative to dry packing (Kolev, 2006; Stichlmair et al., 1989). Hence, the TBR is not affected by flooding or loading conditions and can be applied to wider gas- and liquid-phase flow ranges (Breijer et al., 2008). The trickle flow reactor is only limited by the pressure drop, which causes economic constraints for TBR application. The downside is that the PBR is necessary for equilibrium reactions, which are not easily carried out in a TBR due to the cocurrent nature of the phase flow directions (Al-Dahhan et al., 1997; Kolev, 2006).

The general PBR flow structure is highly dependent on the initial liquid phase flow distribution, liquid velocity, particle shape, particle size, and packing method. The fact that the packing method is influential can be somewhat troubling with random packing because results are harder to replicate once the packing is replaced. On a smaller scale, the flow structure is affected by start-up procedure, wettability, flow modulation, and particle coordination number (number of touching neighbors per particle). The level of the nonuniformity is largely controlled by reactor internals. A properly designed and operated reactor is expected to have uniform flow distribution or at least become stable relatively quickly (Doan et al., 2008; Maiti and Nigam, 2007).

Nonuniform flow has several causes. The first cause is that the initial liquid distribution is not uniform such that the liquid does not enter the packing volume uniformly (shown in Figure 9.16a). If the liquid is not well-distributed and adjustments are not effective or easily implemented, a layer of inert packing particles on top of the reactive packing may lead to some flow improvement. The more common cause is that the packing has not been packed well, damaged, or that its shape makes the flow unstable (shown in Figure 9.16b). The shape may lead to liquid maldistribution in the case that the reactor-to-particle diameter is too small (i.e., the particles are too large relative to the reactor diameter). For example, if the ratio is <20, the liquid starts to show maldistribution near the wall region at higher superficial liquid velocities. Hence, the reactor-to-particle diameter should be at least 20 to ensure proper liquid distribution for nominal liquid velocities (Metaxas and Papayannakos, 2008). If axial dispersion is problematic, a ratio >50 minimizes the influence of axial variations (Schuurman, 2008). It should be noted that liquid flow at the wall requires a bed height-to-diameter ratio of at least 4.0 (Doan et al., 2008). It should be noted that a small reactor-to-particle diameter ratio, or a small bed height-to-diameter ratio, typically results in packing not properly being wetted (shown in Figure 9.16c), and the mistake is often not realized until the packing is replaced, which may not occur for at least 2–3 years (Maiti and Nigam, 2007).

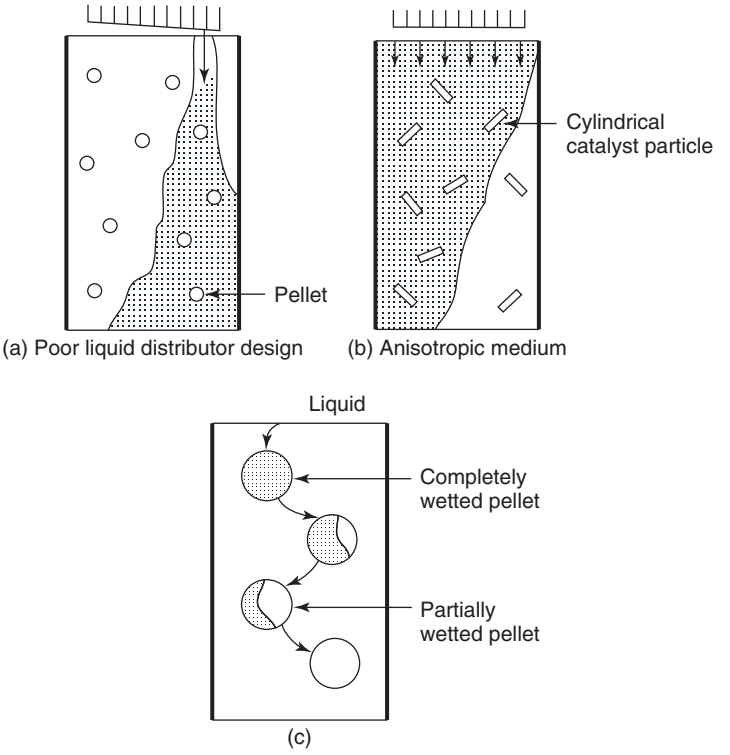

Figure 9.16 (a) Initial liquid maldistribution and (b) restrictive packing leading to (c) different levels of wetted pellets (Maiti and Nigam, 2007).

Packing manufacturers develop and test their packing extensively, but oftentimes do not have the expertise or infrastructure to test packing flow behavior. Engineering firms have the expertise, but are missing the infrastructure and incentives to test packing. Hence, the customer and end-user are expected to experience some trouble that usually requires on-site adjustment (Maiti and Nigam, 2007).

The TBR hydrodynamics are influenced by the operating conditions, reactor design, reactor internals, distributor design, and phase properties (Nacef et al., 2007). There are four basic flow regimes in a TBR. At low superficial liquid and gas velocities, the liquid trickles onto the packing, forming streams and films, while the gas phase flows through the residual voids; this is called the trickle regime. The TBR performance in the trickle regime is dependent on the pressure gradient and liquid saturation. A significant portion of the packing is unwetted in the trickle regime, which is usually minimized by increasing the superficial liquid velocity. The extent of unwetted packing may be used to identify flow nonuniformity and its causes (Liao et al., 2008) since the packing should be completely wetted during the transition from the trickle to pulsing flow regime. The liquid holdup can be

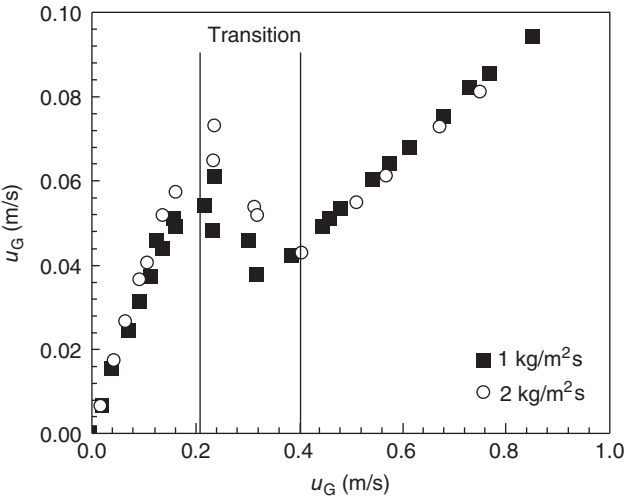

Figure 9.17 Flow regime detection in trickle bed reactors (Nacef et al., 2007).

increased by increasing the liquid flow rate, while increasing the gas flow rate leads to a decrease in the holdup (Burghardt et al., 1995).

At higher superficial liquid velocity, the pulsing regime is formed because the liquid blocks the flow paths and forces alternating liquid- and gas-rich regions in the reactor volume. This is very similar to the slug flow regime in bubble columns. An interesting behavior in the pulsing flow regime is that the liquid holdup is mostly independent of the liquid flow rate although it is still negatively affected by an increase in the gas flow rate (Burghardt et al., 1995). The identification of the pulsing regime is achieved by using the transition between the trickling and pulsing regimes. This transition is defined by a temporary decrease in drift flux (velocity) as the superficial gas velocity is increased, as shown in Figure 9.17. Correlations have been developed that attempt to model the velocity at which the transition may occur; however, these correlations are limited to only a few important parameters (phase velocities, liquid viscosity, particle diameter, and bed height) (Nacef et al., 2007) such that more complicated processes, such as those involving non-Newtonian liquids, are almost impossible to predict.

At high superficial gas and low superficial liquid velocities, a spray regime occurs that is defined by the liquid phase being turned into droplets by the continuous gas phase. At low superficial gas and higher superficial liquid velocities, the dispersed bubble (gas) regime is observed and defined by a continuous liquid phase, which entrains the gas phase as bubbles (Attou et al., 1999). The dispersed bubble is most often used in the TBR, but pulsing regime operation is also common (Burghardt et al., 1995). Biological applications would benefit the most from the dispersed bubble regime while the pulsing regime may cause damage to the microorganisms as well as potential exposure to the gas–liquid interface. A generalized regime map has not been developed because the regime transitions

are dependent on packing material properties such as wettability, size, and shape (Maldonado et al., 2008).

9.4 LIQUID PROPERTIES

Liquid properties influence the behavior of the bubble interface and, consequently, have a strong effect on both the liquid-phase mass transfer coefficient and the interfacial area. Research using organic liquids, which would be very useful for bioreactor and gas–liquid mass transfer optimization, is almost nonexistent for fixed bed reactors.

It should be noted that PBRs operate differently than other gas–liquid reactors covered so far. In the other reactor designs, the gas phase is dispersed in the liquid phase such that bubbles are formed from which the gas phase is transferred to the liquid. The surface area through which the transfer occurs is the interfacial area of the bubbles. In PBRs, general operation yields droplets or liquid films immersed in the gas phase, which causes the main transfer surface to be the droplet–gas or film–gas interface. In order to increase the mass transfer interfacial area, smaller droplets or wavier films have to be produced. This process is often turbulent and may result in liquid breakup and coalescence, which may be destructive to some microorganisms (specifically those that are shear sensitive).

A unique property of fixed bed reactors, in general, is that the wetted particles also become part of the mass transfer interface. This difference is not too important for chemical systems due to the commonly used packing designs, but biological systems may have additional problems. For example, the packing serves as a supporting mechanism for the microorganisms. Hence, the microorganisms feed and breathe through the liquid layer on top of the colonies. If the liquid droplets do not touch or interact in some way with the liquid–microbial interface, mass transfer may not occur. Another design objective has to be added to biological systems, which stipulates that the packing is refreshed with liquid and that the liquid's interaction with the microbial interface is optimized. The liquid properties play a crucial role in this process. The viscosity of the liquid determines the stickiness or the wettability of the packing. The degree to which this property is important is highly variable with the specific microbial needs, and research determining this requirement in fixed bed reactors is nonexistent; however, if trickle- or flooded-bed reactors are used, gas bubbles are the mass transfer mechanisms, and the same bubble behavior and interactions are to be expected as with (three-phase) bubble columns and airlift reactors (Nacef et al., 2007).

Unfortunately for biological applications, the influence of liquid properties is often ignored in fixed bed reactor research. Approximately half the data for fixed bed reactors have been obtained using air–water systems with glass bead packing (Nacef et al., 2007). Hence, a significant problem is apparent. The available data are biased toward a situation that does not occur in industrial settings or biological applications, even if they are for experimental purposes. To make matters worse, experimental phase flow ranges oftentimes differ significantly from industrial practice (Burghardt et al., 1995) such that those results by themselves would have little

meaning for the real-world application. Furthermore, these test systems experience constant properties, such as liquid viscosity or particle density. This state is often not observed in biological systems since microorganisms change the liquid properties and consume or colonize the solid phase. Hence, the effective liquid viscosity and particle density may be unsteady.

9.5 PACKING MATERIAL

Packing is the solid and fixed phase in the reactor volume. It is often used to judge reactor performance and utilization. The wettability or wetting efficiency is the representative parameter of choice and is defined as the ratio of wetted-to-external particle surface area (Metaxas and Papayannakos, 2008). The external area is not equal to the total surface area because the external area excludes the contact areas (Burghardt et al., 1995). The wetting efficiency is a function of phase flow rates, pressure, liquid properties, and packing diameter. In most cases, the wetting efficiency varies between 0.6 and 1.0. The most common approach to measuring wettability is by using tracers and visual inspection. Reaction methods can be used, but are difficult to implement from a theoretical point of view (Nigam and Larachi, 2005). The type of packing generally does not determine wettability directly, but rather influences the liquid distribution, which may lead to non-wetting if flow maldistribution occurs.

As summarized by Nigam and Larachi (2005), wettability may be modeled using saturated pores and solid surfaces. At low wettability, the liquid volume per unit-wetted surface area is large (represented by Figure 9.18a). As the wettability increases and the liquid volume per unit-wetted surface area decreases, the contact angle and the wetting efficiency also increases (Figure 9.18b); however, this is followed by a small contact angle and a decrease in efficiency (transition between Figure 9.18b and c) and then a resumption of the nominal increases (Figure 9.18c). A further increase in wettability causes a steep contact angle and a quick increase in wetting efficiency (transition between Figure 9.18c and d), which is followed again by a contact angle and efficiency decrease (Figure 9.18d). As the wetted pores reach each other, the contact angle becomes stationary and further liquid flattening is not possible such that wetting efficiency is abnormally high (transition between Figure 9.18d and e). If there are any partially solid surfaces left, the liquid film ruptures and a quick decrease in wetting efficiency is observed (Figure 9.18f). The result of higher wetting efficiency is a thinner liquid film, which would also represent a smaller resistive mass transfer force (Liao et al., 2008; Nigam and Larachi, 2005). Hence, porosity has a significant impact on wetting efficiency and hysteresis behavior.

The start-up procedure for fixed bed reactors often involves prewetting the packing in order to limit operational variations. Interestingly, reactors may demonstrate better or worse performance due to a different start-up procedure. In other words, the pressure drop or liquid holdup are not good indicators of flow uniformity, but rather show significant dependence on the start-up and prewetting procedure. The

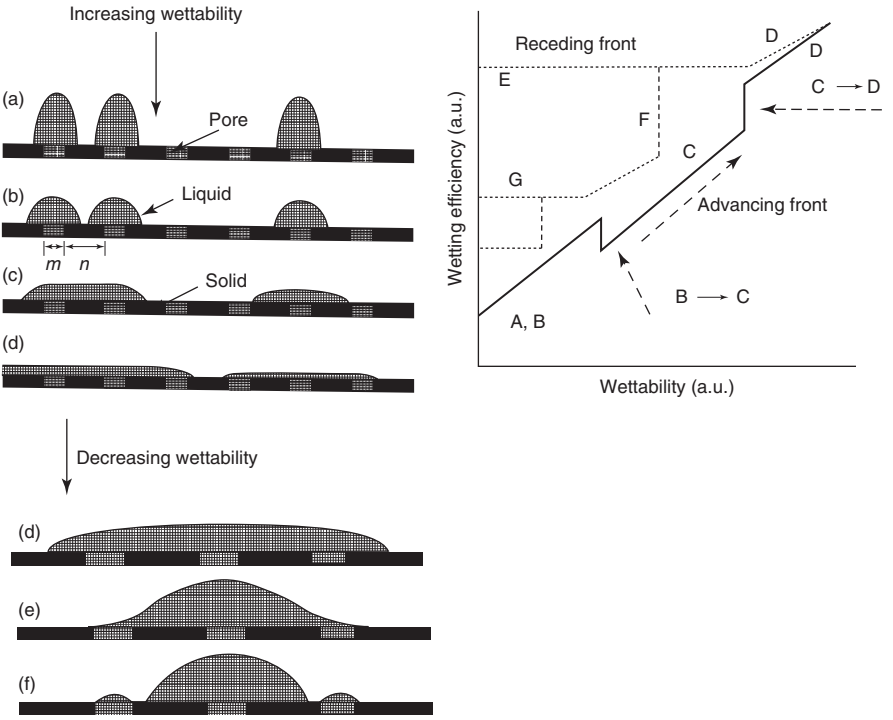

Figure 9.18 Wetting efficiency dependence on the contact angle movement (Nigam and Larachi, 2005).

possible start-up procedures include a dry, Levec, Kan liquid, Super, and Kan gas mode. The dry mode starts the process with the packing dry. The Levec mode prewets the packing for about 20 min by flooding the reactor volume and then allows the liquid to drain out after which the liquid is reintroduced and the process is allowed to start normal operation. The Kan liquid mode prewets the packing by cycling the reactor between the pulsing regime and the operating set point. The Super mode simply floods the reactor volume and then reduces the phase flow rates to the operational set points. The Kan gas mode prewets the packing by operating in the pulsing regime. The pulsing regime is achieved by increasing the gas flow to the critical pulsing point after which the phase flow rates are adjusted to the operational set point (van der Westhuizen et al., 2007). Prewetting has not been studied with biological media so that its influence is currently unknown for this application.

9.5.1 Random Packing

There are two basic types of packing materials: random and structured packings. Random packings are commonly formed from different shapes such as rings, shown in Figure 9.19, or saddles, shown in Figure 9.20. They are constructed out of ceramic, metal, plastics, or coke with the most popular metal application being

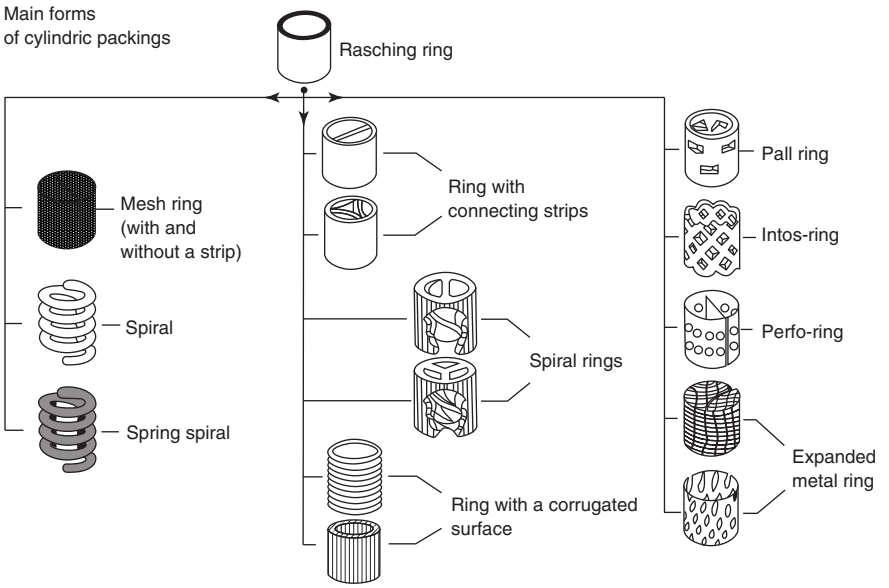

Figure 9.19 Raschig ring packing examples (Reichelt, 1974).

stainless steel. A chemical treatment may be applied to the surface in order to increase the wettability and process efficiency (Kolev, 2006; Strigle, 1994).

The simplest random packings are spherical, but are not used very often in industry. The most commonly used packing are the Raschig rings and its descendants. The historical development of random packing is summarized in Figure 9.21. Each alteration stems from the need to improve packing performance for the particular process. The most common goal is to increase the surface area available for mass transfer and reaction. The great advantage of random packing is the ease with which it can be produced and loaded into the column. Typically, the packing is simply loaded from the top onto the support plate and secured by the hold-down plates. On the other hand, the random and unstructured distribution of the packing also leads to poor phase distribution, possible flow channeling, and higher pressure drop (Kolev, 2006; Strigle, 1994). The pressure drop, on the other hand, may also be an advantage as it leads to a higher level of turbulence and, hence, higher gas–liquid mass transfer efficiency relative to structured packing (Schultes, 2003).

The first and most logical adaptation has been to add dividers, internal spirals, and corrugated surfaces to the Raschig ring. Although these rings effectively increase the area, the pressure losses and gas clogging/slugging can be significant, which may limit the operating range. The second adaptation has been to make the rings out of mesh and spirals. Finally, the rings can be perforated. Interestingly, the pall ring has been determined to fulfill most mass transfer requirements and a better random packing has not been found in the last 30 years; however, other options, such as the Hiflow ring, Ralu-Flow, IMTP, Nutter ring, and Raschig Super Ring,

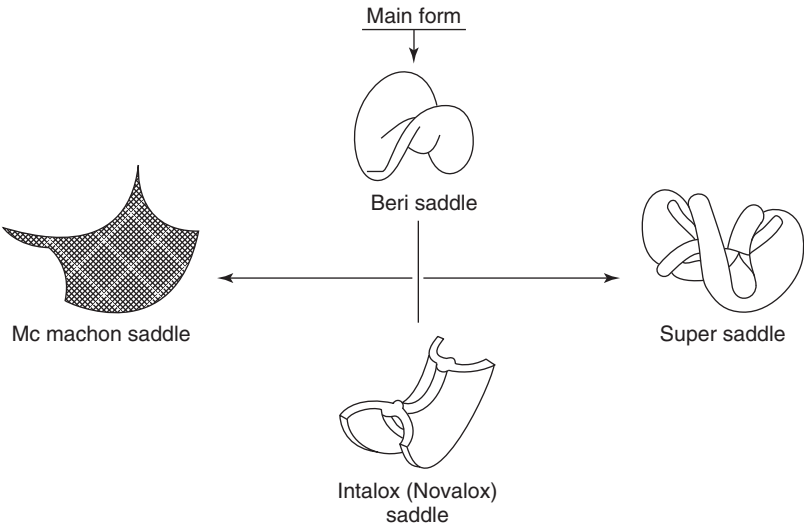

Figure 9.20 Saddle-type packing examples (Reichelt, 1974).

are available and provide satisfactory mass transfer results. Although statistics and performance measures are collected, they are highly dependent on the reactor diameter such that results presented in the literature may vary greatly and be a challenge to reproduce (Kolev, 2006).

The mass transfer requirement stipulates that the patella (connecting strip) cannot be larger than 5 mm in width. If the patella is larger than that, a droplet will form on the surface, which will effectively reduce the wetted surface available for the reaction. If the patella is less than 5 mm in width, the liquid is capable of moving over the surface without accumulating. The result is that the operating range is widened. The downside is that as the width is decreased, the pressure drop increases. This increase may limit the economics of the process.

9.5.2 Structured Packing

Structured packing is constructed to provide optimal phase channeling and uniform phase distribution. Structured packing material is very similar to the random packing and includes metals, ceramics, plastics, and other materials like wood. Structured packing is usually subdivided into smooth-walled packing, packing with turbulizers, expanded metal packing, corrugated metal sheet packing, and packing for very low superficial liquid velocities (Kolev, 2006; Strigle, 1994).

Smooth-walled packing is constructed using vertical walls, which attempts to limit the pressure losses for a given operating condition. As such, they provide the lowest pressure drop per mass transfer unit for a given volumetric mass transfer coefficient. The first generation of structured packing was fixed rings, such as Raschig rings. Although the construction was very simple, a significant problem

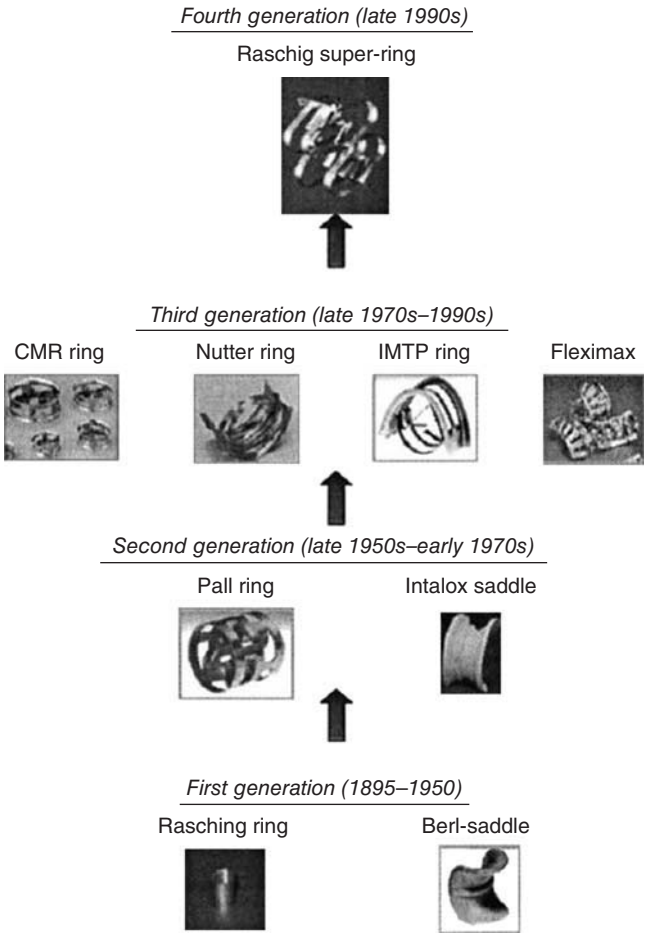

Figure 9.21 Historical random packing development (Schultes, 2003).

became apparent early on. The interior ring channel (labeled 1 in Figure 9.22) is much larger than the exterior ring channel (labeled 2 in Figure 9.22). This discrepancy leads to flow channeling and a dry packing surface. Hence, the natural evolution has been to construct structured packing using similar members and forming them into symmetrical arrangements. Some popular formations are shown in Figure 9.23. Honeycomb has quickly become very popular, largely because they are able to provide a lower pressure drop for a given volumetric mass transfer coefficient. For example, honeycomb packing (Honeycomb No. 1) can provide a pressure drop that was 8.3 times lower than the Raschig rings (Kolev, 2006).

Packing with turbulizers, referred to as Turbo-pack, is made by thermo-pressing or stamping plates such that the packing surface is ribbed, which increases turbulence near the wall. This increased turbulence leads to better heat and mass transfer

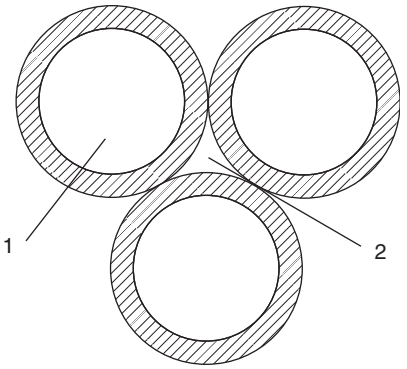

Figure 9.22 Cross section of structured (Raschig) ring packing (Kolev, 2006).

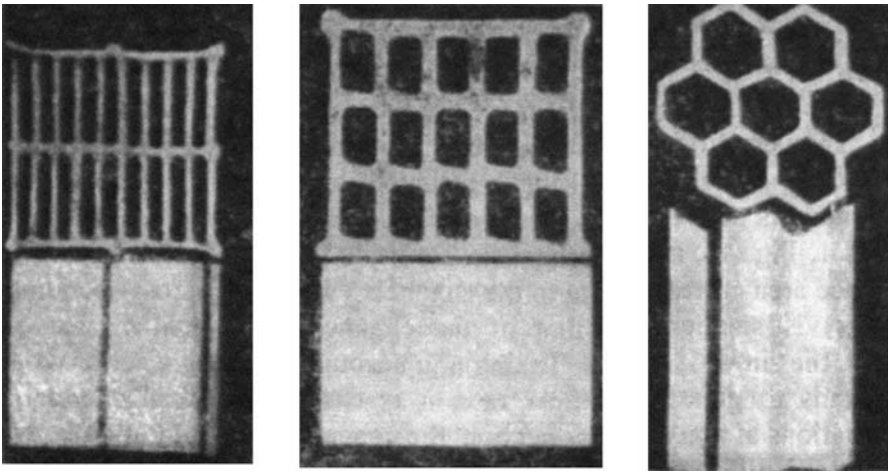

Figure 9.23 Examples of (a) slit block, (b) grid block, and (c) honeycomb block packing structures (Kolev, 2006).

performance. Turbulizers are usually made in the horizontal direction in order to achieve axial flow uniformity. The result of using turbulizers is that the operable superficial gas and liquid velocities are increased. For example, P15-235 (type of structured packing with turbulizers) allows for superficial gas and liquid velocities up to 3.5 and 0.11 m/s (in PBRs), respectively (Kolev, 2006). The interesting behavior of these turbulizers is that at low superficial liquid velocity, the pressure drop of the wetted packing is half the pressure drop experienced by the dry packing. At high superficial liquid velocity, the pressure drop equalizes for wetted and dry packing.

Expanded metal packing is constructed by stamping or otherwise forming a channel from metal plates. The greatest advantage of this type of packing is that the channels are exclusively in the vertical direction such that the pressure drop is lower relative to the other packing types. Another derived advantage is that this also allows for much higher superficial gas velocities, potentially reaching 2.5–3.5 m/s. In order to achieve even higher gas velocities, the gas phase is input and extracted horizontally from the vessel, which allows operational superficial gas velocities up to 6 m/s. The most important disadvantage is that the vertical channel leads to the liquid preferentially wetting the leading edges. Hence, this packing requires more rigorous collection and redistribution than the other options. The exact behavior of the expanded metal packing is highly dependent on its construction, which can vary significantly. Major design considerations are the pitch, step height, and the existence and extent of perforations. The pitch, for example, can be designed so that the packing may be almost completely wet at relatively low superficial liquid velocities or able to handle an extreme (relative to other packing) amount of liquid (Kolev, 2006; Strigle, 1994).

The structured packing of corrugated sheets attempts to fix a major disadvantage of the smooth-walled packing: the possibility of free-falling liquid through the open cross-sectional area. The corrugated sheets are designed to intercept liquid (usually within one half of a wave) and enhance axial mixing (Kolev, 2006). The downside is that the pressure drop is larger relative to other structured packing options, but lower than random packing.

Certain processes, such as those relying on equilibrium absorption with low initial concentration of highly soluble gases, require very low superficial liquid velocities in the countercurrent configuration such that existent packing does not perform well. The operator has the option of using very easily wettable materials or using a highly specific packing form. This circumstance is rarely encountered in biological applications.

9.6 BIOLOGICAL CONSIDERATIONS

Biocatalysis and microorganisms have become great hopes and are seen as possible solutions to a multitude of problems. As such, research efforts are starting to turn toward suspending microorganisms on packing material to perform similar roles as reactive packing or perhaps completely new functions (Llamas et al., 2008). Biological microorganisms are typically attached to the packing surface since the microorganisms perform better when either the cell adhesion occurs or the cells are highly shear sensitive and need to be protected. Hence, fixed bed reactor performance is highly dependent on the liquid distribution uniformity. It should be noted that the liquid phase usually serves as the food source for the microorganisms. So, if the packing is not wetted, microorganisms will not colonize that section of the reactor. This, in turn, can severely limit reactor performance (Doan et al., 2008).

In addition, reactor internals may be of significant importance. Even though the perforated plate is a simple and effective device, it tends to provide minimal wall

wetting and tends to channel liquid through the central region. This effect can cause interesting performance variations at different liquid flow rates and may make comparisons between different research work a challenge. If the outer regions need to have liquid exposure, a better liquid distributor should be selected. Similar channeling can also be experienced by uneven cellular growth rates within the reactor volume.

Biomass and microorganisms tend to have a positive effect on fixed bed performance. Packing is usually judged on the basis of wettability, which biomass seems to increase. Doan et al. (2008) compared the wettability of plastic spheres with the same plastic spheres in the presence of microorganisms. The result has been that the liquid holdup increased by about 20% in the presence of microorganisms.

Liquid flow distribution and gas solubility issues can be enhanced with periodic liquid flushing of the reactor volume. The flushing tends to renew interfaces and reduce the gas-phase transport resistance (Nigam and Larachi, 2005). This practice may also have additional benefits in controlling microorganism growth. If the microorganisms do very well, the colonies might grow too thick and kill the lower cell layers. In order to prevent buildup in the reactor volume, a flushing cycle could be performed to detach a specific region or amount of microbial growth.

9.7 CORRELATIONS

Correlations for fixed bed reactors, which are shown in Tables 9.2 and 9.3, are currently available for specific operating regimes and packing types. Some aspects can be generalized; however, correlations are developed for either random or structured packing even though the same principal theories are used to explain gas–liquid mass transfer and behavior (Larachi et al., 2008). Current fixed bed correlations are very design specific, and any broad correlations produce highly variable and sometimes impractical results. This has been at least partially the result of many experiments being conducted at much lower pressure than those observed during industrial application (Attou et al., 1999). Kolev (2006) collected gas–liquid mass transfer correlations for the packed bubble column for his book on packed bed columns; however, the number of correlations was small because research was limited to gas–liquid mass transfer in PBRs. The most recent correlation (other than Kolev's) is from Billet (1989). Most of the work seems to have been done in the 1950s and 1960s. Since then, correlations have been seldom formed.

Perhaps the reason for the lack of correlations is twofold. First, the more important information for chemical engineers is the pressure and temperature predictions. With these in hand, chemical engineers are able to predict the other factors of importance. Biological processes are not expected to behave like this, and more work would need to be done for this purpose.

A second reason is the complexity of the interactions, which has lead to a data mining exercise by Professor Larachi's research group at Laval University. They have been at the forefront of providing correlations capable of predicting fixed

TABLE 9.2 Gas–liquid Mass Transfer Correlations for Fixed Bed Reactors

Researcher(s)	Reactor	Packing	Correlation
Billet (1989)		RP	$k_L a = C_L \frac{a^{2/3}}{d_h^{0.50}} D_L^{0.50} \left(\frac{g\rho_L}{\mu_L}\right)^{1/6} U_L^{1/3} \frac{a_e}{a}$ where C_L is an experimental, packing dependent constant
Fujita and Hayakawa (1956)	PBR	Rings 5–35 mm Saddles 13–40 mm	$Sh_L = 0.025 \left(\frac{h_P}{\delta}\right)^{-0.19} Re_L^{0.67} Sc_L^{0.50}$
Kasatkin and Ziparis (1952)	PBR	Rings 8–20 mm	$Sh_L = 0.0021\ Re_L^{0.75} Sc_L^{0.50}$
Hikita and Ono (1959)	PBR	Wetted single element	$Sh_L = 0.27 \left(\frac{d_P}{\delta}\right)^{-0.50} Re_L^{0.545} Sc_L^{0.50}$
Krevelen and Hoftijzer (1948)	PBR	Rings, coke, and others	$Sh_L = 0.00595\ Re_L^{0.67} Sc_L^{0.33}$

(*continued*)

TABLE 9.2 (*Continued*)

Researcher(s)	Reactor	Packing	Correlation
Koch et al. (1949)	PBR	RP	$k_L a = 0.25 L_m^{0.96}$ $k_L a = 0.0085 U_L$
Kolev (1976)		RP	$Sh_L = 0.030\ Re_{Le}^{0.5}\ Ga_L^{0.28}\ Sc_L^{0.50}$ $Re_{Le} = \left(\frac{4U_L}{a_e \nu_L}\right)$ Sh_L and Ga_L determined by d_P
Kolev and Daraktschiev (1976)		Holpack	$Sh_L = 0.00113\ Re_L^{0.635}\ Sc_L^{0.50}\ Ga_{Lh}^{0.366}\ (s/t_P)^{4.0}\ (at_P)^{0.1}$
Kolev and Semkov (1983)		RP	$Sh_L = 0.0115\ Re_L^{0.33}\ Ga_L^{0.42}\ Sc_L^{0.5}\ (ad_P)^{-0.37}$
Kolev and Nakov (1994)		FP with turbulizers	$Sh_L = 0.0077\ Sc_L^{0.5}\ Re_L^{0.70}\ (ah_P)^{-0.29} (as)^{-0.19}$

Larachi et al. (2008)	Correlation Excel files available at http://www.gch.ulaval.ca/bgrandjean or http://www.gch.ulaval.ca/flarachi		
Mangers and Ponter (1980)		RP	$\frac{k_L a}{D_L} = 0.0039 \left(\frac{U_L \rho_L}{\mu_L}\right)^{\alpha} \left(\frac{\mu_L}{\rho_L D_L}\right)^{0.50} \left(\frac{\rho_L{}^2 g d_P{}^3}{\mu_L{}^2}\right)^{0.70} \left(\frac{\rho_L \sigma^3}{\mu_L{}^4 g}\right)^{0.33} \left(\frac{1}{\text{MWR}}\right)^{1.67}$ $\alpha = 0.484\text{MWR}^{0.108}$ $\text{MWR} = 1.12 \left[(1-\cos\theta_\theta)^{0.60} \left(\frac{\rho_L \sigma^3}{\mu_L{}^4 g}\right)^{0.33}\right]$ where θ_θ is the contact angle
Onda et al. (1961)		RP	$Sh_L = 0.01\, Re_L{}^{0.50}\, Sc_L{}^{0.50}$
Onda et al. (1958)	PBR	Rings 6–10 mm	$Sh_L = 0.00625\, Re_L{}^{0.50}\, Sc_L{}^{0.50}$
Onda et al. (1959)	PBR	Rings 6–10 mm	$Sh_L = 0.0107\, Re_L{}^{0.90}\, Sc_L{}^{0.50}$
Ramm and Chagina (1965)	PBR	FP	$k_L a = 11.6 U_L{}^{0.768}\, h_P{}^{-0.185}$
		Raschig rings 25 and 50 mm	$Sh_L = 0.00216\, Re_L{}^{0.77}\, Sc_L{}^{0.50}$
		Pall rings 50 mm	$Sh_L = 0.0036\, Re_L{}^{0.77}\, Sc_L{}^{0.50}$

(*continued*)

TABLE 9.2 (*Continued*)

Researcher(s)	Reactor	Packing	Correlation
Raschig LTD		FP	$Sh_L = 0.01019\ Re_L^{1.1-0.4\varepsilon}\ Sc_L^{0.50}\ Ga_L^{-0.01}\ (ah_P)^{-0.35\varepsilon}\ \varepsilon^{2.9}$ $Sh_L = 0.0026\ Re_L^{0.66-0.4(1-\varepsilon)}\ Sc_L^{0.5}\ Ga_L^{0.07-0.25(1-\varepsilon)}\ (ah_P)^{-0.41+0.6(1-\varepsilon)}\ (1-\varepsilon)^{-0.2}$
Scherwood and Holloway (1940)	PBR	Rings 25–50 mm	$Sh_L = 0.00204\ Re_L^{0.78}\ Sc_L^{0.50}$
		Rings 12, 5 mm	$Sh_L = 0.00333\ Re_L^{0.65}\ Sc_L^{0.50}$
		Saddles 12.5–38 mm	$Sh_L = 0.00285\ Re_L^{0.72}\ Sc_L^{0.50}$
Shulman et al. (1955)		RP	$Sh_L = 5\left(\frac{F_f^{2/3}}{1-\varepsilon}\right)^{0.55} Re_L^{0.45}\ Sc_L^{0.50}\ (a\delta)^{33}$ $F_f = \frac{483\nu_L^{2/3}}{a_s}$
Yoshida and Koyanagi (1962)	PBR	Rings 15–25 mm Saddles 12–25 mm	$Sh_L = 0.236\left(\frac{d_P}{\delta}\right)^{-0.50} Re_{Le}^{0.50}\ Sc_L^{0.50}$ $Re_{Le} = \left(\frac{4U_L}{a_e\nu_L}\right)$

Adapted from Kolev (2006).

TABLE 9.3 Liquid-Phase Mass Transfer Correlations for Fixed Bed Reactors

Researcher(s)	Reactor	Packing	Correlation
Billet (1993)		RP	$k_L = C\left(\frac{D_L}{4\varepsilon}\right)^{0.5}\left(\frac{\rho_L g}{\mu_L}\right)^{1/3}\mu_L^{1/3}$ where C is an experimental, packing dependent constant
Billet and Schultes (1993)		RP	$k_L = C_{LB}12^{1/16}\left(\frac{U_L}{\varepsilon_L}\right)^{0.5}\left(\frac{D_L}{d_h}\right)^{0.5}$ where C_{LB} is an experimental, packing dependent constant
Kolev and Daraktschiev (1976)		Holpack	$\frac{k_L t_P}{D_L} = 0.00113\, Re_L^{0.635}\, Sc_L^{0.5}\, Ga_{Lh}^{0.366}\,(s/t_P)^{4.0}\,(at_P)^{0.1}$ $Re_L = \frac{4d_L}{a_e\nu_L}$ and $Ga_{Lh} = \frac{gt_P^3}{\nu_L^2}$

(*continued*)

TABLE 9.3 (*Continued*)

Researcher(s)	Reactor	Packing	Correlation
Norman and Sammak (1963)	Disk column	RP	$\frac{k_L d_d}{d_R} = 0.13 \left(\frac{4U_{LI}}{\mu_L}\right)^{0.61} \left(\frac{\mu_L}{\rho_L d_R}\right)^{0.50} \left(\frac{\rho_L{}^2 g d_d{}^3}{\mu_L{}^2}\right)^{0.17}$
Onda et al. (1959)		RP	$k_L = 0.0051 \left(\frac{\mu_L g}{\rho_L}\right)^{1/3} \left(\frac{U_L \rho_L}{a_e \mu_L}\right)^{1/3} \left(\frac{D_L \rho_L}{\mu_L}\right)^{1/3} (a d_P)^{0.4}$
Shi and Mersmann (288)		RP	$k_L = 0.91 \left(\frac{6D_L}{\pi d_P}\right)^{0.5} \frac{U_L{}^{0.19} g^{0.22} \varepsilon^{0.2} \rho_L{}^{0.23}}{\mu_L{}^{0.23} a^{0.4}} \left(\frac{\sigma}{\rho_L}\right)^{0.05} (1–0.93 \cos\theta_\theta)^{1/3}$
Zech (1978)		RP	$k_L = C \left(\frac{\rho_L g d_P{}^2}{\sigma}\right)^{-0.15} \left(\frac{U_L g d_P}{3}\right)^{1/6} \left(\frac{6D_L}{\pi d_P}\right)^{0.5}$ where C is an experimental, packing dependent constant

Adapted from Kolev (2006).

bed performance for a wide variety of packing and designs. Their approach has been based on developing a large database, which incorporates 861 and 4291 experiments for structured and random packings, respectively, and the use of a neural network to determine the most important factors in predicting the necessary output. The resulting average error varies between 20.9 and 29.2% among six different mass transfer parameters. They have created separate correlation Excel files for the packed, flooded, and TBRs, which can be accessed from Professor Larachi's homepage at Laval University (Larachi et al., 2008; Piché et al., 2001a; Piché et al., 2001b; Piché et al., 2001c); the link to this site is http://www.gch.ulaval.ca/bgrandjean/pbrsimul/pbrsimul.html. This is currently the best and most comprehensive resource for gas–liquid mass transfer information relative to fixed bed reactors.

9.8 NEEDED RESEARCH

Fixed bed reactors have been largely used by the chemical and related industries. Industrial biological applications are limited. Since fixed bed reactors operate at lower superficial gas and liquid velocities, it is going to be very hard for these reactor types to compete with bubble columns, airlift reactors, or membrane reactors (Gottschalk, 2008). A second competitive problem is that interfacial area in fixed bed reactors is made of liquid droplets and wetted packing. If fixed bed reactors are to be used in biological applications, more research needs to be directed toward increasing the surface area available for mass transfer. One solution that could use more investigation is the operation in the flooded regime, which would allow for more bubbles and a larger interfacial area; however, the problem with this approach is that such operation may be described as more bubble column than fixed bed reactor. So far, biological research has been focused on waste treatment, or the need to provide a support mechanisms for highly shear-sensitive media, such as mammalian cell structures. In other words, if the microorganism is tough enough for a bubble column or airlift reactor, the fixed bed reactor is not effective.

The current research effort in fixed bed reactors is directed toward the improvement of packing. The view is that the packing choice can make or break the success of the operation, and that current operations are so large that even minimal improvements would yield tremendous savings. Although the reactive function is very important given the supporting role packing has in chemical reactions, biological systems are going to be less dependent on this packing function and would be better served with packing that supports larger amounts of microorganisms.

9.9 SUMMARY

Fixed bed reactors use packed, fixed material with the purpose of achieving higher reaction rates than would be possible with two-phase interaction alone. In order to conform to different types of reactions, several styles and forms of fixed bed reactors and packing are in use. The PBR is a countercurrent model, where

liquid is injected from the top of the reactor and gas from the bottom. The TBR is a downward flowing cocurrent reactor. If the flow occurs in the upward direction, it is referred to as a FBR. As far as the packing goes, the designer and operator have a wide array of options, which are mainly due to a tremendous amount of customization that has occurred over the years. This experimentation has led to dozens of different packing materials and classifications.

Generally speaking, fixed bed reactors are not able to transfer as much mass when compared to previously covered reactor types because the phase flow rates in fixed beds are usually much lower. This is due to the fact that the pressure drop across the bed would increase to a value that would make almost any operation either unprofitable or nonreactive. Hence, the general application of fixed bed reactors is to provide a support structure on which microorganisms can grow. Another application of the fixed bed reactor is to serve as a biofiltration device.

There is still a lot of work—including more basic research—left to do on fixed bed reactors for biological applications. Most of the data, conclusions, and designs have been developed for chemical processes and reactions, which usually require very high pressures and temperatures. Microorganisms often have very different requirements and interactions, which have not been explored very deeply, if at all. For example, there is not a single gas–liquid mass transfer correlation that is directly applicable to microbial design mainly because most of them have been developed in the 1940–1960s. So, if the fixed bed reactor limitations are kept in mind, the design can be adapted to serve roles currently supplied by chemical reactions or open the doors to new applications.

10 Novel Bioreactors

10.1 INTRODUCTION

Novel bioreactors are nonstandard devices, which attempt to deliver better performance, bring new features, or introduce production through a new method. Novel designs accomplish these tasks by either introducing new or significantly adjusting components in standard devices, or by introducing a completely new approach and/or concept into the production. This section will concentrate on both aspects of novel bioreactor design, but more attention will be paid to novel bioreactor design strategies. Note that new novel bioreactors are being developed all the time, and this chapter is not intended to be an exhaustive review of novel bioreactors.

10.2 NOVEL BUBBLE-INDUCED FLOW DESIGNS

Novel bubble-induced flow designs apply a plethora of mechanisms that help differentiate each specific design from other novel and standard devices. Some changes are structural and include use of different materials and internals. Others include the use of novel methods to excite the bubble interface and induce gas–liquid mass transfer. Novel methods exclude devices that are created to study specific events relating to standard devices. For example, the study by Sotiriadis et al. (2005) using a specially designed bubble column where the phases move downward to specifically study bubble behavior, bubble size, and gas–liquid mass transfer in the downcomer of airlift reactors would fall in the excluded devices.

Perhaps the simplest variation to aerated designs is to inject the phase(s) using the jetting principle. Such devices are often grouped as jet reactors. It should be noted that jet reactors do not necessarily share any other commonalities besides the phase input techniques. The reactor internals and phase flow can vary significantly. Jet reactors use liquid jets and injection devices in order to achieve high liquid velocities and turbulence. The higher turbulence generally yields to better gas–liquid mass transfer performance, which is its largest advantage. On the other hand, the shear rates, especially in the injection vicinity, tend to be much higher than the average. Microorganism growth could produce uneven reactor performance. Furthermore, the generated shear stresses are potentially too high for

An Introduction to Bioreactor Hydrodynamics and Gas-Liquid Mass Transfer, First Edition.
Enes Kadic and Theodore J. Heindel.

microorganisms to survive. Hence, the current application of jet reactors is limited to strictly chemical processes, and research with microorganisms is limited.

Some examples of jet reactors include submerged- and plunging-jet reactors, ejector reactors, hydrocyclones, and venturi devices. Plunging-jet reactors throw a liquid jet through a gas phase, which is usually reactive, into the liquid volume. In other words, these reactors attempt to transfer the gas phase by creating gas entrainment at the liquid surface. This jet reactor requires jet velocities of up to 30 m/s (Charpentier, 1981). Submerged-jet reactors pump a liquid phase through a venturi where the liquid is combined with the gas phase. The result is a mixture that has a very bubbly appearance. The generated bubbles are very small and would be expected to have a large gas–liquid interfacial area. Varley (1995) reported a Sauter mean diameter of 0.29–1.92 mm in a 72-l submerged-jet reactor using $U_{\mathrm{L}} = 3 - 12\ \mathrm{m/s}$.

The ejector reactor uses a similar injection device as the submerged-jet reactor, but the created jet is injected into an airlift-like vessel. The gas–liquid mixture is allowed to go through a riser and into a separator. Since the gas phase separates, a density difference is created and liquid recirculates into the injection zone. These reactors are capable of operating with liquid velocities of at least 20 m/s. With this kind of turbulence, the ejector reactor outperforms stirred-tank reactors at equivalent operating conditions (Charpentier, 1981).

Venturi-based reactors work similarly to submerged-jet and ejector reactors, but the big difference is that the liquid is injected into a high velocity gas-phase field, whereas the ejector reactors inject gas into a high velocity liquid-phase field. Hence, the venturi-based reactors create small liquid droplets similar to an atomizer. Venturi-based reactors are used as scrubbers or with quantities of gas phase present in the reactor volume. In contrast, ejector reactors create small bubbles that are used in liquid-phase dominated reactor volumes (Charpentier, 1981).

Jet injectors may also be combined with monolith reactors. Monoliths are usually tube reactors with channeled flow. The reaction occurs at the gas–liquid interface as well as on the channel wall, which are usually catalytic or coated with catalytic material. Monoliths can be made into vertical (similar to bubble column) or horizontal tubes, airlift devices (whereby the riser would a monolith), or even into a mechanically stirred device. Usually, however, monoliths are designed like bubble columns or airlift reactors (Broekhuis et al., 2001).

Monolith reactors could be considered a novel class on their own. The problem is that the monolith reactor relies on the catalytic properties of the wall in order to have better mass transfer and reaction performance than the other reactor types. If these properties do not exist, as they are not expected to with biological applications, the channels are too small and cause gas to slug. Hence, a monolith reactor would be limited by the amount of biological media and phase flow media, specifically the gas phase. If the microorganisms grow well, the channels could be plugged and extensive cleaning may be necessary. For most biological applications, monoliths do not provide theoretical advantages to a fixed bed reactor, bubble column, or airlift reactor. This fact is reflected in the lack of biological application of traditional monolithic reactors; however, monolith-like principles are sometimes

hidden within fixed bed reactors. In these cases, the monolith-like packing is used as a support mechanism for cellular growth. For available biological studies, monolith reactors tend to compete with trickle-down (fixed bed) or membrane reactors. For example, the 2007 AIChE Annual Meeting held in Salt Lake City, UT, had a conference section dedicated to monoliths and membranes (Bauer et al., 2007). It is also a popular option to design monolith microreactors (Schönfeld et al., 2004), which are basically scaled-down versions of the large-scale reactors.

Researchers have also combined reactor types. Guo et al. (1997), for example, designed an external loop airlift reactor that incorporates a fluidized bed within the downcomer section, shown in Figure 10.1. The fluidized bed section is used to immobilize microorganisms on carrier particles in order to protect them from damage. The design is meant for the production of enzymes, biofluidization, and wastewater treatment. Although shear rates were minimized, bubbles were not entrained within the downcomer. Furthermore, the gas–liquid mass transfer coefficient was observed to increase with gas holdup. The result was that the gas–liquid mass transfer was limited due to the fact that global gas holdup for the reactor was strictly defined by the riser gas holdup without any addition by the downcomer.

Wastewater treatment plants oftentimes use vessels that combine the (slurry) bubble column with a mechanical extractor and/or a mixer. The mechanical extractor is used to scrape heavy residue at strategically located divider walls. Such a system implies that the liquid flows across the gas flow field. Siemens' proprietary Attached Growth Airlift Reactor (AGAR)-Moving Bed Bioreactor is an example of such a device.

Wastewater treatment may also require the use of UVA–UVB rays as a mechanism to kill any unwanted cellular material. Unsparged photoelectrochemical

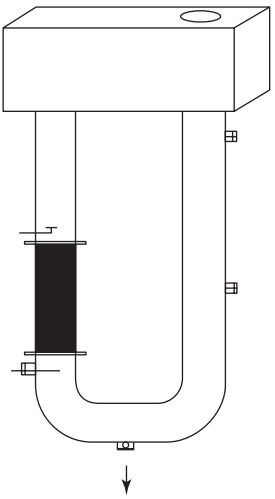

Figure 10.1 Novel external-loop airlift reactor designed by Guo et al. (1997).

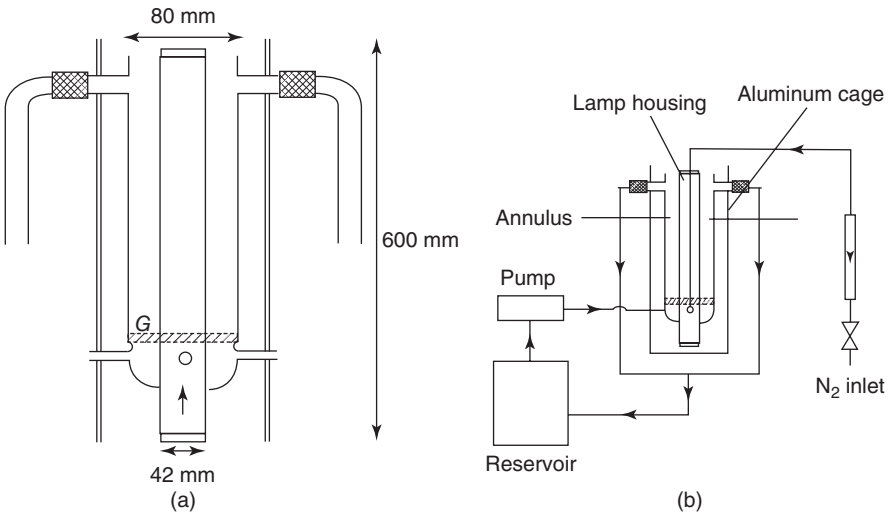

Figure 10.2 (a) Novel sparged photoelectrochemical reactor cross section and (b) schematic diagram used by Harper et al. (2001).

reactors, which resemble unsparged slurry bubble columns, are standard devices for such an operation. Harper et al. (2001), however, experimented with a modified aerated airlift reactor, shown in Figure 10.2. The design uses an UVA–UVB lamp core around which the photochemical reaction is allowed to occur. The liquid and gas can be recirculated to maximize output and conversion and optimize residence times. A similar design could be very useful for photosynthetic microorganism growth, such as algae, but no information on such a system has been found in the open literature.

Ellenberger and Krishna (2002) introduced vibrations in order to reduce the bubble rise velocity, destabilized the bubble surface, and reduced surface tension forces. These changes lead to an improved liquid-phase mass transfer coefficient and, hence, gas–liquid mass transfer coefficient. This goal has been accomplished using mechanical vibration devices in previous studies cited by the authors. In contrast, Ellenberger and Krishna (2002) introduced sinusoidal pressure variations at a frequency on the order of 100 Hz and amplitude of 0.0025–0.01 mm; this led to a reduction in the bubble diameter by 40–50% and an increase by 100–300% in gas holdup and 200% in the gas–liquid mass transfer coefficient when compared to the no pressure variation system.

Another less commonly applied adjustment with bubble columns and airlift reactors is to introduce additional turbulence by pumping or mechanically exciting the liquid phase. Such adjustments have long been viewed as being advantageous and increasing gas–liquid mass transfer, but they have also been seen as very expensive options (Lundgren and Russel, 1956). The advantage of such a system is that it allows more control of the liquid phase flow, but the cost is usually represented by the additional power required by the pump or impeller motor. The need for

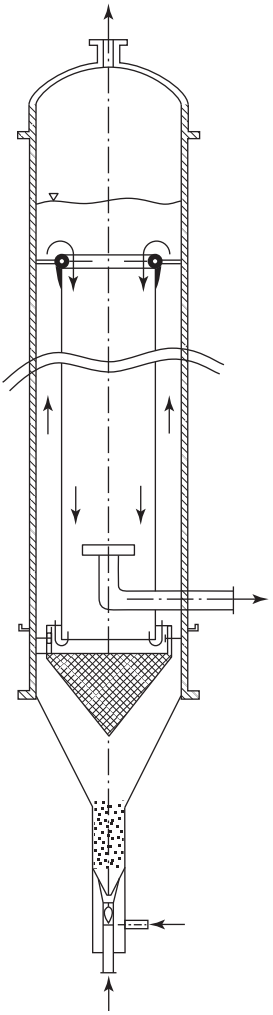

Figure 10.3 Experimental pumped circulation column proposed by Fadavi and Chisti (2005).

such a device stems from the potentially limiting suspension capabilities, liquid circulation rates, and axial nutrient gradients provided by standard airlift reactors. These issues are exaggerated with height. The pumped circulation column is shown in Figure 10.3. As expected, the high liquid flow rate ($Q_L = 2$ m^3/h) used by Fadavi and Chisti (2005) added to the turbulence and nearly doubled gas–liquid mass transfer relative to an airlift reactor. Liquid flow in an airlift reactor generally does not contribute significantly to bubble breakage, but the fast liquid flow in the pumped variant did so and led to a smaller average bubble diameter.

A mechanically induced circulation loop reactor is shown in Figure 10.4. This variant works on similar principles as the pumped circulation column.

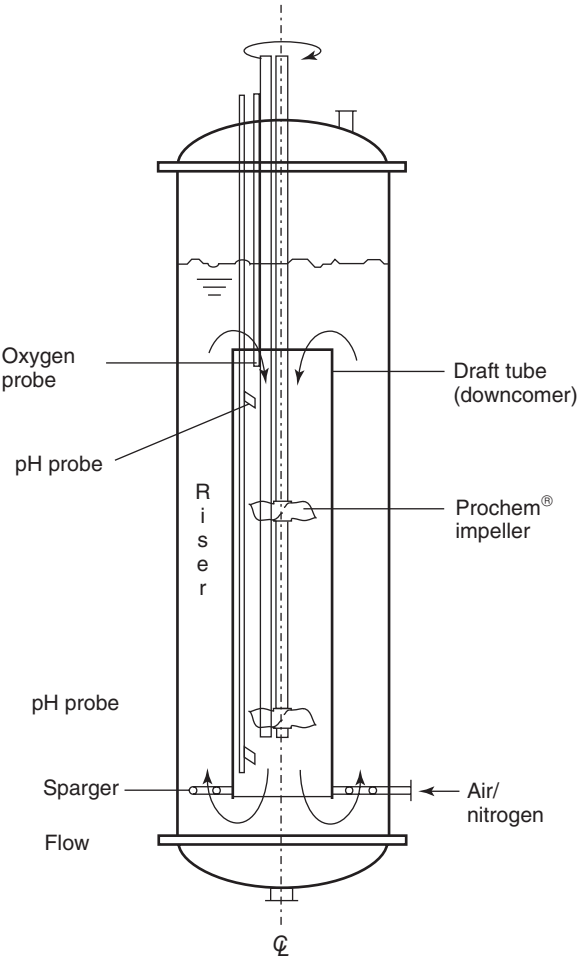

Figure 10.4 Experimental mechanically induced circulation loop reactor proposed by Chisti and Jauregui-Haza (2002).

The mechanically induced circulation loop reactor attempts to increase liquid velocity using impeller sets. Chisti and Jauregui-Haza (2002) accomplished this by imbedding a down-pumping Prochem Maxflo T hydrofoil impeller. Air is injected into the annular region of the reactor for several reasons. First, the impellers may flood with the higher gas flow rates usually applied in airlift reactors. Second, the operational set becomes easier to handle if the impellers are placed in the reactor center. Finally, the impellers are used to increase the liquid velocity rather than bubble breakage. So, the impellers used for pumping, such as the Prochem Maxflo T, do not necessarily handle gas well, and placing them in the riser would make the situation unnecessarily more complicated. In addition, the riser flow is already influenced by the gas flow rate. It should be noted that many airlift reactor issues

can be solved with proper airlift reactor design and phase flow rates; however, these hybrid variants are useful when high gas flow rates are not possible or for more control. Generally, mechanically agitated airlift reactors are still seen as economically prohibitive except for a set of specialized cases.

Another area of reactor modifications has been to add or adjust column internals. For airlift reactors, some research has gone into replacing the draught tube with a net draught tube that would allow for bubble breakage near the wall region (Fu et al., 2004; Fu et al., 2003). This additional bubble breakage leads to a smaller bubble diameter in the riser, which in turn leads to higher gas–liquid mass transfer. If the process is mass transfer limited, it is expected that an increase in productivity would be observed. Although the net draught tube reactor has the potential to easily increase gas–liquid mass transfer, it also has the potential to be easily plugged by biomass growth or otherwise foul in an industrial setting.

Static mixers can be installed in bubble columns or airlift reactors to provide additional mixing efficiency. Such devices are used to break bubbles before they have a chance to coalesce. The performance of these devices range greatly, but increase in gas–liquid mass transfer by 500% has been observed (Chisti et al., 1990; Fadavi and Chisti, 2005). Such increases, however, are to be expected with highly viscous media. Viscosities that are nearer to water are going to see much smaller performance increases. Operators interested in adding static mixers to their bubble column or airlift reactor also have to consider the additional cleaning requirements that may come from such devices. In other words, static mixers may not provide enough of an improvement in low viscosity fluids to pay for their additional maintenance costs.

10.3 MINIATURIZED BIOREACTORS

Miniaturized bioreactors can be divided into two categories based on scale: microreactors and nanoreactors. These bioreactors present several fundamental advantages and open new venues. Miniaturized reactors allow for bench-scale chemical and biochemical production, which can be used by researchers. They also allow for cost-effective production when smaller quantities of a chemical are required. Other larger bioreactors are often not feasible because the production is not cost effective if the product is not very valuable or if the production is not consistent or pure enough for higher value chemicals. Miniaturized bioreactors, however, provide a great deal of control over reaction kinetics and hydrodynamics.

Another very important advantage of miniaturized bioreactors is that scale-up takes on a different form. The scale-up procedure for standard bioreactors and miniaturized bioreactors is compared in Figure 10.5. The scale-up procedure for standard bioreactors involves a complicated iteration processes. A laboratory bioreactor is designed as a proof-of-concept. Next, an experimental-scale bioreactor is designed to ensure production viability. After a few iterations, a small-scale pilot plant is constructed to test and finalize the production process, equipment placement, and economic viability. Once this step is accomplished, a large-scale

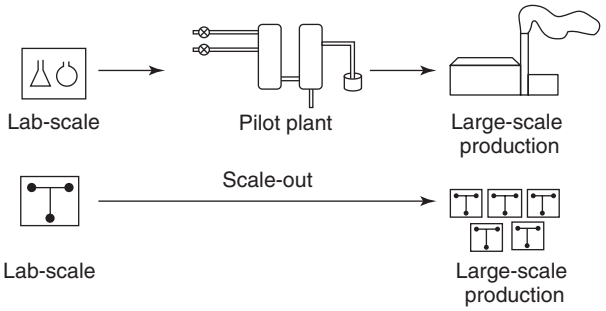

Figure 10.5 Scale-up procedure comparison (Watts and Wiles, 2007).

plant is constructed. The iteration requirement stems from the significant changes in hydrodynamics and/or reaction kinetics that are experienced as scale is increased (Watts and Wiles, 2007).

With miniaturized bioreactors, however, scale-up is a much simpler process. The procedure involves putting miniaturized bioreactors into series and/or parallel in order to produce larger output quantities. This approach keeps the reaction kinetics and hydrodynamics predictable for each component regardless of plant scale. Hence, the process is often referred to as numbering-up. In other words, the laboratory bioreactor is very similar to the industrial production, with the bioreactor quantity and controls being the most significant differences. This property keeps the start-up and development costs lower and more flexible (Ehrfeld et al., 2000; Watts and Wiles, 2007).

The numbering-up method also introduces another potential advantage. The scaled model operates as a continuous bioreactor rather than batch while providing the operator with the same control advantages of the batch operation at the same time. Therefore, the process time is expected to be shorter with miniaturized bioreactors since most standardized bioreactors use a process time that is longer than the kinetic minimum. Safety is also increased tremendously since the process can be stopped at any point in the process flow (Ehrfeld et al., 2000). These controls can be instituted automatically without the need for human supervision.

10.3.1 Microreactors

Microreactors are defined by their size rather than construction. Microreactors are miniaturized with channels between the (sub-)millimeter scale and nanometer scale. Microreactors mix the gas and liquid phases pneumatically or mechanically. The size of the complete bioreactor construction is less important. A microreactor example is shown in Figure 10.6. Microreactors are generally compounded into microreactor elements, which are placed into mixing units. These units are placed into microreactor devices, which have inputs and outputs for all the microreactor units placed within it. Microreactor devices are placed in parallel or in series in order to achieve the necessary conversion. Finally, the output is treated

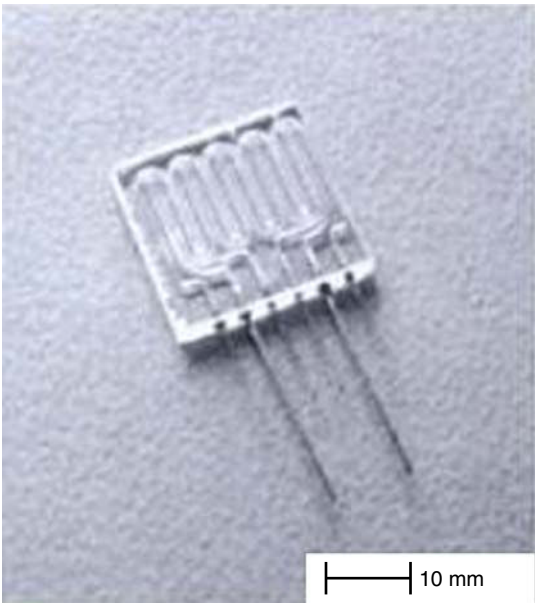

Figure 10.6 Microreactor example (Ehrfeld et al., 2000).

(Ehrfeld et al., 2000; Watts and Wiles, 2007). A typical microreactor assembly is shown in Figure 10.7.

Microreactor construction can be accomplished using numerous tools. Costs, however, dominate the construction options. Hence, possible construction techniques are defined by channel flow scale, precision, reliability, and material selection. Naturally, as the bioreactor scale becomes smaller and precision requirements become higher, the costs tend to increase as well. An accepted approach when constructing microreactors out of metals, ceramics, or plastics is using lithography, electroplating, and molding (LIGA, Lithographie, Galvanik und Abformung). LIGA is a three-step process in which a laser, electron beam, ion beam, UV-ray lithography, or X-ray lithography are used to print microstructures. Then, electroforming is used to generate a metal layer onto the microstructure. This metal structure can be used as a mold or embossing tool for mass production (Ehrfeld et al., 2000; Hruby, 2002; Wirth, 2008). The available construction techniques are summarized in Figure 10.8. Ehrfeld et al. (2000) and Wirth (2008) are good and recent sources for the current construction techniques and their applications.

Mixing in microreactors is almost exclusively assumed to be laminar due to the small flow channel width. Laminar flow through microchannels requires the phase flow to be alternated in some fashion in order to create the mixing environment. This operation is important because mass transfer, in this case, is driven only by molecular diffusion. Hence, the creation of larger gas–liquid interfaces is the only practical course of action for gas-limited operations. Miniaturized bubble columns are able to accomplish this task well. For example, a standard reactor can create

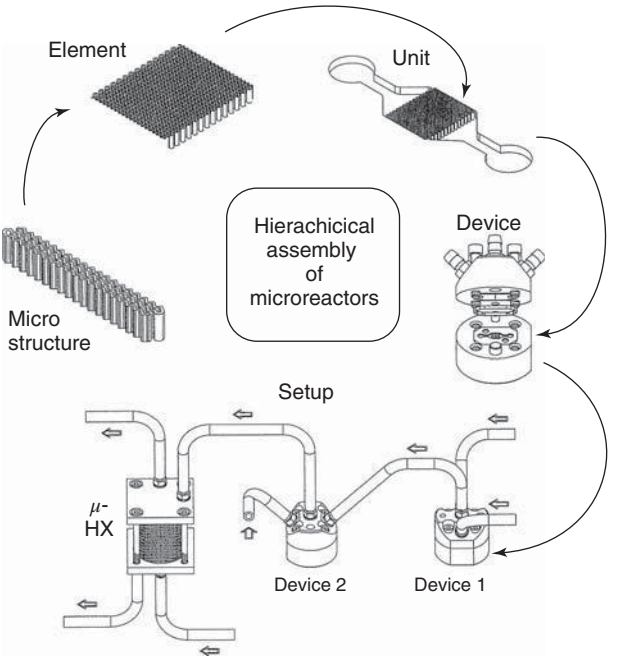

Figure 10.7 Microreactor assembly (Ehrfeld et al., 2000).

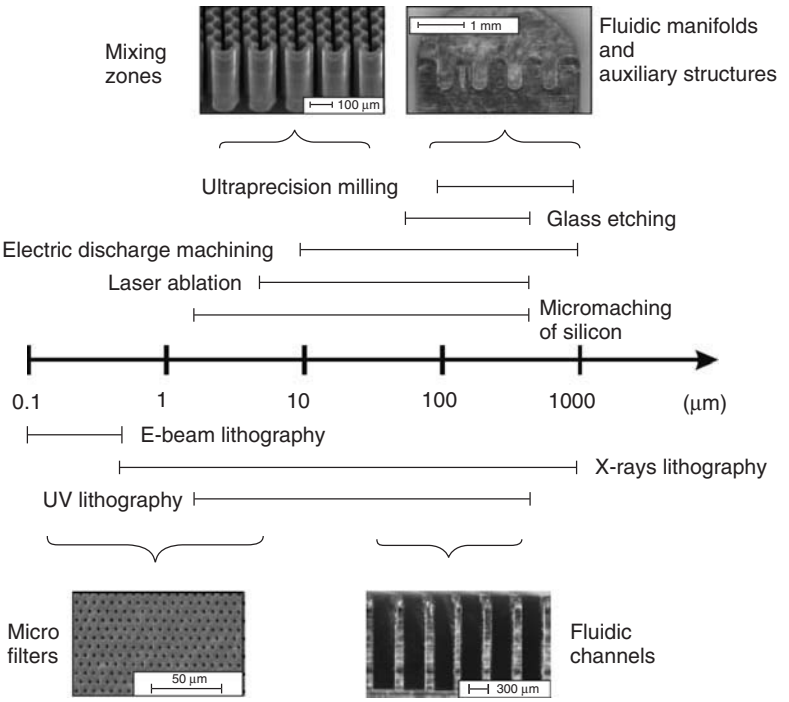

Figure 10.8 Microreactor construction techniques (Ehrfeld et al., 2000).

interfacial areas in the range of 2000 m^2/m^3, while a single-channel microbubble column and a microbubble column with channel arrays can create interfacial areas of 1700–25,300 and 5100–16,600 m^2/m^3, respectively (Ehrfeld et al., 2000).

Unfortunately, the extreme numbers are somewhat misleading. In order to properly understand their context for biological application, an understanding of microbubble column flow regimes is necessary. Bubble velocity in microreactors is defined by a gas space velocity. This velocity is similar to the superficial gas velocity, but it tends to be slower due to very significant wall effects. So, the gas space velocity is approximated using a sample bubble velocity.

Bubbles in microbubble columns are observed to be separated by a liquid film from the wall at almost all gas space velocities. At low gas space velocities, the microbubble column experiences bubbly flow. The bubbly flow is defined by microbubbles, which are spherical and as large as the channel diameter. Since bubbles of this size are highly unstable without surfactants, the gas space velocity has to be low enough to allow enough space between bubbles in order to prevent coalescing.

As the gas space velocity increases, bubbles tend to coalesce and a slug flow regime develops. The slug flow regime is defined by bubbles that are longer than the channel diameter and are still separated by some amount of liquid. Increasing the gas space velocity leads to the slugs coalescing even further, and a slug-annular flow regime is observed. The slug-annular regime experiences very long bubbles, which are separated by a very small amount of liquid. Further increasing the gas space velocity combines the elongated bubbles into an annular gas flow (annular flow regime).

The extreme interfacial values are experienced by the latter two regimes and are most likely useless for biological applications. The channel diameters are very small to begin with, and the liquid film that develops in the slug, slug-annular, and annular flow regimes is not sufficient to support microorganism growth. In order to have microorganisms survive in microbubble columns, the reactor would almost certainly have to be operated in the bubbly regime, which experiences interfacial areas of $1700 - 5100\ m^2/m^3$. Lower values are observed with microbubble columns with a diameter of 1100 μm, whereas the larger values are experienced with a channel diameter of approximately 300 μm (Ehrfeld et al., 2000). Even though these values are higher than those for standard equipment, the advantage for microbubble columns is not astronomical, and competition and performance are likely to be more comparable and competitive.

Although microbubble columns are popular, other microreactor mixing methods exist, such as the falling film principle. In such a system, the liquid phase would be input into the microreactor's reaction chamber from the top while the gas phase input is at the bottom. The principle is very similar to the annular flow regime in the microbubble columns. The liquid would line the reactor walls while the gas phase would move through the annular region. The difference with the falling film reactor is that the liquid is fed at a rate and way that it would guarantee flow only at the wall region and would prevent the liquid phase from mixing into the gas phase (Zhang et al., 2009).

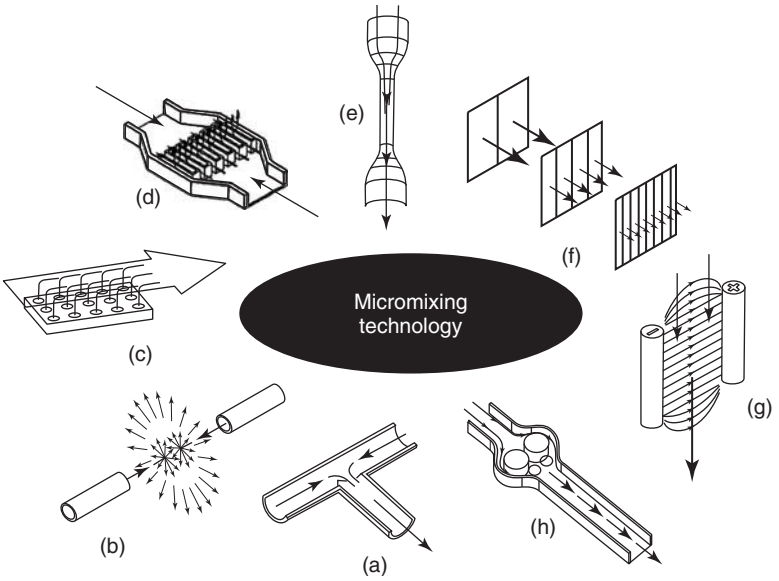

Figure 10.9 Micromixing arrangements: (a) substream contacting, (b) high energy substream contacting, (c) multiple substream injection into major stream, (d) multiple substream contacting, (e) flow restriction, (f) stream splitting, (g) forced mass transfer, and (h) periodic fluid injection (Löwe et al., 2000).

In addition to the microbubble column and falling film microreactor, several other theoretical schemes exist in order to achieve proper mixing conditions of two phases. The simplest mechanism is defined by the phases entering a tee intersection either as single streams, shown in Figure 10.9a, or as numerous substreams, shown in Figure 10.9d. Control over the mixing is provided by the phase flow rates. A more energetic method is to collide high energy (velocity) streams in order to create large interfacial areas due to atomization or spraying (Figure 10.9b). This method is most likely not useful for biological applications as it would damage the microorganisms. It could, however, be used as a phase premixer for semisuspended microorganisms. One of the phases could also be broken down into substreams, which are then injected into a larger stream of the other phase (Figure 10.9c). For example, gas could be injected into a liquid stream in order to generate bubbles with liquid intervals.

An interesting method for mass transfer problems is to channel the phase flows into a constricted area, which would increase velocity and decrease the diffusion path (Figure 10.9e). Although useful in this regard, it could create problems in biological systems by either damaging the microorganisms or not allowing enough room for the microorganisms to pass through. A more popular approach is to use splitting arrays (Figure 10.9f). The phases would be mixed into a single stream and then continuously broken apart by alternating horizontal and vertical splitters, which get finer as the mixture moves along. Although this method is popular in

the chemical industry, microorganism growth would most likely cause blockage. Naturally, these methods can be combined into a single, more complex device. These mixing schemes have been applied to liquid–liquid contacting problems, but only substream tee contacting and substream injection have been tested for gas–liquid problems (Ehrfeld et al., 2000).

The natural cause for a lack of microreactor research in gas–liquid processes is that most miniaturized reactor research is concentrated on problems experienced in the chemical industry, specifically catalyzed liquid–liquid reactions. Gas–liquid, and especially biological reactions, have not been widely attempted since the field of microreactor engineering is emerging to fulfill the highest margin needs first. Biological applications are still being mastered with standardized equipment, and economic viability using microreactors seems to be some distance away. Another issue is that much of the work is still not published. For example, Ehrfeld et al. (2000) includes numerous unpublished reports and correspondences, such as the interfacial areas data. The same information for standard bioreactors, however, is easily obtained across different print media.

10.3.2 Nanoreactors

A differentiation between nanoscaled and microscaled miniaturized reactors is necessary because the naming convention is not universally applied. Nanoscaled reactors were introduced in the late 1990s and are the possible microreactor alternatives for the chemical industry (Ostafin and Landfester, 2009). An example of a nanoreactor in nature is the mitochondrion, which is the energy-producing portion in most complex cells. Nanoreactors are more accurately described as molecular reactors, and the reactor volume is defined by the number of molecules confined within the reactor rather than a standard volumetric measurement. Nanoreactor's biological applications, however, will most likely stay very limited. The nanoreactor has some critical faults and problematic characteristics for biological application. The first and largest problem is that the channel size is too small for most microorganisms of interest, such as bacteria. Nanoreactors are usually on the nanometer scale while smaller bacteria are in the micrometer scale. Hence, no additional discussion on nanoreactors will be presented.

10.4 MEMBRANE REACTOR

Some products or intermediaries in biological processes are highly shear sensitive. Standard bioreactors may not be able to protect the microorganisms sufficiently. Membrane reactors allow for semisuspension of cells by placing the cellular material within or between (semi)permeable membranes. Membranes are not novel ideas for the chemical industry for which membranes have $9 billion in component sales in 2006 (Nunes and Peinemann, 2006), but their biological application is novel. The chemical industry, however, has used membrane technology for experiments since the 1920s and for industrial applications since the 1960s, while

the membrane bioreactor concept has been first defined in the literature in 1979 (Hall et al., 2001; Nunes and Peinemann, 2006). It should be noted that permeation and membrane concepts were first scientifically described in 1748 (Baker, 2004).

The initial membrane bioreactors cross-flowed the liquid phase through the membrane, which increased energy costs significantly. Currently viable membrane bioprocesses submerge the membrane in the liquid phase whereby the liquid flows parallel to the membrane matrices. This creates low pressure drops and makes the economic viability a reality. Current membrane reactors also tend to vary the volumetric membrane amount or carrier particles at 60–70% (Leiknes and Odegaard, 2007).

Membranes allow the gas phase to transfer the microorganisms without exposing the microorganisms to the bubble interface or other potentially high shear areas. This allows high cell densities which, in turn, allows for higher conversion effectiveness (Ko et al., 2008). The membrane may also allow the product to permeate away to a collection area. Since the microorganisms have little exposure to bubbles and the gas has to travel through the membrane, the membrane reactor allows for relatively small amount of gas–liquid mass transfer to occur and almost any other reactor types outperform it on that measure. Unfortunately, some microorganisms, such as animal cells, are so shear sensitive that they are able to survive only in a membrane-protected environment (Bellgardt, 2000b).

The most significant disadvantage of membrane bioreactors is that they are very costly to construct and maintain, and their long-term viability is yet to be proven (Dudukovic, 1999; Kumar et al., 2008). For example, microporous membranes have to be replaced every 3 years, which leads to operating and maintenance costs that are approximately 10 times higher than with a conventional gas treatment options (Kumar et al., 2008). Long-term viability may be problematic because the current membrane technology has permeate mass fluxes which are an order of magnitude that are too small to be competitive on a volumetric productivity basis. Furthermore, membranes provide an additional heat transfer barrier, which introduces temperature control issues that are generally not present in standard bioreactor designs (Dudukovic, 1999).

Mass transfer through a membrane occurs in several steps, which differentiate it from mass transfer in standard reactors. The first two processes are very similar. First, the gas is injected into the reactors volume. Then, the gas is transported into the liquid phase. This is usually accomplished by molecular diffusion. The mixing is not turbulent enough for bubble interface excitement. The diffused gas phase transports through the membrane, which adds a significant mass transfer resistance. Membrane transportation is a two-part process whereby the gas phase is first absorbed by the membrane and then diffuses through the membrane. This process may lead to the separation of the transfer material, which is an advantageous property of membranes for specific product removal. For example, this property would allow separate gas phases to enter the biofilm at different rates or would allow for protein separation (Gottschalk, 2008) or filtration (Ko et al., 2008). Hence,

membrane reactors can be split into permselective and nonpermselective categories (Dudukovic, 1999).

The dissolved gas phase then has to diffuse through the biofilm, and the reaction is allowed to occur. The biofilm is usually attached to the membrane rather than being allowed to float (Henstra et al., 2007). Additional problems are created because any by-products, which may be toxic if they are allowed to concentrate, have to leave the reactor through the same manner. In other words, microbial operation may have significant effects on the gas phase concentrations (gas–liquid mass transfer driving force), which could become an additional restriction on total gas–liquid mass transfer (Kumar et al., 2008).

Membranes can be classified by either geometry (symmetrical or anisotropic) or construction (dense, porous, or composite). Membrane selection becomes the main design criterion for a membrane bioreactor. The membrane can be very dense and complex, which would allow for a high degree of selectivity while microporous materials would allow gas, regardless of identity, to permeate easier. Composite membranes have been developed, which attempt to allow the gas phase to permeate easily while allowing a high degree of selectivity. Biological applications make extensive use of microporous membranes, and some attempts have been made to incorporate composite membranes. The most commonly encountered problem with microporous membranes is that they easily plug, which leads to even higher maintenance costs (Kumar et al., 2008). In such a case, the operation becomes limited by the net material accumulation at or within the membrane. This accumulation can be controlled if the fouling is reversible by backwashing; however, some fouling is irreversible and requires chemical treatment, which would force the membrane bioreactor to be shut down and then restarted after the cleaning procedure (Leiknes and Odegaard, 2007).

Hence, issues have led the membrane bioreactor to be a perfect choice for a select few problems. Interestingly, even with its advantages for those shear-sensitive microorganisms, their industrial viability and application have yet to be proven. In practical terms, membrane bioreactors have to compete with fixed-bed bioreactors, hybrid systems (fixed bed incorporated into an airlift), bubble columns, and airlift reactors, all of which are able to provide much higher gas–liquid mass transfer rates. In other words, production could be optimized within an environment that is less friendly than the membrane bioreactor simply because the higher productivity due to higher amounts of gas–liquid mass transfer could offset the productivity losses due to microorganism shear damage. More information on membrane technology for chemical and biological applications can be found in Baker (2004), Nunes and Peinemann (2006), and Peinemann and Nunes (2008a, 2008b).

10.5 SUMMARY

Novel bioreactors can be represented by many different designs and variations, but the most novel and promising approach may turn out to be miniaturized reactors.

Novel mechanical or bubble-induced flow designs are not trendsetters nor do they solve many of the and gas–liquid mass transfer problems. Miniaturized reactors, however, could decrease process design and implementation significantly. The numbering-up method for these reactors reduces the time and amount of work necessary for scale-up; the process is determined for one experimental unit and then the unit is copied multiple times. The rest of the work is spent on the industrial and economic problems rather than hydrodynamic and gas–liquid mass transfer issues commonly found in scale-up issues for other bioreactors.

11 Figures of Merit

Figures of merit are quantities used to compare reactor performance across all reactor types or just the different designs of stirred-tank bioreactors. This section summarizes some reactor-specific figures of merit and problems that have prevented meaningful and significant figures of merit being developed as well as some possibilities that could be considered for further research. The figures of merit are also oriented toward stirred-tank reactors, bubble columns, and airlift reactors since these are the most common gas–liquid and gas–liquid–solid bioreactors. Fixed bed reactors use a much smaller gas and liquid flow rate so that they are not able to compete with the other reactors unless the microorganisms have to be suspended or otherwise protected.

Figures of merit for stirred-tank reactors are especially difficult because of the wide variety of equipment and arrangements used and the high degree of phase interaction complexity. Although the impeller is always used for gas breakup, mixing, and dispersion, the effects of different impellers, setups, inputs, or microorganisms make universal conclusions on hydrodynamics almost impossible. The varieties of microorganisms also make predictions on production or conversion very difficult. Furthermore, a practical model describing conditions for stirred-tank reactors across wide operational ranges and scales is currently unavailable. Since this underlying information is not available, a figure of merit, which is applicable across a wide variety of designs, control variables, inputs, and microorganisms, is also not easily within reach and rarely addressed in available research.

The task, however, is not impossible. A practical representation of the mass transfer performance is $k_L a/(P_G/\forall_L)$. It represents the mass transfer rate per unit power input. This figure of merit does not attempt to predict output or conversion, but that outcome is implied if the process is still gas–liquid mass transfer limited. If other microorganisms' performance measures are important, a time-dependent representation of output in terms of systems size (e.g., units of mass/liter-hour) can be used. Its downfall is that design or control variables are not accounted for, but it can still be used in tandem with the previous mass transfer-based figure of merit or as a long-term assessment tool.

These measures have not been extended to the different reactor designs, but they certainly could be. A few fundamental issues exist. The first arises from the fact that variable costs differ significantly between the reactor designs. For example, the

An Introduction to Bioreactor Hydrodynamics and Gas-Liquid Mass Transfer, First Edition.
Enes Kadic and Theodore J. Heindel.

power draw in the stirred-tank reactor varies with impeller diameter raised to the fifth power and impeller speed raised to the third power. Hence, increasing the scale of a stirred-tank reactor increases the power usage at a fast pace. At the same time, larger mechanical systems, such as the motor and gear systems, may require more or more expensive maintenance. These properties ultimately lead to the operational cost growing faster than with the bubble column or airlift reactor; however, the stirred-tank reactor may be able to produce smaller bubbles if it is properly designed and setup. As scale increases, a theoretical inflection point may exist at which the advantages of the stirred-tank reactor are surpassed by the power usage and the bubble column or airlift reactor becomes a superior economic alternative. This inflection point has not been studied, and such comparisons between stirred-tank reactors, bubble columns, and/or airlift reactors are very rare. So, such a study could produce a map that could be microorganism specific, which shows the preferred reactor for a given scale and gas or liquid flow rate(s). Many variations and variables would not be included but a process-specific guide could be developed.

A second issue with figures of merit is more of a derived problem. The scale-up procedure for any given reactor design is highly variable. The stirred-tank reactor alone has numerous alternatives such as constant power density, impeller velocity, impeller tip speed, or a variation/combination of these variables. Bubble column scale-up might be even harder since the gas and liquid hydrodynamics are not easily controlled or predicted. The airlift reactor scale-up is perhaps easier due to the more controlled gas and liquid flow patterns. Regardless, the scale-up for each reactor design varies significantly, and, more importantly, the reactors do not have a standard, optimal, or commonly applied and agreed upon scale-up procedure. For example, bubble columns have to be scaled up by increasing the experimental reactor by a factor of 5–10 for each iteration. By approximately 300 l, the reactor is supposed to be scale independent and a pilot plant can be seriously considered. The airlift reactors seem to show this property at a much earlier point, 32 l (see Figure 8.14). The stirred-tank reactor, on the other hand, may never lose its scale dependence (after accounting for the power usage). In other words, comparison of industrial bubble columns and airlift reactors could be well defined, but the experimental and pilot-scaled reactors may not be. Since most research is done with experimental (small) reactors, figures of merit are often not attempted.

It is clear that a defined winner among the reactor designs does not exist. More importantly, the reactors may not be interchangeable and design competition is not clearly defined. The previously discussed issues shed light on the lack of interchangeability. The specific project or process helps to further explain the lack of figures of merit in published research. Many of the reactor applications are process or project specific. Without having an idea of the microorganism requirements or its influence on the liquid properties over time, it may be difficult to predict which reactor would be better without experience. At best, some reactors could be ruled out.

An example of the problem difficulty can be simulated by assuming economic product qualities. Let us assume that the product of interest is highly valuable, and that its quality impacts the earned price significantly. The bioreactor for such a

product should be chosen on its ability to consistently produce the same product quality. In other words, the bioreactor design that can accomplish this task can get away with costing more (feed, maintenance cost, variable cost, capital cost, etc.) on an annualized output basis. Specifically, it can cost more on a marginal or variable basis since the marginal product price would be able to at least cover those expenses. Such a product also implies a certain degree of pricing power on the part of the producer. An example of such production is often encountered with patented products (proteins, antibiotics, medicines, etc.). Such a producer may be perfectly happy employing stirred-tank reactors regardless of scale.

A commoditized product, on the other hand, requires that the marginal product cost be optimize using whatever method works. The producer does not have significant pricing power. If the cost of capital is low or the economies of scale are large, the bioreactor of choice may be quite complicated and the facility may be very large such as many refineries in the United States. If the cost of capital is high, input prices are variable, and the price risks are not easily accounted for, producers may be interested in smaller facilities with a smaller initial investment and higher variable cost such as many of the early ethanol facilities. The bioreactor choice becomes dependent on preference, economic resourcefulness, and a reflection of the producer's risk appetite. The bioreactor selection for such a producer becomes much more important. It should be noted that competitive market theory calls for commodity producers to optimize the marginal cost rather than the average.

Some figures of merit, however, could be defined without accounting for the economic impact and trying to judge a bioreactor's efficiency and feasibility for a given process. The scale of interest for such figures of merit would not be industrial. By the time a process reaches even the pilot stage, the designer has to start considering the economic impact, and the economic decisions become more and more important. The efficiency and feasibility of production has to be decided early in the experimental and scale-up portion of the project. Hence, figures of merit are going to be highly dependent on the bioreactor scale-up procedures and knowledge thereof. So, more research would need to be directed into producing a unified or at least more uniform scale-up procedure set in order to predict and compare the potential output gains between the bioreactors.

Cost analysis is usually implemented based on a previous project that used similar components. A size ratio is introduced to relate the base design to the current design. A scaling factor is used to properly represent the equipment relative to its scale basis. The scale basis is determined by the type of equipment and process and commonly includes flow, volume, area, and power. An installation multiplier is introduced that is based on the material cost and type of equipment. This factor hopes to account for the necessary machining, design, and installation costs. For example, a carbon steel agitator has a multiplier of 1.3 while a stainless steel version has one of 1.2. If different equipment has a higher design and installation cost, such as heat exchangers, they carry a higher multiple (2.1 in this case) (Aden et al., 2002; Wooley et al., 1999).

In order to account for inflation in the monetary supply and fluctuations in equipment costs due to technology and commodity prices, an equipment index, such as

the Chemical Engineering Purchased Equipment Index (CE Index), is used. This index, in particular, is popular because bioreactors are completely based on chemical reactor principles such that the index properly reflects fluctuations for bioreactor equipment. Proper usage should project prices to the year when purchasing decisions and commitments are to be made. A formula for the practice can be summarized by (Aden et al., 2002; Wooley et al., 1999)

$$\text{Cost} = \text{InstalledBaseCost}^{*}\left(\frac{\text{Base}}{\text{Current}}\right)^{\text{ScalingExp}} {}^{*}\text{InstallationFactor}^{*}\left(\frac{\text{CEIndexBase}}{\text{CEIndexCurrent}}\right) \tag{11.1}$$

Equation (11.1) assumes economies of scale, which is only true for relatively cheap materials such as mild steel. If the material is more expensive, this relationship breaks down. For medium material costs ($\sim\$10/\text{kg}$), a break-even point (diminishing returns) develops such that larger reactors prove too expensive in terms of capital, but smaller reactors are too energy intensive such that the variable costs are higher. As the material becomes more expensive, the break-even point shifts toward a smaller scale. The opposite is true for cheaper material costs. Capital and input (labor, electricity, or feed) costs also induce similar behavior. As the cost of capital increases, operators prefer smaller scales such that continued operation is used to pay for variable costs that occur during the same period (may be offset due to payment arrangements). Therefore, lower capital and input costs induce larger scales (Patwardhan and Joshi, 1999).

Economies of scale also explain industrial practices for processes that turn from low viscosity Newtonian to viscous and/or non-Newtonian liquids. If feed costs are reduced, the process is more likely to yield a positive return with scale (Ogut and Hatch, 1988) even though the amount of unused volume and discarded feed would increase as well. The rate of diminishing returns would be dependent on product price(s), material costs, and other input costs (electricity, labor) such that the operator may be inclined to halt operation (Ogut and Hatch, 1988) once the power draw becomes economically unbearable. On the other hand, if input costs are too high, the reactor design would require maximum conversion and recycling, leading to diminishing returns such that the amount of equipment may limit the scale of operation.

Equipment selection and recommendations are dependent on a proper cash flow analysis that includes costs and price shocks to inputs, capital costs (debt facilities, lines of credit), and products (Aden et al., 2002; Patwardhan and Joshi, 1999; Wooley et al., 1999). The ultimate goal hinges on investment criteria. Operation can be optimized to meet a certain level of output, maximize profit, maximize the return on equity/capital, or a combination of those that would depend on the investors and their priorities.

12 Concluding Remarks

The interesting aspect of the bioreactor design developments has been that the different designs are more complementary than competitive in nature. For example, the stirred-tank bioreactor is capable of producing small bubbles, but costs too much to operate at a large scale. The fix has been the bubble column bioreactor. Under certain conditions, the bubble column has too much backmixing. The solution is the airlift reactor. If suspension is necessary, one can use a fixed bed reactor. Ultimately, these relationships may be a significant cause that research work rarely attempts to describe more than two reactor designs. In addition, any comparisons that are done have been accomplished at the experimental scale where the stirred-tank bioreactor weaknesses are not as apparent.

For gas–liquid mass transfer purposes, the stirred-tank bioreactor ranks better than the bubble column or airlift bioreactor, and the bubble column outperforms the airlift bioreactor most of the time. The fixed bed bioreactors cannot compete unless the microorganisms or biological material is highly shear sensitive. On a cost basis, the bubble column is the cheapest followed by the airlift bioreactor. The stirred-tank bioreactors have high power costs associated with impeller scaling, whereas the fixed bed bioreactors tend to have significant pressure drops and packing and maintenance costs. However, the airlift bioreactor is the easiest to scale based on hydrodynamics. The bubble column is harder to scale effectively while the stirred-tank bioreactor has the largest variety of published scale-up procedures. These procedures also tend to have variable success as defined by the process and depend on the reference and final scale.

The ultimate success of the reactor will depend on the comfort and well-being of the microorganisms in the bioreactor. In addition to gas–liquid mass transfer, the bioreactor also has to provide efficient mixing, a friendly shear environment, and proper pressure and temperature controls so that the microorganism output can be optimized. Hence, bioreactor design can have significant variation depending on the microorganism employed by the process.

The information that is available for the different bioreactor designs provides a good understanding of each bioreactor operation, construction, advantages, and disadvantages. These aspects have been summarized qualitatively in Table 12.1 for each reactor design where the relative benefit of a particular reactor type (indicated by the number of "+" signs) or challenge (−) is provided. A summary of some of the less common or novel bioreactor options is presented in Table 12.2.

An Introduction to Bioreactor Hydrodynamics and Gas-Liquid Mass Transfer, First Edition.
Enes Kadic and Theodore J. Heindel.

TABLE 12.1 Bioreactor Comparison with Relative Benefit (+) or Challenge (−)

	Reactor Type	Brief Description	Economics	Operations/ Maintenance	Hydro-dynamics	Design	Scalability	Comments
Gas-liquid	Bubble column (BC)	Column reactor in which the medium is aerated and mixed by gas introduced at its base.	+++	++	++	+++	−−−	Lack of control; high shear gradients; reactor of choice for gas conversion; no moving parts
	Airlift reactor (ALR)	Modified BC with a channel for up- and downflow. Driving force is supplied by a density difference between these sections. More control than BC. Two major variants.						Flow defined by reactor design; minimum fluid level; modifications possible leading to further improvements
	Internal loop airlift reactor (ILALR)	ILALR has an internal flow separator creating channels for up- and downflow.	++	++	+++	++	++	Limited flow control
	External loop airlift reactor (ELALR)	ELALR has distinct conduits for fluid flow which are connected at the base and gas separator sections.	+	+++	+++	++	++	Even more control and design flexibility; better hydrodynamics than ILALR
	Stirred tank reactor (STR)	Mechanically agitated and mixed vessel with flow dependent on impeller design. High power consumption.	−−	−	+++	++	+	High shear gradients; ideally mixed; limited economical operating range
	Packed bed reactors	Reactor in which liquid flows over immobilized solid material also known as packing material. Solids cannot be present in inputor product.						Large units possible; usually counter current configuration which is limited by flooding
	Trickle bed reactor (TBR)	Liquid is sprayed over packing with product extraction at the bottomof the reactor.	+	−−	+	−	+	
	Packed-bubble column (PBC)	Packed BC.	+	−−	+	−	+	Liquid flow is negligible
Gas–liquid–solid	Slurry bubble column (SBC)	G–L–S or G–S bubble column. The G–S SBC has analogous hydrodynamic behavior as the G–S bubbling FBR.	+++	++	+	+++	−−−	
	Fluidized bed reactor (FBR)	Reactor in which the solid phase is suspended in medium.						Many variants are available; usually operated as gas–solid system. Typically not used as bioreactors.
	Bubbling	BC variant that can also be operated in G–S mode.	+++	++	+	+++	−−−	
	Circulating	ALR variant.	++	++	+++	++	++	Internal or external

TABLE 12.2 Summary of Less Important and Novel Bioreactors

	Description	Comments
Others:		
Jet reactors	Reactor in which the liquid (submerged-jet reactor) or gas (ejector reactor) is introduced at a high velocity. Another variant, the venturi scrubber reactor, injects liquid into a high velocity gas stream causing the liquid to atomize.	Large interfacial areas allowing high mass and heat transfer; not applicable to most organic substances
Membrane reactor	G–L–S or G–L reactor in which liquid is diffused through a membrane and converted by the bioflim, which is attached to the membrane, to the final product. Biofouling or clogging is possible. High construction and operating cost.	Four membrane types: microporous, porous, dense, and composite.
Plate columns	Liquid is channeled by plates (such as a muffler and run counter currently with the gas phase. Able to handle large variations in flow rates and high pressures.	Two major variants: bubble-cap and sieve plates
Tube Reactors	Cocurrent BC variant with pipelines or coils serving as guidelines. Very similar to heat exchanger.	horizontal, vertical or coiled; variety of flow regimes
Spray towers/column	Usually treated as a gas–liquid reactor. Liquid is sprayed counter currently to gas flow. Used for corrosive and liquids containing substantial amount of solid materials.	Higher energy usage and capital investment
Torus reactor	Mechanically agitated loop reactor. Lower power consumption, better mixing, and good heat transfer capacity than STR.	Many variants based on different cross-sectional shapes
Wetted wall reactor	Verticalreactor with liquid phase entering at the top and flowing along its wall with gas flowing through its core.	
Novel bioreactors:		
Magnetically stabilized FBR	FBR in which a magnetic field is used to stabilize magnetic particles in the fluidized bed.	
Dually injected turbulent separation FBR	FBR variant in which large and small particles are injected separately allowing for separate residence times.	Size and cost of the reactor are minimized
Continuous centrifugal bioreactor	FBR variant in which cells are fluidized using centrifugal forces. Allows high density cell cultivation.	May not be suitable for three phase fermentation
Inverse FBR	FBR variant in which low density particles with a biofilm are used. The biofilm causes a change in its thickness over time causing the bed to growing downward.	Superior to ALR for aerobic waste water treatment with certain cultures

(*continued*)

TABLE 12.2 (*Continued*)

	Description	Comments
Blenke-cascade reactor	Baffled tower separating the reactor into different sections being mixed by upward flowing gas. Similar to plate columns.	Liquid or liquid–solid mixture can be operated co- or countercurrently
Contained FBR	FBR variant that uses a retaining mesh or grid to contain solids and allow a liquid-only product.	
Double-entry FBR	FBR variant that uses top and bottom inlets to minimize gas logging (gas phase lifts solids to reactor surface).	

13 Nomenclature

a	Gas–liquid interfacial area (per unit liquid volume) (m^2/m^3)
$a(V_b, V_b')$	Coalescence frequency between bubbles of volume V_b and V_b' (s^{-1})
a_e	Effective surface area (per unit liquid volume) (m^2/m^3)
a_s	Surface area of a single element (m^2)
A	Constant (−)
A_d	Downcomer cross-sectional area (m^2)
A_r	Riser cross-sectional area (m^2)
Abs	Absorption value (−)
$b(V_b')$	Breakup frequency of bubbles of volume V_b' (s^{-1})
b_1	Constant (−)
b_2	Constant (−)
B	Constant (−)
B_i	Wall baffle length (m)
B_{ij}	Turbulent modeling coefficient (−)
B_W	Baffle width (m)
c_s	Solid concentration (kg/m^3)
C	Experimental constant; dissolved gas concentration in the liquid phase (−; mol/m^3)
C_B	Experimental constant (−)
C_{BP}	Virtual mass coefficient (−)
C_{BT}	Bubble-induced turbulence constant (−)
C_c	Cell concentration (kg/m^3)
C_{c0}	Initial cell concentration (kg/m^3)
C_{CO}	Carbon monoxide concentration (mol/m^3)
C_D	Drag coefficient (−)
C_E	Gas concentration at the electrode (mol/m^3)
C_i	Impeller clearance from the bottom of an STR (m)
C_L	Experimental constant (−)
C_o	Initial liquid-phase gas concentration (mol/m^3)

An Introduction to Bioreactor Hydrodynamics and Gas-Liquid Mass Transfer, First Edition.
Enes Kadic and Theodore J. Heindel.

C_p	Myoglobin concentration (mol/m^3)
C_s	Substrate concentration (kg/m^3)
$C_{1\epsilon}$, $C_{2\epsilon}$, $C_{\mu,i}$ $k-\epsilon$	Turbulence model parameters (−)
C_2	Constant (−)
C^*	Gas concentration in the gas phase (mol/m^3)
C_∞	Dissolved gas concentration at a steady state (mol/m^3)
d_B	Average bubble diameter (m)
d_d	Downcomer (hydraulic) diameter (m)
d_{disc}	Disc diameter of the disc column (m)
d_D	Draught tube diameter (m)
d_h	Hydraulic diameter of the packing (m)
d_m	Membrane thickness (m)
d_p	Average particle diameter (m)
d_P	Packing diameter (m)
d_R	Reactor diameter; riser diameter (m; m)
d_{SM}	Sauter mean bubble diameter (m)
d_o	Diameter of sparger orifice (m)
D	Diffusivity; constant (m^2/s; −)
D_d	Gas distributor diameter (m)
D_c	Column internal diameter (m)
D_i	Impeller diameter (m)
D_L	Liquid diffusivity; axial dispersion coefficient (m^2/s; m^2/s)
D_m	Membrane diffusion coefficient (m^2/s)
D_R	Reactor diameter (m)
D_T	Tank diameter (m)
e	Constant (−)
E	Constant (−)
E_{ij}	Turbulent energy exchange rate coefficient ($kg/m^3\,s$)
$f(\vec{x}, V_b, t)$	Bubble number density function (m^{-3})
F	Constant; volumetric flow rate (−; m^3/s)
F_f	Coefficient (−)
$\vec{F}_{vm}$	Virtual mass force (N/m^3)
g	Gravitational acceleration (m/s^2)
G_i	Production of turbulent kinetic energy (m^2/s^3)
h_c	Downcomer clearance height (m)
h_{DC}	Critical downcomer sparger distance (m)
h_P	Packing height (m)
h_R	Effective reactor height (m)
H	Static or unaerated liquid height (m)
H_b	Liquid height with bubbling (m)
H_0	Ungassed liquid height (m)
I	Ion strength (g-ion/L)
J	Mass flux ($kg/s\,m^2$)
k_G	Gas-phase mass transfer coefficient (m/s)

k_L	Liquid-phase mass transfer coefficient (m/s)
$k_L a$	Volumetric gas–liquid mass transfer coefficient (s^{-1})
k	Turbulent kinetic energy per unit mass; rate constant (m^2/s^2; s^{-1})
K	Constant (−)
$\overrightarrow{K}_{dc}$	Drag force (N/m^3)
K_{ij}	Interfacial momentum exchange coefficient (kg/m^3)
K_s	Saturation constant (kg/m^3)
L_c	Tube connector length (−)
L_D	Draught tube length (−)
L_h	Reactor height; used by Choi (2001) (−)
L_m	Liquid mass superficial velocity ($kmol/m^2\,s$)
m	Parameter group (−)
$m(V_b')$	Mean number of daughter bubbles produced by breakup of a parent bubble of volume V_b' (−)
n	Constant; exponent (− ; −)
N	Impeller speed (rev/min)
N_A	Avogadro's number (mol^{-1})
N_{CD}	Impeller speed at which a transition in flow regime occurs from loaded to completely dispersed (rev/min)
N_{CSA}	Critical impeller speed for surface aeration (rev/min)
N_F	Flooded regime impeller speed (rev/min)
N_{FL}	Impeller speed at which a transition in flow regime occurs from flooded to loaded (rev/min)
N_R	Gross recirculation regime impeller speed (rev/min)
N_o	Constant (−)
Δp	Pressure drop (Pa)
P	Pressure; power (Pa; W)
$P(V_b, V_b')$	Probability density function of daughter bubbles produced upon breakup of a parent bubble of volume V_b' (m^{-3})
P_B	Bubble pressure (Pa)
P_o	Ungassed impeller power draw (W)
P_g	Gassed impeller power draw (W)
P_{sat}	Saturation pressure (Pa)
P_{TOT}	Total power (W)
P_v	Energy dissipation rate (kW/m^3)
qX	Microbial gas consumption rate (mol/s)
Q_G	Volumetric gas flow rate (m^3/s)
r_B	Bubble radius (m)
r_c	Gas-phase reaction rate at the liquid interface ($mol/m^3\,s$)
r_U	Radius of the gas particle (m)
R	Universal gas constant; source term (kJ/K kmol; kg/m s)

R_A	Gas distributor open area ratio (−)
s	Surface renewal rate; thickness of the sloped metal sheet (s; m)
S_p	Source/sink term due to bubbles being added/subtracted from the bubble class of volume V_b due to pressure change (m^3/s)
S_{ph}	Source/sink term due to bubbles being added/subtracted from the bubble class of volume V_b due to phase change (m^3/s)
S_r	Source/sink term due to bubbles being added/subtracted from the bubble class of volume V_b due to a reaction (m^3/s)
SS	Percent match to saturated carbon monoxide spectrum (%)
t	Time (s)
t_c	Circulation time (s)
t_P	Thickness of expanded metal sheets (m)
T	Temperature; STR tank diameter (°C; m)
T_o	Initial temperature (°C)
T_∞	Final temperature (°C)
$\vec{u}$	Velocity (m/s)
$\vec{u}_b(\vec{x}, V_b, t)$	Local bubble velocity function (m/s)
U_b	Bubble terminal velocity (m/s)
U_c	Mean circulation velocity (m/s)
U_G	Superficial gas velocity (m/s)
U_{Gr}	Riser superficial gas velocity (m/s)
U_L	Superficial liquid velocity (m/s)
U_{Lc}	Liquid circulation velocity (m/s)
U_{Ld}	Superficial liquid velocity in the downcomer (m/s)
U_{Ll}	Peripheral liquid flow rate (kg/m s)
U_{Lr}	Superficial liquid velocity in the riser (m/s)
U_{Ls}	Liquid velocity in the separator (m/s)
U_o	Gas velocity through orifice (m/s)
U_P	Superficial velocity losses to the surroundings (m/s)
U_R	Bubble rise velocity (m/s)
U_{sG}	Average slip velocity (m/s)
U_t	Terminal bubble velocity (m/s)
U_{trans}	Superficial gas velocity at which flow transitions out of the homogeneous flow regime into the transition flow regime (m/s)
U_∞	Terminal rise velocity (m/s)
vvm	Gas volume per unit liquid volume per minute (m^3/m^3 min)
V_b	Bubble volume (m^3)
V_L	Liquid linear velocity; liquid volume (m/s; m^3)
$V_{L,D}$	Downcomer liquid velocity (m/s)

$V_L(0)$	Center-line liquid velocity; used by Zehner (1989) (m/s)
$\forall_g$	Gas volume (m^3)
$\forall_L$	Liquid volume (m^3)
Vol_L	Liquid volume (m^3)
Vol_S	Volume of dissolved carbon monoxide liquid sample (m^3)
Vol_T	Total cuvette liquid volume (m^3)
W	Impeller blade width (m)
W_L	Found in Kantarci et al. (2005) but not defined (−)
W_s	Found in Kantarci et al. (2005) but not defined (−)
x	Constant (−)
$\vec{x}$	Position vector (m)
x_c	Circulation path (m)
y	Distance normal to surface (m)
z	Axial location (m)
Δz	Axial distance (m)

Abbreviations

ALR	Airlift reactor
A-310	Lightnin A-310 axial flow impeller (hydrofoil)
A-315	Lightnin A-315 axial flow impeller (hydrofoil)
BC	Bubble column
BIP	Bubble-induced pressure
BP	Bubble pressure
BPBE	Bubble population balance equation
BT-6	Concave blade disc turbine (radial flow impeller)
Carbopol	Carboxypolymethylene
CFD	Computational fluid dynamics
CMC	Carboxymethylcellulose
CS	Cylindrical sintered sparger
DGD	Dynamic gas disengagement
DNS	Direct numerical simulation
DR	Dilution ratio
DSF	Decision support framework
DT-ILALR	Draught tube airlift reactor
ELALR	External-loop airlift reactor
FBR	Flooded bed reactor; fluidized bed reactor
FP	Fixed packing
GTR	Gas transfer rate
HETP	Height equivalent to a theoretical plate
ILALR	Internal-loop airlift reactor
MCE	Maximum efficiency capacity
NS	Narcissus impeller (radial flow impeller)
PBD	Down-pumping pitched blade turbine
PBR	Packed bed reactor

PBT	Pitched blade disc turbine
PBU	Up-pumping pitched blade turbine
PP	Perforated plate or tube
PS	(Perforated) plane sparger (as cited by Merchuk et al. (1998))
RP	Random packing
RT	Rushton-type impeller (radial flow impeller)
RTD	Residence time distribution
STR	Stirred-tank reactor
TBR	Trickle bed reactor
TX	Techmix 335 (axial flow impeller)
TXD	Down-pumping Techmix 335
TXU	Up-pumping Techmix 335

Greek Symbols

α	Constant; volumetric phase fraction (−; −)
a_{dcp}	Gas holdup at close packing (−)
β	Constant (−)
γ	Shear rate (s^{-1})
δ	Diffusion layer thickness; modified film thickness, $\delta = (\mu_L{}^2/\rho_L{}^2 g)^{1/3}$ (m; m)
δ_{eff}	Liquid-phase film layer (m)
δ_o	Viscous sublayer thickness (m)
ϵ	Overall gas holdup or void fraction; turbulent energy dissipation rate (−; m^2/s^3)
ϵ_b	Baseline gas holdup used by Salvacion et al. (1995) (−)
ϵ_d	Downcomer gas holdup (−)
ϵ_G	Gas holdup (−)
ϵ_L	Liquid void fraction (−)
ϵ_m	Protein extinction coefficient (mol/m)
ϵ_r	Riser gas holdup (−)
ϵ_s	Solid holdup (−)
ϵ_0	Gas holdup at atmospheric pressure used by Kojima et al. (1997) (−)
$\overline{\epsilon}$	Average gas holdup (−)
θ_θ	Contact angle of wettability (degrees)
λ	Cuvette path length (m)
λ_L	Liquid thermal conductivity (W/m K)
μ	Liquid dynamic viscosity; specific cellular growth rate (Pa-s; s^{-1})
μ_a	Apparent dynamic viscosity (Pa-s)
μ_G	Gas dynamic viscosity (Pa-s)
μ_L	Liquid dynamic viscosity (Pa-s)
μ_m	Maximum specific cellular growth rate (s^{-1})

μ_t	Turbulent viscosity (Pa-s)
μ_w	Dynamic viscosity of tap water (Pa-s)
v_L	Liquid kinematic viscosity (m^2/s^2)
ρ	Density (kg/m^3)
ρ_G	Gas density (kg/m^3)
ρ_L	Liquid density (kg/m^3)
ρ_m	Slurry density in the absence of gas (kg/m^3)
ρ_s	Density of solids (kg/m^3)
$\Delta\rho$	Phase density difference (kg/m^3)
σ	Liquid-phase surface tension (mN/m or dyn/cm)
σ_i	Turbulent parameters in $k-\epsilon$ equations (N/m)
σ_w	Surface tension of tap water (mN/m or dyn/cm)
τ	Contact time (s)
$\tau\delta$	Dead time (s)
τ_e	Electrode time constant (s)
τ_g	Gas-phase residence time (s)
$\tau_{i\phi}$	Time constant in turbulent dissipation (s)
τ_w	Wall shear stress (N/m^2)
$\overline{\tau}_w$	Average wall shear stress (N/m^2)
$\overline{\overline{\tau}}$	Effective shear tensor (N/m^3)
φ_s	Volumetric solid fraction (−)

Dimensionless Numbers

Bo	Bond number, $Bo = \rho_L g D_R^2/\sigma$
Fl_G	Gas flow number, $Fl_G = Q_G/ND^3$
Fr	Froude number, $Fr = U_G/\sqrt{gD_R}$
Ga	Galileo number, $Ga = gD_R{}^3/v_L{}^2$
Ga_L	Galileo number, $Ga_L = g\rho_L{}^2/a^3\mu_L{}^2$
Ga_{Lh}	Galileo number, $Ga_{Lh} = gt_P{}^3/\nu_L{}^2$
G	Grashof number, $Gr = d_{Bs}{}^3\rho_L\Delta\rho g/\mu_L{}^2$
Ha	Hatta number, ratio of species absorption with and without reaction
Mo	Morton number, $Mo = g\mu_L{}^4/\rho_L\sigma^3$
Mo_m	Modified Morton number, $Mo_m = (\xi\mu_L)^4 g/\rho_m\sigma^3$ where $\ln\xi = 4.6\epsilon_s\{5.7\epsilon_s^{0.58}\sinh[-0.71\exp(-5.8\epsilon_s)\ln Mo^{0.22}] + 1\}$
N_{Pg}	Gassed power number, $N_{Pg} = P_g/\rho N^3 D^5$
N_{Po}	Ungassed power number, $N_{Po} = P_o/\rho N^3 D^5$
Re	Reynolds number, $Re = \rho ND^2/\mu$
Re_B	Bubble Reynolds number, $Re_B = \rho_c\lvert\vec{u}_d - \vec{u}_c\rvert d_B/\mu_c$
Re_L	Liquid-phase Reynolds number, $Re_L = \rho_L U_L D_R/\mu_L$
Re_{Le}	Reynolds number, $Re_{Le} = 4U_L/a_e\nu_L$
Re_P	Reynolds number used by Mena et al. (2005); defined in terms of particle diameter

Re_T	Reynolds number used by Kantarci et al. (2005); not defined
Sc or Sc_L	Schmidt number, $Sc = \nu_L/D_L$
Sh	Sherwood number, usually $Sh = k_L a d_R/D_L$
Sh_L	Sherwood number, usually $Sh_L = k_L d_P/D_L$
We	Weber number, $We = \rho_L U_L{}^2 D_R/\sigma$

Bibliography

Abashar, M.E., Narsingh, U., Rouillard, A.E., and Judd, R. (1998), "Hydrodynamic flow regimes, gas holdup, and liquid circulation in airlift reactors," *Industrial & Engineering Chemistry Research*, 37: 1251–1259.

Aden, A., Ruth, M., Ibsen, K., Jechura, J., Neeves, K., Sheehan, J., Wallace, B., Montague, L., Slayton, A., and Lukas, J. (2002), *Lignocellulosic biomass to ethanol process design and economics utilizing co-current dilute acid prehydrolysis and enzymatic hydrolysis for corn stover*, Golden, Colorado, National Renewable Energy Laboratory.

Aiba, S., Ohashi, M., and Huang, S.Y. (1968), "Rapid determination of oxygen permeability of polymer membranes," *Industrial & Engineering Chemistry, Fundamentals*, 7(3): 497–502.

Akita, K., and Yoshida, F. (1973), "Gas holdup and volumetric mass transfer coefficient in bubble columns," *Industrial & Engineering Chemistry, Process Design and Development*, 12(1): 76–80.

Akita, K., and Yoshida, F. (1974), "Bubble size, interfacial area, and liquid-phase mass transfer coefficient in bubble columns," *Industrial & Engineering Chemistry, Process Design and Development*, 13(1): 84–91.

Al-Dahhan, M.H., Larachi, F., Dudukovic, M.P., and Laurent, A. (1997), "High-pressure trickle-bed reactors: A review," *Industrial & Engineering Chemistry Research*, 36(8): 3292–3314.

Al-Masry, W.A. (1999), "Effect of liquid volume in the gas-separator on the hydrodynamics of airlift reactors," *Journal of Chemical Technology & Biotechnology*, 74(10): 931–936.

Al-Masry, W.A. (2001), "Gas holdup in circulating bubble columns with pseudoplastic liquids," *Chemical Engineering & Technology*, 24(1): 71–76.

Albijanic, B., Havran, V., Petrovic, L., Duric, M., and Tekic, M.N. (2007), "Hydrodynamics and mass transfer in a draft tube airlift reactor with dilute alcohol solutions," *AIChE Journal*, 53(11): 2897–2904.

Alix, P., and Raynal, L. (2008), "Liquid distribution and liquid hold-up in modern high capacity packings," *Chemical Engineering Research & Design*, 86(6): 585–591.

Álvarez, E., Gomez-Diaz, D., Navaza, J.M., and Sanjurjo, B. (2008), "Continuous removal of carbon dioxide by absorption employing a bubble column," *Chemical Engineering Journal*, 137(2): 251–256.

An Introduction to Bioreactor Hydrodynamics and Gas-Liquid Mass Transfer, First Edition.
Enes Kadic and Theodore J. Heindel.

Álvarez, E., Sanjurjo, B., Cancela, A., and Navaza, J.M. (2000), "Mass transfer and influence of physical properties of solutions in a bubble column," *Chemical Engineering Research & Design*, 78(6): 889–893.

Anabtawi, M.Z.A., Abu-Eishah, S.I., Hilal, N., and Nabhan, M.B.W. (2003), "Hydrodynamic studies in both bi-dimensional and three-dimensional bubble columns with a single sparger," *Chemical Engineering and Processing*, 42(5): 403–408.

Andre, G., Moo-Young, M., and Robinson, C.W. (1981), "Improved method for the dynamic measurement of mass transfer coefficient for application to solid-substrate fermentation," *Biotechnology and Bioengineering*, 23(7): 1611–1622.

Anonymous (2005), "4500-o oxygen (dissolved)," in *Standard Methods for the Examination of Water and Wastewater* 21st Edition, M.A.H. Franson, Editor, New York, American Public Health Association, American Water Works Association, & Water Pollution Control Federation: 4.136–4.143.

Antonini, E., and Brunori, M. (1971), "Memoglobin and myoglobin in their reactions with ligands," in *Frontiers in Biology*, A. Neuberger, and E.L. Tatum, Editors, Amsterdam-London, North-Holland Reserach Monographs. **21**.

Ascanio, G., Castro, B., and Galindo, E. (2004), "Measurement of power consumption in stirred vessels—a review," *Chemical Engineering Research and Design: Transactions of the Institution of Chemical Engineers Part A*, 82(A9): 1282–1290.

Attou, A., Boyer, C., and Ferschneider, G. (1999), "Modelling of the hydrodynamics of the cocurrent gas-liquid trickle flow through a trickle-bed reactor," *Chemical Engineering Science*, 54(6): 785–802.

Azbel, D. (1981), *Two-Phase Flows in Chemical Engineering*, Cambridge University Press, New York.

Azzopardi, B.J., Mudde, R.F., Lo, S., Morvan, H., Yan, Y., and Zhao, D. (2011), *Hydrodynamics of Gas-Liquid Reactors: Normal Operation and Upset Conditions*, West Sussex, UK, John Wiley & Sons.

Bach, H.F., and Pilhofer, T. (1978), "Variation of gas hold-up in bubble columns with physical properties of liquids and operating parameters of columns," *German Chemical Engineering*, 1(5): 270–275.

Baker, R.W. (2004), *Membrane Technology and Applications*, John Wiley & Sons, Ltd., West Sussex, England.

Bakker, A. (1992), "Hydrodynamics of stirred gas-liquid dispersion," PhD Thesis, Delft University of Technology, Delft, The Netherlands.

Bakker, A., and Oshinowo, L.M. (2004), "Modelling of turbulence in stirred vessels using large eddy simulation," *Chemical Engineering Research & Design*, 82(9 SPEC ISS): 1169–1178.

Barakat, T.M.M., and Sorensen, E. (2008), "Simultaneous optimal synthesis, design and operation of batch and continuous hybrid separation processes," *Chemical Engineering Research & Design*, 86(3): 279–298.

Bauer, T., Haase, S., Al-Dahhan, M.H., and Lange, R. (2007), "Paper 559d - Monolithic reactor and particle-packed monolithic reactor for three-phase catalytic reactions", in *The 2007 Annual Meeting*, Salt Lake City, UT, AIChE.

Beck, M.S., and Williams, R.A. (1996), "Process tomography: A European innovation and its applications," *Measurement Science and Technology*, 7: 215–224.

Beenackers, A.A.C.M., and Van Swaaij, W.P.M. (1993), "Mass transfer in gas-liquid slurry reactors," *Chemical Engineering Science*, 48(18): 3109–3139.

Behkish, A., Men, Z., Inga, J.R., and Morsi, B.I. (2002), "Mass transfer characteristics in a large-scale slurry bubble column reactor with organic liquid mixtures," *Chemical Engineering Science*, 57(16): 3307–3324.

Bellgardt, K.-H. (2000a), "Bioprocess models," in *Bioreaction Engineering: Modeling and Control*, K. Schugerl, and K.-H. Bellgardt, Editors, Berlin, Springer: 44–105.

Bellgardt, K.-H. (2000b), *Bioreaction Engineering: Modeling and Control*, Springer, New York City, New York.

Bellgardt, K.-H. (2000c), "Introduction," in *Bioreaction Engineering: Modeling and Control*, K. Schugerl, and K.-H. Bellgardt, Editors, Berlin, Springer: 1–18.

Bello, R.A. (1981), "A characterization study of airlift contactors for applications to fermentation," PhD Thesis, University of Waterloo, Ontario, Canada.

Bello, R.A., Robinson, C.W., and Moo-Young, M. (1984), "Liquid circulation and mixing characteristics of airlift contactors," *Canadian Journal of Chemical Engineering*, 62(5): 573–577.

Bello, R.A., Robinson, C.W., and Moo-Young, M. (1985a), "Gas holdup and overall volumetric oxygen transfer coefficient in airlift contactors," *Biotechnology and Bioengineering*, 27(3): 369–381.

Bello, R.A., Robinson, C.W., and Moo-Young, M. (1985b), "Prediction of the volumetric mass transfer coefficient in pneumatic contactors," *Chemical Engineering Science*, 40(1): 53–58.

Bendjaballah, N., Dhaouadi, H., Poncin, S., Midoux, N., Hornut, J.-M., and Wild, G. (1999), "Hydrodynamics and flow regimes in external loop airlift reactors," *Chemical Engineering Science*, 54(21): 5211–5221.

Bentifraouine, C., Xuereb, C., and Riba, J.-P. (1997a), "Effect of gas liquid separator and liquid height on the global hydrodynamic parameters of an external loop airlift contactor," *Chemical Engineering Science*, 66: 91–95.

Bentifraouine, C., Xuereb, C., and Riba, J.-P. (1997b), "An experimental study of the hydrodynamic characteristics of external loop airlift contactors," *Journal of Chemical Technology & Biotechnology*, 69: 345–349.

Benz, G.T. (2008), "Piloting bioreactors for agitation scale-up," *Chemical Engineering Progress*, 104(2): 32–34.

Beyerlein, S.W., Cossmann, R.K., and Richter, H.J. (1985), "Prediction of bubble concentration profiles in vertical turbulent two-phase flow," *International Journal of Multiphase Flow*, 11(5): 629–641.

Biesheuvel, A., and Gorissen, W.C.M. (1990), "Void fraction disturbances in a uniform bubbly fluid," *International Journal of Multiphase Flow*, 16(2): 211–231.

Billet, R. (1989), "Packed column analysis and design," PhD Thesis, Ruhr-Universität Bochum, Bochum, Germany.

Billet, R. (1993), "Process engineering evaluation of packings and the limits of their development," *Chemie-Ingenieur-Technik*, 65(2): 157–166.

Billet, R., and Schultes, M. (1993), "Physical model for the prediction of liquid hold-up in two-phase countercurrent columns," *Chemical Engineering & Technology*, 16(6): 370–375.

Birch, D., and Ahmed, N. (1996), "Gas sparging in vessels agitated by mixed flow impellers," *Powder Technology*, 88(1): 33–38.

Birch, D., and Ahmed, N. (1997), "The influence of sparger design and location on gas dispersion in stirred vessels," *Chemical Engineering Research & Design*, 75(5): 487–496.

Bisang, J.M. (1997), "Modelling the startup of a continuous parallel plate electrochemical reactor," *Journal of Applied Electrochemistry*, 27(4): 379–384.

Blanch, H.W. and Clark, D.S. (1997), *Biochemical Engineering*, Marcel Dekker, New York.

Blazej, M., Annus, J., and Markos, J. (2004a), "Comparison of gassing-out and pressure-step dynamic methods for $k_l a$ measurement in an airlift reactor with internal loop," *Chemical Engineering Research and Design*, 82(10): 1375–1382.

Blazej, M., Jurascik, M., Annus, J., and Markos, J. (2004b), "Measurement of mass transfer coefficient in an airlift reactor with internal loop using coalescent and non-coalescent liquid media," *Journal of Chemical Technology & Biotechnology*, 79(12): 1405–1411.

Blazej, M., Kisa, M., and Markos, J. (2004c), "Scale influence on the hydrodynamics of an internal loop airlift reactor," *Chemical Engineering and Processing*, 43(12): 1519–1527.

Blenke, H. (1979), "Loop reactors," *Advances in Biochemical Engineering*, 13: 121–214.

Bliem, R., and Katinger, H. (1988a), "Scale-up engineering in animal cell technology: Part I," *Trends in Biotechnology*, 6(8): 190–195.

Bliem, R., and Katinger, H. (1988b), "Scale-up engineering in animal cell technology: Part II," *Trends in Biotechnology*, 6(9): 224–230.

Boden, S., Bieberle, M., and Hampel, U. (2008), "Quantitative measurement of gas hold-up distribution in a stirred chemical reactor using X-ray cone-beam computed tomography," *Chemical Engineering Journal*, 139(2): 351–362.

Bouaifi, M., Hebrard, G., Bastoul, D., and Roustan, M. (2001), "A comparative study of gas hold-up, bubble size, interfacial area, and mass transfer coefficients in stirred gas-liquid reactors and bubble columns," *Chemical Engineering and Processing*, 40(2): 97–111.

Bouaifi, M., and Roustan, M. (2001), "Power consumption, mixing time and homogenisation energy in dual-impeller agitated gas-liquid reactors," *Chemical Engineering and Processing*, 40(2): 87–95.

Boyer, C., Duquenne, A.M., and Wild, G. (2002), "Measuring techniques in gas-liquid and gas-liquid-solid reactors," *Chemical Engineering Science*, 57: 3185–3215.

Branyik, T., Vicente, A.A., Dostalek, P., and Teixeira, J.A. (2005), "Continuous beer fermentation using immobilized yeast cell bioreactor systems," *Biotechnology Progress*, 21(3): 653–663.

Bredwell, M.D., Srivastava, P., and Worden, R.M. (1999), "Reactor design issues for synthesis-gas fermentations," *Biotechnology Progress*, 15(5): 834–844.

Bredwell, M.D., and Worden, R.M. (1998), "Mass-transfer properties of microbubbles: I. Experimental studies," *Biotechnology Progress*, 14(1): 31–38.

Breijer, A.A.J., Nijenhuis, J., and van Ommen, J.R. (2008), "Prevention of flooding in a countercurrent trickle-bed reactor using additional void space," *Chemical Engineering Journal*, 138(1–3): 333–340.

Bridgwater, A.V. (1995), "The technical and economic feasiblity of biomass gasification for power generation," *Fuel*, 74: 631–653.

Broder, D., and Sommerfeld, M. (2003), "Combined PIV/PTV-measurements for the analysis of bubble interactions and coalescence in a turbulent flow," *The Canadian Journal of Chemical Engineering*, 81(3–4): 756–763.

Broekhuis, R.R., Machado, R.M., and Nordquist, A.F. (2001), "The ejector-driven monolith loop reactor: Experiments and modeling," *Catalysis Today*, 69(1–4): 87–93.

Brown, R.C. (2005), "Biomass refineries based on hybrid thermochemical/biological processing – An overview," in *Biorefineries, Biobased Industrial Processes and Products*, B. Kamm, P.R. Gruber, and M. Kamm, Editors, Weinheim, Germany, Wiley-VCH Verlag: 1–24.

Burghardt, A., Bartelmus, G., Jaroszynski, M., and Kolodziej, A. (1995), "Hydrodynamics and mass transfer in a three-phase fixed-bed reactor with cocurrent gas-liquid downflow," *The Chemical Engineering Journal and the Biochemical Engineering Journal*, 58(2): 83–99.

Cabaret, F., Fradette, L., and Tanguy, P.A. (2008), "Gas-liquid mass transfer in unbaffled dual-impeller mixers," *Chemical Engineering Science*, 63(6): 1636–1647.

Cai, J., Nieuwstad, T.J., and Kop, J.H. (1992), "Fluidization and sedimentation of carrier material in a pilot-scale airlift internal-loop reactor," *Water Science & Technology*, 26(9–11): 2481–2484.

Calderbank, P.H. (1958), "Physical rate processes in industrial fermentation. Part I: The interfacial area in gas-liquid contacting with mechanical agitation," *Transactions of IChemE, Part A, Chemical Engineering Research and Design*, 36: 443–463.

Calderbank, P.H., and Moo-Young, M.B. (1961), "The continuous phase heat and mass-transfer properties of dispersion," *Chemical Engineering Science*, 16(1–2): 39–54.

Carroll, J.J. (1991), "What is Henry's law?," *Chemical Engineering Progress*, 87(9): 48–52.

Ceccio, S.L., and George, D.L. (1996), "A review of electrical impedance techniques for the measurement of multiphase flows," *Journal of Fluids Engineering - Transactions of the ASME*, 118: 391–399.

Chakravarty, M., Begum, S., Singh, H.D., Baruah, J.N., and Iyengar, M.S. (1973), "Gas holdup distribution in a gas-lift column," *Biotechnology and Bioengineering Symposium*, 4: 363–378.

Chakravarty, M., Singh, H.D., Baruah, J.N., and Lyengar, M.S. (1974), "Gas holdup distribution in a gas-lift column," *Indian Chemical Engineer*, 16: 17–22.

Chand Eisenmann Metallurgical, (2008), "Spargers," Retrieved August 7, 2008, from http://www.chandeisenmann.com/products/spargers.asp.

Chandrasekharan, K., and Calderbank, P.H. (1981), "Further observations on the scale-up of aerated mixing vessels," *Chemical Engineering Science*, 36(5): 818–823.

Chang, H.N., Halard, B., and Moo-Young, M. (1989), "Measurement of $k_L a$ by a gassing-in method with oxygen-enriched air," *Biotechnology and Bioengineering*, 34(9): 1147–1157.

Chaouki, J., Larachi, F., and Dudukovic, M.P. (eds) (1996), *Non-Invasive Monitoring of Multiphase Flows*, Elsevier, New York.

Chaouki, J., Larachi, F., and Dudukovic, M.P. (1997), "Noninvasive tomography and velocimetric monitoring of multiphase flows," *Industrial & Engineering Chemistry Research*, 36: 4476–4503.

Charpentier, J.-C. (1981), "Mass-transfer rates in gas-liquid absorbers and reactors," in *Advances in Chemical Engineering*, T.B. Drew, G.E. Cokelet, J.W. Hoopes, Jr., and T. Vermeulen, Editors, New York City, New York, Academic Press. **11**: 1–133.

Chaumat, H., Billet-Duquenne, A.M., Augier, F., Mathieu, C., and Delmas, H. (2005), "Mass transfer in bubble column for industrial conditions: Effects of organic medium, gas and liquid flow rates and column design," *Chemical Engineering Science*, 60(22): 5930–5936.

Chen, P., Sanyal, J., and Dudukovic, M.P. (2005), "Numerical simulation of bubble column flows: Effect of different breakup and coalescence closures," *Chemical Engineering Science*, 60: 1085–1101.

Chen, R.C., Reese, J., and Fan, L.S. (1994), "Flow structure in a three-dimensional bubble column and three-phase fluidized bed," *AIChE Journal*, 40(7): 1093–1104.

Chen, Z.D., and Chen, J.J. (1999), "Comparison of mass transfer performance for various single and twin impellers," *Chemical Engineering Research & Design*, 77(2): 104–109.

Cheremisinoff, N.P. (1986), "Measurement techniques for multiphase flows," in *Encyclopedia of Fluid Mechanics Volume 1 - Flow Phenomena and Measurement*, N.P. Cheremisinoff, Editor, Houston, Gulf Publishing Company: 1280–1338.

Chilekar, V.P., Warnier, M.J.F., van der Schaaf, J., Kuster, B.F.M., Schouten, J.C., and van Ommen, J.R. (2005), "Bubble size estimation in slurry bubble columns from pressure fluctuations," *AIChE Journal*, 51(7): 1924–1937.

Chisti, M.Y. (1989), *Airlift Bioreactors*, Elsevier Applied Science, London.

Chisti, M.Y., Halard, B., and Moo-Young, M. (1988a), "Liquid circulation in airlift reactors," *Chemical Engineering Science*, 43(3): 451–457.

Chisti, M.Y., and Moo-Young, M. (1987), "Airlift reactors: Characteristics, applications, and design considerations," *Chemical Engineering Communications*, 60: 195–242.

Chisti, Y., Fujimoto, K., and Moo-Young, M. (1988b), *Biotechnology Progress*, 5: 72–76.

Chisti, Y., and Jauregui-Haza, U.J. (2002), "Oxygen transfer and mixing in mechanically agitated airlift bioreactors," *Biochemical Engineering Journal*, 10(2): 143–153.

Chisti, Y., Kasper, M., and Moo-Young, M. (1990), "Mass transfer in external-loop airlift bioreactors using static mixers," *Canadian Journal of Chemical Engineering*, 68(2): 45–50.

Chisti, Y., and Moo-Young, M. (1986), "Disruption of microbial cells for intracellular products," *Enzyme and Microbial Technology*, 8(4): 194–204.

Cho, J.S., and Wakao, N. (1988), "Determination of liquid-side and gas-side volumetric mass transfer coefficients in a bubble column," *Journal of Chemical Engineering of Japan*, 21(6): 576–581.

Choi, J.H., and Lee, W.K. (1993), "Circulating liquid velocity, gas holdup and volumetric oxygen transfer coefficient in external-loop airlift reactors," *Journal of Chemical Technology & Biotechnology*, 56: 51–58.

Choi, K.H. (2001), "Hydrodynamic and mass transfer characteristics of external-loop airlift reactors without an extension tube above the downcomer," *Korean Journal of Chemical Engineering*, 18(2): 240–246.

Cockx, A., Roustan, M., Line, A., and Hebrard, G. (1995), "Modelling of mass transfer coefficient k_L in bubble columns," *Chemical Engineering Research & Design*, 73(A6): 627–631.

Daly, J.G., Patel, S.A., and Bukur, D.B. (1992), "Measurement of gas holdups and Sauter mean bubble diameters in bubble column reactors by dynamic gas disengagement method," *Chemical Engineering Science*, 47(13/14): 3647–3654.

Dang, N.D.P., Karrer, D.A., and Dunn, I.J. (1977), "Oxygen transfer coefficients by dynamic model moment analysis," *Biotechnology and Bioengineering*, 19(6): 853–865.

Dechsiri, C., Ghione, A., van de Weil, F., Dehling, H.G., Paans, A.M.J., and Hoffmann, A.C. (2005), "Positron emission tomography applied to fluidization engineering," *The Canadian Journal of Chemical Engineering*, 83: 88–96.

Deckwer, W.-D. (1992), *Bubble Column Reactors*, Wiley & Sons, New York, NY.

Delnoij, E., Kuipers, J.A.M., and van Swaaij, W.P.M. (1997a), "Computational fluid dynamics applied to gas-liquid contactors," *Chemical Engineering Science*, 52(21/22): 3623–3638.

Delnoij, E., Kuipers, J.A.M., and van Swaaij, W.P.M. (1997b), "Dynamic simulation of gas-liquid two-phase flow: Effect of column aspect ratio on the flow structure," *Chemical Engineering Science*, 52(21/22): 3759–3772.

Delnoij, E., Lammers, F.A., Kuipers, J.A.M., and van Swaaij, W.P.M. (1997c), "Dynamic simulation of dispersed gas-liquid two-phase flow using a discrete bubble model," *Chemical Engineering Science*, 52(9): 1429–1458.

Demirel, B., and Yenigün, O. (2002), "Two-phase anaerobic digestion processes: A review," *Journal of Chemical Technology & Biotechnology*, 77(7): 743–755.

Deshpande, N.S., Dinkar, M., and Joshi, J.B. (1995), "Disengagement of the gas phase in bubble columns," *International Journal of Multiphase Flow*, 21(6): 1191–1201.

Devanathan, N., Moslemian, D., and Dudukovic, M.P. (1990), "Flow mapping in bubble columns using CARPT," *Chemical Engineering Science*, 45(8): 2285–2291.

Dhaouadi, H., Poncin, S., Hornut, J.M., and Midoux, N. (2008), "Gas-liquid mass transfer in bubble column reactor - Analytical solution and experimental confirmation," *Chemical Engineering and Processing Process Intensification*, 47(4): 548–556.

Díaz, M.E., Montes, F.J., and Galán, M.A. (2008), "Experimental study of the transition between unsteady flow regimes in a partially aerated two-dimensional bubble column," *Chemical Engineering and Processing Process Intensification*, 47(9–10): 1867–1876.

Dijkhuizen, W., Roghair, I., van Sint Annaland, M., and Kuipers, J.A.M. (2010), "DNS of gas bubbles behaviour using an improved 3D front tracking model—model development," *Chemical Engineering Science*, 65(4): 1427–1437.

Doan, H.D., Wu, J., and Eyvazi, M.J. (2008), "Effect of liquid distribution on the organic removal in a trickle bed filter," *Chemical Engineering Journal*, 139(3): 495–502.

Domingues, L., and Teixeira, N.L.J.A. (2000), "Contamination of a high-cell-density continuous bioreactor," *Biotechnology and Bioengineering*, 68(5): 584–587.

Donati, G., and Paludetto, R. (1999), "Batch and semibatch catalytic reactors (from theory to practice)," *Catalysis Today*, 52(2–3): 183–195.

Doran, P.M. (2013), *Bioprocess Engineering Principles*, 2nd edn, Elsevier, Oxford, UK.

Drake, J.B., and Heindel, T.J. (2011), "The repeatability and uniformity of 3D fluidized beds," *Powder Technology*, 213(1–3): 148–154.

Drake, J.B., and Heindel, T.J. (2012), "Local time-average gas holdup comparisons in cold flow fluidized beds with side-air injection," *Chemical Engineering Science*, 68(1): 157–165.

Du, B., Warsito, W., and Fan, L.S. (2006), "Imaging the choking transition in gas-solid risers using electrical capacitance tomography," *Industrial & Engineering Chemistry Research*, 45(15): 5384–5395.

Dudukovic, M.P. (1999), "Trends in catalytic reaction engineering," *Catalysis Today*, 48(1–4): 5–15.

Dudukovic, M.P. (2000), "Opaque multiphase reactors: Experimentation, modeling and troubleshooting," *Oil & Gas Science and Technology*, 55(2): 135–158.

Dudukovic, M.P. (2002), "Opaque multiphase flows: Experiments and modeling," *Experimental Thermal and Fluid Science*, 26(6–7): 747–761.

Dunn, I.J., and Einsele, A. (1975), "Oxygen transfer coefficients by the dynamic method," *Journal of Applied Chemistry and Biotechnology*, 25(9): 707–720.

Dunn, I.J., Heinzle, E., Ingham, J., and Prenosil, J.E. (2003), *Biological Reaction Engineering*, Wiley-VCH, Weinheim.

Ehrfeld, W., Hessel, V., and Lowe, H. (2000), *Microreactors: New Technology for Modern Chemistry*, Wiley-VCH, New York, NY.

Ellenberger, J., and Krishna, R. (1994), "A unified approach to the scale-up of gas-solid fluidized bed and gas-liquid bubble column reactors," *Chemical Engineering Science*, 49(24B): 5391–5411.

Ellenberger, J., and Krishna, R. (2002), "Improving mass transfer in gas-liquid dispersions by vibration excitement," *Chemical Engineering Science*, 57(22–23): 4809–4815.

Fadavi, A., and Chisti, Y. (2005), "Gas-liquid mass transfer in a novel forced circulation loop reactor," *Chemical Engineering Journal*, 112(1–3): 73–80.

Fadavi, A., Chisti, Y., and Chriascarontel, L. (2008), "Bubble size in a forced circulation loop reactor," *Journal of Chemical Technology & Biotechnology*, 83(1): 105–108.

Fair, J.R. (1967), "Designing gas-sparged reactors," *Chemical Engineering*, 74(14): 67–74.

Figueiredo, M.M.L.d., and Calderbank, P.H. (1979), "The scale-up of aerated mixing vessels for specified oxygen dissolution rates," *Chemical Engineering Science*, 34: 1333–1338.

Fogler, H.S. (2005), *Elements of Chemical Reaction Engineering*, Upper Saddle River, NJ, Prentice Hall.

Ford, J.J., Heindel, T.J., Jensen, T.C., and Drake, J.B. (2008), "X-ray computed tomography of a gas-sparged stirred-tank reactor," *Chemical Engineering Science*, 63: 2075–2085.

Franka, N.P., and Heindel, T.J. (2009), "Local time-averaged gas holdup in a fluidized bed with side air injection using X-ray computed tomography," *Powder Technology*, 193: 69–78.

Fransolet, E., Crine, M., Marchot, P., and Toye, D. (2005), "Analysis of gas holdup in bubble columns with non-Newtonian fluid using electrical resistance tomography and dynamic gas disengagement technique," *Chemical Engineering Science*, 60: 6118–6123.

Freitas, C., and Teixeira, J.A. (2001), "Oxygen mass transfer in a high solids loading three-phase internal-loop airlift reactor," *Chemical Engineering Journal*, 84(1): 57–61.

Fu, C.-C., Lu, S.-Y., Hsu, Y.-J., Chen, G.-C., Lin, Y.-R., and Wu, W.-T. (2004), "Superior mixing performance for airlift reactor with a net draft tube," *Chemical Engineering Science*, 59(14): 3021–3028.

Fu, C.-C., Wu, W.-T., and Lu, S.-Y. (2003), "Performance of airlift bioreactors with net draft tube," *Enzyme and Microbial Technology*, 33(4): 332–342.

Fuchs, R., Ryu, D.D.Y., and Humphrey, A.E. (1971), "Effect of surface aeration on scale-up proceedures for fermentation process," *Industrial & Engineering Chemistry Process Design and Development*, 10(2): 190–196.

Fujasova, M., Linek, V., and Moucha, T. (2007), "Mass transfer correlations for multiple-impeller gas-liquid contactors. Analysis of the effect of axial dispersion in gas

and liquid phases on "local" $k_L a$ values measured by the dynamic pressure method in individual stages of the vessel," *Chemical Engineering Science*, 62(6): 1650–1669.

Fujita, S., and Hayakawa, T. (1956), "Liquid-film mass transfer coefficients in packed towers and rod-like irrigation towers," *Kagaku Kogaku*, 20(3): 113–117.

Fukuma, M., Muroyama, K., and Yasunishi, A. (1987), "Specific gas-liquid interfacial area and liquid-phase mass transfer coefficient in a slurry bubble column," *Journal of Chemical Engineering of Japan*, 20(3): 321–324.

Gaddis, E.S. (1999), "Mass transfer in gas-liquid contactors," *Chemical Engineering and Processing*, 38(4–6): 503–510.

Gagnon, H., Lounes, M., and Thibault, J. (1998), "Power consumption and mass transfer in agitated gas-liquid columns: A comparative study," *Canadian Journal of Chemical Engineering*, 76(3): 379–389.

Gamio, J.C., Castro, J., Rivera, L., Alamilla, J., Garcia-Nocetti, F., and Aguilar, L. (2005), "Visualization of gas-oil two-phase flows in pressurized pipes using electrical capacitance tomography," *Flow Measurement and Instrumentation*, 16(2–3): 129–134.

Garcia-Ochoa, F., and Gomez, E. (2009), "Bioreactor scale-up and oxygen transfer rate in microbial processes: An overview," *Biotechnology Advances*, 27(2): 153–176.

Garcia-Ochoa, F.F., and Gomez, E. (1998), "Mass transfer coefficient in stirred tank reactors for xanthan gum solutions," *Biochemical Engineering Journal*, 1(1): 1–10.

Garcia-Ochoa, F.F., and Gomez, E. (2004), "Theoretical prediction of gas-liquid mass transfer coefficient, specific area and hold-up in sparged stirred tanks," *Chemical Engineering Science*, 59(12): 2489–2501.

Garner, A.E., and Heindel, T.J. (2000), "The effect of fiber type on bubble size," *Journal of Pulp and Paper Science*, 26(7): 266–269.

George, D.L., Torczynski, J.R., O'Hern, T.J., Shollenberger, K.A., Tortora, P.R., and Ceccio, S.L. (2001), "Quantitative electrical-impedance tomography in an electrically conducting bubble-column vessel," in *ASME 2001 Fluids Engineering Division Summer Meeting*, New Orleans, LA, ASME Press.

George, D.L., Torczynski, J.R., Shollenberger, K.A., O'Hern, T.J., and Ceccio, S.L. (2000), "Validation of electrical-impedance tomography for measurements of material distribution in two-phase flows," *International Journal of Multiphase Flow*, 26: 549–581.

Gestrich, W., Esenwein, H., and Kraus, W. (1978), "Liquid-side mass transfer coefficient in bubble layers," *International Chemical Engineering*, 18(1): 38–47.

Gestrich, W. and Rahse, W. (1975), "Der relative gasgehalt von blasenschichten," *Chemie-Ingenieur-Technik*, 47(1): 8–13.

Gezork, K.M., Bujalski, W., Cooke, M., and Nienow, A.W. (2000), "The transition from homogeneous to heterogeneous flow in a gassed, stirred vessel," *Chemical Engineering Research & Design*, 78(3): 363–370.

Gezork, K.M., Bujalski, W., Cooke, M., and Nienow, A.W. (2001), "Mass transfer and hold-up characteristics in a gassed, stirred vessel at intensified operating conditions," *Chemical Engineering Research & Design*, 79(8): 965–972.

Gharat, S.D., and Joshi, J.B. (1992), "Transport phenomena in bubble colunm reactor II: Pressure drop," *The Chemical Engineering Journal*, 48(3): 153–166.

Ghirardini, M., Donati, G., and Rivetti, F. (1992), "Gas lift reactors: Hydrodynamics, mass transfer, and scale up," *Chemical Engineering Science*, 47(9–11): 2209–2214.

Giovannettone, J.P., Tsai, E., and Gulliver, J.S. (2009), "Gas void ratio and bubble diameter inside a deep airlift reactor," *Chemical Engineering Journal*, 149(1–3): 301–310.

Glazer, B.T., Marsh, A.G., Stierhoff, K., and Luther III, G.W. (2004), "The dynamic response of optical oxygen sensors and voltammetric electrodes to temporal changes in dissolved oxygen concentrations," *Analytica Chimica Acta*, 518(1–2): 93–100.

Godbole, S.P., Honath, M.F., and Shah, Y.T. (1982), "Holdup structure in highly viscous Newtonian and non-Newtonian liquids in bubble columns," *Chemical Engineering Communications*, 16: 119–134.

Godbole, S.P., and Shah, Y.T. (1986), "Design and operation of bubble column reactors," in *Encyclopedia of Fluid Mechanics: Gas-Liquid Flows*, N.P. Cheremisinoff, Editor, Houston, Gulf Publishing Company. **3**: 1216–1239.

Gogate, P.R., and Pandit, A.B. (1999a), "Mixing of miscible liquids with density differences: Effect of volume and density of the tracer fluid," *Canadian Journal of Chemical Engineering*, 77(5): 988–996.

Gogate, P.R., and Pandit, A.B. (1999b), "Survey of measurement techniques for gas-liquid mass transfer coefficient in bioreactors," *Biochemical Engineering Journal*, 4(1): 7–15.

Gonzalez, J., Aguilar, R., Alvarez-Ramirez, J., and Barren, M.A. (1998), "Nonlinear regulation for a continuous bioreactor via a numerical uncertainty observer," *Chemical Engineering Journal*, 69(2): 105–110.

Gottschalk, U. (2008), "Bioseparation in antibody manufacturing: The good, the bad and the ugly," *Biotechnology Progress*, 24(3): 496–503.

Grover, G.S., Rode, C.V., and Chaudhari, R.V. (1986), "Effect of temperature on flow regime and gas hold-up in a bubble column," *Canadian Journal of Chemical Engineering*, 64(3): 501–504.

Guo, Y.X., Rathor, M.N., and Ti, H.C. (1997), "Hydrodynamics and mass transfer studies in a novel external-loop airlift reactor," *Chemical Engineering Journal*, 67(3): 205–214.

Guy, C., Carreau, P.J., and Paris, J. (1986), "Mixing characteristics and gas hold-up of a bubble column," *Canadian Journal of Chemical Engineering*, 64(1): 23–35.

Hadjiev, D., Sabiri, N.E., and Zanati, A. (2006), "Mixing time in bioreactors under aerated conditions," *Biochemical Engineering Journal*, 27(3): 323–330.

Hall, D.W., Scott, K., and Jachuck, R.J.J. (2001), "Determination of mass transfer coefficient of a cross-corrugated membrane reactor by the limiting-current technique," *International Journal of Heat and Mass Transfer*, 44(12): 2201–2207.

Hallaile, M. (1993), *Biotechnology*, Ben-Gurion University of the Negev, Israel.

Hamidipour, M., Chen, J., and Larachi, F. (2012), "CFD study on hydrodynamics in three-phase fluidized beds—Application of turbulence models and experimental validation," *Chemical Engineering Science*, 78(0): 167–180.

Hammer, H. (1984), *Frontiers in Chemical Reaction Engineering*, Halsted Press, New Delhi, India.

Han, L., and Al-Dahhan, M.H. (2007), "Gas-liquid mass transfer in a high pressure bubble column reactor with different sparger designs," *Chemical Engineering Science*, 62(1–2): 131–139.

Haque, M.W., Nigam, K.D.P., and Joshi, J.B. (1986), "Hydrodynamics and mixing in highly viscous pseudo-plastic non-Newtonian solutions in bubble columns," *Chemical Engineering Science*, 41(9): 2321–2331.

Harnby, N., Edwards, M.F., and Nienow, A.W. (1992), *Mixing in the Process Industry*, Butterworth-Heinemann Ltd. Boston.

Harper, J.C., Christensen, P.A., Egerton, T.A., and Scott, K. (2001), "Mass transport characterization of a novel gas sparged photoelectrochemical reactor," *Journal of Applied Electrochemistry*, 31: 267–276.

Harvel, G.D., Hori, K., Kawanishi, K., and Chang, J.S. (1999), "Cross-sectional void fraction distribution measurements in a vertical annulus two-phase flow by high speed X-ray computed tomography and real-time neutron radiography techniques," *Flow Measurement and Instrumentation*, 10(4): 259–266.

Heijnen, P., and Lukszo, Z. (2006), "Continuous improvement of batch wise operation: A decision support framework," *Production Planning & Control*, 17(4): 355–366.

Heindel, T.J. (1999), "Bubble size measurements in a quiescent fiber suspension," *Journal of Pulp and Paper Science*, 25(3): 104–110.

Heindel, T.J. (2000), "Gas flow regime changes in a bubble column filled with a fiber suspension," *The Canadian Journal of Chemical Engineering*, 78(5): 1017–1022.

Heindel, T.J. (2002), "Bubble size in a cocurrent fiber slurry," *Industrial & Engineering Chemistry Research*, 41(3): 632–641.

Heindel, T.J. (2011), "A review of X-ray flow visualization with applications to multiphase flows," *Journal of Fluids Engineering - Transactions of the ASME*, 133(7): 074001 (16 pages).

Heindel, T.J., and Garner, A.E. (1999), "The effect of fiber consistency on bubble size," *Nordic Pulp and Paper Research Journal*, 14(2): 171–178.

Henstra, A.M., Sipma, J., Rinzema, A., and Stams, A.J. (2007), "Microbiology of synthesis gas fermentation for biofuel production," *Current Opinion in Biotechnology*, 2007(18): 200–206.

Herringe, R.A., and Davis, M.R. (1978), "Flow structure and distribution effects in gas-liquid mixture flows," *International Journal of Multiphase Flow*, 4(5–6): 461–486.

Hewitt, G.F. (1978), *Measurement of Two Phase Flow Parameters*, Academic Press, New York.

Hewitt, G.F. (1982), "Measurement techniques: Overall measurements - measurement of void fraction," in *Handbook of Multiphase Systems*, G. Hetsroni, Editor, New York, Hemisphere Publishing Corp.: Chapter 10.2.1.2.

Hickman, A.D. (1988), "Gas-liquid oxygen transfer and scale-up. A novel experimental technique with results for mass transfer in aerated agitated vessels," in *Proceedings of the 6th European Conference on Mixing*, Pavia, Italy, 369–374.

Hikita, H., Asai, S., Tanigawa, K., Segawa, K., and Kitao, M. (1980), "Gas hold-up in bubble columns," *Chemical Engineering Journal*, 20(1): 59–67.

Hikita, H., Asai, S., Tanigawa, K., Segawa, K., and Kitao, M. (1981), "The volumetric liquid-phase mass transfer coefficient in bubble columns," *Chemical Engineering Journal*, 22(1): 61–69.

Hikita, H., and Kikukawa, H. (1974), "Liquid-phase mixing in bubble columns: Effect of liquid properties," *Chemical Engineering Journal and the Biochemical Engineering Journal*, 8(3): 191–197.

Hikita, H., and Ono, Y. (1959), "Mass transfer into a liquid film flowing over a packing piece," *Kagaku Kogaku*, 23(12): 808–813.

Hills, J.H. (1976), "The operation of a bubble column at high throughputs. I – Gas holdup measurements," *The Chemical Engineering Journal*, 12: 89–99.

Hoffmann, A., Mackowiak, J.F., Gorak, A., Haas, M., Loning, J.M., Runowski, T., and Hallenberger, K. (2007), "Standardization of mass transfer measurements: A basis for the description of absorption processes," *Chemical Engineering Research & Design*, 85(1): 40–49.

Hoffmann, R.A., Garcia, M.L., Veskivar, M., Karim, K., Al-Dahhan, M.H., and Angenent, L.T. (2008), "Effect of shear on performance and microbial ecology of continuously stirred anaerobic digesters treating animal manure," *Biotechnology and Bioengineering*, 100(1): 38–48.

Hol, P.D., and Heindel, T.J. (2005), "Local gas holdup variation in a fiber slurry," *Industrial & Engineering Chemistry Research*, 44: 4778–4784.

Hruby, J. (2002), "Overview of liga microfabrication," in *5th Workshop on High Energy Density and High Power RF*, Snowbird, Utah (USA), American Institute of Physics, 55–62.

Huang, Z.-B., and Cheng, Z.-M. (2011), "Determination of liquid multiscale circulation structure in a bubble column by tracing the liquid flowing trajectory," *Industrial & Engineering Chemistry Research*, 50(21): 11843–11852.

Hubers, J.L., Striegel, A.C., Heindel, T.J., Gray, J.N., and Jensen, T.C. (2005), "X-ray computed tomography in large bubble columns," *Chemical Engineering Science*, 60(22): 6124–6133.

Hughmark, G.A. (1967), "Holdup and mass transfer in bubble columns," *Industrial & Engineering Chemistry Process Design and Development*, 6(2): 218–220.

Idogawa, K., Ikeda, K., Fukuda, T., and Morooka, S. (1987), "Effect of gas and liquid properties on the behavior of bubbles in a column under high pressure," *International Chemical Engineering*, 27(1): 93–99.

Ismail, I., Gamio, J.C., Bukhari, S.F.A., and Yang, W.Q. (2005), "Tomography for multi-phase flow measurement in the oil industry," *Flow Measurement and Instrumentation*, 16(2–3): 145–155.

Ityokumbul, M.T., Kosaric, N., and Bulani, W. (1994), "Gas hold-up and liquid mixing at low and intermediate gas velocities: 1. Air-water system," *The Chemical Engineering Journal and The Biochemical Engineering Journal*, 53(3): 167–172.

Jade, A.M., Jayaraman, V.K., Kulkarni, B.D., Khopkar, A.R., Ranade, V.V., and Sharma, A. (2006), "A novel local singularity distribution based method for flow regime identification: Gas-liquid stirred vessel with Rushton turbine," *Chemical Engineering Science*, 61(2): 688–697.

Jakobsen, H.A., Lindborg, H., and Dorao, C.A. (2005a), "Modeling of bubble column reactors: Progress and limitations," *Industrial & Engineering Chemistry Research*, 44: 5107–5151.

Jakobsen, H.A., Lindborg, H., and Dorao, C.A. (2005b), "Modeling of bubble column reactors: Progress and limitations," *Industrial & Engineering Chemistry Research*, 44(14): 5107–5151.

Jean, R.-H., and Fan, L.-S. (1987), "On the particle terminal velocity in a gas-liquid medium with liquid as the continuous phase," *Canadian Journal of Chemical Engineering*, 65(6): 881–886.

Jia, X., Wen, J., Feng, W., and Yuan, Q. (2007), "Local hydrodynamics modeling of a gas-liquid-solid three-phase airlift loop reactor," *Industrial & Engineering Chemistry Research*, 46(15): 5210–5220.

Jin, H., Yang, S., He, G., Guo, Z., and Tong, Z. (2005), "An experimental study of holdups in large-scale p-xylene oxidation reactors using the γ-ray attenuation approach," *Chemical Engineering Science*, 60: 5955–5961.

Jones, S.T. (2007), "Gas-liquid mass transfer in an external airlift loop reactor for syngas fermentation," PhD Thesis, Iowa State University, Ames, Iowa.

Jones, S.T., and Heindel, T.J. (2007), "A review of dissolved oxygen concentration measurement methods for biological fermentations", in *ASABE Annual Meeting*, Minneapolis, Minnesota, ASABE: 2–15.

Jordan, U., and Schumpe, A. (2001), "The gas density effect on mass transfer in bubble columns with organic liquids," *Chemical Engineering Science*, 56(21–22): 6267–6272.

Jordan, U., Terasaka, K., Kundu, G., and Schumpe, A. (2002), "Mass transfer in high-pressure bubble columns with organic liquids," *Chemical Engineering & Technology*, 25(3): 262–265.

Joshi, J.B. (2001), "Computational flow modelling and design of bubble column reactors," *Chemical Engineering Science*, 56: 5893–5933.

Joshi, J.B., Ranade, V.V., Gharat, S.D., and Lele, S.S. (1990), "Sparged loop reactors," *The Canadian Journal of Chemical Engineering*, 68(October): 705–741.

Joshi, J.B., and Sharma, M.M. (1979), "Circulation cell model for bubble columns," *Chemical Engineering Research & Design*, 57(4): 244–251.

Kak, A.C., and Slaney, M. (1988), *Principles of Computerized Tomographic Imaging*, Society of Industrial and Applied Mathematics, New York.

Kang, Y., Cho, Y.J., Woo, K.J., and Kim, S.D. (1999), "Diagnosis of bubble distribution and mass transfer in pressurized bubble columns with viscous liquid medium," *Chemical Engineering Science*, 54(21): 4887–4893.

Kantarci, N., Borak, F., and Ulgen, K.O. (2005), "Bubble column reactors," *Process Biochemistry*, 40(7): 2263–2283.

Kantzas, A. (1994), "Computation of holdups in fluidized and trickle beds by computer-assisted tomography," *AIChE Journal*, 40(7): 1254–1261.

Kapic, A. (2005), "Mass transfer measurements for syngas fermentation," MS Thesis, Iowa State University, Ames, Iowa.

Kapic, A., and Heindel, T.J. (2006), "Correlating gas-liquid mass transfer in a stirred-tank reactor," *Chemical Engineering Research & Design*, 84(3A): 239–245.

Kapic, A., Jones, S.T., and Heindel, T.J. (2006), "Carbon monoxide mass transfer in a syngas mixture," *Industrial & Engineering Chemistry Research*, 45(26): 9150–9155.

Kara, S., Kelkar, B.G., Shah, Y.T., and Carr, N.L. (1982), "Hydrodynamics and axial mixing in a three-phase bubble column," *Industrial and Engineering Chemistry Process Design and Development*, 21: 584–594.

Karamanev, D.G., Chavarie, C., and Samson, R. (1996), "Hydrodynamics and mass transfer in an airlift reactor with a semipermeable draft tube," *Chemical Engineering Science*, 51(7): 1173–1176.

Kasatkin, A.G., and Ziparis, I.N. (1952) *Chim Prom*, 7, 203.

Kashiwa, B.A., Padial, N.T., Rauenzahn, R.M., and VanderHeyden, W.B. (1993), "Cell-centered ice method for multiphase flow simulations", U.S. Department of Energy, Los Alamos National Laboratory, Report: LA-UR-93-3922.

Kato, Y., and Nishiwaki, A. (1972), "Longitudinal dispersion coefficient of a liquid in a bubble column," *International Journal of Chemical Reactor Engineering*, 12(1): 182–187.

Kawase, Y., Halard, B., and Moo-Young, M. (1987), "Theoretical prediction of volumetric mass transfer coefficients in bubble columns for Newtonian and non-Newtonian fluids," *Chemical Engineering Science*, 42(7): 1609–1617.

Kawase, Y., and Moo-Young, M. (1986a), "Influence of non-Newtonian flow behaviour on mass transfer in bubble columns with and without draft tubes," *Chemical Engineering Communications*, 40(1–6): 67–83.

Kawase, Y., and Moo-Young, M. (1986b), "Mixing and mass transfer in concentric-tube airlift fermenters: Newtonian and non-Newtonian media," *Journal of Chemical Technology and Biotechnology*, 36(11): 527–538.

Kawase, Y., and Moo-Young, M. (1987), "Heat transfer in bubble column reactors with Newtonian and non-Newtonian fluids," *Chemical Engineering Research & Design*, 65(2): 121–126.

Kawase, Y., and Moo-Young, M. (1988), "Volumetric mass transfer coefficients in aerated stirred tank reactors with Newtonian and non-Newtonian media," *Chemical Engineering Research & Design*, 66(3): 284–288.

Kawase, Y., and Moo-Young, M. (1992), "Correlations for liquid-phase mass transfer coefficient in bubble column reactor with Newtonian and non-Newtonian fluids," *Canadian Journal of Chemical Engineering*, 70(1): 48–54.

Kawase, Y., Tsujimura, M., and Yamaguchi, T. (1995), Gas hold-up in external-loop airlift bioreactors. *Bioprocess and Biosystems Engineering*, 12(1–2): 21–27.

Kawase, Y., Umeno, S., and Kumagai, T. (1992), "The prediction of gas hold-up in bubble column reactors: Newtonian and non-Newtonian fluids," *Chemical Engineering Journal*, 50(1): 1–7.

Keitel, G., and Onken, U. (1981), "Errors in the determination of mass transfer in gas-liquid dispersions," *Chemical Engineering Science*, 36(12): 1927–1932.

Kemblowski, Z., Przywarski, J., and Diab, A. (1993), "An average gas hold-up and liquid circulation velocity in airlift reactors with external loop," *Chemical Engineering Science*, 48(23): 4023–4035.

Kertzscher, U., Seeger, A., Affeld, K., Goubergrits, L., and Wellnhofer, E. (2004), "X-ray based particle tracking velocimetry - A measurement technique for multi-phase flows and flows without optical access," *Flow Measurement and Instrumentation*, 15(4): 199–206.

Khopkar, A.R., Rammohan, A.R., Ranade, V.V., and Dudukovic, M.P. (2005), "Gas-liquid flow generated by a rushton turbine in stirred vessel: CARPT/CT measurements and CFD simulations," *Chemical Engineering Science*, 60(8–9): 2215–2229.

Khudenko, B.M., and Shpirt, E. (1986), "Hydrodynamic parameters of diffused air systems," *Water Research*, 20(7): 905–915.

Kiambi, S.L., Kiriamiti, H.K., and Kumar, A. (2011), "Characterization of two phase flows in chemical engineering reactors," *Flow Measurement and Instrumentation*, 22(4): 265–271.

Kim, D.J., and Chang, H.N. (1989), "Dynamic measurement of $k_L a$ with oxygen-enriched air during fermentation," *Journal of Chemical Technology and Biotechnology*, 45(1): 39–44.

Kim, S.D., Baker, C.G.J., and Bergougnou, M.A. (1972), "Hold-up and axial mixing characteristics of two and three phase fluidized beds," *Canadian Journal of Chemical Engineering*, 50(6): 695–691.

Kluytmans, J.H.J., Kuster, B.F.M., and Schouten, J.C. (2001), "Gas holdup in a slurry bubble column: Influence of electrolyte and carbon particles," *Industrial & Engineering Chemistry Research*, 40(23): 5326–5333.

Ko, C.-H., Chiang, P.-N., Chiu, P.-C., Liu, C.-C., Yang, C.-L., and Shiau, I.-L. (2008), "Integrated xylitol production by fermentation of hardwood wastes," *Journal of Chemical Technology & Biotechnology*, 83(4): 534–540.

Koch, H.A., Stutzman, L.F., Blum, L.F., and Hutchings, H.A. (1949), "Liquid transfer coefficients for the carbon dioxide-air-water system," *Chemical Engineering Progress*, 45(11): 677–682.

Koeneke, R., Comte, A., Juergens, H., Kohls, O., Lam, H., and Scheper, T. (1999), "Fiber optic oxygen sensors for use in biotechnology, environmental, and food industries," *Chemical Engineering and Technology*, 22(8): 666–671.

Kohls, O., and Scheper, T. (2000), "Setup of a fiber optical oxygen multisensor-system and its applications in biotechnology," *Sensors and Actuators, B: Chemical*, 70(1–3): 121–130.

Koide, K., Horibe, K., Kawabata, H., and Ito, S. (1985), "Gas holdup and volumetric liquid-phase mass transfer coefficient in solid-suspended bubble column with draught tube," *Journal of Chemical Engineering of Japan*, 18(3): 248–254.

Koide, K., Kimura, M., Nitta, H., and Kawabata, H. (1988), "Liquid circulation in bubble column with draught tube," *Journal of Chemical Engineering of Japan*, 21(4): 393–399.

Koide, K., Kurematsu, K., Iwamoto, S., Iwata, Y., and Horibe, K. (1983a), "Gas holdup and volumetric liquid-phase mass transfer coefficient in bubble column with draught tube and with gas dispersion into tube," *Journal of Chemical Engineering of Japan*, 16(5): 413–418.

Koide, K., Morooka, S., Ueyama, K., Matsuura, A., Yamashita, F., Iwamoto, S., Kato, Y., Inoue, H., Shigeta, M., Suzuki, S., and Akehata, T. (1979), "Behavior of bubbles in large scale bubble column," *Journal of Chemical Engineering of Japan*, 12(2): 98–104.

Koide, K., Sato, H., and Iwamoto, S. (1983b), "Gas holdup and volumetric liquid-phase mass transfer coefficient in bubble column with draught tube and with gas dispersion into annulus," *Journal of Chemical Engineering of Japan*, 16(5): 407–413.

Koide, K., Takazawa, A., Komura, M., and Matsunaga, H. (1984), "Gas holdup and volumetric liquid-phase mass transfer coefficient in solid-suspended bubble columns," *Journal of Chemical Engineering of Japan*, 17(5): 459–466.

Kojima, H., Sawai, J., and Suzuki, H. (1997), "Effect of pressure on volumetric mass transfer coefficient and gas holdup in bubble column," *Chemical Engineering Science*, 52(21–22): 4111–4116.

Kolev, N. (1976), "Wirkungsweise von füllkörperschüttungen," *Chemie-Ingenieur-Technik*, 48(12): 1105–1112.

Kolev, N. (2006), *Packed Bed Columns: For Absorption, Desorption, Rectification and Direct Heat Transfer*, Elsevier, Amsterdam, The Netherlands.

Kolev, N., and Daraktschiev, R. (1976), "Issledobanie massoobmena w gorizontalbnoi listowoi nasadke," *Theoretical Fundamentals of Chemical Technology*, 10(4): 611–614.

Kolev, N., and Nakov, S. (1994), "Performance characteristics of a packing with boundary layer turbulizers. III. Liquid film controlled mass transfer," *Chemical Engineering and Processing*, 33(6): 437–442.

Kolev, N., and Semkov, K. (1983), "Axial mixing in the liquid phase in packed columns," *Verfahrenstechnik*, 17(8): 474–479, 488.

Krevelen, D.V.V., and Hoftijzer, P.J. (1948), "Kinetics of simultaneous absorption and chemical reaction," *Chemical Engineering Progress*, 44(7): 529–536.

Krishna, R., De Swart, J.W.A., Ellenberger, J., Martina, G.B., and Maretto, C. (1997), "Gas holdup in slurry bubble columns: Effect of column diameter and slurry concentrations," *AIChE Journal*, 43(2): 311–316.

Krishna, R., and Ellenberger, J. (1996), "Gas holdup in bubble column reactors operating in the churn-turbulent flow regime," *AIChE Journal*, 42(9): 2627–2634.

Krishna, R., Urseanu, M.I., de Swart, J.W.A., and Ellenberger, J. (2000), "Gas hold-up in bubble columns: Operation with concentrated slurries versus high viscosity liquid," *The Canadian Journal of Chemical Engineering*, 78(6): 442–448.

Krishna, R., Urseanu, M.I., van Baten, J.M., and Ellenberger, J. (1999), "Influence of scale on the hydrodynamics of bubble columns operating in the churn-turbulent regime: Experiments vs. Eulerian simulations," *Chemical Engineering Science*, 54(21): 4903–4911.

Krishna, R., van Baten, J.M., and Urseanu, M.I. (2001), "Scale effects on the hydrodynamics of bubble columns operating in the homogeneous flow regime," *Chemical Engineering & Technology*, 24(5): 451–458.

Kulkarni, A.A., Ekambara, K., and Joshi, J.B. (2007), "On the development of flow pattern in a bubble column reactor: Experiments and CFD," *Chemical Engineering Science*, 62(4): 1049–1072.

Kumar, A., Degaleesan, T.E., Laddha, G.S., and Hoelscher, H.E. (1976), "Bubble swarm characteristics in bubble columns," *Canadian Journal of Chemical Engineering*, 54(6): 503–508.

Kumar, A., Dewulf, J., and Van Langenhove, H. (2008), "Membrane-based biological waste gas treatment," *Chemical Engineering Journal*, 136(2–3): 82–91.

Kumar, S.B., and Dudukovic, M.P. (1996), "Computer assisted gamma and X-ray tomography: Applications to multiphase flow systems," in *Non-Invasive Monitoring of Multiphase Flows*, J. Chaouki, F. Larachi, and M.P. Dudukovic, Editors, New York, Elsevier: 47–103.

Kumar, S.B., Dudukovic, M.P., and Toseland, B.A. (1997), "Measurement techniques for local and global fluid dynamic quantities in two and three phase systems," in *Non-Invasive Monitoring of Multiphase Flows*, J. Chaouki, F. Larachi, and M.P. Dudukovic, Editors, New York, Elsevier: 1–45.

Kumar, S.B., Moslemian, D., and Dudukovic, M.P. (1995), "A γ-ray tomographic scanner for imaging voidage distribution in two-phase flow systems," *Flow Measurement and Instrumentation*, 6(1): 61–73.

Kundu, S., Premer, S.A., Hoy, J.A., Trent, J.T., and Hargrove, M.S. (2003), "Direct measurements of equilibrium constants for high-affinity hemoglobins," *Biophysical Journal*, 84(6): 3931–3940.

Laari, A., and Turunen, I. (2005), "Prediction of coalescence properties of gas bubbles in a gas-liquid reactor using persistence time measurements," *Chemical Engineering Research & Design*, 83(7): 881–886.

Lance, M., and Bataille, J. (1991), "Turbulence in the liquid phase of a uniform bubbly air–water flow," *Journal of Fluid Mechanics*, 222: 95–118.

Larachi, F., Levesque, S., and Grandjean, B.P.A. (2008), "Seamless mass transfer correlations for packed beds bridging random and structured packings," *Industrial & Engineering Chemistry Research*, 47(9): 3274–3284.

Lau, R., Peng, W., Velazquez-Vargas, L.G., Yang, G.Q., and Fan, L.S. (2004), "Gas-liquid mass transfer in high-pressure bubble columns," *Industrial & Engineering Chemistry Research*, 43(5): 1302–1311.

Law, D., Battaglia, F., and Heindel, T.J. (2008), "Model validation for low and high superficial gas velocity bubble column flows," *Chemical Engineering Science*, 63(18): 4605–4616.

Lee, D.-H., Grace, J.R., and Epstein, N. (2000), "Gas holdup for high gas velocities in a gas-liquid cocurrent upward-flow system," *Canadian Journal of Chemical Engineering*, 78(5): 1006–1010.

Lee, D.J., Luo, X., and Fan, L.-S. (1999), "Gas disengagement technique in a slurry bubble column operated in the coalesced bubble regime," *Chemical Engineering Science*, 54: 2227–2236.

Lee, Y.H., and Luk, S. (1983), "Aeration," *Annual Reports on Fermentation Processes*, 6: 101–147.

Lee, Y.H., and Tsao, G.T. (1979), "Dissolved oxygen electrodes," *Advances in Biochemical Engineering*, 13: 35–86.

Leiknes, T., and Odegaard, H. (2007), "The development of a biofilm membrane bioreactor," *Desalination*, 202(1–3): 135–143.

León-Becerril, E., Cockx, A., and Liné, A. (2002), "Effect of bubble deformation on stability and mixing in bubble columns," *Chemical Engineering Science*, 57(16): 3283–3297.

León-Becerril, E., and Liné, A. (2001), "Stability analysis of a bubble column," *Chemical Engineering Science*, 56(21–22): 6135–6141.

Letzel, H.M., Schouten, J.C., Krishna, R., and van den Bleek, C.M. (1999), "Gas holdup and mass transfer in bubble column reactors operated at elevated pressure," *Chemical Engineering Science*, 54(13–14): 2237–2246.

Levin, Y., and Flores-Mena, J.E. (2001), "Surface tension of strong electrolytes," *Europhysics Letters*, 56(2): 187–192.

Li, G.Q., Yang, S.Z., Cai, Z.L., and Chen, J.Y. (1995), "Mass transfer and gas-liquid circulation in an airlift bioreactor with viscous non-Newtonian fluids," *The Chemical Engineering Journal and the Biochemical Engineering Journal*, 56(2): b101–b107.

Li, H., and Prakash, A. (1997), "Heat transfer and hydrodynamics in a three-phase slurry bubble column," *Industrial & Engineering Chemistry Research*, 36(11): 4688–4694.

Li, H., and Prakash, A. (2000), "Influence of slurry concentrations on bubble population and their rise velocities in a three-phase slurry bubble column," *Powder Technology*, 113(1–2): 158–167.

Liao, Q., Tian, X., Chen, R., and Zhu, X. (2008), "Mathematical model for gas-liquid two-phase flow and biodegradation of a low concentration volatile organic compound (VOC) in a trickling biofilter," *International Journal of Heat and Mass Transfer*, 51(7–8): 1780–1792.

Lin, T.-J., Tsuchiya, K., and Fan, L.-S. (1998), "Bubble flow characteristics in bubble columns at elevated pressure and temperature," *AIChE Journal*, 44(3): 545–560.

Linek, V. (1972), "Determination of aeration capacity of mechanically agitated vessels by fast response oxygen probe," *Biotechnology and Bioengineering*, 14(2): 285–289.

Linek, V. (1988), *Measurement of Oxygen by Membrane-Covered Probes: Guidelines for Applications in Chemical and Biochemical Engineering*, Halsted Press, New York.

Linek, V., Benes, F., and Hovorka, F. (1981), "Role of interphase nitrogen transport in the dynamic measurement of the overall volumetric mass transfer coefficient in air-sparged systems," *Biotechnology and Bioengineering*, 23(2): 301–319.

Linek, V., Benes, P., and Sinkule, J. (1990), "Critical assessment of the steady-state Na_2SO_3 feeding method for k_La measurements in fermentors," *Biotechnology and Bioengineering*, 35(8): 766–770.

Linek, V., Benes, P., and Sinkule, J. (1991a), "Hollow blade agitator for mass transfer in gas-liquid bioreactors," *Food and Bioproducts Processing*, 69(3): 145–148.

Linek, V., Benes, P., Sinkule, J., and Moucha, T. (1993), "Non-ideal pressure step method for k_La measurement," *Chemical Engineering Science*, 48(9): 1593–1599.

Linek, V., Benes, P., and Vacek, V. (1979), "Oxygen probe dynamics in flowing fluids," *Industrial & Engineering Chemistry, Fundamentals*, 18(3): 240–245.

Linek, V., Benes, P., and Vacek, V. (1984), "Experimental study of oxygen probe linearity and transient characteristics in the high oxygen concentration range," *Journal of Electroanalytical Chemistry and Interfacial Electrochemistry*, 169(1–2): 233–257.

Linek, V., Benes, P., and Vacek, V. (1989), "Dynamic pressure method for k_La measurement in large-scale bioreactors," *Biotechnology and Bioengineering*, 33(11): 1406–1412.

Linek, V., Kordac, M., Fujasova, M., and Moucha, T. (2004), "Gas-liquid mass transfer coefficient in stirred tanks interpreted through models of idealized eddy structure of turbulence in the bubble vicinity," *Chemical Engineering and Processing*, 43(12): 1511–1517.

Linek, V., Kordac, M., and Moucha, T. (2005a), "Mechanism of mass transfer from bubbles in dispersions: Part II. Mass transfer coefficients in stirred gas-liquid reactor and bubble column," *Chemical Engineering and Processing*, 44(1): 121–130.

Linek, V., Moucha, T., Dousova, M., and Sinkule, J. (1994), "Measurement of k_La by dynamic pressure method in pilot-plant fermentor," *Biotechnology and Bioengineering*, 43(6): 477–482.

Linek, V., Moucha, T., and Kordac, M. (2005b), "Mechanism of mass transfer from bubbles in dispersions: Part I. Danckwerts' plot method with sulphite solutions in the presence of viscosity and surface tension changing agents," *Chemical Engineering and Processing*, 44(3): 353–361.

Linek, V., Moucha, T., and Sinkule, J. (1996a), "Gas-liquid mass transfer in vessels stirred with multiple impellers–I. Gas-liquid mass transfer characteristics in individual stages," *Chemical Engineering Science*, 51(12): 3203–3212.

Linek, V., Moucha, T., and Sinkule, J. (1996b), "Gas-liquid mass transfer in vessels stirred with multiple impellers–II. Modelling of gas-liquid mass transfer," *Chemical Engineering Science*, 51(15): 3875–3879.

Linek, V., and Sinkule, J. (1990), "Comments on validity of dynamic measuring methods of oxygen diffusion coefficients in fermentation media with polarographic oxygen electrodes," *Biotechnology and Bioengineering*, 35(10): 1034–1041.

Linek, V., Sinkule, J., and Benes, P. (1991b), "Critical assessment of gassing-in methods for measuring k_La in fermentors," *Biotechnology and Bioengineering*, 38(4): 323–330.

Linek, V., Sinkule, J., and Benes, P. (1992), "Critical assessment of the dynamic double-response method for measuring $k_L a$. Experimental elimination of dispersion effects," *Chemical Engineering Science*, 47(15–16): 3885–3894.

Linek, V., Sinkule, J., and Vacek, V. (1985), "Dissolved oxygen probes," in *Comprehensive Biotechnology*, Oxford, England, Pergamon Press, 4: 363–394.

Linek, V., Vacek, V., and Benes, P. (1987), "A critical review and experimental verification of the correct use of the dynamic method for the determination of oxygen transfer in aerated agitated vessels to water, electrolyte solutions and viscous liquids," *Chemical Engineering Journal*, 34(1): 11–34.

Lines, P.C. (1999), "Gas-liquid mass transfer: Surface aeration in stirred vessels with dual impellers," *Institution of Chemical Engineers Symposium Series*, 146: 199–216.

Lines, P.C. (2000), "Gas-liquid mass transfer using surface-aeration in stirred vessels, with dual impellers," *Chemical Engineering Research & Design*, 78(3): 342–347.

Liu, T.-J. (1997), "Investigation of the wall shear stress in vertical bubbly flow under different bubble size conditions," *International Journal of Multiphase Flow*, 23(6): 1085–1109.

Llamas, J.-D., Pérat, C., Lesage, F., Weber, M., D'Ortona, U., and Wild, G. (2008), "Wire mesh tomography applied to trickle beds: A new way to study liquid maldistribution," *Chemical Engineering and Processing Process Intensification*, 47(9–10): 1765–1770.

Lo, C.-S., and Hwang, S.-J. (2003), "Local hydrodynamic properties of gas phase in an internal-loop airlift reactor," *Chemical Engineering Journal*, 91(1): 3–22.

Lockett, M.J., and Kirkpatrick, R.D. (1975), "Ideal bubbly flow and actual flow in bubble columns," *Transactions of the Institution of Chemical Engineers*, 1975(53): 267–273.

Lopez, J.L., Rodriguez Porcel, E.M., Oller Alberola, I., Ballesteros Martin, M.M., Sanchez Perez, J.A., Fernandez Sevilla, J.M., and Chisti, Y. (2006), "Simultaneous determination of oxygen consumption rate and volumetric aoxygen transfer coefficient in pnuematically agitated airlift bioreactors," *Industrial & Engineering Chemistry Research*, 2006: 1167–1171.

Lorenz, O., Schumpe, A., Ekambara, K., and Joshi, J.B. (2005), "Liquid phase axial mixing in bubble columns operated at high pressures," *Chemical Engineering Science*, 60(13): 3573.

Löwe, H., Ehrfeld, W., Hessel, V., Richter, T., and Schiewe, J. (2000), "Micromixing technology", in *4th International Conference on Microreaction Technology*, Atlanta, GA, AIChE: 31–47.

Lundgren, D.G., and Russel, R.T. (1956), "An air-lift laboratory fermentor," *Applied and Environmental Microbiology*, 4(1): 31–33.

Luo, H.-P., and Al-Dahhan, M.H. (2008), "Local characteristics of hydrodynamics in draft tube airlift bioreactor," *Chemical Engineering Science*, 63(11): 3057–3068.

Luo, X., Jiang, P., and Fan, L.-S. (1997), "High-pressure three-phase fluidization: Hydrodynamics and heat transfer," *AIChE Journal*, 43(10): 2432–2445.

Luo, X., Lee, D.J., Lau, R., Yang, G., and Fan, L.-S. (1999), "Maximum stable bubble size and gas holdup in high-pressure slurry bubble columns," *AIChE Journal*, 45(4): 665–680.

Magaud, F., Souhar, M., Wild, G., and Boisson, N. (2001), "Experimental study of bubble column hydrodynamics," *Chemical Engineering Science*, 56(15): 4597–4607.

Maiti, R.N., and Nigam, K.D.P. (2007), "Gas-liquid distributors for trickle-bed reactors: A review," *Industrial & Engineering Chemistry Research*, 46(19): 6164–6182.

Majirova, H., Pinelli, D., Machon, V., and Magelli, F. (2004), "Gas flow behavior in a two-phase reactor stirred with triple turbines," *Chemical Engineering & Technology*, 27(3): 304–309.

Makkawi, Y.T., and Wright, P.C. (2002), "Fluidization regimes in a conventional fluidized bed characterized by means of electrical capacitance tomography," *Chemical Engineering Science*, 57: 2411–2437.

Makkawi, Y.T., and Wright, P.C. (2004), "Electrical capacitance tomography for conventional fluidized bed measurements–Remarks on the measuring technique," *Powder Technology*, 148(2–3): 142–157.

Maldonado, J.G.G., Bastoul, D., Baig, S., Roustan, M., and Hébrard, G. (2008), "Effect of solid characteristics on hydrodynamic and mass transfer in a fixed bed reactor operating in co-current gas-liquid up flow," *Chemical Engineering and Processing Process Intensification*, 47(8): 1190–1200.

Mangers, R.J., and Ponter, A.B. (1980), "Effect of viscosity on liquid film resistance to mass transfer in a packed column," *Industrial & Engineering Chemistry, Process Design and Development*, 19(4): 530–537.

Marashdeh, Q., Fan, L.S., Du, B., and Warsito, W. (2008), "Electrical capacitance tomography – A perspective," *Industrial & Engineering Chemistry Research*, 47(10): 3708–3719.

Marchot, P., Toye, D., Pelsser, A.-M., Crine, M., L'Homme, G.L., and Olujic, Z. (2001), "Liquid distribution images on structured packing by X-ray computed tomography," *AIChE Journal*, 47(6): 1471–1476.

Martín, M., García, J.M., Montes, F.J., and Galán, M.A. (2008a), "On the effect of the orifice configuration on the coalescence of growing bubbles," *Chemical Engineering and Processing Process Intensification*, 47(9–10): 1799–1809.

Martín, M., Montes, F.J., and Galan, M.A. (2008b), "Influence of impeller type on the bubble breakup process in stirred tanks," *Industrial & Engineering Chemistry Research*, 47(16): 6251–6263.

Martín, M., Montes, F.J., and Galán, M.A. (2009), "Theoretical modelling of the effect of surface active species on the mass transfer rates in bubble column reactors," *Chemical Engineering Journal*, 155(1–2): 272–284.

Martin, Y., and Vermette, P. (2005), "Bioreactors for tissue mass culture: Design, characterization, and recent advances," *Biomaterials*, 26(35): 7481–7503.

Mashelkar, R.A. (1970), "Bubble columns," *British Chemical Engineering*, 1970(15): 1297–1304.

McFarlane, C.M., and Nienow, A.W. (1995), "Studies of high solidity ratio hydrofoil impellers for aerated bioreactors. 1. Review," *Biotechnology Progress*, 11(6): 601–607.

McFarlane, C.M., and Nienow, A.W. (1996a), "Studies of high solidity ratio hydrofoil impellers for aerated bioreactors. 3. Fluids of enhanced viscosity and exhibiting coalescence repression," *Biotechnology Progress*, 12(1): 1–8.

McFarlane, C.M., and Nienow, A.W. (1996b), "Studies of high solidity ratio hydrofoil impellers for aerated bioreactors. 4. Comparison of impeller types," *Biotechnology Progress*, 12(1): 9–15.

McFarlane, C.M., Zhao, X.-M., and Nienow, A.W. (1995), "Studies of high solidity ratio hydrofoil impellers for aerated bioreactors. 2. Air-water studies," *Biotechnology Progress*, 11(6): 608–618.

McManamey, W.J., and Wase, D.A.J. (1986), "Relationship between the volumetric mass transfer coefficient and gas holdup in airlift fermentors," *Biotechnology and Bioengineering*, 28(9): 1446–1448.

Medeiros, E.B.M., Petrissans, M., Wehrer, A., and Zoulalian, A. (2001), "Comparative study of two cocurrent downflow three phase catalytic fixed bed reactors: Application to the sulphur dioxide catalytic oxidation on active carbon particles," *Chemical Engineering and Processing*, 40(2): 153–158.

Mehrnia, M.R., Towfighi, J., Bonakdarpour, B., and Akbarnejad, M.M. (2005), "Gas hold-up and oxygen transfer in a draft-tube airlift bioreactor with petroleum-based liquids," *Biochemical Engineering Journal*, 22(2): 105–110.

Mena, P.C., Ruzicka, M.C., Rocha, F.A., Teixeira, J.A., and Drahos, J. (2005), "Effect of solids on homogeneous-heterogeneous flow regime transition in bubble columns," *Chemical Engineering Science*, 60(22): 6013–6026.

Merchuk, J.C. (1985), "Hydrodynamics and hold-up in air-lift reactors," in *Encyclopedia of Fluid Mechanics*, N.P. Cheremisinoff, Editor, Houston, Texas, Gulf Publishing Company, Chapter 3: 1485–1511.

Merchuk, J.C. (1986), "Gas hold-up and liquid velocity in a two-dimensional air lift reactor," *Chemical Engineering Science*, 41(1): 11–16.

Merchuk, J.C., Contreras, A., García, F., and Molina, E. (1998), "Studies of mixing in a concentric tube airlift bioreactor with different spargers," *Chemical Engineering Science*, 53(4): 709–719.

Merchuk, J.C., and Gluz, M. (1999), "Bioreactors: Air-lift reactors," in *Encyclopedia of Bioprocess Technology: Fermentation, Biocatalysis, and Bioseperations*, M.C. Flickinger, and S.W. Drew, Editors, New York City, New York, John Wiley & Sons, Inc. **1**: 320–353.

Merchuk, J.C., Ladwa, N., Cameron, A., Bulmer, M., and Pickett, A. (1994), "Concentric-tube airlift reactors: Effects of geometrical design on performance," *AIChE Journal*, 40(7): 1105–1117.

Merchuk, J.C., and Stein, Y. (1981), "Local hold-up and liquid velocity in air-lift reactors," *AIChE Journal*, 27(3): 377–388.

Merchuk, J.C., Yona, S., Siegel, M.H., and Zvi, A.B. (1990), "On the first-order approximation to the response of dissolved oxygen electrodes for dynamic $k_L a$ estimation," *Biotechnology and Bioengineering*, 35(11): 1161–1163.

Mersmann, A. (1977), "Auslegung und maβstabsvergrösserung von blasen- und tropfensäulen," *Chemie-Ingenieur-Technik*, 49(9): 679–691.

Metaxas, K., and Papayannakos, N. (2008), "Gas-liquid mass transfer in a bench-scale trickle bed reactor used for benzene hydrogenation," *Chemical Engineering & Technology*, 31(10): 1410–1417.

Miller, D.N. (1974), "Scale-up of agitated vessels gas-liquid mass transfer," *AIChE Journal*, 20(3): 445–453.

Mishra, V.P., and Joshi, J.B. (1994), "Flow generated by a disc turbine: Part IV: Multiple impellers," *Chemical Engineering Research & Design*, 72(A5): 657–668.

Miyahara, T., Hamaguchi, M., Sukeda, Y., and Takehashi, T. (1986), "Size of bubbles and liquid circulation in a bubble column with draught tube and sieve plate," *Canadian Journal of Chemical Engineering*, 64: 718–725.

Mizukami, M., Parthasarathy, R.N., and Faeth, G.M. (1992), "Particle-generated turbulence in homogeneous dilute dispersed flows," *International Journal of Multiphase Flow*, 18(3): 397–412.

Moilanen, P., Laakkonen, M., Visuri, O., Alopaeus, V., and Aittamaa, J. (2008), "Modelling mass transfer in an aerated 0.2 m^3 vessel agitated by Rushton, Phasejet and Combijet impellers," *Chemical Engineering Journal*, 142(1): 95–108.

Mok, Y.S., Kim, Y.H., and Kim, S.Y. (1990), "Bubble and gas holdup characteristics in a bubble column of CMC solution," *The Korean Journal of Chemical Engineering*, 7(1): 31–39.

Molina, E., Contreras, A., and Chisti, Y. (1999), "Gas holdup, liquid circulation and mixing behaviour of viscous Newtonian media in a split-cylinder airlift bioreactor," *Food and Bioproducts Processing*, 77(1): 27–32.

Monahan, S.M., Vitankar, V.S., and Fox, R.O. (2005), "CFD predictions for flow-regime transitions in bubble columns," *AIChE Journal*, 51(7): 1897–1923.

Moo-Young, M., and Blanch, H.W. (1981), "Design of biochemical reactors mass transfer criteria for simple and complex systems," *Advances in Biochemical Engineering*, 19: 1–69.

Moucha, T., Linek, V., and Prokopova, E. (2003), "Gas hold-up, mixing time and gas-liquid volumetric mass transfer coefficient of various multiple-impeller configurations: Rushton turbine, pitched blade and techmix impeller and their combinations," *Chemical Engineering Science*, 58(9): 1839–1846.

Mouza, A.A., Dalakoglou, G.K., and Paras, S.V. (2005), "Effect of liquid properties on the performance of bubble column reactors with fine pore spargers," *Chemical Engineering Science*, 60(5): 1465–1475.

Mudde, R.F. (2010a), "Advanced measurement techniques for gls reactors," *The Canadian Journal of Chemical Engineering*, 88(4): 638–647.

Mudde, R.F. (2010b), "Time-resolved X-ray tomography of a fluidized bed," *Powder Technology*, 199(1): 55–59.

Mudde, R.F., Bruneau, P.R.P., and van der Hagen, T.H.J.J. (2005), "Time-resolved γ-densitometry imaging within fluidized beds," *Industrial & Engineering Chemistry Research*, 44: 6181–6187.

Muller, C.R., Holland, D.J., Sederman, A.J., Mantle, M.D., Gladden, L.F., and Davidson, J.F. (2008), "Magnetic resonance imaging of fluidized beds," *Powder Technology*, 183(1): 53–62.

Murthy, B.N., Ghadge, R.S., and Joshi, J.B. (2007), "CFD simulations of gas-liquid-solid stirred reactor: Prediction of critical impeller speed for solid suspension," *Chemical Engineering Science*, 62(24): 7184–7195.

Muthukumar, K., and Velan, M. (2006), "Volumetric mass transfer coefficients in an internal loop airlift reactor with low-density particles," *Journal of Chemical Technology & Biotechnology*, 81(4): 667–673.

Nacef, S., Poncin, S., Bouguettoucha, A., and Wild, G. (2007), "Drift flux concept in two- and three-phase reactors," *Chemical Engineering Science*, 62(24): 7530–7538.

Nakanoh, M., and Yoshida, F. (1980), "Gas absorption by Newtonian and non-Newtonian liquids in a bubble column," *Industrial & Engineering Chemistry Process Design and Development*, 19(1): 190–195.

Nakanoh, M., and Yoshida, F. (1983), "Transient characteristics of oxygen probes and determination of $k_L a$," *Biotechnology and Bioengineering*, 25(6): 1653–1654.

Nauman, E.B., and Buffman, B.A. (1983), *Mixing in Continuous Flow Systems*, John Wiley & Sons, New York.

Nedeltchev, S. (2003), "Correction of the penetration theory applied for prediction of mass transfer coefficients in a high-pressure bubble column operated with gasoline and toluene," *Journal of Chemical Engineering of Japan*, 36(5): 630–633.

Ni, X., Gao, S., Cumming, R.H., and Pritchard, D.W. (1995), "A comparative study of mass transfer in yeast for a batch pulsed baffled bioreactor and a stirred tank fermenter," *Chemical Engineering Science*, 50(13): 2127–2136.

Nicolella, C., van Loosdrecht, M.C.M., and Heijnen, J.J. (1998), "Mass transfer and reaction in a biofilm airlift suspension reactor," *Chemical Engineering Science*, 53(15): 2743–2753.

Nielsen, J., Villadsen, J., and Liden, G. (2003), *Bioreaction Engineering Principles*, Kluwer Academic/Plenum Publishers, New York.

Nielsen, J., and Volladsen, J. (1993), "Description and modelling," in *Bioprocessing*, H.-J. Rehm, G. Reed, A. Puehler, and P. Stadler, Editors, New York, NY, Wiley-VCH. **3**: 79–102.

Nienow, A.W. (1996), "Gas-liquid mixing studies: A comparison of Rushton turbines with some modern impellers," *Chemical Engineering Research & Design*, 74(A4): 417–423.

Nienow, A.W., Kendall, A., Moore, I.P.T., Ozcan-Taskin, G.N., and Badham, R.S. (1995), "The characteristics of aerated 12- and 18-blade Rushton turbines at transitional Reynolds numbers," *Chemical Engineering Science*, 50(4): 593–599.

Nienow, A.W., Warmoeskerken, M.M.C.G., Smith, J.M., and Konno, M. (1985), "On the flooding/loading transition and the complete dispersal condition in aerated vessels agitated by a Rushton-turbine," in *Fifth European Conference on Mixing*, Wuerzburg, West Germany, BHRA, Cranfield, England: 143–154.

Nienow, A.W., Wisdom, D.J., and Middleton, J.C. (1977), "The effect of scale and geometry on flooding, recirculation, and power in gassed stirred vessels," in *Second European Conference on Mixing*, Cambridge, England: **F1**: 1–16.

Nigam, K.D.P., and Larachi, F. (2005), "Process intensification in trickle-bed reactors," *Chemical Engineering Science*, 60(22): 5880–5894.

Nishikawa, M., Nakamura, M., and Hashimoto, K. (1981), "Gas absorption in aerated mixing vessels with non-Newtonian liquid," *Journal of Chemical Engineering of Japan*, 14(3): 227–232.

Nishikawa, M., Nishioka, S., and Kayama, T. (1984), "Gas absorption in an aerated mixing vessel with multi-stage impellers," *Journal of Chemical Engineering of Japan*, 17(5): 541–543.

Nocentini, M. (1990), "Mass transfer in gas-liquid, multiple-impeller stirred vessels: A discussion about experimental techniques for $k_L a$ measurement and models comparison," *Chemical Engineering Research & Design*, 68(3): 287–294.

Nocentini, M., Fajner, D., Pasquali, G., and Magelli, F. (1993), "Gas-liquid mass transfer and holdup in vessels stirred with multiple Rushton turbines: Water and water-glycerol solutions," *Industrial & Engineering Chemistry Research*, 32(1): 19–26.

Nocentini, M., Pinelli, D., and Magelli, F. (1998), "Analysis of the gas behavior in sparged reactors stirred with multiple Rushton turbines: Tentative model validation and scale-up," *Industrial & Engineering Chemistry Research*, 37(4): 1528–1535.

Norman, W.S., and Sammak, F.Y.Y. (1963), "Gas absorption in a packed column part I: The effect of liquid viscosity on the mass transfer coefficient," *Transactions of the Institution of Chemical Engineers*, 41(3): 109–116.

Nunes, S.P., and Peinemann, K.-V. (eds) (2006), *Membrane Technology in the Chemical Industry*, Wiley-VCH Verlag GmbH & Co., Weinheim, Germany.

Ogut, A., and Hatch, R.T. (1988), "Oxygen transfer into Newtonian and non-Newtonian fluids in mechanically agitated vessels," *Canadian Journal of Chemical Engineering*, 66(1): 79–85.

Ohki, Y., and Inoue, H. (1970), "Longitudinal mixing of the liquid phase in bubble columns," *Chemical Engineering Science*, 25(1): 1–16.

Oldshue, J.Y. (1983), *Fluid Mixing Technology*, McGraw-Hill Publications Co., New York, NY.

Olmos, E., Gentric, C., and Midoux, N. (2003), "Numerical description of flow regime transitions in bubble column reactors by a multiple gas phase model," *Chemical Engineering Science*, 58(10): 2113–2121.

Onda, K., Sada, E., and Murase, Y. (1959), "Liquid-side mass transfer coefficients in packed towers," *AIChE Journal*, 5(2): 235–239.

Onda, K., Sada, E., and Otubo, F. (1958), "Liquid-side mass-transfer coefficient for a tower packed with Raschig rings," *Kagaku Kogaku*, 22(4): 194–199.

Onda, K., Sada, E., and Saito, M. (1961), "Gas-side mass transfer coefficients in packed tower," *Kagaku Kogaku*, 25(N11): 820–828.

Ostafin, A. and Landfester, K. (eds) (2009), Nanoreactor Engineering: Engineering in Medicine & Biology, Artech House, Boston.

Ozturk, S.S., Schumpe, A., and Deckwer, W.D. (1987), "Organic liquids in a bubble column: Holdups and mass transfer coefficients," *AIChE Journal*, 33(9): 1473–1480.

Padial, N.T., VanderHeyden, W.B., Rauenzahn, R.M., and Yarbro, S.L. (2000), "Three-dimensional simulation of a three-phase draft-tube bubble column," *Chemical Engineering Science*, 55(16): 3261–3273.

Pan, Y., Dudukovic, M.P., and Chang, M. (2000), "Numerical investigation of gas-driven flow in 2-D bubble columns," *AIChE Journal*, 46(3): 434–449.

Parthasarathy, R.N., and Faeth, G.M. (1990a), "Turbulence modulation in homogeneous dilute particle-laden flows," *Journal of Fluid Mechanics*, 220: 485–514.

Parthasarathy, R.N., and Faeth, G.M. (1990b), "Turbulent dispersion of particles in self-generated homogeneous turbulence," *Journal of Fluid Mechanics*, 220: 515–537.

Patel, S.A., Daly, J.G., and Bukur, D.B. (1989), "Holdup and interfacial area measurements using dynamic gas disengagement," *AIChE Journal*, 35(6): 931–942.

Patwardhan, A.W., and Joshi, J.B. (1998), "Design of stirred vessels with gas entrained from free liquid surface," *Canadian Journal of Chemical Engineering*, 76(3): 339–364.

Patwardhan, A.W., and Joshi, J.B. (1999), "Design of gas-inducing reactors," *Industrial & Engineering Chemistry Research*, 38(1): 49–80.

Paul, E.L., Atiemo-Obeng, V.A., and Kresta, S.M. (eds) (2004), *Handbook of Industrial Mixing*, John Wiley & Sons, Inc., Hoboken, New Jersey.

Peinemann, K.-V., and Nunes, S.P. (2008a), "Membranes for energy conversion," in *Membrane Technology*, K.-V. Peinemann, and S.P. Nunes, Editors, Weinheim, Germany, Wiley-VCH Verlag GmbH & Co. KGaA.

Peinemann, K.-V., and Nunes, S.P. (2008b), "Membranes for life sciences," in *Membrane Technology*, K.-V. Peinemann, and S.P. Nunes, Editors, Weinheim, Germany, Wiley-VCH Verlag GmbH & Co. KGaA.

Piché, S., Larachi, F., and Grandjean, B.P.A. (2001a), "Flooding capacity in packed towers: Database, correlations, and analysis," *Industrial & Engineering Chemistry Research*, 40(1): 476–487.

Piché, S., Larachi, F., and Grandjean, B.P.A. (2001b), "Loading capacity in packing towers: Database, correlations and analysis," *Chemical Engineering & Technology*, 24(4): 373–380.

Piché, S.R., Larachi, F., and Grandjean, B.P.A. (2001c), "Improving the prediction of irrigated pressure drop in packed absorption towers," *The Canadian Journal of Chemical Engineering*, 79(4): 584–594.

Pinelli, D., Bakker, A., Myers, K.J., Reeder, M.F., Fasano, J., and Magelli, F. (2003), "Some features of a novel gas dispersion impeller in a dual-impeller configuration," *Chemical Engineering Research & Design*, 81(A4): 448–454.

Pollack, J.K., Li, Z.J., and Marten, M.R. (2008), "Fungal mycelia show lag time before re-growth on endogenous carbon," *Biotechnology and Bioengineering*, 100(3): 458–465.

Poorte, R.E.G., and Biesheuvel, A. (2002), "Experiments on the motion of gas bubbles in turbulence generated by an active grid," *Journal of Fluid Mechanics*, 461: 127–154.

Popovic, M., and Robinson, C.W. (1984), "Estimation of some important design parameters for non-Newtonian liquids in pneumatically-agitated fermenters," in *Proceedings of the 34th Canadian Chemical Engineering Conference*, Quebec City, Canada, 258–263.

Popovic, M., and Robinson, C.W. (1988), "External-circulation-loop airlift bioreactors: Study of the liquid circulating velocity in highly viscous non-Newtonian liquids," *Biotechnology and Bioengineering*, 32(7): 301–312.

Posarac, D., and Petrovic, D. (1988), "An experimental study of the minimum fluidization velocity in a three-phase external loop airlift-reactor," *Chemical Engineering Science*, 43(5): 1161–1165.

Poughon, L., Duchez, D., Cornet, J.F., and Dussap, C.G. (2003), "$k_L a$ determination: Comparative study for a gas mass balance method," *Bioprocess and Biosystems Engineering*, 25(6): 341–348.

Powell, R.L. (2008), "Experimental techniques for multiphase flows," *Physics of Fluids*, 20(4): 040605–040622.

Prasser, H.M. (2008), "Novel experimental measuring techniques required to provide data for CFD validation," *Nuclear Engineering and Design*, 238(3): 744–770.

Prasser, H.M., Misawa, M., and Tiseanu, I. (2005), "Comparison between wire-mesh sensor and ultra-fast X-ray tomograph for an air-water flow in a vertical pipe," *Flow Measurement and Instrumentation*, 16(2–3): 73–83.

Pugsley, T., Tanfara, H., Malcus, S., Cui, H., Chaouki, J., and Winters, C. (2003), "Verification of fluidized bed electrical capacitance tomography measurements with a fiber optic probe," *Chemical Engineering Science*, 58: 3923–3934.

Puthli, M.S., Rathod, V.K., and Pandit, A.B. (2005), "Gas-liquid mass transfer studies with triple impeller system on a laboratory scale bioreactor," *Biochemical Engineering Journal*, 23(1): 25–30.

Rados, N., Shaikh, A., and Al-Dahhan, M. (2005), "Phase distribution in a high pressure slurry bubble column via a single source computed tomography," *The Canadian Journal of Chemical Engineering*, 83: 104–112.

Ramaswamy, S., Cutright, T.J., and Qammar, H.K. (2005), "Control of a continuous bioreactor using model predictive control," *Process Biochemistry*, 40(8): 2763–2770.

Ramm, W.M., and Chagina, Z.W. (1965), "Issledowanie teplootdachi pri powerxnostnom kipenii rastworow neletuchix weshestw," *Khimicheskaia Promyshlennost*, 23: 219–222.

Rampure, M.R., Buwa, V.V., and Ranade, V.V. (2003), "Modelling of gas-liquid/gas-liquid-solid flows in bubble columns: Experiments and CFD simulations," *The Canadian Journal of Chemical Engineering*, 81: 692–706.

Raschig Jaeger Technologies (2006), "Product bulletin 1100," *Raschig Jaeger Technologies Brochures*(1100): 1–20.

Raschig LTD, "Prospectus of packings", Ludwigshafen, Germany, Raschig LTD.

Reddy, G.P., and Chidambaram, M. (1995), "Near-optimal productivity control of a continuous bioreactor," *IEEE Proceedings: Control Theory and Applications*, 142(6): 633–637.

Rees, A.C., Davidson, J.F., Dennis, J.S., Fennell, P.S., Gladden, L.F., Hayhurst, A.N., Mantle, M.D., Muller, C.R., and Sederman, A.J. (2006), "The nature of the flow just above the perforated plate distributor of a gas-fluidised bed, as imaged using magnetic resonance," *Chemical Engineering Science*, 61(18): 6002–6015.

Reichelt, W. (1974), *Stromung und stoffaustausch in fullkorperapparaten bei gegenstrom einer flussigen und einer gasformigen phase*, Weinheim/Bergstr, Verlag Chemie.

Reilley, I.G., Scott, D.S., De Bruijin, T., Jain, A., and Pixkorz, J. (1986), "A correlation for gas holdup in turbulent coalescing bubble columns," *Canadian Journal of Chemical Engineering*, 1986(64): 705–717.

Rewatkar, V.B., Deshpande, A.J., Pandit, A.B., and Joshi, J.B. (1993), "Gas hold-up behavior of mechanically agitated gas-liquid reactors using pitched blade downflow turbines," *Canadian Journal of Chemical Engineering*, 71(2): 226–237.

Rewatkar, V.B., and Joshi, J.B. (1993), "Role of sparger design on gas dispersion in mechanically agitated gas-liquid contactors," *Canadian Journal of Chemical Engineering*, 71(2): 278–291.

Ribeiro Jr., C.P. (2008), "On the estimation of the regime transition point in bubble columns," *Chemical Engineering Journal*, 140(1–3): 473–482.

Ribeiro Jr., C.P., and Lage, P.L.C. (2005), "Gas-liquid direct-contact evaporation: A review," *Chemical Engineering & Technology*, 28(10): 1081–1107.

Riggs, S.S., and Heindel, T.J. (2006), "Measuring carbon monoxide gas-liquid mass transfer in a stirred tank reactor for syngas fermentation," *Biotechnology Progress*, 22(3): 903–906.

Rodgers, T.L., Gangolf, L., Vannier, C., Parriaud, M., and Cooke, M. (2011), "Mixing times for process vessels with aspect ratios greater than one," *Chemical Engineering Science*, 66(13): 2935–2944.

Ros, M., and Zupancic, G.D. (2002), "Thermophilic aerobic digestion of waste activated sludge," *Acta Chimica Slovenica*, 49(4): 931–943.

Roy, N.K., Guha, D.K., and Rao, M.N. (1963), "Fractional gas holdup in two-phase and three-phase batch-fluidized bubble-bed and foam-systems," *Indian Chemical Engineer*, 1963: 27–31.

Roy, S., Dhotre, M.T., and Joshi, J.B. (2006), "CFD simulation of flow and axial dispersion in external loop airlift reactor," *Transactions of IChemE, Part A, Chemical Engineering Research and Design*, 84(A8): 677–690.

Roy, S., and Joshi, J.B. (2008), "CFD study of mixing characteristics of bubble column and external loop airlift reactor," *Asia-Pacific Journal of Chemical Engineering*, 3(2): 97–105.

Ruchti, G., Dunn, I.J., and Bourne, J.R. (1981), "Comparison of dynamic oxygen electrode methods for the measurement of $k_L a$," *Biotechnology and Bioengineering*, 23(2): 277–290.

Ruckenstein, E. (1964), "On mass transfer in the continuous phase from spherical bubbles or drops," *Chemical Engineering Science*, 19(2): 131–148.

Ruen-ngam, D., Wongsuchoto, P., Limpanuphap, A., Charinpanitkul, T., and Pavasant, P. (2008), "Influence of salinity on bubble size distribution and gas-liquid mass transfer in airlift contactors," *Chemical Engineering Journal*, 141(1–3): 222–232.

Ruthiya, K.C., Chilekar, V.P., Warnier, M.J.F., van der Schaaf, J., Kuster, B.F.M., Schouten, J.C., and van Ommen, J.R. (2005), "Detecting regime transitions in slurry bubble columns using pressure time series," *AIChE Journal*, 51(7): 1951–1965.

Ruzicka, M.C., Drahos, J., Fialová, M., and Thomas, N.H. (2001a), "Effect of bubble column dimensions on flow regime transition," *Chemical Engineering Science*, 56(21–22): 6117–6124.

Ruzicka, M.C., Drahos, J., Mena, P.C., and Teixeira, J.A. (2003), "Effect of viscosity on homogeneous-heterogeneous flow regime transition in bubble columns," *Chemical Engineering Journal*, 96(1–3): 15–22.

Ruzicka, M.C., Zahradník, J., Drahos, J., and Thomas, N.H. (2001b), "Homogeneous-heterogeneous regime transition in bubble columns," *Chemical Engineering Science*, 56(15): 4609–4626.

Sada, E., Katoh, S., Yoshii, H., Yamanishi, T., and Nakanishi, A. (1984), "Performance of the gas bubble column in molten salt systems," *Industrial & Engineering Chemistry, Process Design and Development*, 23(1): 151–154.

Salvacion, J.L., Murayama, M., Ohtaguchi, K., and Koide, K. (1995), "Effects of alcohols on gas holdup and volumetric liquid-phase mass transfer coefficient in gel-particle suspended bubble column," *Journal of Chemical Engineering of Japan*, 28(4): 434.

Sankaranarayanan, K., and Sundaresan, S. (2002), "Lift force in bubbly suspensions," *Chemical Engineering Science*, 57: 3521–3542.

Sanyal, J., Marchisio, D.L., Fox, R.O., and Dhanasekharan, K. (2005), "On the comparison between population balance models for CFD simulation of bubble columns," *Industrial & Engineering Chemistry Research*, 44: 5063–5072.

Sardeing, R., Aubin, J., Poux, M., and Xuereb, C. (2004a), "Gas-liquid mass transfer: Influence of sparger location," *Chemical Engineering Research & Design*, 82(9): 1161–1168.

Sardeing, R., Aubin, J., and Xuereb, C. (2004b), "Gas-liquid mass transfer: A comparison of down- and up-pumping axial flow impellers with radial impellers," *Chemical Engineering Research & Design*, 82(12): 1589–1596.

Sato, Y., Sadatomi, M., and Sekoguchi, K. (1981), "Momentum and heat transfer in two-phase bubble flow I," *International Journal of Multiphase Flow*, 7(2): 167–177.

Sato, Y., and Sekoguchi, K. (1975), "Liquid velocity distribution in two-phase bubble flow," *International Journal of Multiphase Flow*, 2(1): 79–95.

Saxena, S.C., Patel, D., Smith, D.N., and Ruether, J.A. (1988), "An assessment of experimental techniques for the measurement of bubble size in a bubble slurry reactor as applied to indirect coal liquefaction," *Chemical Engineering Communications*, 63: 87–127.

Scargiali, F., D'Orazio, A., Grisafi, F., and Brucato, A. (2007), "Modelling and simulation of gas-liquid hydrodynamics in mechanically stirred tanks," *Chemical Engineering Research & Design*, 85(5): 637–646.

Schäfer, R., Merten, C., and Eigenberger, G. (2002), "Bubble size distributions in a bubble column reactor under industrial conditions," *Experimental Thermal and Fluid Science*, 26(6–7): 595–604.

Scherwood, T.K., and Holloway, F.A.L. (1940) "Performance of packed towers—Liquid film data for several packings," *Transactions of the American Institute of Chemical Engineers*, 36(1): 36–69.

Schiller, L., and Naumann, A. (1933), "Uber die grundlegenden berechnungen bei der schwerkraftaufbereitung," *Zeitung des vereins deutscher ingenieure*, 77: 318–320.

Schmit, C.E., and Eldridge, R.B. (2004), "Investigation of X-ray imaging of vapor-liquid contactors: 1 – Studies involving stationary objects and a simple flow system," *Chemical Engineering Science*, 59: 1255–1266.

Schmit, C.E., Perkins, J., and Eldridge, R.B. (2004), "Investigation of X-ray imaging of vapor-liquid contactors: 2 - Experiments and simulations of flows in an air-water contactor," *Chemical Engineering Science*, 59: 1267–1283.

Schönfeld, H., Hunger, K., Cecilia, R., and Kunz, U. (2004), "Enhanced mass transfer using a novel polymer/carrier microreactor," *Chemical Engineering Journal*, 101(1–3): 455–463.

Schultes, M. (2003), "Raschig super-ring: A new fourth generation packing offers new advantages," *Chemical Engineering Research & Design*, 81(1): 48–57.

Schumacher, J. (2000), "A framework for batch-operation analysis within the context of disturbance management," *Computers & Chemical Engineering*, 24(2–7): 1175–1180.

Schumpe, A., and Deckwer, W.D. (1987), "Viscous media in tower bioreactors: Hydrodynamic characteristics and mass transfer properties," *Bioprocess and Biosystems Engineering*, 1987(2): 79–94.

Schumpe, A., and Grund, G. (1986), "The gas disengagement technique for studying gas holdup structure in bubble columns," *The Canadian Journal of Chemical Engineering*, 64(6): 891–896.

Schuurman, Y. (2008), "Aspects of kinetic modeling of fixed bed reactors," *Catalysis Today*, 138(1–2): 15–20.

Seeger, A., Affeld, K., Goubergrits, L., Kertzscher, U., and Wellnhofer, E. (2001a), "X-ray-based assessment of the three-dimensional velocity of the liquid phase in a bubble column," *Experiments in Fluids*, 31: 193–201.

Seeger, A., Affeld, K., Kertzscher, U., Goubergrits, L., and Wellnhofer, E. (2001b), "Assessment of flow structures in bubble columns by X-ray based particle tracking velocimetry," in *4th International Symposium on Particle Image Velocimetry*, Gottingen, Germany.

Seeger, A., Kertzscher, U., Affeld, K., and Wellnhofer, E. (2003), "Measurement of the local velocity of the solid phase and the local solid hold-up in a three-phase flow by X-ray based particle tracking velocimetry (XPTV)," *Chemical Engineering Science*, 58: 1721–1729.

Shah, Y.T., Kelkar, B.G., Godbole, S.P., and Deckwer, W.-D. (1982), "Design parameters estimation for bubble column reactors," *AIChE Journal*, 28(3): 353–379.

Shaikh, A., and Al-Dahhan, M. (2005), "Characterization of the hydrodynamic flow regime in bubble columns via computed tomography," *Flow Measurement and Instrumentation*, 16(2–3): 91–98.

Shariati, F.P., Bonakdarpour, B., and Mehrnia, M.R. (2007), "Hydrodynamics and oxygen transfer behaviour of water in diesel microemulsions in a draft tube airlift bioreactor," *Chemical Engineering and Processing*, 46(4): 334–342.

Sharma, M., and Yashonath, S. (2006), "Breakdown of the Stokes-Einstein relationship: Role of interactions in the size dependence of self-diffusivity," *The Journal of Physical Chemistry. B*, 110(34): 17207–17211.

Shewale, S.D., and Pandit, A.B. (2006), "Studies in multiple impeller agitated gas-liquid contactors," *Chemical Engineering Science*, 61(2): 489–504.

Shpirt, E. (1981), "Role of hydrodynamic factors in ammonia desorption by diffused aeration," *Water Research*, 15(6): 739–743.

Shulman, H.L., Ulrich, C.E., Proulz, A.Z., and Zimmerman, L.O. (1955), "Wetted and effective: Interfacial areas, gas- and liquid-phase mass transfer rates," *AIChE Journal*, 1(2): 253–258.

Siegel, M.H., and Merchuk, J.C. (1988), "Mass transfer in a rectangular air-lift reactor: Effects of geometry and gas recirculation," *Biotechnology and Bioengineering*, 32(9): 1128–1137.

Siegel, M.H., Merchuk, J.C., and Schugerl, K. (1986), "Air-lift reactor analysis: Interrelationships between riser, downcomer, and gas-liquid separator behavior, including gas recirculation effects," *AIChE Journal*, 32(10): 1585–1596.

Simon, J., Wiese, J., and Steinmetz, H. (2006), "A comparison of continuous flow and sequencing batch reactor plants concerning integrated operation of sewer systems and wastewater treatment plants," *Water Science & Technology*, 54(11): 241–248.

Sivashanmugam, P., and Prabhakaran, S. (2008), "Simulation of an effect of a baffle length on the power consumption in an agitated vessel," *International Journal of Food Engineering*, 4(2): Article 3.

Smith, D.N., Fuchs, W., Lynn, R.J., and Smith, D.H. (1983), *Bubble Behavior in a Slurry Bubble Column Reactor Model*, ACS, Washington, DC, USA 526.

Smith, J.M. (1991), "Simple performance correlations for agitated vessels," in *Proceedings of the 7th European Congress on Mixing*, Brugge, Belgium: 233–241.

Smith, J.M., Van't Riet, K., and Middleton, J.C. (1977), "Scale-up of agitated gas-liquid reactors for mass transfer", in *Proceedings of the Second European Conference on Mixing*, H.S. Stephens and J.A. Clarke, Editors, Crafield, UK, BHRA Fluid Engineering: 51–66.

Smith, J.M., and Warmoeskerken, M.M.C.G. (1985), "Dispersion of gases in liquids with turbines," in *Fifth European Conference on Mixing*, Wuerzburg, West Germany, BHRA, Cranfield, England, 115–126.

Snape, J.B., Zahradnik, J., Fialova, M., and Thomas, N.M. (1995), "Liquid-phase properties and sparger design effects in an external-loop airlift reactor," *Chemical Engineering Science*, 50(20): 3175–3186.

Sobotka, M., Prokop, A., Dunn, I.J., and Einsele, A. (1982), "Review of methods for the measurement of oxygen transfer in microbial systems," *Annual Reports on Fermentation Processes*, 5: 127–210.

Sokol, W., and Migiro, C.L.C. (1996), "Controlling a continuous stirred-tank bioreactor degrading phenol in the stability range," *The Chemical Engineering Journal and The Biochemical Engineering Journal*, 62(1): 67–72.

Sokolichin, A., and Eigenberger, G. (1994), "Gas-liquid flow in bubble columns and loop reactors: Part I. Detailed modeling and numerical simulation," *Chemical Engineering Science*, 49(24): 5735–5746.

Sokolichin, A., Eigenberger, G., and Lapin, A. (2004), "Simulation of buoyancy driven bubbly flow: Established simplifications and open questions," *AIChE Journal*, 50(1): 24–45.

Sokolov, V.N., and Aksenova, E.G. (1982), "Mass transfer in bubble columns," *Journal of Applied Chemistry of the USSR*, 55(10): 2158–2159.

Sotelo, J.L., Benitez, F.J., Beltran-Heredia, J., and Rodriguez, C. (1994), "Gas holdup and mass transfer coefficients in bubble columns. 1. Porous glass-plate diffusers," *International Chemical Engineering*, 34(1): 82–90.

Sotiriadis, A.A., Thorpe, R.B., and Smith, J.M. (2005), "Bubble size and mass transfer characteristics of sparged downwards two-phase flow," *Chemical Engineering Science*, 60(22): 5917–5929.

Spelt, P.D.M., and Sangani, A.S. (1998), "Properties and averaged equations for flows of bubbly liquids," *Applied Scientific Research*, 58(1): 337–386.

Sriram, K., and Mann, R. (1977), "Dynamic gas disengagement: A new technique for assessing the behavior of bubble columns," *Chemical Engineering Science*, 32: 571–580.

Stegeman, D., Ket, P.J., Kolk, K.A.v.d., Bolk, J.W., Knop, P.A., and Westerterp, K.R. (1995), "Interfacial area and gas holdup in an agitated gas-liquid reactor under pressure," *Industrial & Engineering Chemistry Research*, 34(1): 59–71.

Stenberg, O., and Andersson, B. (1988a), "Gas-liquid mass transfer in agitated vessels–I. Evaluation of the gas-liquid mass transfer coefficient from transient-response measurements," *Chemical Engineering Science*, 43(3): 719–724.

Stenberg, O., and Andersson, B. (1988b), "Gas-liquid mass transfer in agitated vessels–II. Modelling of gas-liquid mass transfer," *Chemical Engineering Science*, 43(3): 725–730.

Stichlmair, J., Bravo, J.L., and Fair, J.R. (1989), "General model for prediction of pressure drop and capacity of countercurrent gas/liquid packed columns," *Gas Separation & Purification*, 3(March): 19–28.

Strigle, R.F.J. (1994), *Packed Tower Design and Applications: Random and Structured Packings*, Gulf Publishing Company, Houston, TX.

Su, X., and Heindel, T.J. (2003), "Gas holdup in a fiber suspension," *The Canadian Journal of Chemical Engineering*, 81: 412–418.

Su, X., and Heindel, T.J. (2004), "Gas holdup behavior in Nylon fiber suspensions," *Industrial & Engineering Chemistry Research*, 43(9): 2256–2263.

Su, X., and Heindel, T.J. (2005a), "Effect of perforated plate open area on gas holdup in Rayon fiber suspensions," *ASME Journal of Fluids Engineering - Transactions of the ASME*, 127(4): 816–823.

Su, X., and Heindel, T.J. (2005b), "Modeling gas holdup in gas-liquid-fiber semibatch bubble columns," *Industrial & Engineering Chemistry Research*, 44(24): 9355–9363.

Su, X., Hol, P.D., Talcott, S.M., Staudt, A.K., and Heindel, T.J. (2006), "The effect of bubble column diameter on gas holdup in fiber suspensions," *Chemical Engineering Science*, 61(10): 3098–3104.

Syeda, S.R., Afacan, A., and Chuang, K.T. (2002), "Prediction of gas hold-up in a bubble column filled with pure and, binary liquids," *Canadian Journal of Chemical Engineering*, 80(1): 44–50.

Talvy, S., Cockx, A., and Liné, A. (2007), "Modeling of oxygen mass transfer in a gas-liquid airlift reactor," *AIChE Journal*, 53(2): 316–326.

Tang, C., and Heindel, T.J. (2004), "Time-dependent gas holdup variation in an air-water bubble column," *Chemical Engineering Science*, 59(3): 623–632.

Tang, C., and Heindel, T.J. (2005a), "Effect of fiber type on gas holdup in a cocurrent air-water-fiber bubble column," *Chemical Engineering Journal*, 111(1): 21–30.

Tang, C., and Heindel, T.J. (2005b), "Gas-liquid-fiber flow in a cocurrent bubble column," *AIChE Journal*, 51(10): 2665–2674.

Tang, C., and Heindel, T.J. (2006a), "Estimating gas holdup via pressure difference measurements in a cocurrent bubble column," *International Journal of Multiphase Flow*, 32(7): 850–863.

Tang, C., and Heindel, T.J. (2006b), "Similitude analysis for gas-liquid-fiber flows in cocurrent bubble columns," in *Proceedings of FEDSM06: ASME Joint US-European Fluids Engineering Summer Meeting*, Miami, Florida.

Tang, C., and Heindel, T.J. (2007), "Effect of fiber length distribution on gas holdup in a cocurrent air-water-fiber bubble column," *Chemical Engineering Science*, 62(5): 1408–1417.

Tatterson, G.B. (1991), *Fluid Mixing and Gas Dispersion in Agitated Tanks*, McGraw-Hill, Inc., New York.

Tatterson, G.B. (1994), *Scaleup and Design of Industrial Mixing Processes*, McGraw-Hill, Inc., New York.

Tecante, A., and Choplin, L. (1993), "Gas-liquid mass transfer in non-Newtonian fluids in a tank stirred with a helical ribbon screw impeller," *Canadian Journal of Chemical Engineering*, 71(6): 859–865.

Terasaka, K., Hullmann, D., and Schumpe, A. (1998), "Mass transfer in bubble columns studied with an oxygen optode," *Chemical Engineering Science*, 53(17): 3181–3184.

Thatte, A.R., Ghadge, R.S., Patwardhan, A.W., Joshi, J.B., and Singh, G. (2004), "Local gas holdup measurement in sparged and aerated tanks by γ-ray attenuation technique," *Industrial & Engineering Chemistry Research*, 43(17): 5389–5399.

Titchener-Hooker, N.J., and Hoare, P.D.M. (2008), "Micro biochemical engineering to accelerate the design of industrial-scale downstream processes for biopharmaceutical proteins," *Biotechnology and Bioengineering*, 100(3): 473–487.

Tobajas, M., and Garcia-Calvo, E. (2000), "Comparison of experimental methods for determination of the volumetric mass transfer coefficient in fermentation processes," *Heat and Mass Transfer/Waerme- und Stoffuebertragung*, 36(3): 201–207.

Torré, J.-P., Fletcher, D.F., Lasuye, T., and Xuereb, C. (2007), "An experimental and computational study of the vortex shape in a partially baffled agitated vessel," *Chemical Engineering Science*, 62(7): 1915–1926.

Tortora, P.R., Ceccio, S.L., O'Hern, T.J., Trujillo, S.M., and Torczynski, J.R. (2006), "Quantitative measurement of solids distribution in gas-solid riser flows using electrical impedance tomography and gamma densitometry tomography," *International Journal of Multiphase Flow*, 32(8): 972–995.

Toye, D., Fransolet, E., Simon, D., Crine, M., L'Homme, G., and Marchot, P. (2005), "Possibilities and limits of application of electrical resistance tomography in hydrodynamics of bubble columns," *The Canadian Journal of Chemical Engineering*, 83: 4–10.

Toye, D., Marchot, P., Crine, M., and L'Homme, G. (1996), "Modelling of multiphase flow in packed beds by computer-assisted X-ray tomography," *Measurement Science and Technology*, 7(3): 436–443.

Tribe, L.A., Briens, C.L., and Margaritis, A. (1995), "Determination of the volumetric mass transfer coefficient ($k_L a$) using the dynamic 'gas out-gas in' method: Analysis of errors caused by dissolved oxygen probes," *Biotechnology and Bioengineering*, 46(4): 388–392.

Trilleros, J., Díaz, R., and Redondo, P. (2005), "Three-phase airlift internal loop reactor: Correlations for predicting the main fluid dynamic parameters," *Journal of Chemical Technology & Biotechnology*, 80(5): 515–522.

Tse, K., Martin, T., McFarlane, C.M., and Nienow, A.W. (1998), "Visualisation of bubble coalescence in a coalescence cell, a stirred tank and a bubble column," *Chemical Engineering Science*, 53(23): 4031–4036.

Turner, A.P.F., and White, S.F. (1999), "Process monitoring," in *Encyclopedia of Process Technology: Fermentation, Biocatalysis, and Bioseperation*, M.C. Flickinger and S.W. Drew, Editors, New York, John Wiley. 4: 2056–2070.

Tzeng, J.-W., Chen, R.C., and Fan, L.S. (1993), "Visualization of flow characteristics in a 2-D bubble column and three-phase fluidized bed," *AIChE Journal*, 39(5): 733–744.

Ueyama, K., Tsuru, T., and Furusaki, S. (1989), "Flow transition in a bubble column," *International Chemical Engineering*, 29(3): 523–529.

Ulbrecht, J.J., and Patterson, G.K. (1985), *Mixing of Liquids by Mechanical Agitation*, Gordon and Breach Science Publishers, New York.

Ungerman, A.J. (2006), "*Mass transfer enhancement for syngas fermentation*," MS Thesis, Iowa State University, Ames, Iowa.

Ungerman, A.J., and Heindel, T.J. (2007), "Carbon monoxide mass transfer for syngas fermentation in a stirred tank reactor with dual impeller configurations," *Biotechnology Progress*, 23(3): 613–620.

Utomo, M.B., Warsito, W., Sakai, T., and Uchida, S. (2001), "Analysis of distributions of gas and TiO_2 particles in slurry bubble column using ultrasonic computed tomography," *Chemical Engineering Science*, 56: 6073–6079.

Van't Riet, K. (1979), "Review of measuring methods and results in nonviscous gas-liquid mass transfer in stirred vessels," *Industrial and Engineering Chemistry Process Design and Development*, 18(3): 357–364.

Van't Riet, K. and Tramper, J. (1991), *Basic Bioreactor Design*, Marcel Dekker, Inc., New York, New York.

van Benthum, W.A.J., van den Hoogen, J.H.A., van der Lans, R.G.J.M., van Loosdrecht, M.C.M., and Heijnen, J.J. (1999a), "The biofilm airlift suspension extension reactor. Part I: Design and two-phase hydrodynamics," *Chemical Engineering Science*, 54(12): 1909–1924.

van Benthum, W.A.J., van der Lans, R.G.J.M., van Loosdrecht, M.C.M., and Heijnen, J.J. (1999b), "Bubble recirculation regimes in an internal-loop airlift reactor," *Chemical Engineering Science*, 54(18): 3995–4006.

van Dam-Mieras, M.C.E., de Jue, W.H., de Vries, J., Currell, B.R., James, J.W., Leach, C.K., and Patmore, R.A. (1992), *Operational Modes of Bioreactors*, Elsevier Science & Technology Books, San Diego.

van der Meer, A.B., Beenackers, A.A.C.M., Burghard, R., Mulder, N.H., and Fok, J.J. (1992), "Gas/liquid mass transfer in a four-phase stirred fermentor: Effects of organic phase hold-up and surfactant concentration, " *Chemical Engineering Science*, 47(9–11): 2369–2374.

van der Schaaf, J., Chilekar, V.P., van Ommen, J.R., Kuster, B.F.M., Tinge, J.T., and Schouten, J.C. (2007), "Effect of particle lyophobicity in slurry bubble columns at elevated pressures," *Chemical Engineering Science*, 62(18–20): 5533–5537.

van der Westhuizen, I., Du Toit, E., and Nicol, W. (2007), "Trickle flow multiplicity: The influence of the prewetting procedure on flow hysteresis, " *Chemical Engineering Research & Design*, 85(12): 1604–1610.

van Elk, E.P., Knaap, M.C., and Versteeg, G.F. (2007), "Application of the penetration theory for gas-liquid mass transfer without liquid bulk: Differences with systems with a bulk," *Chemical Engineering Research & Design*, 85(4): 516–524.

van Sint Annaland, M., Dijkhuizen, W., Deen, N.G., and Kuipers, J.A.M. (2006), "Numerical simulation of behavior of gas bubbles using a 3-D front-tracking method," *AIChE Journal*, 52(1): 99–110.

Vandu, C.O., and Krishna, R. (2004), "Influence of scale on the volumetric mass transfer coefficients in bubble columns," *Chemical Engineering and Processing*, 43(4): 575–579.

Vardar, F., and Lilly, M.D. (1982), "The measurement of oxygen-transfer coefficients in fermentors by frequency response techniques," *Biotechnology and Bioengineering*, 24(7): 1711–1719.

Varley, J. (1995), "Submerged gas-liquid jets: Bubble size prediction," *Chemical Engineering Science*, 50(5): 901–905.

Vasconcelos, J.M.T., Orvalho, S.C.P., Rodrigues, A.M.A.F., and Alves, S.S. (2000), "Effect of blade shape on the performance of six-bladed disk turbine impellers," *Industrial & Engineering Chemistry Research*, 39(1): 203–213.

Vasquez, G., Antorrena, G., Navaza, J.M., Santos, V., and Rodriguez, T. (1993), "Adsorption of CO_2 in aqueous solutions of various viscosities in the presence of induced turbulence," *International Chemical Engineering*, 1993(4): 649–655.

Vasquez, G., Cancela, M.A., Riverol, C., Alvarez, E., and Navaza, J.M. (2000), "Determination of interfacial areas in a bubble column by different chemical methods," *Industrial & Engineering Chemistry Research*, 39: 2541–2547.

Vatai, G., and Tekic, M.N. (1986), "Effect of pseudoplasticity on hydrodynamic characteristics of air-lift loop contactor," *Rheologica Acta*, 26: 271.

Vatanakul, M., Zheng, Y., and Couturier, M. (2004), "Application of ultrasonic technique in multiphase flows," *Industrial & Engineering Chemistry Research*, 43: 5681–5691.

Vázquez, G., Cancela, M.A., Riverol, C., Alvarez, E., and Navaza, J.M. (2000), "Application of the Danckwerts method in a bubble column: Effects of surfactants on mass transfer coefficient and interfacial area," *Chemical Engineering Journal*, 78(1): 13–19.

Vazquez, G., Cancela, M.A., Varela, R., Alvarez, E., and Navaza, J.M. (1997), "Influence of surfactants on absorption of CO_2 in a stirred tank with and without bubbling," *Chemical Engineering Journal*, 67(2): 131–137.

Veera, U.P., and Joshi, J.B. (1999), "Measurement of gas hold-up profiles by gamma ray tomography: Effect of sparger design and height of dispersion in bubble columns," *Chemical Engineering Research & Design*, 77(4): 303–317.

Veera, U.P., Kataria, K.L., and Joshi, J.B. (2004), "Effect of superficial gas velocity on gas hold-up profiles in foaming liquids in bubble column reactors," *Chemical Engineering Journal*, 99(1): 53–58.

Veera, U.P., Patwardhan, A.W., and Joshi, J.B. (2001) "Measurement of gas hold-up profiles in stirred tank reactors by gamma ray attenuation technique," *Transactions of IChemE, Part A Chemical Engineering Research and Design*, 79(6): 684–688.

Vega, J.L., Antorrena, G.M., Clausen, E.C., and Gaddy, J.L. (1989), "Study of gaseous substrate fermentations: Carbon monoxide conversion to acetate. 2. Continuous culture," *Biotechnology and Bioengineering*, 34(6): 785–793.

Verma, A.K., and Rai, S. (2003), "Studies on surface to bulk ionic mass transfer in bubble column," *Chemical Engineering Journal*, 94(1): 67–72.

Vermeer, D.J., and Krishna, R. (1981), "Hydrodynamics and mass transfer in bubble columns operating in the churn-turbulent regime," *Industrial and Engineering Chemistry Process Design and Development*, 20: 475–482.

Vesselinov, H.H., Stephan, B., Uwe, H., Holger, K., Günther, H., and Wilfried, S. (2008), "A study on the two-phase flow in a stirred tank reactor agitated by a gas-inducing turbine," *Chemical Engineering Research & Design*, 86(1): 75–81.

Vial, C., Bendjaballah-Lalaoui, N., Poncin, S., Wild, G., and Midoux, N. (2003), "Comparison, combination, and validation of measuring techniques for flow and turbulence analysis in bubble columns and airlift reactors," *The Canadian Journal of Chemical Engineering*, 81(3–4): 749–755.

Vial, C., Camarasa, E., Poncin, S., Wild, G., Midoux, N., and Bouillard, J. (2000), "Study of hydrodynamic behaviour in bubble columns and external loop airlift reactors through analysis of pressure fluctuations," *Chemical Engineering Science*, 55(15): 2957–2973.

Vial, C., Laine, R., Poncin, S., Midoux, N., and Wild, G. (2001), "Influence of gas distribution and regime transitions on liquid velocity and turbulence in a 3-D bubble column," *Chemical Engineering Science*, 56(3): 1085–1093.

Waghmare, Y.G., Rice, R.G., and Knopf, F.C. (2008), "Mass transfer in a viscous bubble column with forced oscillations," *Industrial & Engineering Chemistry Research*, 47(15): 5386–5394.

Wallis, G.B. (1969), *One-Dimensional Two-Phase Flow*, McGraw-Hill, New York.

Walter, J.F., and Blanch, H.W. (1986), "Bubble break-up in gas-liquid bioreactors: Break-up in turbulent flows," *Chemical Engineering Journal*, 32(1): B7–B17.

Warsito, W., and Fan, L.-S. (2003a), "3D-ECT velocimetry for flow structure quantification of gas-liquid-solid fluidized beds," *The Canadian Journal of Chemical Engineering*, 81(3–4): 875–884.

Warsito, W., and Fan, L.-S. (2003b), "ECT imaging of three-phase fluidized bed based on three-phase capacitance model," *Chemical Engineering Science*, 58: 823–832.

Warsito, W., and Fan, L.-S. (2005), "Dynamics of spiral bubble plume motion in the entrance region of bubble columns and three phase fluidized beds using 3D ECT," *Chemical Engineering Science*, 60: 6073–6084.

Watts, P., and Wiles, C. (2007), "Micro reactors: A new tool for the synthetic chemist," *Organic and Biomolecular Chemistry*, 5(5): 727–732.

Wei, C., Xie, B., and Xiao, H. (2000), "Hydrodynamics in an internal loop airlift reactor with a convergence-divergence draft tube," *Chemical Engineering & Technology*, 23(1): 38–45.

Wei, Y., Tiefeng, W., Malin, L., and Zhanwen, W. (2008), "Bubble circulation regimes in a multi-stage internal-loop airlift reactor," *Chemical Engineering Journal*, 142(3): 301–308.

Weiland, P. (1984), "Influence of draft tube diameter on operation behavior of airlift loop reactors," *German Chemical Engineering*, 7(6): 374–385.

Weiland, P., and Onken, U. (1981), "Fluid dynamics and mass transfer in an airlift fermenter with external loop," *German Chemical Engineering*, 4(1): 42–50.

Westerterp, K.R., and Molga, E.J. (2006), "Safety and runaway protection in batch and semibatch reactors: A review," *Chemical Engineering Research & Design*, 84(A7): 543–552.

White, F.M. (1974), *Viscous Fluid Flow*, McGraw-Hill, New York.

Whitton, M.J., and Nienow, A.W. (1993), "Scale-up correlations fr gas hold-up and mass transfer coefficients in stirred tank reactors" in *Proceedings of the 3rd International Conference on Bioreactor and Bioprocess Fluid Dynamics*, 135–149.

Wilkin, R.T., McNeil, M.S., Adair, C.J., and Wilson, J.T. (2001), "Field measurement of dissolved oxygen: A comparison of methods," *Ground Water Monitoring and Remediation*, 21(4): 124–132.

Wilkinson, P.M. (1991), "Physical aspect and scale-up of high pressure bubble column," PhD Thesis, University of Groningen, Groningen, The Netherlands.

Wilkinson, P.M., Spek, A.P., and van Dierendonck, L.L. (1992), "Design parameters estimation for scale-up of high-pressure bubble columns," *AIChE Journal*, 38(4): 544–554.

Williams, J.A. (2002), "Keys to bioreactor selection," *Chemical Engineering Progress*, 98(3): 34–41.

Williams, R.A., and Beck, M.S., (eds) (1995), *Process Tomography: Principles, Techniques and Applications*, Butterworth-Heinemann Ltd, Oxford.

Wirth, T. (ed.) (2008), Microreactors in Organic Synthesis and Catalysis*, Weinheim*, Wiley-VCH Verlag GmbH & KGaA, Germany.

Wooley, R., Ruth, M., Sheehan, J., Ibsen, K., Majdeski, H., and Galvez, A. (1999), "Lignocellulosic biomass to ethanol process design and economics utilizing co-current dilute acid prehydrolysis and enzymatic hydrolysis current and futuristic scenarios", National Renewable Energy Laboratory, Golden, Colorado.

Worden, R.M., and Bredwell, M.D. (1998), "Mass transfer properties of microbubbles: II. Analysis using a dynamic model," *Biotechnology Progress*, 14(1): 39–46.

Worden, R.M., Bredwell, M.D., and Grethlein, A.J. (1997), "Engineering issues in synthesis-gas fermentations," in *ACS Symposium Series: Fuels and Chemicals from Biomass*, B.C. Saha, and J. Woodward, Editors, Washington, DC, American Chemical Society. 666: 320–335.

Yakhnin, V.Z., and Menzinger, M. (2008), "Estimating spectral properties of the thermal instability in packed-bed reactors," *Chemical Engineering Science*, 63(6): 1480–1489.

Yawalkar, A.A., Heesing, A.B.M., Versteeg, G.F., and Pangarkar, V.G. (2002a), "Gas-liquid mass transfer coefficient in stirred tank reactors," *The Canadian Journal of Chemical Engineering*, 80: 840–848.

Yawalkar, A.A., Pangarkar, V.G., and Beenackers, A.A.C.M. (2002b), "Gas hold-up in stirred tank reactors," *The Canadian Journal of Chemical Engineering*, 80: 158–166.

Yin, F., Afacan, A., Nandakumar, K., and Chuang, K.T. (2002), "Liquid holdup distribution in packed columns: Gamma ray tomography and CFD simulation," *Chemical Engineering and Processing*, 41: 473–483.

Yoshida, F., and Koyanagi, T. (1962), "Mass transfer and effective interfacial areas in packed columns," *AIChE Journal*, 8(3): 309–316.

Zahradnik, J., Fialová, M., and Linek, V. (1999a), "The effect of surface-active additives on bubble coalescence in aqueous media," *Chemical Engineering Science*, 54(21): 4757–4766.

Zahradnik, J., Fialova, M., Ruzicka, M., Drahos, J., Kastanek, F., and Thomas, N.H. (1997), "Duality of the gas-liquid flow regimes in bubble column reactors," *Chemical Engineering Science*, 52(21/22): 3811–3826.

Zahradnik, J., and Kastanek, F. (1979), "Gas holdup in uniformly aerated bubble column reactors," *Chemical Engineering Communications*, 3(4–5): 413–429.

Zahradnik, J., Kuncová, G., and Fialová, M. (1999b), "The effect of surface active additives on bubble coalescence and gas holdup in viscous aerated batches," *Chemical Engineering Science*, 54(13–14): 2401–2408.

Zech, J.B. (1978), "Liquid flow and mass transfer in an irrigated packed column," PhD Thesis, TU Munchen, Munchen, Germany.

Zehner, P. (1989), "Mehrphasenstromungen in gas-flussigkeits-reaktoren," *Dechema-Monograph*, 1989(114): 215–233.

Zeng, A.-P., and Deckwer, W.-D. (1996), "Bioreaction techniques under microaerobic conditions: From molecular level to pilot plant reactors," *Chemical Engineering Science*, 51(10): 2305–2314.

Zhang, H., Chen, G., Yue, J., and Yuan, Q. (2009), "Hydrodynamics and mass transfer of gas-liquid flow in a falling film microreactor," *AIChE Journal*, 55(5): 1110–1120.

Zheng, Y., and Zhang, Q. (2004), "Simultaneous measurements of gas and solid holdups in multiphase systems using ultrasonic technique," *Chemical Engineering Science*, 59: 3505–3514.

Zhong, J.-J. (2010), "Recent advances in bioreactor engineering," *Korean Journal of Chemical Engineering*, 27(4): 1035–1041.

Zhu, H., Shanks, B.H., and Heindel, T.J. (2008), "Enhancing CO-water mass transfer by functionalized MCM41 nanoparticles," *Industrial & Engineering Chemistry Research*, 47(20): 7881–7887.

Zhu, H., Shanks, B.H., and Heindel, T.J. (2009), "Effect of electrolytes on CO-water mass transfer," *Industrial & Engineering Chemistry Research*, 48(6): 3206–3210.

Zhu, Y., Bandopadhayay, P.C., and Wu, J. (2001), "Measurement of gas-liquid mass transfer in an agitated vessel-A comparison between different impellers," *Journal of Chemical Engineering of Japan*, 34(5): 579–584.

Zou, R., Jiang, X., Li, B., Zu, Y., and Zhang, L. (1988), "Studies on gas holdup in a bubble column operated at elevated temperatures," *Industrial & Engineering Chemistry Research*, 27(10): 1910–1916.

Index

An Introduction to Bioreactor Hydrodynamics and Gas-Liquid Mass Transfer, First Edition.
Enes Kadic and Theodore J. Heindel.